



**MONASH** University

**Formation, reaction rates and stability of hydrotalcite-group  
minerals: applications for carbon mineralisation**

*Connor Charles Turvey*

*Bachelor of Science (Honours), Monash University, 2013*

A thesis submitted for the Degree of Doctor of Philosophy at Monash  
University in 2018

School of Earth, Atmosphere and Environment



## **Copyright notice**

© Connor Charles Turvey (2018).

I certify that I have made all reasonable efforts to secure copyright permissions for third-party content included in this thesis and have not knowingly added copyright content to my work without the owner's permission.

## Thesis including published works declaration

I hereby declare that this thesis contains no material which has been accepted for the award of any other degree or diploma at any university or equivalent institution and that, to the best of my knowledge and belief, this thesis contains no material previously published or written by another person, except where due reference is made in the text of the thesis.

This thesis includes 0 original papers published in peer reviewed journals and 0 submitted publications. The core theme of the thesis is tracing and understanding the role of hydrotalcite minerals is carbon mineralisation. The ideas, development and writing up of all the papers in the thesis were the principal responsibility of myself, the student, working within the School of Earth, Atmosphere and Environment under the supervision of Dr Siobhan Alexandra Wilson.

(The inclusion of co-authors reflects the fact that the work came from active collaboration between researchers and acknowledges input into team-based research.)

In the case of Chapter 3, 4, 5 and 6 my contribution to the work involved the following:

Thesis Chapter	Publication Title	Status (published, in press, accepted or returned for revision, submitted)	Nature and % of student contribution	Co-author name(s) Nature and % of Co-author's contribution*	Co-author(s), Monash student Y/N*
3	<i>Comparison of Rietveld-compatible structureless fitting analysis methods for accurate quantification of carbon dioxide fixation in ultramafic mine tailings</i>	<i>Returned for revision</i>	75%. Concept, experimental design, conducted experiments, collected and analysed data, writing and editing.	1. Jessica L. Hamilton, Experimental design and data Analysis 5% 2. Siobhan A. Wilson, Supervisory role, concept, assisted with data analysis and had input into the manuscript 20%	Yes  No
4	<i>Hydrotalcites and hydrated Mg-carbonates as carbon sinks in serpentinite mineral wastes from the Woodsreef Chrysotile Mine, New South Wales, Australia: CO<sub>2</sub></i>	<i>Submitted</i>	60%. Concept, conducted fieldwork, experimental design, conducted experiments, collected and analysed data, writing and editing.	1. Siobhan A. Wilson, supervisory role, fieldwork, assisted with data analysis and had input into the manuscript 15%. 2. Jessica L. Hamilton, field work, data analysis 10%. 3. Alistair W. Tait, field work, data analysis 10%.	No  Yes  No

	<i>limitation controls mineralogy and efficiency of CO2 air capture in mine tailings</i>			<p>4. Jenine McCutcheon, field work 1%.</p> <p>5. Andreas Beinlich, data analysis 1%.</p> <p>6. Stewart J. Fallon, data analysis 1%.</p> <p>7. Gregory M. Dipple, supervisory role 1%.</p> <p>8. Gordon Southam, supervisory role, fieldwork 1%.</p>	<p>No</p> <p>No</p> <p>No</p> <p>No</p> <p>No</p>
5	<i>Stable magnesium isotope signatures of alteration minerals during carbon mineralisation in ultramafic mineral wastes</i>	<i>In preparation</i>	60%. Concept, conducted fieldwork, experimental design, conducted experiments, collected and analysed data, writing and editing.	<p>1. Hans C. Oskierski, supervisory role, field work, assisted with data interpretation and had input into the manuscript 15%.</p> <p>2. Siobhan A. Wilson, Supervisory role, field work, assisted with data interpretation and had input into the manuscript 15%.</p> <p>3. Vasileios Mavromatis, sample preparation and data analysis 10%.</p> <p>4. Jessica L. Hamilton, fieldwork 3%.</p> <p>5. Bogdan Dlugogorski, fieldwork. 2%</p>	<p>No</p> <p>No</p> <p>No</p> <p>Yes</p> <p>No</p>
6	<i>Mg exchange between pyroaurite [Mg<sub>6</sub>Fe<sup>3+</sup><sub>2</sub>CO<sub>3</sub>(OH)<sub>16</sub>·4H<sub>2</sub>O] and aqueous Mg(II): Implications for carbon mineralisation and contaminant release</i>	<i>In preparation</i>	75%. Concept, experimental design, conducted experiments, collected and analysed data, writing and editing.	<p>1. Andrew Frierdich, supervisory role, experimental design, data analysis and interpretation and had input into the manuscript 20%.</p> <p>2. Sasha A. Wilson, supervisory role, assisted with data interpretation and had input into the manuscript 5%.</p>	<p>No</p> <p>No</p>

*\*If no co-authors, leave fields blank*

I have renumbered sections of submitted or published papers in order to generate a consistent presentation within the thesis.

**Student signature:**

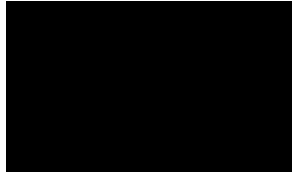


**Date:**

22/03/2018

The undersigned hereby certify that the above declaration correctly reflects the nature and extent of the student's and co-authors' contributions to this work. In instances where I am not the responsible author I have consulted with the responsible author to agree on the respective contributions of the authors.

**Main Supervisor signature:**



**Date:** 22/03/2018

## Publications during enrolment

Mervine, E., Wilson, S.A., Power, I.M., Dipple, G.M., Turvey, C.C., Hamilton, J.L., Vanderzee, S., Raudsepp, M., Southam, C., Matter, J.M., Kelemen, P.B., Stiefenhofer, J., Miya, Z., and Southam, G. (2018). Carbon Storage Potential of Kimberlite Mine Tailings. Accepted in press, *Mineralogy and Petrology*.

Hamilton, J.L., Wilson, S.A., Morgan, B., Turvey, C.C., Paterson, D., Jowitt, S.M., McCutcheon, J. and Southam, G. (2018). Fate of transition metals during passive carbonation of ultramafic mine tailings via air capture with potential for metal resource recovery. Accepted in press, *International Journal of Greenhouse Gas Control*.

Turvey, C.C., Wilson, S.A., Hamilton, J.L. and Southam, G. (2017) Field-based accounting of CO<sub>2</sub> sequestration in ultramafic mine wastes using portable X-ray diffraction. *American Mineralogist* **102**, 1302-1310.

McCutcheon, J., Turvey, C.C., Wilson, S., Hamilton, J.L. and Southam, G. (2017). Field-based deployment of microbial carbonation for carbon sequestration and stabilization of asbestos mine tailings. *Minerals* **7**, 191.

Hebbard, E.R., Wilson, S.A., Jowitt, S.M., Tait, A.W., Turvey, C.C., Wilson, H. (2017) Regrowth of arsenate-sulfate efflorescences on processing plant walls at the Ottery arsenic-tin mine, New South Wales, Australia: Implications for arsenic mobility and remediation of contaminated processing sites. *Applied Geochemistry* **79**, pages 91-106.

Hamilton, J.L., Wilson, S.A., Morgan, B., Turvey, C.C., Paterson, D., MacRae, C., McCutcheon, J. and Southam, G. (2016). Nesquehonite sequesters transition metals and CO<sub>2</sub> during accelerated carbon mineralisation. *International Journal of Greenhouse Gas Control* **55**, 73-81.

## **Dedication**

To my loving and supportive family and friends

## Acknowledgements

Firstly I would like to acknowledge the amazing contribution of my supervisor Sasha Wilson, she gave me the opportunity to work on this research, advice when I needed it and never failed to help when I had a problem to work through. I would also like to thank my fellow student and friend Jessica Hamilton who went on this journey with me, from field work, to our first conference together, we shared so much of this and she made the entire experience a pleasure.

Thanks also go to Dr. Carlos Rodriguez-Navarro and Professor Martin Dietzel, who examined this thesis, and whose constructive comments helped to improve the science and language within.

My PhD candidature was supported by an Australian Government Research training Program (RTP) Scholarship and a MDS/MRS and Donors Scholarship. Funding for this research was provided by grants from Carbon Management Canada and the New South Wales Department of Industry to Sasha Wilson. We would also like to thank Kate Maddison, Nick Staheyeff, Catherine Karpel and Brad Mullard for granting us access to the Woodsreef Chrysotile mine and supporting us in the field. I would like to thank the Mineralogical Society of Great Britain & Ireland, Mineralogical Association of Canada and the AusIMM for providing additional funding that allowed me to conduct experiments at the University of British Columbia. Furthermore I would like to acknowledge the contributions of the International Centre for Diffraction Data, Rotary Club of Balwyn, Australian X-ray Analytical Association and the Mineralogical Society of Great Britain & Ireland whose financial contributions allowed me to present my research at national and international conferences.

My thanks to all staff at the School of Earth, Atmosphere and Environment for their support during my time at Monash University. Particularly Ian Cartwright, Andrew Frierdich, Andrew Tomkins, Vanessa Wong, Xuan Zhu and Roberto Weinberg for their invaluable contributions and suggestions as members of my milestone committees. I would like to acknowledge all the hard work by Yuzhou Lin for making sure my scholarships and reimbursements were in order, and my appreciation goes to Rachelle Pierson, Junnel Alegado and Massimo Raveggi for their assistance in the laboratories at the School of Earth, Atmosphere and Environment.

I would also like to thank Bree Morgan for being a constant source of advice and compassion throughout my research. Thanks to Greg Dipple, Kate Carrol and Bart De Baere for helping me with my research, hosting me and making me feel home at the University of British Columbia and to Simon Jowitt, Ben Mililli and Katherine Barta for undertaking field work with me. And I would like to acknowledge the contributions of Ben Grguric for providing us with samples from Mount Keith, Anna Harrison for transporting samples for Mg isotope analysis, and Andreas Beinlich for advice on stable Mg isotope analyses.

Finally, I wish to thank all my family and friends for helping support me throughout my research. Special thanks go to Anna B, Anna G, Penelope and Andrew as they are a constant source of light and happiness in my life.



## Table of contents

Copyright notice .....	III
Thesis including published works declaration.....	IV
Publications during enrolment.....	VII
Dedication.....	VIII
Acknowledgements.....	IX
Table of contents.....	XII
List of figures.....	XVI
List of tables .....	XIX
List of Abbreviations .....	XX
Abstract.....	XXII
Chapter 1: Introduction.....	1
1.1 Significance of the study.....	2
1.2 Carbon mineralisation in ultramafic tailings.....	4
1.3 Hydrotalcite minerals.....	6
1.4 Aims and objectives of the thesis.....	7
1.5 Organisation and outcomes of the thesis.....	10
1.6 References.....	14
Chapter 2: Carbon mineralisation and hydrotalcites: background and current knowledge.	23
2.1 Introduction.....	24
2.2 Carbon mineralisation in Ultramafic Mine Wastes.....	26
2.2.1 The Woodsreef chrysotile mine .....	27
2.2.2 The Mount Keith nickel mine .....	31
2.2.3 The Dundas mineral field.....	32
2.3 Hydrotalcites: current geochemical knowledge and gaps.....	33
2.3.1 Structures of hydrotalcites.....	34
2.3.2 Anion exchange in hydrotalcites .....	39
2.3.3 Formation of hydrotalcites .....	41
2.3.4 Uses and applications of hydrotalcites .....	42
2.3.5 Reaction rates in hydrotalcites .....	44
2.3.6 Stable isotope geochemistry of hydrotalcites .....	45
2.4 Summary .....	47
2.5 References.....	49
Declaration for Thesis Chapter 3 .....	66

Chapter 3: Comparison of Rietveld-compatible structureless fitting analysis methods for accurate quantification of carbon dioxide fixation in ultramafic mine tailings .....	67
3.0 Abstract .....	68
3.1 Introduction .....	70
3.2 Experimental method .....	75
3.2.1 Synthetic tailings samples.....	75
3.2.2 Instrument details.....	76
3.2.3 Rietveld refinement strategy .....	78
3.3 Results and discussion.....	89
3.3.1 Comparison of results from the three refinement methods.....	89
3.3.2 Carbon sequestration and carbonation potential estimates .....	95
3.3.3 Method comparison .....	104
3.4 Implications .....	104
3.5 Acknowledgements .....	107
3.6 References .....	108
Declaration for Thesis Chapter 4 .....	120
Chapter 4: Hydrotalcites and hydrated Mg-carbonates as carbon sinks in serpentinite mineral wastes from the Woodsreef Chrysotile Mine, New South Wales, Australia: CO <sub>2</sub> limitation controls mineralogy and efficiency of CO <sub>2</sub> air capture in mine tailings .....	121
4.0 Abstract .....	122
4.1 Introduction .....	123
4.2 Material and methods .....	128
4.2.1 Field site and sampling methods.....	128
4.2.2 X-ray diffraction methods.....	130
4.2.3 Scanning electron microscopy .....	134
4.2.4 Stable carbon and oxygen isotope analysis.....	135
4.2.5 Radiocarbon analysis .....	136
4.2.6 Anion exchange experiment .....	136
4.2.7 Total carbon analysis and carbon accounting .....	138
4.3 Results .....	139
4.3.1 X-ray diffraction .....	139
4.3.2 Scanning electron microscopy results.....	146
4.3.3 Radiocarbon and stable carbon and oxygen isotopes .....	148
4.3.4 Anion exchange experiment .....	152
4.3.5 Total carbon .....	155

4.4 Discussion .....	157
4.4.1 Mineralogy as a function of depth in the tailings pile .....	157
4.4.2 Formation of coalingite and pyroaurite from brucite .....	163
4.4.3 Radiocarbon and stable carbon and oxygen isotope results reflect formation under carbon limited conditions .....	165
4.4.4 Differentiating metamorphic and sedimentary hydrotalcite minerals in mine tailings and natural environments.....	176
4.4.5 CO <sub>2</sub> limitation controls mineralogy and capture of CO <sub>2</sub> from air in mine tailings .....	179
4.4.6 Carbon sequestration rate estimates .....	181
4.5 Conclusions .....	186
4.6 Acknowledgements .....	189
4.7 References .....	189
Declaration for Thesis Chapter 5 .....	204
Chapter 5: Stable magnesium isotope signatures of alteration minerals during carbon mineralisation in ultramafic mineral wastes .....	205
5.0 Abstract .....	206
5.1 Introduction.....	207
5.2 Field sites .....	211
5.2.1 The Woodsreef chrysotile mine .....	212
5.2.2 The Mount Keith nickel mine .....	214
5.2.3 The Dundas mineral field .....	216
5.2.4 Sampling details .....	217
5.3 Analytical methods .....	220
5.3.1 Powder X-ray diffraction.....	220
5.3.2 Selective acid extractions .....	220
5.3.3 Stable Mg isotope analysis .....	221
5.4 Results.....	222
5.4.1 The Woodsreef chrysotile mine .....	223
5.4.2 The Mount Keith nickel mine .....	225
5.4.3 The Dundas mineral field .....	227
5.5 Discussion .....	228
5.5.1 Stable Mg isotope signatures of serpentine undergoing weathering .....	228
5.5.2 Effects of selective acid leaching treatments on stable Mg isotope signatures of serpentinite samples .....	231
5.5.3 Stable Mg isotope signature of hydrotalcites .....	234

5.5.4 Tracing serpentinite weathering and carbonation using stable Mg isotopes .....	236
5.6 Conclusions .....	240
5.7 Acknowledgements .....	242
5.8 References .....	242
Declaration for Thesis Chapter 6 .....	256
Chapter 6: Mg exchange between pyroaurite [ $\text{Mg}_6\text{Fe}^{3+}_2\text{CO}_3(\text{OH})_{16}\cdot 4\text{H}_2\text{O}$ ] and aqueous Mg(II): Implications for carbon mineralisation and contaminant release.....	257
6.0 Abstract .....	258
6.1 Introduction .....	259
6.2 Materials and methods.....	263
6.2.1 Pyroaurite synthesis .....	263
6.2.2 Isotopic exchange experiments.....	264
6.2.3 ICP-MS Analysis and %Mg exchange calculations .....	265
6.3 Results and discussion.....	267
6.3.1 Interactions between pyroaurite and aqueous Mg .....	267
6.3.2 Degree of Mg exchange.....	274
6.3.3 Implications for tracing the origins of hydrotalcite minerals and for contaminant release .....	279
6.4 Acknowledgements .....	281
6.5 References .....	281
Conclusions and future research .....	290
7.1 Outcomes of the thesis .....	291
7.2 Improved methods for tracing carbon mineralisation .....	293
7.3 Determining the origin of hydrotalcites at the Woodsreef chrysotile mine .....	298
7.4 Implications of <i>in situ</i> formation of hydrotalcite minerals for carbon sequestration in ultramafic tailings storage facilities .....	300
7.5 Understanding stable isotopic signatures and elemental exchange in hydrotalcites	302
7.6 Suggestions for future research .....	305
7.7 References .....	308
Appendix 1: Supplemental Information for Chapter 6: Mg exchange between pyroaurite [ $\text{Mg}_6\text{Fe}^{3+}_2\text{CO}_3(\text{OH})_{16}\cdot 4\text{H}_2\text{O}$ ] and aqueous Mg(II): Implications for carbon mineralisation and contaminant release .....	315
S1. Control experiments .....	316
S2. Mg % Exchange calculations .....	320
S3. Estimate of the fraction of Mg atoms at the pyroaurite surface.....	322
S4. Crystallite size calculations and results.....	324

## List of figures

### Chapter 2

**Figure 2.1** Generalised structure of a hydrotalcite mineral, illustrating the relationship between the hydroxide layers and interlayer galleries. Inset shows the atomic positions within the brucite-like hydroxide layer (modified from Woodhouse, 2006).....35

**Figure 2.2** Layering within hydrotalcites, showing the difference between O and P-type interlayers, modified from Bookin and Drits (1993).....38

### Chapter 3

**Figure 3.1** Modelling pyroaurite using with the PONKCS method and **a)** no March-Dollase preferred orientation, and a March-Dollase correction with **b)** no minimum value **c)** a minimum of 0.6 and **d)** a minimum of 0.75. Refined pyroaurite abundance (absolute error) and  $R_{wp}$  is reported for each of the conditions.....85

**Figure 3.2** Modelling pyroaurite using with the Pawley/internal standard method and **a)** no March-Dollase preferred orientation, and a March-Dollase correction with **b)** no minimum value **c)** a minimum of 0.6 and **d)** a minimum of 0.75. Refined pyroaurite abundance (absolute error) and  $R_{wp}$  is reported for each of the conditions.....87

**Figure 3.3** Results of Rietveld refinements for each mineral phase in the synthetic tailings using both the PONKCS and Rietveld spike method.....88

**Figure 3.4** Relative and absolute error values between the weighed compositions of the artificial tailings samples and the compositions calculated via Rietveld refinement for **a)** absolute error values for PONKCS method **b)** relative error values for PONKCS method **c)** absolute error values for Rietveld spike method **d)** relative error values for Rietveld spike method.....92

**Figure 3.5** Estimates for carbon sequestration and remaining carbonation potential of the artificial tailings based on the abundance of (1) hydromagnesite and pyroaurite and (2) brucite, respectively according to their weighed and refined abundances. Two values are included for brucite to represent the potential for it to form hydromagnesite (high C) or pyroaurite (low C).....96

### Chapter 4

**Figure 4.1** **(a)** Map showing the location of the Woodsreef chrysotile mine. **(b)** Aerial photograph of the Woodsreef chrysotile mine.....123

**Figure 4.2** Field photographs of **(a)** loose shallow tailings (14WRP-1, 15cm ruler for scale), **(b)** loose shallow tailings (14WRP-4, 15cm ruler for scale), **(c)** vertical crusts forming on the surface of the tailings (hammer for scale) and **(d)** horizontal crusts on the surface of the tailings (multi-tool for scale).....123

**Figure 4.3** Quantitative XRD results for the vertical tailings profiles, showing the abundance (wt%) of serpentine, hydromagnesite, pyroaurite, brucite, coalingite, forsterite and magnetite with depth below the tailings pile surface.....139

**Figure 4.4** SEM micrograph and EDS results for tailings samples showing (a) serpentine and magnetite grains and an amorphous Mg-Si carbonate, (b) carbonated brucite and pyroaurite grains and (c) heavily dissolved and carbonated brucite grains.....141

**Figure 4.5** Stable carbon and radiocarbon results of tailings material and pyroaurite grains showing (a)  $F^{14}C$  vs  $\delta^{13}C$  (bedrock and atmospheric carbonate fields are replotted from Oskierski et al. 2013), (b)  $F^{14}C$  vs depth and (c)  $\delta^{13}C$  vs depth. Tailings samples are replotted from Hamilton et al., in prep-b.....143

**Figure 4.6** Stable carbon ( $\delta^{13}C_{VPDB}$ ) and oxygen ( $\delta^{18}O_{VSMOW}$ ) results for pyroaurite, tailings and surface crusts from the Woodsreef tailings pile (bedrock and atmospheric carbonate fields and the bedrock carbonate, crusts and cements are taken from Oskierski et al. 2013). Pyr: pyroaurite, Hmgs: hydromagnesite.....146

**Figure 4.7** XRD pattern showing the change in the 0 0 3 and 0 0 6 reflections that occurs during anion exchange from iowaite to pyroaurite after 46 hours in the high carbon treatment.....147

**Figure 4.8** Stable carbon and radiocarbon results for the anion exchange experiment indicating (a) the  $\delta^{13}C$  versus time exchanged; (b)  $F^{14}C$  versus time exchanged; and (c) the  $F^{14}C$  compared to  $\delta^{13}C$  results.....148

**Figure 4.9** Inorganic carbon content (wt%) versus depth for the vertical tailings profiles, as analysed by total carbon (LECO) and quantitative XRD analysis.....151

**Figure 4.10** Diagram comparing the quantity of atmospheric carbon sequestered in the tailings at various depths according to XRD and total carbon data.....178

## Chapter 5

**Figure 5.1** (a) Map of Australia showing the locations of the Woodsreef chrysotile mine, Mount Keith nickel mine and Dundas mineral field. Aerial photographs of (b) the Woodsreef chrysotile mine, (c) the Mount Keith nickel mine and (d) the Dundas mineral field, highlighting the sampling locations.....208

**Figure 5.2** (a) Serpentinite waste rock with pyroaurite coating at Woodsreef. (b) Thin, surficial carbonate crust formed on the Woodsreef tailings pile. (c) Serpentinite tailings containing visible pyroaurite at Woodsreef. (d) Serpentinite wasterock with visible grains of woodallite from the Mount Keith nickel mine. (e) Serpentinite cobble with visible intergrown brucite and iowaite collected from the pit at the Mount Keith nickel mine. (f) Intergrown brucite and iowaite vein collected from the pit at the Mount Keith nickel mine. (g-h) Serpentinite cobbles with visible stichtite and aragonite collected from Murchison Creek (Dundas, Tasmania).....213

**Figure 5.3**  $\delta^{25}Mg$ – $\delta^{26}Mg$  diagram (3-isotope plot) showing the stable Mg isotopic composition of serpentine, brucite, hydrotalcite and carbonate specimens used for this study from the Woodsreef chrysotile mine, the Mount Keith nickel mine and the Dundas mineral

field. Samples are differentiated depending on whether the sample was separated by picking or by acid leaching, either in the leachate or the acid leached residue. The typical  $\delta^{25}\text{Mg}$ – $\delta^{26}\text{Mg}$  compositions of mafic and ultramafic rocks (according to Beinlich et al., 2014 and Bourdon et al., 2010) are indicated as a single field. The lines indicate the slopes for equilibrium and kinetic mass dependent fractionation (Young and Galy, 2004).....216

**Figure 5.4**  $\delta^{25}\text{Mg}$ – $\delta^{26}\text{Mg}$  diagram (3-isotope plot) showing the stable Mg isotopic composition of serpentine, hydrotalcite and carbonate specimens from the Woodsreef chrysotile mine. Samples are differentiated depending on whether the sample was separated by picking or by acid leaching, either in the leachate or the acid leached residue. The typical  $\delta^{25}\text{Mg}$ – $\delta^{26}\text{Mg}$  compositions of mafic and ultramafic rocks (according to Beinlich et al., 2014 and Bourdon et al., 2010) are indicated as a single field. The lines indicate the slopes for equilibrium and kinetic mass dependent fractionation (Young and Galy, 2004).....218

**Figure 5.5**  $\delta^{25}\text{Mg}$ – $\delta^{26}\text{Mg}$  diagram (3-isotope plot) showing the stable Mg isotopic composition of serpentine, brucite and hydrotalcite specimens from the Mount Keith nickel mine. The typical  $\delta^{25}\text{Mg}$ – $\delta^{26}\text{Mg}$  compositions of mafic and ultramafic rocks (according to Beinlich et al., 2014 and Bourdon et al., 2010) are indicated as a single field. The lines indicate the slopes for equilibrium and kinetic mass dependent fractionation (Young and Galy, 2004).....220

**Figure 5.6**  $\delta^{25}\text{Mg}$ – $\delta^{26}\text{Mg}$  diagram (3-isotope plot) showing the stable Mg isotopic composition of serpentine, and hydrotalcite specimens from the Dundas mineral field. Samples are differentiated depending on whether the sample was separated by picking or by acid leaching, either in the leachate or the acid leached residue. The typical  $\delta^{25}\text{Mg}$ – $\delta^{26}\text{Mg}$  compositions of mafic and ultramafic rocks (according to Beinlich et al., 2014 and Bourdon et al., 2010) are indicated as a single field. The lines indicate the slopes for equilibrium and kinetic mass dependent fractionation (Young and Galy, 2004).....222

**Figure 5.7**  $\delta^{25}\text{Mg}$ – $\delta^{26}\text{Mg}$  diagram (3-isotope plot) showing the stable Mg isotopic composition of leachate and residue samples from acid leaching. Samples are differentiated depending on whether the sample is from leachate or the acid leached residue. The typical  $\delta^{25}\text{Mg}$ – $\delta^{26}\text{Mg}$  compositions of mafic and ultramafic rocks (according to Beinlich et al., 2014 and Bourdon et al., 2010) are indicated as a single field. The lines indicate the slopes for equilibrium and kinetic mass dependent fractionation (Young and Galy, 2004).....226

## Chapter 6

**Figure 6.1** Graph of the total Mg concentration in solution over time. Duplicate results are included for each time step.....263

**Figure 6.2** Graph of the evolving fraction Mg composition of the solution over time. Duplicate results are included for each time step.....264

**Figure 6.3** Comparison between normalised XRD patterns of **a**) the (0 0 3) peak and **b**) whole pattern for the pyroaurite before reaction and after 1, 10 and 60 days. XRD patterns are normalised to the intensity of the (0 0 3) peak ( $\sim 12^\circ 2\theta$ ) to allow for comparison between individual patterns.....266

**Figure 6.4** Graph of the % Mg exchange over time calculated using  $f^{25}\text{Mg}$ .....271

## S.I. 1

- Figure S1.** ICP-MS results for control experiment 1, showing change in concentration over time for experiments using pH 9.4 and pH 10.5 carbonate–bicarbonate buffers (experiments using pH 10, 10.3, 10.6 and 11.5 are not included as they were only collected at one time point). .....311
- Figure S2.** ICP-MS results for control experiment 1, showing negligible change in Mg concentration for a range of pH values (for pH 9.4 and pH 10.5 multiple data points are from various time points see Figure S1.).....311
- Figure S3.** ICP-MS results for control experiment 2, showing change in concentration for multiple pyroaurite masses, over a range of pH values.....313
- Figure S4.** % Mg results for control experiment 2, showing the amount of Mg which has entered solution for multiple pyroaurite masses, over a range of pH values.....313
- Figure S5.** Comparison of the % Mg exchange values calculated using  $f^{24}\text{Mg}$  and  $f^{26}\text{Mg}$  relative to using  $f^{25}\text{Mg}$ .....314
- Figure S6.** Geometry of Mg atoms (yellow) at the pyroaurite surface for the (0 0 1) and (1 0 0), (0 1 0) surfaces.....316
- Figure S7.** Crystallite size ( $LVol-IB$ ) over time for pyroaurite undergoing Mg exchange. Error bars represent the estimated standard deviation ( $2\sigma$ ) that was calculated using Topas V.5 (BrukerAXS).....319

## List of tables

### Chapter 3

- Table 3.1** Weighed composition of artificial tailings samples.....76
- Table 3.2** Sources of crystal-structure data for Rietveld refinement.....78
- Table 3.3** Refinement results for PONKCS method.....88
- Table 3.4** Refinement results for Pawley/internal standard method.....89
- Table 3.5** Refinement results for combined PONKCS-Pawley/internal standard method...90
- Table 3.6** Estimated carbon sequestration plus carbonation potential (from brucite only) of artificial tailings.....97

### Chapter 4

- Table 4.1** Sources of crystal-structure data for Rietveld refinement.....126
- Table 4.2** Sample descriptions and qualitative XRD results for Woodsreef tailings and waste rock.....134
- Table 4.3** Quantitative XRD results for Woodsreef tailings and waste rock.....136
- Table 4.4** Radiocarbon and stable carbon values for Woodsreef tailings samples.....144

<b>Table 4.5</b>	Stable carbon and oxygen isotope results for Woodsreef tailings samples.....	145
<b>Table 4.6</b>	Radiocarbon, stable carbon and total carbon for anion exchange experiments..	147
<b>Table 4.7</b>	Comparison of carbonate minerals and carbon sequestration estimate using XRD and elemental carbon data.....	156
<b>Table 4.8</b>	Comparison of atmospheric carbon sequestration rate estimates using XRD and total carbon (LECO) data.....	177
<b>Chapter 5</b>		
<b>Table 5.1</b>	Woodsreef chrysotile mine sample descriptions and Mg isotope results.....	218
<b>Table 5.2</b>	Mount Keith nickel mine sample descriptions and Mg isotope results.....	219
<b>Table 5.3</b>	Dundas mineral field sample descriptions and Mg isotope results.....	221
<b>Chapter 6</b>		
<b>Table 6.1</b>	Mg concentration and Mg fraction.....	262
<b>Table 6.2</b>	% Mg Exchange.....	263
<b>S.I. 1</b>		
<b>Table S1.</b>	Surface fraction calculations.....	317
<b>Table S2.</b>	Crystallite size and strain for pyroaurite over time.....	318

## List of Abbreviations

AFM	Atomic Force Microscopy
BSE	Back Scattered Electron
CCS	Carbon Capture and Storage
DIC	Dissolved Inorganic Carbonate
EDS	Energy Dispersive Spectroscopy
FEG	Field Emission Gun
IAEA	International Atomic Energy Agency
ICDD	International Centre for Diffraction Data
ICP-MS	Inductively Coupled Plasma Mass Spectrometry
IPCC	Intergovernmental Panel on Climate Change
IRMS	Isotope-Ratio Mass Spectrometry
LAS	Laser Absorption Spectrometry
LDH	Layered Double Hydroxide

MCEM	Monash Centre for Electron Microscopy
OA-ICOS	Off-Axis Integrated Cavity Output Spectrometer
RIR	Reference Intensity Ratio
SSAMS	Single Stage Accelerator Mass Spectrometer
SE	Secondary Electron
SEM	Scanning Electron Microscope
SIMS	Secondary Ion Mass Spectrometry
VPDB	Vienna Pee Dee Belemnite
VSMOW	Vienna Standard Mean Ocean Water
XRD	X-Ray Diffraction

## Abstract

Carbon mineralisation is one method that is being developed to manage the concentration of anthropogenic CO<sub>2</sub> in the atmosphere, and mitigate the potential impacts of climate change. Carbon mineralisation in ultramafic mine tailings has been suggested as a low-cost way to sequester atmospheric CO<sub>2</sub> and reduce the greenhouse gas emissions of mine sites. This process involves dissolution of Mg-hydroxide and silicate minerals, and precipitation of Mg-carbonate minerals. Much of the research on the carbonation of mine tailings has focussed on the formation of hydrated Mg-carbonate minerals such as hydromagnesite [Mg<sub>5</sub>(CO<sub>3</sub>)<sub>4</sub>(OH)<sub>2</sub>·4H<sub>2</sub>O]. Minerals from the hydrotalcite supergroup may also be a carbon sink at some ultramafic mine sites; however, their role in CO<sub>2</sub> sequestration is poorly understood. Hydrotalcites are layered double hydroxide (LDH) minerals that have the capacity to sequester atmospheric CO<sub>2</sub> via *in situ* formation within tailings by carbonation of Fe-rich brucite or via anion exchange, whereby they incorporate atmospheric CO<sub>2</sub> into their interlayer spaces. This thesis aims to better understand the carbon sequestration potential of hydrotalcites by assessing their formation at the Woodsreef chrysotile mine and improving our understanding of their stability in near surface environments such as tailings. Hydrotalcites can form during hydrothermal alteration of spinel minerals, or via low-temperature carbonation of Fe-rich brucite, a hydrotalcites origin will determine whether it is sequestering atmospheric CO<sub>2</sub>. At the Woodsreef chrysotile mine, the hydrotalcite minerals pyroaurite [Mg<sub>6</sub>Fe<sup>3+</sup><sub>2</sub>(CO<sub>3</sub>)(OH)<sub>16</sub>·4H<sub>2</sub>O] and coalingite [Mg<sub>10</sub>Fe<sup>3+</sup><sub>2</sub>(CO<sub>3</sub>)(OH)<sub>24</sub>·2H<sub>2</sub>O] are present in the tailings. Samples were taken from multiple depths across the tailings storage facility at Woodsreef to investigate the origins of hydrotalcites and to see how their abundance varied with depth into the tailings pile. Multiple quantitative X-ray diffraction (XRD) methods were trialled to accurately quantify the composition of the tailings. Quantitative XRD results using the Pawley/internal standard

method reveal that pyroaurite abundances are highest in the shallow tailings and that this mineral is forming at the expense of brucite to a depth of at least 120 cm. Radiocarbon analysis reveals that pyroaurite at Woodsreef contained significant abundances of modern atmospheric carbon, and SEM images show platy pyroaurite and coalingite crystals forming on dissolving brucite surfaces, supporting *in situ* formation of hydrotalcites within the tailings and implying that they are sequestering atmospheric CO<sub>2</sub>. Quantitative XRD and elemental C data were used to estimate the amount of CO<sub>2</sub> that has been sequestered Woodsreef, determining that 3,900–6,900 t of CO<sub>2</sub> have been sequestered since 1983.

Stable C and O isotopes were used to trace the origins of the hydrotalcites, however an anion exchange experiment revealed that the C and O isotopic composition of hydrotalcites varies over time through anion exchange. Stable Mg isotopes undergo significant fractionation during low-temperature processes and so may offer an alternative way to determine the origin of hydrotalcites that is more resistant to exchange than stable C and O isotopes. Hydrotalcite minerals, serpentine, hydromagnesite and brucite from three ultramafic mine sites were analysed for their Mg isotopic compositions. Weathered serpentine samples tended to be enriched in <sup>25</sup>Mg and <sup>26</sup>Mg, and hydrotalcite minerals had similar stable Mg isotope signatures regardless of origin, implying that post-formation processes were overprinting their original isotope compositions. To investigate this possibility an exchange experiment was undertaken using synthetic pyroaurite and a <sup>25</sup>Mg-enriched aqueous tracer over 90 days. ICP-MS results indicated that the stable Mg isotopic composition of the fluid changed over time, indicating that hydrotalcite minerals undergo both anion and cation exchange with the local environment at ambient conditions. Hydrotalcites have the capacity to sequester significant amounts of atmospheric CO<sub>2</sub> at ultramafic mine sites, however their ability to undergo anion and cation exchange with the local environment complicates attempts to trace the CO<sub>2</sub> sequestration processes using isotope geochemistry.



# **Chapter 1**

## **Introduction**

Connor C. Turvey<sup>1</sup>

<sup>1</sup>School of Earth, Atmosphere & Environment, Monash University, Clayton, Melbourne,  
Victoria 3800, Australia

## 1.1 Significance of the study

The increased input of anthropogenic carbon dioxide (CO<sub>2</sub>) and other greenhouse gases (such as CH<sub>4</sub> and N<sub>2</sub>O) into the atmosphere is resulting in potentially irreversible warming of the Earth's climate system, with a 1.5–2°C increase in global average surface temperature predicted before the end of the 21<sup>st</sup> century (Cleugh et al., 2011; Houghton et al., 2001; IPCC, 2005; IPCC, 2013; IPCC, 2014; Millar et al., 2017). This warming will have far reaching negative impacts including the increasing prevalence of extreme weather events, ocean acidification (owing to increased uptake of CO<sub>2</sub> into the oceans), thawing of permafrost, melting of the polar icecaps, sea level rise, creation of climate refugees and food insecurity (Biermann and Boas, 2010; IPCC, 2013; National Academies of Sciences and Medicine, 2016; Wheeler and Von Braun, 2013). In an effort to lessen these effects, various governing bodies have worked together to set national and international targets for limiting or eliminating greenhouse gas emissions, such as the Paris Agreement, which was ratified by 192 countries, although notably the United States withdrew from the agreement in 2017 (Ghezloun et al., 2017; Zhang et al., 2017). Under these agreements, solutions are being developed to reduce the input of CO<sub>2</sub> into the atmosphere, including regulatory measures such as carbon trading schemes, the creation of increasingly efficient and cost effective renewable energy sources, and the development of carbon sequestration technologies (Cleugh et al., 2011; Houghton et al., 2001; IPCC, 2005; IPCC, 2013; IPCC, 2014).

Carbon sequestration is unique amongst these methods because it can be used to actively lower current greenhouse gas emissions by capturing CO<sub>2</sub> from the air, as well as preventing emissions of CO<sub>2</sub> into the atmosphere (IPCC, 2005). Carbon mineralisation reactions represent one pathway for carbon sequestration whereby atmospheric or industrial waste CO<sub>2</sub> is trapped as solid carbonate minerals (Lackner, 2002; Lackner et al., 1995; Seifritz,

1990). Various carbon mineralisation strategies have been proposed including the use of *ex situ* carbonation reactors (e.g., Lackner, 2002; Lackner, 2003; Gerdemann et al., 2007), injection of CO<sub>2</sub> into mafic and ultramafic geological formations (e.g., Kelemen and Matter, 2008; Matter and Kelemen, 2009; Matter et al., 2016) and the carbonation of ultramafic mineral wastes generated by mining (tailings) (e.g., Wilson et al., 2006; Wilson et al. 2009a; Power et al. 2013). Carbon mineralisation, occurs naturally as part of weathering reactions. Chemical weathering of mafic and ultramafic rock releases divalent metal cations (typically Mg<sup>2+</sup> and Ca<sup>2+</sup>) into solution, where they react with CO<sub>3</sub><sup>2-</sup><sub>(aq)</sub> sourced from atmospheric CO<sub>2</sub>, to precipitate Ca- and Mg-carbonate minerals. Amongst the Mg-carbonate minerals, magnesite [MgCO<sub>3</sub>], hydromagnesite [Mg<sub>5</sub>(CO<sub>3</sub>)<sub>4</sub>(OH)<sub>2</sub>·4H<sub>2</sub>O], dypingite [Mg<sub>5</sub>(CO<sub>3</sub>)<sub>4</sub>(OH)<sub>2</sub>·~5H<sub>2</sub>O], nesquehonite (MgCO<sub>3</sub>·3H<sub>2</sub>O), and landsfordite (MgCO<sub>3</sub>·5H<sub>2</sub>O) are common products of carbon mineralisation (Beinlich and Austrheim, 2012; Hamilton et al., 2016; Morgan et al., 2015; Power et al., 2013b; Power et al., 2014), with environmental and geochemical conditions dictating which carbonate species will form (e.g., Davies and Bubela, 1973; Königsberger et al., 1999; Morgan et al., 2015). The carbonates that form during carbon sequestration contain atmospheric CO<sub>2</sub> in the form of CO<sub>3</sub><sup>2-</sup> within their crystal structures (Lackner et al., 1995; Oelkers et al., 2008; Power et al., 2013b). It has been estimated that by enhancing the natural rates of silicate weathering and carbonation reactions, it may be possible to sequester significant amounts of CO<sub>2</sub> (Kelemen and Matter, 2008; Lackner, 2002; Lackner et al., 1995; Oelkers et al., 2008; Power et al., 2013a; Seifritz, 1990), with Kelemen and Matter (2008) estimating that the Samail ophiolite in Oman sequesters ~10<sup>4</sup>–10<sup>5</sup> t of CO<sub>2</sub> per year and Power et al. (2013b) estimating that carbon sequestration could be used to offset the emissions of individual industrial operations (10<sup>5</sup> to 10<sup>6</sup> t of CO<sub>2</sub> per year).

The majority of previous carbon mineralisation research has focussed on the formation of magnesite and hydrated Mg-carbonates minerals, as they represent the most efficient carbon sinks, in terms of the amounts of water, reactant mineral and physical space (volume) required to sequester a given amount of CO<sub>2</sub> (Power et al., 2013b). This thesis aims to investigate the potential to sequester atmospheric CO<sub>2</sub> in hydrotalcite minerals. Hydrotalcites are layered double hydroxide (LDH) minerals, part of the hydrotalcite supergroup of minerals, they are capable of sequestering carbonate within their crystal structures, similar to hydrated Mg-carbonates, but they have been relatively underexplored in carbon mineralisation studies. Hydrotalcite minerals are present at significant abundances in many ultramafic rock formations, ultramafic-hosted ore deposits, and in the tailings storage facilities for ultramafic mine tailings. By understanding some of the fundamental processes by which they form, and exploring their carbon sequestration capacity in mine tailings, it may be possible to use hydrotalcites to sequester atmospheric CO<sub>2</sub> in certain ultramafic landscapes and mine sites.

## **1.2 Carbon mineralisation in ultramafic tailings**

It has been estimated that over geologic time, all anthropogenic CO<sub>2</sub> emissions will eventually be sequestered within carbonate minerals (Kump et al., 2000), and this represents a permanent method of CO<sub>2</sub> storage as carbonate minerals are stable at Earth's surface conditions (Lackner et al., 1995). However, the natural rate of silicate weathering and carbonate formation does not occur rapidly enough to meaningfully offset anthropogenic CO<sub>2</sub> emissions (e.g., Power et al., 2013b; Wilson et al., 2009a). For carbon mineralisation, the availability of CO<sub>2</sub> (Beinlich and Austrheim, 2012), dissolution rate of Mg- or Ca-bearing feedstock minerals (typically hydroxides and silicates) and subsequent release of metal cations tends to be the rate-limiting steps in these reactions, rather than the

precipitation of carbonate minerals from solution (Lackner et al., 1995; Oelkers et al., 2008). As such ultramafic minerals that are relatively unpolymerised [e.g., forsterite ( $\text{Mg}_2\text{SiO}_4$ )] or very fine-grained (e.g., serpentine group minerals) are typically used in carbonation reactions because they are relatively reactive and so will rapidly release Mg into solution to promote carbonation reactions (Lackner et al., 1995; Oelkers et al., 2008; Power et al., 2013b).

The tailings storage facilities of ultramafic-hosted mine sites are ideal locations to investigate enhanced weathering and carbonation reactions, and their potential to sequester atmospheric  $\text{CO}_2$  (e.g., Power et al., 2013b). Ultramafic mine tailings contain Mg-bearing silicate and hydroxide minerals that can act as feedstocks for carbonation, and the ore processing that occurs during mining decreases the grain size and increases the reactive surface area of the tailings (Assima et al., 2012; Wilson et al., 2009a; Wilson et al., 2014). This serves to drastically increase the rate of mineral dissolution within the tailings, allowing for faster release of  $\text{Mg}^{2+}$ , and precipitation of carbonate minerals, than observed in natural ultramafic environments. The advantages of using ultramafic tailings for carbonation over injection into ultramafic or mafic rock, or the use of *ex situ* carbonation reactors is that there is less infrastructure, energy and capital required to begin sequestering carbon. Studies of passive (unaccelerated) carbonation of ultramafic mine tailings indicates that at many storage facilities, mines are partially offsetting their own emissions, without the knowledge or intervention of the mine owners (Gras et al., 2017; Lechat et al., 2016; Oskierski et al., 2013; Pronost et al., 2012; Turvey et al., 2017; Wilson et al., 2009a; Wilson et al., 2014; Wilson et al., 2006; Wilson et al., 2009b). There is ongoing research into passive and accelerated carbonation of a variety of ultramafic mine tailings including those from kimberlites (Mervine et al., in review; Wilson et al., 2011; Wilson et al., 2009a), low-grade Ni deposits (Bea et al., 2012; Gras et al., 2017; Hitch et al., 2010; Wilson et al., 2014) and

chrysotile mines (Hamilton et al., 2016; Lechat et al., 2016; McCutcheon et al., 2015; McCutcheon et al., 2016; Oskierski et al., 2013; Pronost et al., 2012; Turvey et al., 2017; Wilson et al., 2009a).

The Woodsreef chrysotile mine is a derelict mine site located 80 km north of Tamworth in New South Wales, Australia (Merril et al., 1980). It was the largest tonnage chrysotile mine in Australia producing 550,000 tons of long fibre chrysotile, 24 Mt of tailings and 75 Mt of waste rock over the lifetime of the mine from 1972 to 1983 (Merril et al., 1980). Previous studies have investigated the surface of the tailings pile and found that it contains a mixture of hydrated Mg-carbonates, such as hydromagnesite, as well as the carbonate-bearing hydrotalcite mineral pyroaurite  $[\text{Mg}_6\text{Fe}^{3+}_2(\text{CO}_3)(\text{OH})_{16}\cdot 4\text{H}_2\text{O}]$  (Oskierski et al., 2013; Turvey et al., 2017). Hydromagnesite is known to be forming *in situ* within the tailings and is sequestering atmospheric  $\text{CO}_2$  (Oskierski et al., 2013; Turvey et al., 2017). The relatively high abundances of pyroaurite at Woodsreef suggest that it may represent an important sink for  $\text{CO}_2$  at Woodsreef; however, it remains to be confirmed that the pyroaurite is forming due to interactions with the atmosphere and sequestering atmospheric  $\text{CO}_2$  (Oskierski et al., 2013; Turvey et al., 2017).

### 1.3 Hydrotalcite minerals

Hydrotalcites are LDH minerals, with the general formula  $[\text{M}^{2+}_{1-x}\text{M}^{3+}_x(\text{OH})_2]^{x+}\text{A}^{n-}_{x/n}\cdot m\text{H}_2\text{O}$ . They consist of brucite-like hydroxide layers containing divalent and trivalent cations as well as interlayer galleries that contain weakly bound  $\text{H}_2\text{O}$  molecules and anions, such as  $\text{SO}_4^{2-}$ ,  $\text{NO}_3^-$  and  $\text{CO}_3^{2-}$  (Mills et al., 2012). Hydrotalcites are commonly formed by two different mechanisms: (1) high temperature hydrothermal alteration of spinel minerals (e.g., Ashwal and Cairncross, 1997; Grguric, 2003; Grguric et al. 2001; Melchiorre et al., 2016; Melchiorre et al., 2018) and (2) low temperature carbonation of Fe-brucite at the Earth's

surface (e.g., Hostetler et al., 1966; Mumpton et al., 1965; Mumpton and Thompson, 1966). Hydrotalcites have the capacity to sequester atmospheric CO<sub>2</sub> if they precipitate at the Earth's surface and contain atmospheric derived CO<sub>3</sub><sup>2-</sup> (Oskierski et al., 2013), similar to hydrated Mg-carbonate minerals.

Hydrotalcite minerals of metamorphic origin could also potentially sequester atmospheric CO<sub>2</sub>, via anion exchange with the local environment (Mills et al., 2011; Woodhouse, 2006). Anion exchange reactions occur when anions held between the hydroxide layers of a hydrotalcite mineral are replaced by another anion that is present in solution at a high concentration (Bish, 1980; Bish and Brindley, 1977; Hudson and Bussell, 1981; Miyata, 1983). At mine sites with atmosphere derived carbonate-rich fluids, non-carbonate bearing hydrotalcites could undergo anion exchange and incorporate carbonate anions. The tailings from many operational and derelict ultramafic-hosted mine sites contain Fe-brucite and hydrotalcite minerals in significant abundances in their tailings storage facilities (e.g., Oskierski et al., 2013; Turvey et al., 2017; Wilson et al., 2014; Wilson et al., 2009b). With their ability to sequester atmospheric CO<sub>2</sub> during both formation at low temperature and via anion exchange, hydrotalcites may already be playing an important part in carbon sequestration efforts at these mine sites.

#### **1.4 Aims and objectives of the thesis**

There is relatively little existing research concerning the application of hydrotalcites to carbon sequestration. Oskierski et al. (2013) and Turvey et al. (2017) both note the presence of pyroaurite in the tailings at Woodsreef, however they did not definitively determine that the pyroaurite is sequestering atmospheric CO<sub>2</sub>. Gras et al. (2017) found that hydrotalcite minerals formed in experimental carbon mineralisation plots at the Dumont nickel project

and were sequestering CO<sub>2</sub>, similarly McCutcheon et al. (2017) found that pyroaurite formed during a microbially mediated carbonation trial at the Woodsreef chrysotile mine.

This thesis aims to improve our understanding of the occurrence, formation, stability and carbon sequestration capacity of hydrotalcite minerals. It focuses primarily on the Woodsreef chrysotile mine where pyroaurite and coalingite [Mg<sub>10</sub>Fe<sup>3+</sup><sub>2</sub>(CO<sub>3</sub>)(OH)<sub>24</sub>·2H<sub>2</sub>O] are found in the tailings material and may play a role in the carbon sequestration capacity of the site (Glen and Butt, 1981; Oskierski et al., 2013; Turvey et al., 2017). The thesis is split between: (1) the laboratory experiments and method development needed to understand the processes that have formed pyroaurite and coalingite at Woodsreef and (2) using and applying the techniques and knowledge gained in laboratory experiments to understand the geochemical processes occurring at Woodsreef and determine what role hydrotalcites play in carbon sequestration.

Quantitative powder X-ray diffraction (XRD) analysis has previously been used to assess the rate of carbonation in mine sites, as it provides a way to separately quantify CO<sub>2</sub> sequestered in carbonates of atmospheric and metamorphic origins (Oskierski et al., 2013; Turvey et al., 2017; Wilson et al., 2006; Wilson et al., 2009b). However the presence of serpentine minerals within the tailings at Woodsreef makes use of standard Rietveld refinements (Bish and Howard, 1988; Hill and Howard, 1987; Rietveld, 1969) problematic, this can be overcome by the use of modified Rietveld refinement methods as seen in Wilson et al., (2006) and Turvey et al., (2017). Before analysing the mineralogy of the tailings at Woodsreef the following must be determined:

1. What is the most accurate XRD method to quantify mineral abundances in ultramafic mine tailings that contain serpentine minerals? (**Chapter 3**)

2. How does quantitative XRD compare to other methods that have been used to quantify CO<sub>2</sub> sequestration rates? (**Chapter 3**)

Because hydrotalcites may be present in ultramafic mine tailings as either gangue minerals (i.e., that were originally part of the ore) or as alteration minerals that form by the carbonation of Fe-rich brucite, this will impact whether or not hydrotalcites at any given mine site are sequestering a net amount of atmospheric CO<sub>2</sub>:

3. To what extent are pyroaurite and coalingite forming *in situ* within the tailings pile at Woodsreef? (**Chapter 4**)

4. Are the hydrotalcites at Woodsreef a net sink for atmospheric CO<sub>2</sub>? (**Chapter 4**)

5. What are the stable C and O isotopic signatures of hydrotalcites that are sequestering atmospheric CO<sub>2</sub>, compared to gangue hydrotalcites? (**Chapter 4**)

6. How much CO<sub>2</sub> are hydrotalcites trapping compared to other carbonate-bearing minerals at the site? (**Chapter 4**)

Using stable C and O isotope data to trace the origin of carbonate anions in hydrotalcites is complicated because no stable C or O isotope fraction factors have been published for hydrotalcite minerals and because the ability of hydrotalcites to undergo anion exchange may continuously reset their stable C isotope compositions. Stable Mg isotopes offer a potential avenue for investigating carbon mineralisation reactions and determining the origin of hydrotalcites but have not previously been used for this purpose. As such, a fundamental understanding of the stable Mg isotope compositions of hydrotalcites is needed:

7. How do Mg-isotope compositions of serpentine, carbonate and hydrotalcite minerals change as carbon mineralisation occurs in ultramafic tailings? (**Chapter 5**)

8. Can stable Mg-isotopes be used to differentiate between hydrotalcites that have hydrothermal and sedimentary origins? (**Chapter 5**)

To correctly interpret the stable Mg isotope compositions of hydrotalcites it is important to determine whether stable Mg isotopes in hydrotalcites are able to undergo exchange with local environment, as this is the case for stable C and O isotopes in hydrotalcites, and which occurs for Mg in some Mg-carbonates (Oelkers et al., 2018).

9. Do hydrotalcites undergo stable Mg isotope exchange with the local environment? (**Chapter 6**)

Answering these questions will give insight into the carbon sequestration potential of hydrotalcites, by investigating the extent to which they form in the tailings of ultramafic mine sites and determining if quantitative XRD and stable C, O and Mg isotopes can be used to identify hydrotalcites that form *in situ* within tailings material via carbon mineralisation and are sequestering atmospheric CO<sub>2</sub>.

### **1.5 Organisation and outcomes of the thesis**

This thesis consists of seven chapters. **Chapter 2** provides a summary of the background literature regarding carbon mineralisation of alkaline wastes, including ultramafic mine tailings, descriptions of field sites used in the thesis and the current understanding regarding the structure, formation and uses of hydrotalcites. **Chapters 3-6** are written as research papers intended for submission to international journals, as such each is a standalone manuscript and so there may be repetition of introductory material in each of these chapters.

**Chapter 3** is under review in *American Mineralogist* and details the methods development needed to quantify the mineralogical composition of the tailings at Woodsreef. Quantifying the abundance of hydrotalcites in the tailings at Woodsreef is vitally important to

determining the impact they have upon the carbon sequestration capacity of the site. However, the presence of serpentine minerals at Woodsreef makes traditional quantitative XRD techniques inappropriate for analysing these, and other, ultramafic tailings. To overcome this, three structureless pattern fitting techniques for use with the Rietveld method (Bish and Howard, 1988; Hill and Howard, 1987; Rietveld, 1969) and XRD data are trialled on artificial tailings samples that were made to mimic the composition of the tailings at Woodsreef. Absolute and relative errors for the different methods are compared to determine the most accurate and appropriate XRD method, which was then used to analyse the tailings at Woodsreef in **Chapter 4**. Furthermore, the utility of XRD to quantify carbon sequestration is assessed and compared to the known elemental carbon content of the artificial tailings samples. The results indicate that XRD typically gives a conservative estimate of the amount of CO<sub>2</sub> sequestered in mine tailings.

**Chapter 4** is in preparation for submission to the *International Journal of Greenhouse Gas Control*. It aims to provide a more complete picture of the formation mechanisms for hydrotalcite minerals at Woodsreef and to understand their role in carbon sequestration. The quantitative XRD methods developed in **Chapter 3** are used to quantify the mineralogical changes that occur in the tailings pile at Woodsreef. Scanning electron microscopy (SEM) is used to provide textural evidence for the formation of pyroaurite and coalingite from gangue brucite that is present in the tailings. Radiocarbon and stable C and O isotope data are used to investigate the origin of the carbon within hydrated Mg-carbonates and hydrotalcites at the site. The information gained from XRD, SEM, stable C and O isotopes and radiocarbon data are combined and collectively used to determine that pyroaurite and coalingite are sequestering atmospheric CO<sub>2</sub> at Woodsreef. Quantitative XRD data and elemental carbon data are used to estimate the amount of CO<sub>2</sub> that has been sequestered at

Woodsreef and to determine how much of the atmospheric carbon sequestered at Woodsreef is bound within hydrotalcite minerals.

**Chapter 5** is in preparation for submission to *Geochimica et Cosmochimica Acta*. This study compares the stable Mg isotope signatures of minerals from the mine wastes of several different ultramafic mine sites, including the Woodsreef chrysotile mine, the Mount Keith nickel mine (Western Australia) and a number of small workings from the Dundas mineral field (Tasmania). Stable Mg isotopes can be used to trace surface processes involved in dissolution and precipitation of minerals, but it is unknown how carbon mineralisation reactions affect the stable Mg isotopic composition of ultramafic tailings. Additionally, when considering the carbon mineralisation potential of mine sites that contain hydrotalcites, it is important to understand the difference between carbonate-bearing hydrotalcite that have formed at high temperature and those that have formed *in situ* within the tailings pile, because only the latter will be sequestering a net amount of atmospheric CO<sub>2</sub>. Stable Mg isotopes are indifferent to fractionation at high temperature but will fractionate readily during low temperature surface processes such as soil formation or carbonate precipitation (Opfergelt et al., 2012; Shirokova et al., 2013). This makes it likely that high temperature and low temperature hydrotalcites will have distinct stable Mg isotope signatures that could be resistant to anion exchange reactions and so could be used to differentiate between the two hydrotalcite formation pathways. Samples of serpentine minerals, hydromagnesite, brucite and the hydrotalcite minerals pyroaurite, stichtite [Mg<sub>6</sub>Cr<sup>3+</sup><sub>2</sub>(CO<sub>3</sub>)(OH)<sub>16</sub>·4H<sub>2</sub>O], woodallite [Mg<sub>6</sub>Cr<sup>3+</sup><sub>2</sub>(Cl<sub>2</sub>)(OH)<sub>16</sub>·4H<sub>2</sub>O] and iowaite [Mg<sub>6</sub>Fe<sup>3+</sup><sub>2</sub>(Cl<sub>2</sub>)(OH)<sub>16</sub>·4H<sub>2</sub>O], from three study sites were collected and their stable Mg compositions were analysed and compared. This was done to determine whether there are differences in stable Mg isotope compositions of hydrotalcites that were formed at high temperature processes (Mount Keith and Dundas) and those that formed *in situ* within the tailings (Woodsreef). The goal of this

study was to investigate the changes that occur in the stable Mg isotope composition of minerals at a site that undergoes carbon mineralisation and to determine whether stable Mg isotopes can be used to infer the origin of hydrotalcites at those sites and other ultramafic tailings storage facilities. The results of the study found that serpentine minerals appear to become enriched in heavy Mg isotopes due to the preferential loss of  $^{24}\text{Mg}$  during carbon mineralisation, and that the stable Mg isotope compositions of hydrotalcites were largely homogeneous, regardless of their origin.

**Chapter 6** is in preparation for submission to *Environmental Science & Technology*. The aim of this chapter is to expand upon the results in **Chapter 5** by detailing a Mg exchange experiment. The results of **Chapter 5** suggest that hydrotalcites may undergo stable Mg isotope exchange with fluids in the local environment, similar to how they undergo anion exchange at ambient conditions. It is possible that such an effect could lead to constant re-equilibration of their stable Mg isotope composition. Thus, an exchange experiment between synthetic pyroaurite and a solution containing an aqueous  $^{25}\text{Mg}$  tracer was conducted over a period of 90 days. The composition of the fluid phase was analysed by ICP-MS to observe whether any magnesium exchange was occurring, and Rietveld refinements were used to trace changes to crystallite size over time. Results found that exchange occurs between the Mg held at the surface of the pyroaurite and the  $\text{Mg}^{2+}$  in solution.

**Chapter 7** summarises the most important findings of the thesis and describes how these findings will affect the current understanding of hydrotalcite formation and carbon sequestration in ultramafic tailings storage facilities. Current limitations and suggestions for future research are also discussed.

## 1.6 References

- Ashwal, L.D., and Cairncross, B. (1997) Mineralogy and origin of stichtite in chromite-bearing serpentinites. *Contributions to Mineralogy and Petrology*, 127(1-2), 75-86.
- Assima, G.P., Larachi, F., Beaudoin, G., and Molson, J. (2012) CO<sub>2</sub> Sequestration in Chrysotile Mining Residues—Implication of Watering and Passivation under Environmental Conditions. *Industrial & Engineering Chemistry Research*, 51(26), 8726-8734.
- Bea, S.A., Wilson, S.A., Mayer, K.U., Dipple, G.M., Power, I.M., and Gamazo, P. (2012) Reactive transport modeling of natural carbon sequestration in ultramafic mine tailings. *Vadose Zone Journal*, 11(2).
- Beinlich, A., and Austrheim, H. (2012) In situ sequestration of atmospheric CO<sub>2</sub> at low temperature and surface cracking of serpentinized peridotite in mine shafts. *Chemical Geology*, 332–333, 32-44.
- Biermann, F., and Boas, I. (2010) Preparing for a Warmer World: Towards a Global Governance System to Protect Climate Refugees. *Global Environmental Politics*, 10(1), 60-88.
- Bish, D.L. (1980) Anion-exchange in takovite: applications to other hydroxyl carbonate minerals. *Bulletin Mineralogie*, 103, 170-175.
- Bish, D.L., and Brindley, G.W. (1977) A reinvestigation of takovite, a nickel aluminium hydroxy-carbonate of the pyroaurite group. *American Mineralogist*, 62, 458-464.
- Bish, D.L., and Howard, S.A. (1988) Quantitative phase analysis using the Rietveld method. *Journal of Applied Crystallography*, 21(2), 86-91.

- Cleugh, H., Smith, M.S., Battaglia, M., and Graham, P. (2011) *Climate Change Science and Solutions for Australia*. CSIRO Publishing, 150 Oxford Street Collingwood VIC Australia.
- Davies, P.J., and Bubela, B. (1973) The transformation of nesquehonite into hydromagnesite. *Chemical Geology*, 12(4), 289-300.
- Gerdemann, S.J., O'Connor, W.K., Dahlin, D.C., Penner, L.R., and Rush, H. (2007) Ex Situ Aqueous Mineral Carbonation. *Environmental Science & Technology*, 41(7), 2587-2593.
- Ghezloun, A., Saidane, A., and Merabet, H. (2017) The COP 22 New commitments in support of the Paris Agreement. *Energy Procedia*, 119, 10-16.
- Glen, R.A., and Butt, B.C. (1981) Chrysotile asbestos at Woodsreef, New South Wales. *Economic Geology and the Bulletin of the Society of Economic Geologists*, 76(5), 1153-1169.
- Gras, A., Beaudoin, G., Molson, J., Plante, B., Bussière, B., Lemieux, J.M., and Dupont, P.P. (2017) Isotopic evidence of passive mineral carbonation in mine wastes from the Dumont Nickel Project (Abitibi, Quebec). *International Journal of Greenhouse Gas Control*, 60, 10-23.
- Grguric, B.A. (2003) Minerals of the MKD5 nickel deposit, Mount Keith, Western Australia. *Australian Journal of Mineralogy*, 9(2), 55-71.
- Grguric, B.A., Madsen, I.C., and Pring, A. (2001) Woodallite, a new strontium analogue of iowaite from the Mount Keith nickel deposit, Western Australia. *Mineralogical Magazine*, 65(3), 427-435.
- Hamilton, J.L., Wilson, S.A., Morgan, B., Turvey, C.C., Paterson, D.J., MacRae, C., McCutcheon, J., and Southam, G. (2016) Nesquehonite sequesters transition metals

and CO<sub>2</sub> during accelerated carbon mineralisation. *International Journal of Greenhouse Gas Control*, 55, 73-81.

Hill, R.J., and Howard, C.J. (1987) Quantitative phase analysis from neutron powder diffraction data using the Rietveld method. *Journal of Applied Crystallography*, 20(6), 467-474.

Hitch, M., Ballantyne, S.M., and Hindle, S.R. (2010) Revaluing mine waste rock for carbon capture and storage. *International Journal of Mining, Reclamation and Environment*, 24(1), 64-79.

Hostetler, P.B., Coleman, R.G., A., M.F., and Evans, B.W. (1966) Brucite in Alpine Serpentinities. *The American Mineralogist*, 51, 75-98.

Houghton, J.T., Ding, Y., Griggs, D.J., Noguer, M., van der Linden, P.J., Dai, X., Maskell, K., and Johnson, C.A. (2001) *Climate Change 2001: The Scientific Basis: Contribution of Working Group 1 to the Third Assessment Report of the Intergovernmental Panel on Climate Change*. Cambridge University Press, U.K.

Hudson, D.R., and Bussell, M. (1981) Mountkeithite, a new pyroaurite-related mineral with an expanded interlayer containing exchangeable MgSO<sub>4</sub>. *Mineralogical Magazine*, 44, 345-350.

IPCC. (2005) *IPCC Special Report on Carbon Dioxide Capture and Storage*. In O.D. Bert Metz, Heleen de Coninck, Manuela Loos, Leo Meyer, Ed, p. 442. Cambridge University Press, 40 West 20th Street, New York, NY 10011-4211, USA.

IPCC. (2013) *Climate Change 2013: The Physical Science Basis*. In IPCC, Ed. IPCC Working Group 1.

IPCC. (2014) *Climate Change 2014 Mitigation of Climate Change*. In IPCC, Ed. IPCC Working Group 3.

- Kelemen, P.B., and Matter, J. (2008) In situ carbonation of peridotite for CO<sub>2</sub> storage. *Proceedings of the National Academy of Sciences*, 105(45), 17295-17300.
- Kump, L.R., Brantley, S.L., and Arthur, M.A. (2000) Chemical Weathering, atmospheric CO<sub>2</sub> and climate. *Annual Review of Earth and Planetary Sciences*, 28, 611-67.
- Lackner, K.S. (2002) Carbonate Chemistry for Sequestering Fossil Carbon. *Annual Review of Energy and the Environment*, 27(1), 193-232.
- Lackner, K.S. (2003) A Guide to CO<sub>2</sub> Sequestration. *Science*, 300, 1677-1678.
- Lackner, K.S., Wendt, C.H., Butt, D.P., Joyce Jr, E.L., and Sharp, D.H. (1995) Carbon dioxide disposal in carbonate minerals. *Energy*, 20(11), 1153-1170.
- Lechat, K., Lemieux, J.M., Molson, J.W., Beaudoin, G., and Hebert, R. (2016) Field evidence of CO<sub>2</sub> sequestration by mineral carbonation in ultramafic milling wastes, Thetford Mines, Canada. *International Journal of Greenhouse Gas Control*, 47, 110-121.
- Matter, J.M., and Kelemen, P.B. (2009) Permanent storage of carbon dioxide in geological reservoirs by mineral carbonation. *Nature Geoscience*, 2(12), 837-841.
- Matter, J.M., Stute, M., Snæbjörnsdóttir, S.Ó., Oelkers, E.H., Gislason, S.R., Aradóttir, E.S., Sigfusson, B., Gunnarsson, I., Sigurdardóttir, H., Gunnlaugsson, E., Axelsson, G., Alfredsson, H.A., Wolff-Boenisch, D., Mesfin, K., Taya, D.F.d.l.R., Hall, J., Dideriksen, K., and Broecker, W.S. (2016) Rapid carbon mineralization for permanent disposal of anthropogenic carbon dioxide emissions. *Science*, 352(6291), 1312-1314.
- McCutcheon, J., Dipple, G.M., Wilson, S.A., and Southam, G. (2015) Production of magnesium-rich solutions by acid leaching of chrysotile: A precursor to field-scale deployment of microbially enabled carbonate mineral precipitation. *Chemical Geology*, 413, 119-131.

- McCutcheon, J., Turvey, C.C., Hamilton, J.L., Wilson, S.A., and Southam, G. (2017) Experimental Deployment of Microbial Mineral Carbonation at an Asbestos Mine: Potential Applications to Carbon Storage and Tailings Stabilization. *Minerals*, 7(191).
- McCutcheon, J., Wilson, S.A., and Southam, G. (2016) Microbially accelerated carbonate mineral precipitation as a strategy for in situ carbon sequestration and rehabilitation of asbestos mine sites. *Environmental Science & Technology*, 50(3), 1419-1427.
- Melchiorre, E.B., Bottrill, R., Huss, G.R., and Lopez, A. (2016) Conditions of Stichtite ( $\text{Mg}_6\text{Cr}_2(\text{OH})_{16}[\text{CO}_3] \cdot 4\text{H}_2\text{O}$ ) formation and its Geochemical and Isotope Record of Early Phanerozoic Serpentinizing Environments. *Geochimica et Cosmochimica Acta*.
- Melchiorre, E.B., Bottrill, R., Huss, G.R., and Lopez, A. (2018) The Early Earth Geochemical and Isotope Record of Serpentinizing Environments from Archean Stichtite ( $\text{Mg}_6\text{Cr}_2(\text{OH})_{16}[\text{CO}_3] \cdot 4\text{H}_2\text{O}$ ). *Precambrian Research*.
- Merril, R.J., Butt, B.C., Forrest, V.C., Purdon, G., and Bramley-Moore, R.A. (1980) Asbestos Production at Chrysotile Corporation of Australia Pty. Limited, Barraba, N.S.W. In J.T. Woodcock, Ed. *Mining and Metallurgical Practices in Australasia*, 10, p. 669-673. The Australasian Institute of Mining and Metallurgy, Clunies Ross House, 191 Royal Parade, Parkville, Victoria, Australia 3052.
- Mervine, E., Wilson, S.A., Power, I.M., Dipple, G.M., Turvey, C.C., Hamilton, J.L., Vanderzee, S., Raudsepp, M., Southam, C., Matter, J.M., Kelemen, P.B., Stiefenhofer, J., Miya, Z., and Southam, G. (in review) Carbon Storage Potential of Kimberlite Mine Tailings. *Mineralogy and Petrology*.
- Millar, R.J., Fuglestedt, J.S., Friedlingstein, P., Rogelj, J., Grubb, M.J., Matthews, H.D., Skeie, R.B., Forster, P.M., Frame, D.J., and Allen, M.J. (2017) Emission budgets and

- pathways consistent with limiting warming to 1.5°C. *Nature Geoscience*, 10, 741-748.
- Mills, S.J., Christy, A.G., Génin, J.M.R., Kameda, T., and Colombo, F. (2012) Nomenclature of the hydrotalcite supergroup: natural layered double hydroxides. *Mineralogical Magazine*, 76(5), 1289-1336.
- Mills, S.J., Whitfield, P.S., Wilson, S.A., Woodhouse, J.N., Dipple, G.M., Raudsepp, M., and Francis, C.A. (2011) The crystal structure of stichtite, re-examination of barbertonite, and the nature of polytypism in MgCr hydrotalcites. *American Mineralogist*, 96(1), 179-187.
- Miyata, S. (1983) Anion-exchange properties of hydrotalcite-like compounds. *Clays and Clay Minerals*, 31(4), 305-311.
- Morgan, B., Wilson, S.A., Madsen, I.C., Gozukara, Y.M., and Habsuda, J. (2015) Increased thermal stability of nesquehonite ( $\text{MgCO}_3 \cdot n\text{H}_2\text{O}$ ) in the presence of humidity and  $\text{CO}_2$ : Implications for low temperature  $\text{CO}_2$  storage. *International Journal of Greenhouse Gas Control*, 39, 366-376.
- Mumpton, F.A., and Thompson, C.S. (1966) The Stability of Brucite in the Weathering Zone of the New Idria Serpentinite. *Clays and Clay Minerals*, 14(1), 249-257.
- National Academies of Sciences, E., and Medicine. (2016) Attribution of Extreme Weather Events in the Context of Climate Change. 186 p. The National Academies Press, Washington, DC.
- Oelkers, E.H., Berninger, U.-N., Pérez-Fernández, A., Chmeleff, J., and Mavromatis, V. (2018) The temporal evolution of magnesium isotope fractionation during hydromagnesite dissolution, precipitation, and at equilibrium. *Geochimica et Cosmochimica Acta*, 226, 36-49.

- Oelkers, E.H., Gislason, S.R., and Matter, J. (2008) Mineral Carbonation of CO<sub>2</sub>. *Elements*, 4, 333-337.
- Opfergelt, S., Georg, R.B., Delvaux, B., Cabidoche, Y.M., Burton, K.W., and Halliday, A.N. (2012) Mechanisms of magnesium isotope fractionation in volcanic soil weathering sequences, Guadeloupe. *Earth and Planetary Science Letters*, 341(Supplement C), 176-185.
- Oskierski, H.C., Dlugogorski, B.Z., and Jacobsen, G. (2013) Sequestration of atmospheric CO<sub>2</sub> in chrysotile mine tailings of the Woodsreef Asbestos Mine, Australia: Quantitative Mineralogy, isotopic fingerprinting and carbonation rates. *Chemical Geology*.
- Power, I.M., Harrison, A.L., Dipple, G.M., Wilson, S.A., Kelemen, P.B., Hitch, M., and Southam, G. (2013a) Carbon Mineralization: From Natural Analogues to Engineered Systems. *Reviews in Mineralogy & Geochemistry*, 77, 305-360.
- Power, I.M., Wilson, S.A., and Dipple, G.M. (2013b) Serpentinite Carbonation for CO<sub>2</sub> Sequestration. *Elements*, 9, 115-121.
- Power, I.M., Wilson, S.A., Harrison, A.L., Dipple, G.M., McCutcheon, J., Southam, G., and Kenward, P.A. (2014) A depositional model for hydromagnesite–magnesite playas near Atlin, British Columbia, Canada. *Sedimentology*, 61(6), 1701-1733.
- Pronost, J., Beaudoin, G., Lemieux, J.M., Hebert, R., Constantin, M., Marcouiller, S., Klein, M., Duchesne, J., Molson, J.W., Larachi, F., and Maldague, X. (2012) CO<sub>2</sub>-depleted warm air venting from chrysotile milling waste (Thetford Mines, Canada): Evidence for in-situ carbon capture from the atmosphere. *Geology*, 40(3), 275-278.
- Rietveld, H. (1969) A profile refinement method for nuclear and magnetic structures. *Journal of Applied Crystallography*, 2(2), 65-71.
- Seifritz, W. (1990) CO<sub>2</sub> disposal by means of silicates *Nature*, 345.

- Shirokova, L.S., Mavromatis, V., Bundeleva, I., Pokrovsky, O.S., Benezeth, P., Gerard, E., Pearce, C., and Oelkers, E.H. (2013) Using Mg isotopes to Trace Cyanobacterially Mediated Magnesium Carbonate Precipitation in Alkaline lakes. *Aquatic Geochemistry*, 19, 1-24.
- Turvey, C.C., Wilson, S.A., Hamilton, J.L., and Southam, G. (2017) Field-based accounting of CO<sub>2</sub> sequestration in ultramafic mine wastes using portable X-ray diffraction. *American Mineralogist*.
- Wheeler, T., and von Braun, J. (2013) Climate Change Impacts on Global Food Security. *Science*, 341(6145), 508-513.
- Wilson, S.A., Dipple, G.M., Power, I.M., Barker, S.L.L., Fallon, S.J., and Southam, G. (2011) Subarctic Weathering of Mineral Wastes Provides a Sink for Atmospheric CO<sub>2</sub>. *Environmental Science & Technology*, 45(18), 7727-7736.
- Wilson, S.A., Dipple, G.M., Power, I.M., Thom, J.M., Anderson, R.G., Raudsepp, M., Gabites, J.E., and Southam, G. (2009a) Carbon Dioxide Fixation within Mine Wastes of Ultramafic-Hosted Ore Deposits: Examples from the Clinton Creek and Cassiar Chrysotile Deposits, Canada. *Economic geology*, 104, 95–112.
- Wilson, S.A., Harrison, A.L., Dipple, G.M., Power, I.M., Barker, S.L.L., Mayer, K.U., Fallon, S.J., Raudsepp, M., and Southam, G. (2014) Offsetting of CO<sub>2</sub> emissions by air capture in mine tailings at the Mount Keith Nickel mine, Western Australia: Rates, controls and prospects for carbon neutral mining. *International Journal of Greenhouse Gas Control*, 25, 121-140.
- Wilson, S.A., Raudsepp, M., and Dipple, G.M. (2006) Verifying and quantifying carbon fixation in minerals from serpentine-rich mine tailings using the Rietveld method with X-ray powder diffraction data. *American Mineralogist*, 91(8-9), 1331-1341.

- Wilson, S.A., Raudsepp, M., and Dipple, G.M. (2009b) Quantifying carbon fixation in trace minerals from processed kimberlite; a comparative study of quantitative methods using X-ray powder diffraction data with applications to the Diavik diamond mine, Northwest Territories, Canada. *Applied Geochemistry*, 24(12), 2312-2331.
- Woodhouse, J. (2006) The characterization of hydrotalcite-group minerals and their anion exchange capabilities at mount keith nickel mine, Western Australia. Unpublished masters thesis.
- Zhang, Y.-X., Chao, Q.-C., Zheng, Q.-H., and Huang, L. (2017) The withdrawal of the U.S. from the Paris Agreement and its impact on global climate change governance. *Advances in Climate Change Research*, 8(4), 213-219.

## **Chapter 2**

### **Carbon mineralisation and hydrotalcites: background and current knowledge**

Connor C. Turvey<sup>1</sup>

<sup>1</sup>School of Earth, Atmosphere & Environment, Monash University, Clayton, Melbourne,  
Victoria 3800, Australia

## 2.1 Introduction

The continued emission of carbon dioxide (CO<sub>2</sub>) and other greenhouse gases into the atmosphere is leading to unprecedented changes to the Earth's climate, with continued heating of the oceans, melting of the polar ice sheets and an anticipated increase in global average surface temperature of 1.5–2°C before the end of the 21<sup>st</sup> century (Cleugh et al., 2011; Houghton et al., 2001; IPCC, 2005; IPCC, 2013; IPCC, 2014; Millar et al., 2017). The threat posed by anthropogenic climate change is driving research into a wide variety of mitigation and prevention strategies (IPCC, 2005; IPCC, 2014). In addition to the continued development of renewable energy, and policy-based initiatives that aim to reduce the amount of greenhouse gases produced (Pacala and Socolow, 2004; Ghezloun et al., 2017), carbon sequestration technologies are being tested (Hamilton et al., in prep-b; McCutcheon et al., 2017) and trialled (Matter et al., 2011; Matter et al., 2016; Pevzner et al., 2011; Shulakova et al., 2015). Carbon sequestration technologies aim to prevent greenhouse gases from entering the atmosphere by removing them from waste gas streams or by removing greenhouse gases, chiefly CO<sub>2</sub>, directly from the atmosphere (Cleugh et al., 2011; IPCC, 2014; Matter and Kelemen, 2009; Van der Zwaan and Smekens, 2009). Carbon sequestration represents an important bridging technology that is necessary to help the world to successfully transition to a more sustainable and carbon neutral way of life by reducing the emissions of polluting technologies that are still in place, until they can be replaced by more carbon neutral alternatives, limiting emissions of greenhouse gases and warming of the climate (IPCC, 2005; IPCC, 2014; Millar et al., 2017).

Most carbon sequestration technologies capture and store CO<sub>2</sub> that is being emitted at a point source of greenhouse gas emissions, such a fossil fuel burning power plant or industrial plant

(Rubin et al., 2007; Stewart and Hessami, 2005; Yang et al., 2008). Once captured the CO<sub>2</sub> can then be stored within a geological reservoir such as depleted oil and gas fields, or injected into mafic or ultramafic rock units to react and form solid carbonate minerals (Lackner, 2002; Oelkers et al., 2008; Power et al., 2013; Yang et al., 2008). Trapping the CO<sub>2</sub> as solid carbonate minerals is referred to carbon mineralisation (or mineral carbonation) and it is considered to be the most secure long-term sink for carbon as many carbonate minerals are stable over geological timescales (Lackner, 2002; Lackner, 2003; Lackner et al., 1995; Seifritz, 1990). Carbonate minerals offer more secure CO<sub>2</sub> storage (Matter et al., 2016; Oelkers et al., 2008; Power et al., 2013; Snæbjörnsdóttir et al., 2014) that limits opportunities for (1) leakage into the atmosphere, a risk associated with stratigraphic trapping of CO<sub>2</sub> in sedimentary reservoirs (Haugan, 2004; IPCC, 2005; Zoback and Gorelick, 2012), and (2) adverse effects on ocean geochemistry and biodiversity in the case of offshore injection projects (Barry et al., 2004; Portner et al., 2004; Tamburri et al., 2000).

Carbon mineralisation works by reacting CO<sub>2(g)</sub> or CO<sub>3<sup>2-</sup>(aq)</sub> with divalent metal cations (most typically Mg<sup>2+</sup><sub>(aq)</sub> or Ca<sup>2+</sup><sub>(aq)</sub>) to form carbonate minerals such as magnesite (MgCO<sub>3</sub>) and the Ca-carbonate polymorphs (CaCO<sub>3</sub>) (Lackner, 2002; Lackner, 2003; Lackner et al., 1995; Seifritz, 1990). There are multiple feedstocks that can be used to provide the source of cations for the carbonation reaction, including ultramafic rocks and alkaline industrial wastes, which include the finely pulverised mineral waste from ultramafic mines (tailings). Industrial wastes that are of use in carbonation reactions include steel slags (e.g., Baciocchi et al., 2009; Bonenfant et al., 2008b; Chang et al., 2011), cement kiln dust (e.g., Huntzinger et al., 2009a; Huntzinger et al., 2009b), alkaline paper mill waste (e.g., Perez-Lopez et al., 2008), red mud produced during aluminium production (e.g., Bobicki et al., 2012; Bonenfant et al., 2008a; Sahu et al., 2010; Yadav et al., 2010), waste ash from power plants and municipal solid waste (e.g., Bobicki et al., 2012; Fernandez et al., 2004; Nam et al., 2012;

Uibu et al., 2010). Mafic and ultramafic rock formations such as those found at mid ocean ridges or recent lava fields (such as in Iceland or the Newer Volcanics province in Australia) are also natural sinks for atmospheric CO<sub>2</sub> within carbonate minerals (Matter et al., 2016; Pevzner et al., 2011; Shulakova et al., 2015; Snæbjörnsdóttir et al., 2014).

Ultramafic and mafic rocks can be carbonated in several ways, such as by injecting the CO<sub>2</sub> into rock units or mining ultramafic material for use in carbonation reactors. Several carbon mineralisation demonstration projects such as CarbFix in Iceland (CarbFix, 2018), CO<sub>2</sub>CRC (CO<sub>2</sub>CRC, 2018) and Mineral Carbonation International (Mineralcarbonation.com, 2018) in Australia and Carbonfree Chemicals in the USA (Carbonfree Chemicals, 2018) are currently underway and have been show to completely convert the CO<sub>2</sub> that they are trying to sequester into carbonate minerals (Matter et al., 2016).

## **2.2 Carbon mineralisation in Ultramafic Mine Wastes**

In addition to high-cost and labour-intensive carbon mineralisation projects that offer fast carbonation rates (Kakizawa et al., 2001; Matter et al., 2016; O'Connor et al., 2002; Park and Fan, 2004; Snæbjörnsdóttir et al., 2014), there are also lower-cost carbon mineralisation projects being researched that seek to enhance the natural rate of carbonation that occurs at Earth's surface conditions (e.g., Gras et al., 2017; Lechat et al., 2016; McCutcheon et al., 2017; Oskierski et al., 2013; Wilson et al., 2014; Zarandi et al., 2017). Carbon mineralisation reactions are natural weathering reactions where the dissolution of feedstock minerals tending to be the rate limiting step (Oelkers et al., 2008), once the limitation of CO<sub>2</sub> availability has been addressed (Harrison et al., 2013; Wilson et al., 2010). In tailings storage facilities, the rate of Mg-silicate mineral dissolution is enhanced due to mine processing drastically increasing the reactive surface area of the minerals (e.g., Gras et al., 2017; Lechat et al., 2016; McCutcheon et al., 2017; Oskierski et al., 2013; Wilson et al., 2009a; Wilson et

al., 2014; Wilson et al., 2009b; Zarandi et al., 2017). This enables passive weathering and carbon mineralisation reactions to occur at a rate that could potentially offset the emissions of some mines (e.g., Gras et al., 2017; Lechat et al., 2016; McCutcheon et al., 2017; Oskierski et al., 2013; Wilson et al., 2006; Wilson et al., 2009a; Wilson et al., 2014; Wilson et al., 2009b; Zarandi et al., 2017). With the mine tailings produced by ultramafic nickel, kimberlitic diamond, or asbestos mines making excellent potential storage sites in which to trap atmospheric CO<sub>2</sub> (Assima et al., 2012; Bea et al., 2012; Beinlich and Austrheim, 2012; Hitch et al., 2010; McCutcheon et al., 2015; Mervine et al., 2017; Oskierski et al., 2013; Pronost et al., 2012; Teir et al., 2007; Wilson et al., 2009a; Wilson et al., 2014; Wilson et al., 2009b; Zarandi et al., 2017).

Multiple carbon bearing minerals can precipitate and trap atmospheric CO<sub>2</sub> within ultramafic tailings storage facilities, the most common minerals to form at low-temperature surface conditions are hydrated Mg-carbonate minerals including nesquehonite (MgCO<sub>3</sub>·3H<sub>2</sub>O), hydromagnesite [Mg<sub>5</sub>(CO<sub>3</sub>)<sub>4</sub>(OH)<sub>2</sub>·4H<sub>2</sub>O] and dypingite [Mg<sub>5</sub>(CO<sub>3</sub>)<sub>4</sub>(OH)<sub>2</sub>·~5H<sub>2</sub>O] (Harrison et al., 2013; Harrison et al., 2015; Wilson et al., 2011; Wilson et al., 2009a; Wilson et al., 2014). This has led to much of the research into CO<sub>2</sub> sequestration at ultramafic mine sites focussing on the formation of these hydrated Mg-carbonates (e.g., Harrison et al., 2013; Harrison et al., 2015; Wilson et al., 2011; Wilson et al., 2009a; Wilson et al., 2014).

### **2.2.1 The Woodsreef chrysotile mine**

The Woodsreef chrysotile deposit is located 80 km N of Tamworth (New South Wales, Australia) and was the site of Australia's only large-tonnage chrysotile mine (Glen and Butt, 1981; Offler et al., 1997). The deposit was identified in 1888 and was first mined on a small scale between 1914 and 1922. A larger mine was operated at the site by the Chrysotile Corporation of Australia Pty Ltd between 1970 and 1983. The mine yielded 34 Mt of ore,

and 500,000 t of long fibre chrysotile, while also producing 24 Mt of tailings and 75 Mt of waste rock over the life of the mine (Merril et al., 1980). The Woodsreef chrysotile deposit is located within the Woodsreef Serpentinite, which itself is a part of the Great Serpentinite Belt: a series of ultramafic bodies that are localised along the NNW-trending Peel fault (Katz, 1986). The belt consists of a *mélange* of different serpentinite bodies that surround tectonic blocks of various compositions and metamorphic grade including basalts, dolerites and plagiogranites, as well as eclogites and amphibolites (Offler et al., 2004; Offler and Shaw, 2006).

The Woodsreef Serpentinite is dominated by three altered ultramafic mineral assemblages: partially serpentinitised harzburgite, schistose serpentinite and the massive serpentinite ore body (Glen and Butt, 1981). The least altered rock type is the partially serpentinitised harzburgite, which is red-brown in colour and consists of >30 wt% serpentine minerals, magnetite and relict pieces of the unaltered harzburgite protolith. The protolith is estimated to have been 65–70 wt% olivine (forsterite 81), 25–30 wt% pyroxene (enstatite 94) and 0–5 wt% chromite (Glen and Butt, 1981). Minor phases that have been reported in the partially serpentinitised harzburgite include tremolite  $[\text{Ca}_2\text{Mg}_5(\text{Si}_8\text{O}_{22})(\text{OH})_2]$ , magnetite ( $\text{Fe}_3\text{O}_4$ ), brucite  $[\text{Mg}(\text{OH})_2]$ , and coalingite  $[\text{Mg}_{10}\text{Fe}^{3+}_2(\text{OH})_{24}[\text{CO}_3]\cdot 2\text{H}_2\text{O}]$  (Glen and Butt, 1981). The massive serpentinite ore body can be distinguished from the partially serpentinitised harzburgite by its black-green colour as well as its finer texture and smooth weathering surfaces. The unit consists of lizardite and chrysotile with minor magnetite, brucite and chlorite phases. Unlike the partially serpentinitised harzburgite, the massive serpentinite lacks relict pyroxene and olivine crystals (Glen and Butt, 1981). The schistose serpentinite is the most abundant rock type in the Woodsreef Serpentinite; it is found along the margins of the serpentinite body and encloses all the other lithologies within the mine. Like the massive serpentinite, it consists of chrysotile and lizardite, magnetite, chlorite and minor chrome

spinel (Glen and Butt, 1981). Minerals within the schistose serpentinite are too deformed to preserve any protolith texture (Glen and Butt, 1981). The similarity between the three main units at Woodsreef led Glen and Butt (1981) to conclude that the rock types were formed by different amounts of deformation and serpentinitisation of a single protolith, with the schistose serpentinite being the most deformed of the three rock types.

The composition of the tailings at Woodsreef is representative of the mineralogy of the massive serpentinite ore body. Weathering reactions occurring in the tailings pile have resulted in precipitation of hydromagnesite as surface crusts (Oskierski et al., 2013; Turvey et al., 2017). These crusts cover horizontal and vertical surfaces and contain up to ~15 wt% hydromagnesite (Oskierski et al., 2013; Turvey et al., 2017). The hydrotalcite minerals, pyroaurite [ $\text{Mg}_6\text{Fe}^{3+}_2(\text{CO}_3)(\text{OH})_{16}\cdot 4\text{H}_2\text{O}$ ] and coalingite [ $\text{Mg}_{10}\text{Fe}^{3+}_2(\text{CO}_3)(\text{OH})_{24}\cdot 2\text{H}_2\text{O}$ ], are also found within the tailings material (Oskierski et al., 2013; Turvey et al., 2017), but their origin is currently unknown as they may be present within serpentinite bodies (e.g., Grguric, 2003; Bottril, 2008) or they may be forming *in situ* by reaction of Fe-rich brucite with atmospheric  $\text{CO}_2$ , as seen in the New Idria Serpentinite, California (Mumpton et al., 1965; Mumpton and Thompson, 1966).

Oskierski et al. (2013) and Turvey et al. (2017) characterised the mineralogy of the tailings pile at Woodsreef using quantitative X-ray diffraction (XRD) methods. They found that surface crusts contain significant abundances of pyroaurite and hydromagnesite, whereas samples taken from deeper within the tailings typically contain no hydromagnesite and lower abundances of pyroaurite than at the surface (Oskierski et al., 2013; Turvey et al., 2017). Oskierski et al. (2013) also investigated the stable and radiogenic carbon isotope composition of the carbonate minerals within the tailings, finding that the horizontal and vertical crusts contained significant radiocarbon, suggesting that they formed from a modern

atmospheric source of carbon. Using quantitative XRD data, Oskierski et al. (2013) estimated that Woodsreef has currently sequestered between 1,400 and 70,000 t of atmospheric CO<sub>2</sub>. As the origin of the pyroaurite was still relatively uncertain the upper bound assumes pyroaurite was forming within the tailings and was sequestering atmospheric CO<sub>2</sub> and the lower bound assumes that it was a metamorphic gangue mineral and was not sequestering net CO<sub>2</sub> (Oskierski et al., 2013).

Multiple studies, conducted at the tailings storage facility at Woodsreef have investigated the potential to increase the carbonation rate at Woodsreef using biotic and abiotic means (Hamilton et al., in prep-a; McCutcheon et al., 2015; McCutcheon et al., 2017). McCutcheon et al., (2016, 2017) conducted investigations into enhancing the passive rate of carbon mineralisation within the tailings at Woodsreef using cyanobacteria. McCutcheon et al. (2016) conducted a series of laboratory experiments using sulfuric-acid leached tailings samples taken from Woodsreef that were subsequently inoculated with cyanobacteria cultivated from one of the mine pits. They found that the cyanobacteria generated localised microenvironments that promoted high concentrations of Mg<sup>2+</sup> and CO<sub>3</sub><sup>2-</sup>, while also acting as a nucleation sites for the precipitation of dypingite, hydromagnesite and nesquehonite (McCutcheon et al., 2016). McCutcheon et al. (2017) applied these techniques in a microbially mediated carbonation trial at the Woodsreef tailings storage facility, where they applied sulfuric acid pre-treatments and then inoculated the tailings with endemic cyanobacteria cultured in the laboratory. Quantitative XRD data showed a doubling in the abundance of hydromagnesite in the 2–4 cm interval of the tailings when inoculated with cyanobacteria (McCutcheon et al., 2017). This increase was less than expected based off of previous laboratory experiments, demonstrating the challenge of scaling up laboratory experiments for implementation in the field, where water and carbon availability both became limiting factors (McCutcheon et al., 2017). Hamilton et al. (in prep-a) performed an

abiotic enhanced carbon mineralisation trial on the tailings at Woodsreef using the addition of periodic water and sulfuric acid treatments via heap leaching to promote rapid dissolution of minerals in the tailings while maintaining tailings pore water conditions within the ideal range (30–60 %, saturation) as described by Assima et al. (2013) and Harrison et al. (2015). The majority of these field studies have focussed primarily on the formation of hydromagnesite, as the formation of Mg-carbonate minerals such as hydromagnesite at Woodsreef is well understood, but the origin of the pyroaurite currently held in the tailings is not (Oskierski et al., 2013; Turvey et al., 2017). Pyroaurite makes up a significant portion of the tailings material; therefore, determining whether or not net sequestration of atmospheric carbon is occurring within pyroaurite will alter estimates of how much CO<sub>2</sub> has been sequestered at Woodsreef.

### **2.2.2 The Mount Keith nickel mine**

The Mount Keith nickel mine is 90 km NE of Leinster in the Goldfields district of Western Australia. It is located atop a disseminated nickel sulphide deposit and is the largest nickel mine in Australia, producing 11 Mt of tailings per year and the equivalent of 370,000 t/yr of CO<sub>2</sub> emissions (BHP, 2005; Grguric, 2003; Wilson et al., 2014). The ore and tailings material have a very high proportion of hydrotalcite minerals, up to 20 wt% (Grguric et al., 2001). Several hydrotalcite minerals species are found in the tailings, with woodallite [Mg<sub>6</sub>Cr<sub>2</sub>(OH)<sub>16</sub>Cl<sub>2</sub>·4H<sub>2</sub>O] and stichtite [Mg<sub>6</sub>Cr<sub>2</sub>(OH)<sub>16</sub>CO<sub>3</sub>·4H<sub>2</sub>O] existing as a solid solution between the chloride and carbonate endmembers of the Mg-Cr hydrotalcites (Grguric, 2003). Similarly, the analogous Mg-Fe hydrotalcites, iowaite [Mg<sub>6</sub>Fe<sub>2</sub>(OH)<sub>16</sub>Cl<sub>2</sub>·4H<sub>2</sub>O] and pyroaurite, are both found within the tailings and intermediate composition are common (Grguric, 2003; Grguric et al., 2001). Woodallite–stichtite and iowaite–pyroaurite formed within the ore body by the hydrothermal alteration of chromite

and magnetite grains, respectively (Grguric, 2003; Grguric et al., 2001). Furthermore Mountkeithite  $[\text{Mg}_{11}(\text{Fe}^{3+})_3(\text{SO}_4)_{3.5}(\text{OH})_{24}\cdot 11\text{H}_2\text{O}]$  has been found to undergo anion exchange with the local environment while in the tailings pile at Mount Keith, where it decomposes and incorporates  $\text{CO}_3^{2-}$ , to form pyroaurite (Hudson and Bussell, 1981). The tailings storage facility at Mount Keith has been studied for its carbon sequestration potential with the dissolution of brucite and serpentine minerals leading to the formation of hydromagnesite (Bea et al., 2012; Harrison et al., 2013; Wilson et al., 2010; Wilson et al., 2014). Wilson et al. (2014) estimated that carbonation in the tailings currently offsets 11% of the mine's annual greenhouse gas emissions and has the potential to offset up to 60%. The hydrotalcites in the tailings were originally present in the ore (Grguric, 2003; Grguric et al., 2001), thus, although they did not sequester atmospheric  $\text{CO}_2$  during their formation, the chloride end members may potentially be trapping atmospheric  $\text{CO}_2$  via anion exchange reactions within the tailings (Mills et al., 2011; Woodhouse, 2006).

### **2.2.3 The Dundas mineral field**

The Dundas Mineral Field is a collection of mostly disused historic mine sites located approximately 5 km E of Zeehan in western Tasmania, Australia. The first mines at Dundas were established by prospectors looking to take advantage of rich silver and lead deposits in the 1880s (Reid, 1925). By the 20<sup>th</sup> century tin and zinc–lead mining had become the focus of the region (Reid, 1925). Many of the historic mines in the field, including the Adelaide, Red Lead, Dundas Extended, West Comet, Platt, Kozminsky and Kapi mines are of continued interest to mineralogists for their excellent specimens of crocoite  $[\text{Pb}(\text{Mn}^{4+}, \text{Mn}^{2+})_8\text{O}_{16}]$ , stichtite and serpentine (Bottrill, 2008; Bottrill and Baker, 2008; Sittinger and Sittinger, 2008). The Dundas mineral field consists mainly of the Cambrian-aged marine sandstone–siltstone–conglomerate units of the Owens Group (Seymour and

McMclenaghan, 2003), siderite–ankerite-rich fault zones that cut through the Owens Group and act as the ore body for the many historic silver–lead “crocoite mines”, and Cambrian-aged serpentinites that contain high levels of chromium within chromite and stichtite (Bottrill, 2008).

Stichtite is a major component of the serpentinite units within the Dundas mineral field, with the Adelaide silver and lead mine being the type locality for stichtite (Ashwal and Cairncross, 1997). The stichtite within the Dundas mineral field formed from the carbonation of chromite and chromium rich magnetite (Bottrill and Baker, 2008; Melchiorre et al., 2016). Both polytypes of stichtite (2H and 3R) are found intergrown as small blebs, coarse patches and vein material with relict grains of chromite found within the contorted masses of stichtite (Bottrill, 2008; Bottrill and Baker, 2008). Melchiorre et al. (2016) investigated the formation of stichtite at Dundas and they argue that that the reaction textures between the stichtite and relict chromite grains, as well the stable C and H isotopic compositions of stichtite can record serpentinisation conditions and provide a window into understanding the early Earth. The Dundas mineral field is not being investigated for its carbon sequestration capacity, as the mine sites are small scale and mostly derelict and the hydrothermal origin of the hydrotalcites at the site is well established; however, Dundas is of interest as a point of comparison to larger scale mine sites where hydrotalcites are forming *in situ* and trapping CO<sub>2</sub>, to see how sedimentary and hydrothermal hydrotalcite minerals differ, and how the behaviour and stable isotope composition of hydrothermal hydrotalcites is affected when exposed to the Earth’s surface.

### **2.3 Hydrotalcites: current geochemical knowledge and gaps**

Hydrotalcites are layered double hydroxide (LDH) minerals that are structurally related to brucite [Mg(OH)<sub>2</sub>]. They are capable of incorporating CO<sub>2</sub> into their crystal structures in

multiple ways, either during formation, via the alteration of brucite or spinel minerals by  $\text{CO}_3^{2-}$  (aq) rich fluids (Grguric, 2003; Melchiorre et al., 2016; Mumpton et al., 1965; Mumpton and Thompson, 1966), or via anion exchange reactions that incorporate  $\text{CO}_3^{2-}$  (aq) from the local environment after formation (Bish, 1980; Hudson and Bussell, 1981; Miyata, 1983). This makes hydrotalcites a potential carbon sink at ultramafic mines, either via carbonation of brucite or via anion exchange (Gras et al., 2017; Oskierski et al., 2013; Turvey et al., 2017).

The hydrotalcite supergroup consists of over 40 naturally occurring LDH minerals. Early researchers struggled to understand the compositional and structural relationships between various members of the supergroup (Foshag, 1920; Frondel, 1941; Petterd et al., 1914). A report compiled by the Tasmanian Geological survey in 1914 linked the mineral stichtite with pyroaurite, brugnatellite  $[\text{Mg}_6\text{Fe}^{3+}\text{CO}_3(\text{OH})_{13}\cdot 4\text{H}_2\text{O}]$  and hydrotalcite  $[\text{Mg}_6\text{Al}_2(\text{OH})_{16}(\text{CO}_3)\cdot 4\text{H}_2\text{O}]$ , (the archetypal mineral for which the supergroup is named), noting their compositional and structural similarity (Petterd et al., 1914). This was further elucidated upon by Foshag (1920) who compared all the compositional analyses to date for the different minerals, referring to them as the hydrotalcite group but also doubting the connection between brugnatellite and the other three minerals (Foshag, 1920).

### **2.3.1 Structures of hydrotalcites**

The structure of a hydrotalcite mineral consists of stacked sheets of brucite-like hydroxide layers that are separated by interlayer galleries that contain  $\text{H}_2\text{O}$  molecules and various anions held together by hydrogen bonding (see Figure 2.1) (Evans and Slade, 2006; Mills et al., 2012). The differences between hydroxide and hydrotalcite minerals occurs due to the presence of trivalent cations, which replace some of the divalent cations in the hydroxide sheets (Cavani et al., 1991; Mills et al., 2012; Vaccari, 1998). The incorporation of trivalent

cations into the divalent hydroxide sites leads to a slight positive charge within the hydroxide layers (Evans and Slade, 2006; Mills et al., 2012). To maintain a stable, charge balanced mineral structure various anions and H<sub>2</sub>O molecules are drawn into the interlayer galleries balancing the positively charged hydroxide layers (Cavani et al., 1991; Evans and Slade, 2006; Mills et al., 2012; Reichle, 1986; Vaccari, 1998).

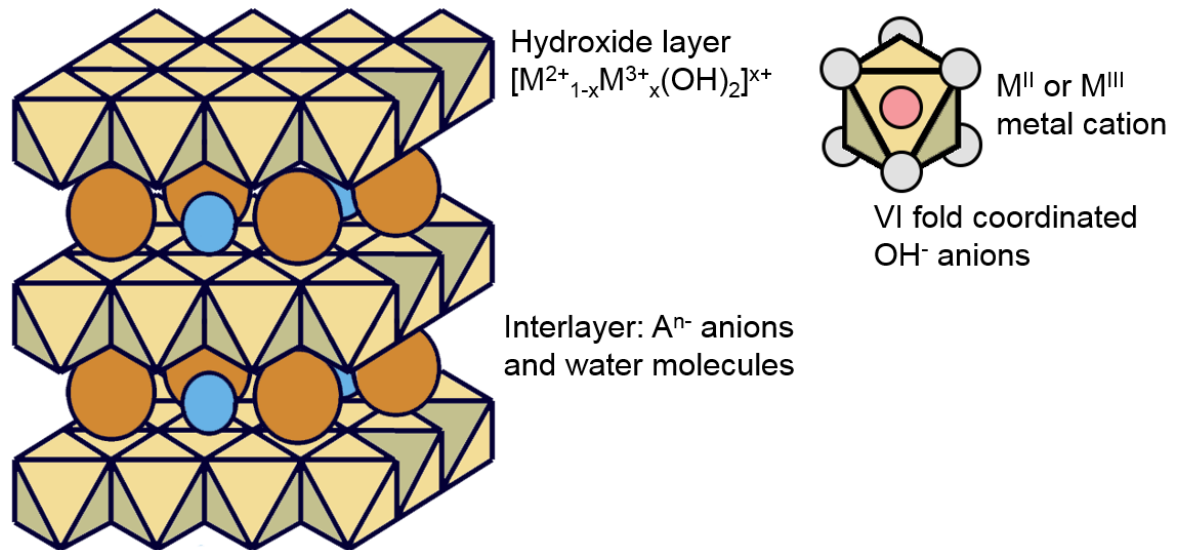


**Figure 2.1** Generalised structure of a hydrotalcite mineral, illustrating the relationship between the hydroxide layers and interlayer galleries. Inset shows the atomic positions within the brucite-like hydroxide layer (modified from Woodhouse, 2006).

The general formula for the hydrotalcite supergroup is  $[M^{2+}_{1-x}M^{3+}_x(OH)_2]^{x+}A^{n-}_{x/n} \cdot mH_2O$  (Evans and Slade, 2006). There is a wide variety of different mineral species within the hydrotalcite supergroup arising from the high degree of variation allowed by this formula. These variations include the identity of divalent and trivalent cations within the hydroxide layers (M<sup>2+</sup> and M<sup>3+</sup>) as well as the molar ratio between the two species (1-x:x) (Evans and Slade, 2006; Mills et al., 2012), the identity of anions and degree of hydration within the interlayer galleries (A<sup>n-</sup><sub>x/n</sub> · mH<sub>2</sub>O) (Cavani et al., 1991; Mills et al., 2012), and the relative position of the stacked hydroxide layers (Bookin et al., 1993a; Bookin and Drits, 1993). There are eight separate groups within the hydrotalcite supergroup, and these groups are

differentiated by interlayer spacing and the  $M^{2+}:M^{3+}$  ratios in the brucite-like layers (Mills et al., 2012).

A wide variety of different cations are incorporated into the structure of hydrotalcite minerals. The most common hydrotalcite forming divalent cations are  $Mg^{2+}$ ,  $Ni^{2+}$ ,  $Fe^{2+}$  and  $Ca^{2+}$  whereas hydrotalcites containing  $Zn^{2+}$ ,  $Cu^{2+}$  and  $Mn^{2+}$  are less common in nature (Mills et al., 2012). A wide variety of trivalent cations are also incorporated into hydrotalcite minerals, with  $Fe^{3+}$  and  $Al^{3+}$  being the most common and  $Co^{3+}$ ,  $Cr^{3+}$ ,  $Ni^{3+}$  and  $Mn^{3+}$  being less common (Mills et al., 2012). The molar ratio between the divalent and trivalent cations in the mineral structure ( $M^{2+}/M^{3+}$ ) is characteristic of the group to which a hydrotalcite supergroup mineral belongs (Mills et al., 2012). Most of these mineral groups have a  $M^{2+}:M^{3+}$  ratio of either 2:1 or 3:1 (Evans and Slade, 2006). Higher molar ratios for cations are found in some hydrotalcites such as brugnatellite [ $Mg_6Fe^{3+}(CO_3)(OH)_{13}\cdot 4H_2O$ ] which has a  $M^{2+}/M^{3+}$  ratio of 6:1; however, ratios higher than 3:1 are typically only found in synthetic LDHs rather than naturally occurring hydrotalcite minerals (Mills et al., 2012). Ratios lower than 2:1 are rare because if three  $M^{3+}$  cations surround a single  $OH^-$  within a hydroxide layer it will lead to severe lengthening of the M–O bond, and edge sharing between multiple highly charged cations is not favoured electrostatically (Evans and Slade, 2006). Local ordering occurs in the hydroxide sheet to prevent the formation of these  $M^{3+}$  clusters in the mineral. This is analogous to the ‘aluminium avoidance principal’ of Loewenstein (1954) found in aluminosilicates (Loewenstein, 1954; Mills et al., 2012). The local order of cations is important in hydrotalcites with a cation ratio of 2:1, and to avoid contact between  $M^{3+}$  cations a honeycomb texture is required giving a  $3 \times 3$  superlattice within the plane of the layer, although the exception to this is hydrotalcites containing  $Cr^{3+}$  (Evans and Slade, 2006). For ratios of 3:1  $M^{3+}$  avoidance can be achieved without long-range order (Mills et al., 2012).

The way the brucite-like layers stack in a hydrotalcite affects the size and shape of the anions that are held in the interlayer spaces (Bookin et al., 1993a; Bookin and Drits, 1993). In brucite  $[\text{Mg}(\text{OH})_2]$  magnesium cations are found in octahedral coordination with hydroxide anions. These magnesium octahedra form infinite layers through edge sharing. The brucite layers are stacked upon each other, with each layer offset from the layers above and below it to allow for the hydrogen atom of one layer to lie in the interstices between three hydrogen atoms of the next layer, with the layers being held together by hydrogen bonding (Cavani et al., 1991; Evans and Slade, 2006; Mills et al., 2012). This atomic arrangement is appropriate for a hydroxide that contains divalent metals cations such as brucite as well as other hydroxide minerals such as amakinite, portlandite, pyrochroite and theophrastite (the  $\text{Fe}^{2+}$ ,  $\text{Ca}^{2+}$ ,  $\text{Mn}^{2+}$  and  $\text{Ni}^{2+}$  equivalents of brucite; Mills et al., 2012). The hydroxide layers in a hydrotalcite mineral stack differently to those of brucite, and can stack in multiple ways. This leads to a high degree of polytypism within hydrotalcites, with one, two, three and six-layer polytypes existing for various hydrotalcite minerals (Mills et al., 2012). What polytypes can occur for a given mineral is dependent on the identity of the anions in the interlayer spaces. Bookin et al. (1993a) determined that for hydrotalcites containing  $\text{CO}_3^{2-}$  two and three-layer polytypes are possible whereas one and three-layer polytypes are possible for hydrotalcite minerals containing  $\text{SO}_4^{2-}$  (Bookin et al., 1993a; Bookin and Drits, 1993; Mills et al., 2012). Layers may exhibit rhombohedral or hexagonal symmetry (Bookin et al., 1993a; Bookin and Drits, 1993; Mills et al., 2012) and stacking of the hydroxide layers will create different interlayer spaces (Bookin et al., 1993a; Bookin et al., 1993b). For instance, if the  $\text{OH}^-$  groups of one layer directly overlie the  $\text{OH}^-$  groups of the next, they will form triangular prisms in the interlayer galleries, which are referred to as P-type interlayers (Figure 2.2). However if the  $\text{OH}^-$  groups do not directly overlie each other, then an octahedral

interlayer space will be formed, and these are referred to as O-type interlayers (Figure 2.2) (Bookin et al., 1993a; Bookin and Drits, 1993; Mills et al., 2012).

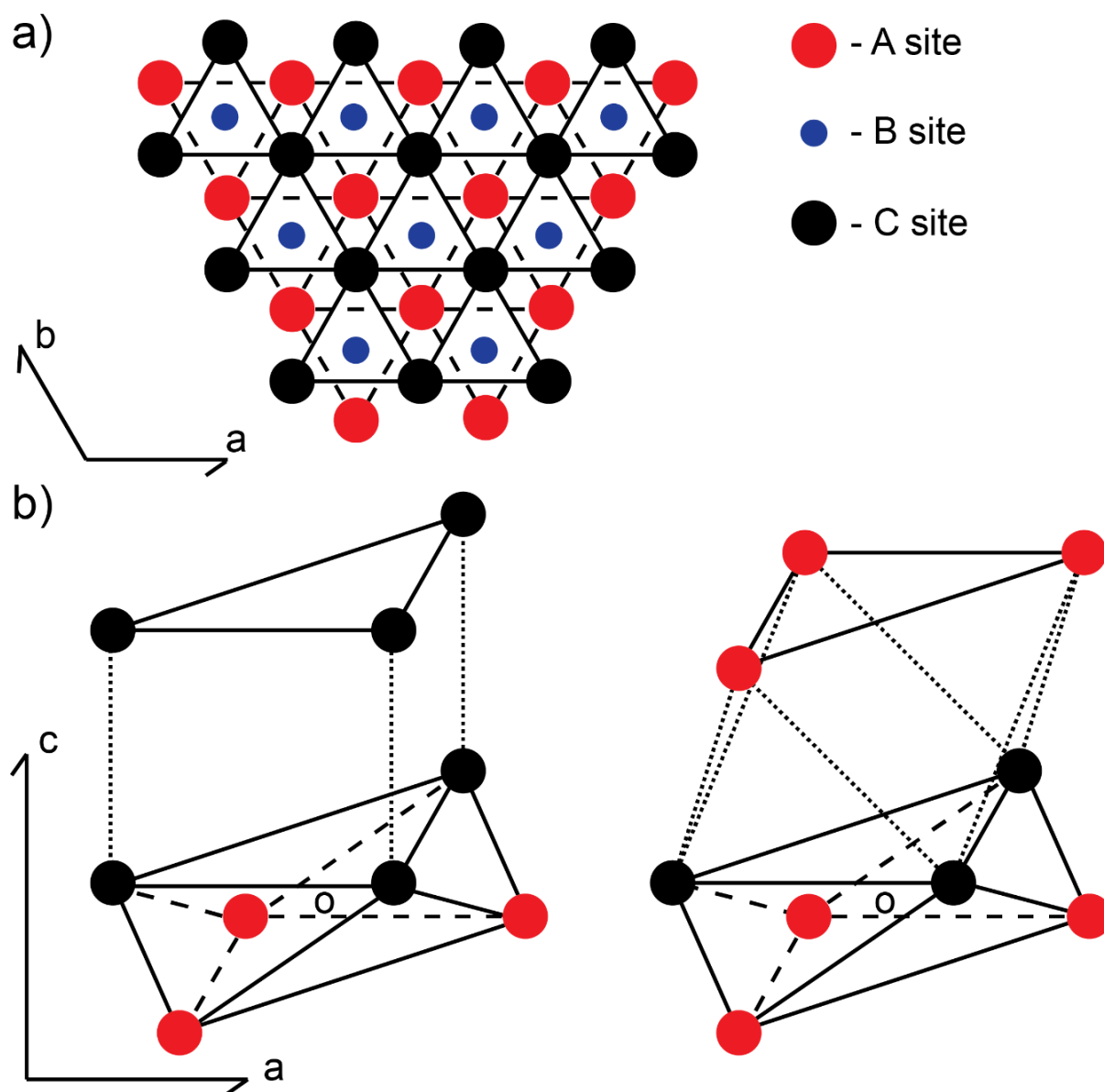


**Figure 2.2** Layering within hydroxalclites, showing the difference between O and P-type interlayers, modified from Bookin and Drits (1993).

The galleries created by the P and O interlayers in a hydroxalclite mineral can incorporate a wide variety of different anions. The anions that are most typically found in natural hydroxalclite minerals are  $\text{Cl}^-$ ,  $\text{OH}^-$ ,  $\text{CO}_3^{2-}$  and  $\text{SO}_4^{2-}$ ,  $\text{S}^{2-}$  and  $[\text{Sb}(\text{OH})_6]^-$  (Mills et al., 2012).

When incorporating these anions, the interlayer spaces in a hydrotalcite can expand to a significant degree. In brucite, which is analogous to a dehydrated and anion-free hydrotalcite, the interlayer spacing is  $\sim 4.7$  Å. However, the interlayer space expands to  $\sim 7.8$  Å to incorporate hydroxide, carbonate and halide groups and up to  $8.5\text{--}9$  Å when incorporating larger sulfate tetrahedra (Mills et al., 2012). The interlayers in hydrotalcites can increase up to a distance of  $\sim 11$  Å for minerals that contain additional H<sub>2</sub>O molecules (such as the glaucocerite group) or large, low charge cationic complexes (Mills et al., 2012). In addition to anionic compounds and water molecules, the interlayer spaces of hydrotalcites may also hold cationic or neutral complexes in the interlayer galleries such as [Na(H<sub>2</sub>O)<sub>6</sub>]<sup>+</sup> or [MgSO<sub>4</sub>]<sup>0</sup> which are found in shigaite [NaAl<sub>3</sub>(Mn<sup>2+</sup>)<sub>6</sub>(SO<sub>4</sub>)<sub>2</sub>(OH)<sub>18</sub>·12H<sub>2</sub>O], or nikischerite [Na(Fe<sup>2+</sup>)<sub>2</sub>Al<sub>3</sub>(SO<sub>4</sub>)<sub>2</sub>(OH)<sub>18</sub>(H<sub>2</sub>O)<sub>12</sub>] and mountkeithite respectively (Mills et al., 2012).

### **2.3.2 Anion exchange in hydrotalcites**

Hydrotalcite group minerals have the ability to undergo anion exchange reactions, where the anions in the interlayer galleries are replaced by different anions sourced from the local environment, without altering the overall hydrotalcite structure (Bish, 1980; Bish and Brindley, 1977; Hudson and Bussell, 1981; Miyata, 1983; Miyata and Okada, 1977). This feature was first recognised when researchers working to synthesise particular hydrotalcites found that great care had to be taken to avoid carbonate anions from being incorporated into the phase they were precipitating (Miyata, 1975). Miyata (1975) synthesised hydrotalcite minerals under controlled conditions that rigorously excluded any carbonate from contaminating the structure. Similarly, Hansen and Taylor (1991) chose to remove carbonate from a synthetic pyroaurite compound via a glycerol intercalation stage that allowed for exchange with SO<sub>4</sub><sup>2-</sup>, NO<sub>3</sub><sup>-</sup> and Cl<sup>-</sup>.

The first study that was specifically conducted to investigate the anion exchange properties of hydrotalcites was Brindley and Bish (1976). They found that it was possible to alter the structure and composition of takovite  $[\text{Ni}_6\text{Al}_2(\text{OH})_{16}(\text{CO}_3,\text{OH})\cdot 4\text{H}_2\text{O}]$  by exposing this mineral to various solutions containing other anions (Brindley and Bish, 1976). Through exposure to these solutions the authors were able to create takovite-like products that included  $\text{Cl}^-$ ,  $\text{NO}_3^-$  and  $\text{SO}_4^{2-}$  within the interlayer spaces rather than  $\text{CO}_3^{2-}$  (Brindley and Bish, 1976). This work was further investigated in Bish and Brindley (1977) where synthetic takovite was treated with dilute  $\text{HCl}_{(\text{aq})}$  to form  $\text{Cl}^-$ -bearing takovite. The reaction product was analysed using infrared spectroscopy and it was determined that the treated takovite was very similar to the untreated material with the exception that it did not show any of the characteristic  $\text{CO}_3^{2-}$  vibrations (Bish and Brindley, 1977). The authors concluded that because the infrared spectra appeared largely unchanged, the hydroxide layers in the takovite were unaffected by the compositional changes that had occurred in the interlayer galleries (Bish and Brindley, 1977). Further experiments were conducted by Bish (1980) where it was determined that hydrotalcite [the Mg-Al endmember of the hydrotalcite group,  $\text{Mg}_6\text{Fe}^{3+}_2\text{CO}_3(\text{OH})_{16}\cdot 4\text{H}_2\text{O}$ ] was also capable of undergoing anion exchange. Samples of takovite and hydrotalcite were treated with dilute solutions of  $\text{HCl}$ ,  $\text{HNO}_3$ ,  $\text{H}_2\text{SO}_4$ ,  $\text{NiSO}_4$ ,  $\text{Al}_2(\text{SO}_4)_3$  and  $\text{KOH}$ . The minerals were placed in powdered form into the solutions at room temperature over times ranging from a few minutes to several days. Changes in the crystal structure of the minerals were tracked using XRD to monitor changes to the size of the interlayer space through observation of the position of the (0 0 3 $l$ ) peak (Bish, 1980). It was concluded that both minerals were capable of undergoing anion exchange at room temperature (Bish, 1980).

Studies by Bish (1980) and Miyata (1983) found that hydrotalcite minerals display a strong preference for some anions over others. Bish (1980) estimated that the order for preference

in exchange and synthesis experiments was  $\text{CO}_3^{2-} > \text{NO}_3^- > \text{OH}^- = \text{Cl}^- > \text{SO}_4^{2-}$ . Miyata (1983) separated the anion preferences into monovalent and divalent anions, the order for monovalent anions was  $\text{OH}^- > \text{F}^- > \text{Cl}^- > \text{Br}^- > \text{NO}_3^- > \text{I}^-$  and for divalent anions it was  $\text{CO}_3^{2-} > \text{Naphthol Yellow S (NYS)} > \text{SO}_4^{2-}$ . These studies both agreed that hydrotalcite minerals have a preference for the carbonate anion over all others due to its divalent nature and small size (Bish, 1980; Miyata, 1983). Preferential uptake of carbonate into the hydrotalcite structure is so great that during synthesis experiments great pains must be taken to exclude sources of aqueous carbonate and  $\text{CO}_2$  gas (Hansen and Taylor, 1991; Miyata, 1975). Additionally a wide variety of organic and complex ionic compounds can be incorporated via anion exchange. This has seen the use of synthetic LDHs as a delivery system for drugs such as Ibuprofen, and for the release of herbicides such as dichlorophenoxy butyrate and chlorophenoxy propionate (Hussein et al., 2012; Parello et al., 2010).

### **2.3.3 Formation of hydrotalcites**

Hydrotalcite group minerals occur naturally and can form by two major formation mechanisms, high temperature hydrothermal alteration of spinel minerals in ultramafic rocks, usually occurring during serpentinisation (Grguric, 2003; Grguric et al., 2001; Melchiorre et al., 2016), and low temperature carbonation of Fe-rich brucite due to weathering reactions, which forms Mg-Fe- $\text{CO}_3^{2-}$  hydrotalcites (Hostetler et al., 1966; Mumpton et al., 1965; Mumpton and Thompson, 1966). Grguric (2003) used textural evidence to determine that magnetite grains in ore from the Mount Keith nickel deposit have been altered and replaced by the formation of iowaite and pyroaurite, with the magnetite providing the divalent and trivalent cations needed to form the hydrotalcites. Similarly, alteration of chromite grains within the Mount Keith nickel deposit forms stichtite and woodallite, with the reacting chromite providing both the  $\text{Mg}^{2+}$  and  $\text{Cr}^{3+}$  necessary for formation of the hydrotalcite

minerals (Grguric, 2003; Grguric et al., 2001). The relationship between stichtite and chromite at Dundas was noted from the first discovery of the mineral (Petterd et al., 1914). A more recent study has proposed that stichtite at the Dundas mineral field was formed from the alteration of chromite grains by methane-rich serpentinising fluids (Melchiorre et al., 2016). Melchiorre et al., (2016, 2018) have estimated the amount of time that several serpentinites spent within the 'stichtite window' by using the degree of replacement by stichtite that chromite grains from Australia, Mexico, South Africa and India have undergone. Low temperature formation of coalingite and pyroaurite from serpentinites has been since the 1960s (Hostetler et al., 1966; Mumpton et al., 1965; Mumpton and Thompson, 1966). Coalingite was first identified by Mumpton et al. (1965) in the surficial weathering zones of the New Idria Serpentinite, California. In addition to petrographic evidence from the serpentinite, Mumpton et al. (1965) found that samples of Fe-rich brucite reacted with the atmosphere in the laboratory over several months to form coalingite. Mumpton and Thompson (1966) observed that brucite was largely absent from the surface weathering zone of the New Idria Serpentinite, despite being present in significant abundances within fresh serpentinite. They determined that formation of coalingite and pyroaurite occurs due to oxidation of  $\text{Fe}^{2+}$  in brucite, whereas exposure of brucite to ground waters leads to dissolution of the brucite, and later re-precipitation of hydromagnesite (Hostetler et al., 1966; Mumpton and Thompson, 1966).

#### **2.3.4 Uses and applications of hydrotalcites**

Hydrotalcites and LDHs (synthetic materials with the same or similar structures and chemical compositions as hydrotalcite minerals) see various uses because of their ability to incorporate and exchange a wide variety of cations and anionic complexes (e.g., Douglas et al., 2014; Douglas et al., 2010; Goh et al., 2008; Hayashi et al., 2009; Hoyo, 2007; Imran et

al., 2016; Johnson and Bullen, 2003; Xu et al., 2006). One use is the controlled dissolution and release of metals and organic complexes for delivery of drugs and fertilizers (Hoyo, 2007; Imran et al., 2016; Xu et al., 2006). Imran et al. (2016) investigated the dissolution and release of  $Zn^{2+}$  from a synthetic LDH for micronutrient release in soils. They demonstrated that a desired metal cation may be incorporated within the structure of a pyroaurite-like LDH and then released via dissolution, and that this may be adapted for Mn or Cu release for use in fertilizers (Imran et al., 2016). LDHs have many potential uses within health sciences and pharmaceuticals (Hoyo, 2007), and they compare favourably with other inorganic nanoparticles that are used for drug delivery because of their high positive surface charge and ability to carry various peptides, proteins and genes (Xu et al., 2006). Parello et al. (2010) investigated the dissolution of biocompatible Mg-Al LDHs at various pH values with and without Ibuprofen intercalated within the interlayers. They found that the Ibuprofen intercalated LDH sample was more soluble and dissolved more rapidly in an acetic/acetate buffer solution than an equivalent LDH with an intercalated carbonate anion (Parello et al. 2010).

LDHs have also been widely studied for their ability to remove aqueous contaminants from waterways (Douglas et al., 2014; Douglas et al., 2010; Goh et al., 2008; Hayashi et al., 2009; Johnson and Bullen, 2003). Reduction of selenate to  $Se^0$  by fougèrite or 'green rust' (a  $Fe^{2+}$ - $Fe^{3+}$  hydroxycarbonate) is the only documented abiotic selenate reduction pathway that is found within nature (Johnson and Bullen, 2003). This is an effective method of contaminant removal as elemental selenium is insoluble in water and has much lower toxicity, reducing potential dangers in waterways (Hayashi et al., 2009). In addition to selenate removal, LDH precipitation is being considered for removal of arsenate, chromate and phosphate from contaminated water, through surface absorption and anion exchange (Goh et al., 2008). Formation of hydroxycarbonates has also been demonstrated to be an effective method for

contaminant removal from uranium mine barren lixiviant and process waters (Douglas et al., 2014; Douglas et al., 2010). Process waters from the Ranger uranium mine, Northern Territory, Australia contain substantial concentrations of Mg, Al, SO<sub>4</sub>, metals and U (Douglas et al., 2014; Douglas et al., 2010). Douglas et al. (2010) describe a method for precipitating hydrotalcites in the process water through the addition of Na-aluminate to achieve a solution pH of > 5 and Mg:Al ratios of 2–3:1. These changes to solution chemistry lead to the formation of hydrotalcite minerals, and their ability to incorporate a wide variety of cations and anions allows them to remove contaminants from the process waters including Cu<sup>2+</sup>, UO<sub>2</sub><sup>2+</sup>, AsO<sub>4</sub><sup>3-</sup> and CrO<sub>4</sub><sup>2-</sup> (Douglas et al., 2010). This method was also demonstrated on barren lixiviant from Heathgate Resources' Beverly North *in situ* recovery mine in South Australia (Douglas et al., 2014). Here, MgCl<sub>2</sub> was added to the lixiviant to provide a source of Mg for precipitation of the hydrotalcite mineral and NaOH was used to neutralise the acidic waste water (Douglas et al., 2014). Formation of hydrotalcite minerals led to trapping and recovery of U and rare earth elements (REE), indicating that hydrotalcite precipitation may not only represent an effective remediation strategy but may also be able to offset remediation costs through recovery of REE resources (Douglas et al., 2014).

### **2.3.5 Reaction rates in hydrotalcites**

There is relatively little research that has been conducted on the dissolution mechanisms and dissolution kinetics of hydrotalcites and LDHs. However, the manner in which these minerals dissolve is important for many of their potential uses. LDHs are considered stable up to pH 12 and are more thermodynamically stable than structurally and chemically related divalent hydroxide minerals (Evans and Slade, 2006).

Of the few studies into dissolution of hydrotalcites and LDHs several relate to the dissolution of LDHs for the delivery of drugs in the body. Parello et al. (2010) found that at acidic

conditions the dissolution rate of Mg-Al LDHs was largely pH dependent due to the equilibrium between protonated and deprotonated (active and inactive) hydroxyl groups. They describe the dissolution mechanism at the mineral surface as occurring in two steps, fast formation of surface reactive sites by protonation of the hydroxyl groups, and slow detachment of metal ions from the surface (Parello et al., 2010). Imran et al. (2016) investigated the release of  $Zn^{2+}$  from pyroaurite-like LDHs over pH conditions ranging from 4-8 when considering the potential use of these compounds for delivering micronutrients to plants. They found that the LDHs dissolved incongruently, preferentially releasing the divalent cations ( $Mg^{2+}$  and  $Zn^{2+}$ ) while leaving behind an  $Fe^{3+}$ -enriched residue, and that with increasing pH values more  $Zn^{2+}$  was retained within the residue (Imran et al., 2016).

### **2.3.6 Stable isotope geochemistry of hydrotalcites**

The stable isotopic signatures of hydrotalcites and LDHs are not well understood as there has been little previous research investigating them. Johnson and Bullen (2003) investigated the fractionation of stable Se isotopes during abiotic selenate reduction by green rust. The authors found that abiotic selenate reduction by green rust produced much greater fractionation of stable Se isotopes than biotic reduction (Johnson and Bullen, 2003). Schellenger and Larese-Casanova (2013) also investigated the reduction of selenate by green rust, using stable oxygen isotope fractionation as an indicator of the processes that occur as selenate is absorbed into the green rust via anion exchange with  $Cl^-$ . The authors determined that reduction was a multi-phase process, with minor enrichment in  $^{18}O$  occurring during uptake of selenate via anion exchange, followed by significant enrichment in  $^{18}O$  caused by electron transfer between selenate held in the hydrotalcite interlayer and structural  $Fe^{2+}$  in the hydroxide layers of the hydrotalcite (Schellenger and Larese-Casanova, 2013). The

results of these studies have potential use for tracking abiotic selenate reduction in the natural environment (Johnson and Bullen, 2003; Schellenger and Larese-Casanova, 2013).

Stable C, O and H isotope compositions have been sporadically investigated for hydrotalcite minerals found in mine tailings and serpentinites. In the absence of mineral-specific isotope microanalysis standards, Melchiorre et al. (2014) trialled a method of correcting microanalysis C and H isotope secondary ion mass spectrometry (SIMS) data for stichtite by calibrating against traditional stable isotope analysis methods. These methods were then applied in Melchiorre et al. (2016) and Melchiorre et al. (2018), where stable C isotope analysis of stichtite was used to explore possible sources for the carbon that led to formation of Phanerozoic stichtite from Dundas, Tasmania and Tehuizingo, Mexico (Melchiorre et al., 2016) and of Archean stichtite from South Africa, Western Australia and Southern India (Melchiorre et al., 2018). The authors concluded that stable carbon isotope values were indicative of marine kerogen and marine carbonate minerals being the source of carbon in these samples of stichtite (Melchiorre et al., 2016; Melchiorre et al., 2018). However, Melchiorre et al., (2016; 2018) make no allowance for post-precipitation processes (e.g., anion exchange) altering the isotopic composition of stichtite, which could potentially overwrite previous isotopic formation signatures related to formation pathways.

O'Neil and Barnes (1971) were the first to report stable C and O isotope data for hydrotalcites, finding that hydrotalcite minerals in the New Idria Serpentinite tended to be enriched in  $^{13}\text{C}$  and have a similar  $\delta^{18}\text{O}$  composition to hydromagnesite found at the same locality. Wilson et al. (2014) found that samples rich in hydrotalcite group minerals from the Mount Keith nickel mine had similar composition to bulk carbonates samples from the site that were rich in bedrock derived magnesite and dolomite, being depleted in  $^{18}\text{O}$  compared to the atmospheric-derived carbonates at the site which formed under highly evaporative

conditions. Oskierski et al. (2013) and Gras et al. (2017) investigated the isotopic compositions of samples that contained pyroaurite and other hydrotalcite minerals at the Woodsreef chrysotile mine and Dumont nickel project (Abitibi, Quebec) respectively. They found hydrotalcite-rich samples tended to be relatively enriched in  $^{13}\text{C}$  compared to bedrock carbonate minerals, but depleted in  $^{13}\text{C}$  compared to atmospheric derived Mg-carbonates such as hydromagnesite and dypingite where they occur at the same localities (Gras et al., 2017; Oskierski et al., 2013). Gras et al. (2017) observe an enrichment trend in  $^{13}\text{C}$  and  $^{18}\text{O}$  that they argue is indicative of the formation of carbonates in an evaporative environment, similar to what was seen for Mg-carbonates in Wilson et al. (2014). A lack of any fractionation factors for stable C and O isotopes for hydrotalcite supergroup minerals makes it difficult to identify carbonate sources in hydrotalcites, and this is further complicated by anion exchange, which may lead to changing isotopic compositions over time, as has been reported for stable carbon and magnesium isotopes in seen for other hydrated carbonate minerals (Mavromatis et al., 2015; Oelkers et al., 2018).

## **2.4 Summary**

Carbon sequestration through enhanced weathering has several advantages over other carbon mineralisation technologies in that it does not require a point source of carbon and requires relatively little in the way of energy or capital (Lackner, 2002; Lackner, 2003; Lackner et al., 1995; Oelkers et al., 2008; Power et al., 2013; Seifritz, 1990). It also has the potential to be an economic asset to some mine sites, either by forming value added mineral products, re-mining wastes or by providing carbon credits if an emissions trading scheme or carbon price is in effect in the jurisdiction of the site. Because these weathering reactions are occurring at some mine sites without any intervention, there is the opportunity to enhance carbon mineralisation through relatively simple techniques such as watering tailings,

introducing cyanobacteria to nucleate carbonate minerals, using acid treatments to dissolve feedstock minerals more rapidly, or altering tailings storage design to maximise reactive surface areas (Hamilton et al., in prep-a; Lechat et al., 2016; McCutcheon et al., 2015; McCutcheon et al., 2017; McCutcheon et al., 2016).

Promoting the formation of hydrotalcites may represent one way to enhance carbon sequestration rates at some mine sites. In addition to being a potential carbon sink through the carbonation of Fe-rich brucite or via anion exchange between tailings fluids and existing non-carbonate-bearing hydrotalcites, these minerals have the potential to offer co-benefits such as safely trapping other contaminants associated with hard-rock mining given the wide variety of cationic and anionic complexes that can be incorporated into their crystal structures. However, before the maximum CO<sub>2</sub> sequestration potential of hydrotalcite minerals can be realised, there are several fundamental knowledge gaps that need to be closed. Understanding the formation and dissolution mechanisms of hydrotalcites is fundamental to harnessing them for sequestering CO<sub>2</sub>, and ensuring that atmospheric CO<sub>2</sub> does not end up being released from these minerals into the atmosphere. A key step in the process is establishing how to determine whether hydrotalcites have formed *in situ* within the tailings or whether they were already present as part of the ore mineralogy, this understanding is necessary to establish whether hydrotalcites are a net sink for atmospheric carbon. Stable C, O and Mg isotopes provide a potential avenue for fingerprinting the origins of hydrotalcite minerals; however, the lack of previous literature regarding stable isotope signatures and fractionation factors of hydrotalcites means that these fundamental aspects must first be researched and understood before they can be applied to the issue of carbon mineralisation.

Once these fundamental questions regarding (1) how hydrotalcites form, (2) their environmental stability and (3) how they sequester carbon are understood, production of hydrotalcite minerals may be a useful addition to carbon mineralisation technologies in the future.

## 2.5 References

- Ashwal, L.D., and Cairncross, B. (1997) Mineralogy and origin of stichtite in chromite-bearing serpentinites. *Contributions to Mineralogy and Petrology*, 127(1-2), 75-86.
- Assima, G.P., Larachi, F., Beaudoin, G., and Molson, J. (2012) CO<sub>2</sub> Sequestration in Chrysotile Mining Residues—Implication of Watering and Passivation under Environmental Conditions. *Industrial & Engineering Chemistry Research*, 51(26), 8726-8734.
- Assima, G.P., Larachi, F., Beaudoin, G., and Molson, J. (2013) Dynamics of carbon dioxide uptake in chrysotile mining residues – Effect of mineralogy and liquid saturation. *International Journal of Greenhouse Gas Control*, 12, 124-135.
- Bacocchi, R., Costa, G., Poletti, A., and Pomi, R. (2009) Influence of particle size on the carbonation of stainless steel slag for CO<sub>2</sub> storage. *Energy Procedia*, 1(1), 4859-4866.
- Barry, J.P., Buck, K.R., Lovera, C.F., Kuhnz, L., Whaling, P.J., Peltzer, E.T., Walz, P., and Brewer, P.G. (2004) Effects of Direct Ocean CO<sub>2</sub> Injection on Deep-Sea Meiofauna. *Journal of Oceanography*, 60(4), 759-766.

- Bea, S.A., Wilson, S.A., Mayer, K.U., Dipple, G.M., Power, I.M., and Gamazo, P. (2012) Reactive transport modeling of natural carbon sequestration in ultramafic mine tailings. *Vadose Zone Journal*, 11(2).
- Beinlich, A., and Austrheim, H. (2012) In situ sequestration of atmospheric CO<sub>2</sub> at low temperature and surface cracking of serpentinized peridotite in mine shafts. *Chemical Geology*, 332–333, 32-44.
- BHP. (2005) Mt Keith Nickel Operations: Environmental Data. BHP Billiton Sustainable Development Reports.
- Bish, D.L. (1980) Anion-exchange in takovite: applications to other hydroxalcalite minerals. *Bulletin Mineralogie*, 103, 170-175.
- Bish, D.L., and Brindley, G.W. (1977) A reinvestigation of takovite, a nickel aluminium hydroxy-carbonate of the pyroaurite group. *American Mineralogist*, 62, 458-464.
- Bobicki, E.R., Liu, Q., Xu, Z., and Zeng, H. (2012) Carbon capture and storage using alkaline industrial wastes. *Progress in Energy and Combustion Science*, 38(2), 302-320.
- Bonenfant, D., Kharoune, L., Sauvé, S.b., Hausler, R., Niquette, P., Mimeault, M., and Kharoune, M. (2008a) CO<sub>2</sub> Sequestration by Aqueous Red Mud Carbonation at Ambient Pressure and Temperature. *Industrial & Engineering Chemistry Research*, 47(20), 7617-7622.
- Bonenfant, D., Kharoune, L., Sauvé, S.b., Hausler, R., Niquette, P., Mimeault, M., and Kharoune, M. (2008b) CO<sub>2</sub> Sequestration Potential of Steel Slags at Ambient Pressure and Temperature. *Industrial & Engineering Chemistry Research*, 47(20), 7610-7616.

- Bookin, A.S., Cherkashin, V.I., and Drits, V.A. (1993a) Polytype diversity of the hydrotalcite-like minerals II. Determination of the polytypes of experimentally studied varieties. *Clays and Clay Minerals*, 41(5), 558-564.
- Bookin, A.S., Cherkashin, V.I., and Drits, V.A. (1993b) Reinterpretation of the X-ray diffraction patterns of stichtite and reevesite. *Clays and Clay Minerals*, 41(5), 631-634.
- Bookin, A.S., and Drits, V.A. (1993) Polytype diversity of the hydrotalcite-like minerals 1. Possible polytypes and their diffraction features. *Clays and Clay Minerals*, 41(5), 551-557.
- Bottrill, R.S. (2008) A mineralogical field guide for a Western tasmania minerals and museums tour. In E.a.R. Department of Infrastructure, Ed. Mineral Resources Tasmania.
- Bottrill, R.S., and Baker, W.E. (2008) A Catalogue of The Minerals of Tasmania. In E.a.R. Department of Infrastructure, Ed. Mineral resources Tasmania.
- Brindley, G.W., and Bish, D.L. (1976) Green rust: a pyroaurite type structure. *Nature*, 263, 353.
- CarbFix. (2018) [www.or.is](http://www.or.is). CarbFix, <https://www.or.is/carbfix>, 21/03/2018. Fjarskipti ehf.
- Cavani, F., Trifirò, F., and Vaccari, A. (1991) Hydrotalcite-type anionic clays: Preparation, properties and applications. *Catalysis Today*, 11(2), 173-301.
- Chang, E.E., Chen, C.H., Chen, Y.H., Pan, S.Y., and Chiang, P.C. (2011) Performance evaluation for carbonation of steel-making slags in a slurry reactor. *J Hazard Mater*, 186(1), 558-64.
- Chemicals, C. (2018) Carbonfree Chemicals | Welcome to an energy company that makes greenhouse gases good for the environment. Carbonfree Chemicals, <http://www.carbonfreechem.com/>, 12/03/2018. Rackspace Hosting.

- Cleugh, H., Smith, M.S., Battaglia, M., and Graham, P. (2011) *Climate Change Science and Solutions for Australia*. CSIRO Publishing, 150 Oxford Street Collingwood VIC Australia.
- CO2CRC. (2018) Home - CO2CRC. CO2CRC, <http://www.co2crc.com.au/>, 12/03/2018. The University of Melbourne.
- Douglas, G., Shackleton, M., and Woods, P. (2014) Hydrotalcite formation facilitates effective contaminant and radionuclide removal from acidic uranium mine barren lixiviant. *Applied Geochemistry*, 42(0), 27-37.
- Douglas, G.B., Wendling, L.A., Pleysier, R., and Trefry, M. (2010) Hydrotalcite Formation for Contaminant Removal from Ranger Mine Process Water. *MINE WATER AND THE ENVIRONMENT*, 29, 108-115.
- Evans, D.G., and Slade, R.C.T. (2006) Structural Aspects of layered Double Hydroxides. In X. Duan, and D.G. Evans, Eds. *Layered Double Hydroxides*, 119, p. 1-87. Springer.
- Fernandez Bertos, M., Li, X., Simons, S.J.R., Hills, C.D., and Carey, P.J. (2004) Investigation of accelerated carbonation for the stabilisation of MSW incinerator ashes and the sequestration of CO<sub>2</sub>. *Green Chemistry*, 6(8), 428-436.
- Foshag, W.F. (1920) The Chemical Composition of Hydrotalcite and the Hydrotalcite Group of Minerals. *Proceedings U. S. National Museum* 58, 147-153.
- Fron del, C. (1941) Constitution and polymorphism of the pyroaurite and sjogrenite groups. *The American Mineralogist*, 26(5), 295-315.
- Ghezloun, A., Saidane, A., and Merabet, H. (2017) The COP 22 New commitments in support of the Paris Agreement. *Energy Procedia*, 119, 10-16.
- Glen, R.A., and Butt, B.C. (1981) Chrysotile asbestos at Woodsreef, New South Wales. *Economic Geology and the Bulletin of the Society of Economic Geologists*, 76(5), 1153-1169.

- Goh, K.H., Lim, T.T., and Dong, Z. (2008) Application of layered double hydroxides for removal of oxyanions: A review. *Water Research*, 42, 1343-1368.
- Gras, A., Beaudoin, G., Molson, J., Plante, B., Bussière, B., Lemieux, J.M., and Dupont, P.P. (2017) Isotopic evidence of passive mineral carbonation in mine wastes from the Dumont Nickel Project (Abitibi, Quebec). *International Journal of Greenhouse Gas Control*, 60, 10-23.
- Grguric, B.A. (2003) Minerals of the MKD5 nickel deposit, Mount Keith, Western Australia. *Australian Journal of Mineralogy*, 9(2), 55-71.
- Grguric, B.A., Madsen, I.C., and Pring, A. (2001) Woodallite, a new strontium analogue of iowaite from the Mount Keith nickel deposit, Western Australia. *Mineralogical Magazine*, 65(3), 427-435.
- Hamilton, J.L., Turvey, C.C., Tait, A.W., and Wilson, S.A. (in prep-a) Accelerating mineral carbonation at ultramafic mines via direct CO<sub>2</sub> reaction and heap leaching, and potential for base metal enrichment and recovery. In preparation.
- Hamilton, J.L., Wilson, S.A., Turvey, C.C., Tait, A.W., McCutcheon, J., Fallon, S.J., and Southam, G. (in prep-b) Field-based deployment of an automated geochemical treatment system for accelerating carbonation of ultramafic mine tailings: Lessons for pilot projects and carbon accounting in mined landscapes. In preparation.
- Hansen, H.C.B., and Taylor, R.M. (1991) The Use of Glycerol Intercalates in the Exchange of CO<sub>3</sub><sup>2-</sup> with SO<sub>4</sub><sup>2-</sup>, NO<sub>3</sub><sup>-</sup> or Cl<sup>-</sup> in Pyroaurite-type Compounds. *Clay Minerals*, 26, 311-327.
- Harrison, A.L., Dipple, G.M., Power, I.M., and Mayer, K.U. (2015) Influence of surface passivation and water content on mineral reactions in unsaturated porous media: Implications for brucite carbonation and CO<sub>2</sub> sequestration. *Geochimica et Cosmochimica Acta*, 148, 477-495.

- Harrison, A.L., Power, I.M., and Dipple, G.M. (2013) Accelerated carbonation of brucite in mine tailings for carbon sequestration. *Environmental Science and Technology*, 47(1), 126-134.
- Haugan, P.M. (2004) Metrics to assess the mitigation of global warming by carbon capture and storage in the ocean and in geological reservoirs. *Geophysical Research Letters*, 31(18).
- Hayashi, H., Kanie, K., Shinoda, K., Marumatsu, A., Suzuki, S., and Sasaki, H. (2009) pH-dependence of selenate removal from liquid phase by reductive Fe(II)–Fe(III)hydroxysulfate compound, green rust. *Chemosphere*, 76, 638-643.
- Hitch, M., Ballantyne, S.M., and Hindle, S.R. (2010) Revaluing mine waste rock for carbon capture and storage. *International Journal of Mining, Reclamation and Environment*, 24(1), 64-79.
- Hostetler, P.B., Coleman, R.G., A., M.F., and Evans, B.W. (1966) Brucite in Alpine Serpentinites. *The American Mineralogist*, 51, 75-98.
- Houghton, J.T., Ding, Y., Griggs, D.J., Noguera, M., van der Linden, P.J., Dai, X., Maskell, K., and Johnson, C.A. (2001) *Climate Change 2001: The Scientific Basis: Contribution of Working Group 1 to the Third Assessment Report of the Intergovernmental Panel on Climate Change*. Cambridge University Press, U.K.
- Hoyo, C.D. (2007) Layered double hydroxides and human health: An overview. *Applied Clay Science*, 36, 103-121.
- Hudson, D.R., and Bussell, M. (1981) Mountkeithite, a new pyroaurite-related mineral with an expanded interlayer containing exchangeable MgSO<sub>4</sub>. *Mineralogical Magazine*, 44, 345-350.

- Huntzinger, D.N., Gierke, J.S., Kawatra, S.K., Eisele, T.C., and Sutter, L.L. (2009a) Carbon dioxide sequestration in cement kiln dust through mineral carbonation. *Environmental Science and Technology*, 43(6), 1986-1992.
- Huntzinger, D.N., Gierke, J.S., Sutter, L.L., Kawatra, S.K., and Eisele, T.C. (2009b) Mineral carbonation for carbon sequestration in cement kiln dust from waste piles. *Journal of Hazardous Materials*, 168(1), 31-37.
- Hussein, M.Z., Rahman, N.S.S.A., Sarijo, S.H., and Zainal, Z. (2012) Herbicide-Intercalated Zinc Layered Hydroxide Nanohybrid for a Dual-Guest Controlled Release Formulation. *International Journal of Molecular Sciences*, 13, 7328-7342.
- Imran, A., López-Rayó, S., Magid, J., and Hansen, H.C.B. (2016) Dissolution kinetics of pyroaurite-type layered double hydroxide doped with Zn: Perspectives for pH controlled micronutrient release. *Applied Clay Science*, 123(Supplement C), 56-63.
- IPCC. (2005) IPCC Special Report on Carbon Dioxide Capture and Storage. In O.D. Bert Metz, Heleen de Coninck, Manuela Loos, Leo Meyer, Ed, p. 442. Cambridge University Press, 40 West 20th Street, New York, NY 10011–4211, USA.
- IPCC. (2013) Climate Change 2013: The Physical Science Basis. In IPCC, Ed. IPCC Working Group 1.
- IPCC. (2014) Climate Change 2014 Mitigation of Climate Change. In IPCC, Ed. IPCC Working Group 3.
- Johnson, T.M., and Bullen, T.D. (2003) Selenium isotope fractionation during reduction by Fe(II)-Fe(III) hydroxide-sulfate(green rust). *Geochimica et Cosmochimica Acta*, 67(3), 413-419.
- Kakizawa, M., Yamasaki, A., and Yanagisawa, Y. (2001) A new CO<sub>2</sub> disposal process via artificial weathering of calcium silicate accelerated by acetic acid. *Energy*, 26(4), 341-354.

- Katz, M.B. (1986) Tectonic analysis of the faulting at Woodsreef Asbestos Mine and its possible relationship to the kinematics of the Peel Fault. *Australian Journal of Earth Sciences*, 33(1), 99-105.
- Lackner, K.S. (2002) Carbonate Chemistry for Sequestering Fossil Carbon. *Annual Review of Energy and the Environment*, 27(1), 193-232.
- Lackner, K.S. (2003) A Guide to CO<sub>2</sub> Sequestration. *Science*, 300, 1677-1678.
- Lackner, K.S., Wendt, C.H., Butt, D.P., Joyce Jr, E.L., and Sharp, D.H. (1995) Carbon dioxide disposal in carbonate minerals. *Energy*, 20(11), 1153-1170.
- Lechat, K., Lemieux, J.M., Molson, J.W., Beaudoin, G., and Hebert, R. (2016) Field evidence of CO<sub>2</sub> sequestration by mineral carbonation in ultramafic milling wastes, Thetford Mines, Canada. *International Journal of Greenhouse Gas Control*, 47, 110-121.
- Loewenstein, W. (1954) The distribution of aluminum in the tetra-hedra of silicates and aluminates. *American Mineralogist*, 39, 92-96.
- Matter, J.M., Broecker, W.S., Gislason, S.R., Gunnlaugsson, E., Oelkers, E.H., Stute, M., Sigurdardóttir, H., Stefansson, A., Alfreðsson, H.A., Aradóttir, E.S., Axelsson, G., Sigfússon, B., and Wolff-Boenisch, D. (2011) The CarbFix Pilot Project—Storing carbon dioxide in basalt. *Energy Procedia*, 4, 5579-5585.
- Matter, J.M., and Kelemen, P.B. (2009) Permanent storage of carbon dioxide in geological reservoirs by mineral carbonation. *Nature Geoscience*, 2(12), 837-841.
- Matter, J.M., Stute, M., Snæbjörnsdóttir, S.Ó., Oelkers, E.H., Gislason, S.R., Aradóttir, E.S., Sigfússon, B., Gunnarsson, I., Sigurdardóttir, H., Gunnlaugsson, E., Axelsson, G., Alfreðsson, H.A., Wolff-Boenisch, D., Mesfin, K., Taya, D.F.d.l.R., Hall, J., Dideriksen, K., and Broecker, W.S. (2016) Rapid carbon mineralization for

permanent disposal of anthropogenic carbon dioxide emissions. *Science*, 352(6291), 1312-1314.

Mavromatis, V., Bundeleva, I.A., Shirokova, L.S., Millo, C., Pokrovsky, O.S., Bénézech, P., Ader, M., and Oelkers, E.H. (2015) The continuous re-equilibration of carbon isotope compositions of hydrous Mg carbonates in the presence of cyanobacteria. *Chemical Geology*, 404(Supplement C), 41-51.

McCutcheon, J., Dipple, G.M., Wilson, S.A., and Southam, G. (2015) Production of magnesium-rich solutions by acid leaching of chrysotile: A precursor to field-scale deployment of microbially enabled carbonate mineral precipitation. *Chemical Geology*, 413, 119-131.

McCutcheon, J., Turvey, C.C., Hamilton, J.L., Wilson, S.A., and Southam, G. (2017) Experimental Deployment of Microbial Mineral Carbonation at an Asbestos Mine: Potential Applications to Carbon Storage and Tailings Stabilization. *Minerals*, 7(191).

McCutcheon, J., Wilson, S.A., and Southam, G. (2016) Microbially accelerated carbonate mineral precipitation as a strategy for in situ carbon sequestration and rehabilitation of asbestos mine sites. *Environmental Science & Technology*, 50(3), 1419-1427.

Melchiorre, E.B., Bottrill, R., Huss, G.R., and Lopez, A. (2016) Conditions of Stichtite ( $\text{Mg}_6\text{Cr}_2(\text{OH})_{16}[\text{CO}_3] \cdot 4\text{H}_2\text{O}$ ) formation and its Geochemical and Isotope Record of Early Phanerozoic Serpentinizing Environments. *Geochimica et Cosmochimica Acta*.

Melchiorre, E.B., Bottrill, R., Huss, G.R., and Lopez, A. (2018) The Early Earth Geochemical and Isotope Record of Serpentinizing Environments from Archean Stichtite ( $\text{Mg}_6\text{Cr}_2(\text{OH})_{16}[\text{CO}_3] \cdot 4\text{H}_2\text{O}$ ). *Precambrian Research*.

- Melchiorre, E.B., Huss, G.R., and Lopez, A. (2014) Carbon and hydrogen stable isotope microanalysis and data correction for rare carbonate minerals: Case studies for stichtite ( $\text{Mg}_6\text{Cr}_2[(\text{OH})_{16}[\text{CO}_3]\cdot\text{H}_2\text{O}]$ ) and malachite ( $\text{Cu}_2\text{CO}_3(\text{OH})_2$ ). *Chemical Geology*, 367, 63-69.
- Merril, R.J., Butt, B.C., Forrest, V.C., Purdon, G., and Bramley-Moore, R.A. (1980) Asbestos Production at Chrysotile Corporation of Australia Pty. Limited, Barraba, N.S.W. In J.T. Woodcock, Ed. *Mining and Metallurgical Practices in Australasia*, 10, p. 669-673. The Australasian Institute of Mining and Metallurgy, Clunies Ross House, 191 Royal Parade, Parkville, Victoria, Australia 3052.
- Mervine, E., Wickens, P., Wilson, S.A., Power, I.M., Vanderzee, S., Turvey, C.C., Hamilton, J.L., Dipple, G., Southam, G., Miya, Z., and Fulop, A. (2017) Carbon Storage Potential of Kimberlite Mine Tailings. Oppenheimer-De Beers Group Research Conference, Ormonde, Johannesburg, South Africa.
- Millar, R.J., Fuglestedt, J.S., Friedlingstein, P., Rogelj, J., Grubb, M.J., Matthews, H.D., Skeie, R.B., Forster, P.M., Frame, D.J., and Allen, M.J. (2017) Emission budgets and pathways consistent with limiting warming to 1.5°C. *Nature Geoscience*, 10, 741-748.
- Mills, S.J., Christy, A.G., Génin, J.M.R., Kameda, T., and Colombo, F. (2012) Nomenclature of the hydrotalcite supergroup: natural layered double hydroxides. *Mineralogical Magazine*, 76(5), 1289-1336.
- Mills, S.J., Whitfield, P.S., Wilson, S.A., Woodhouse, J.N., Dipple, G.M., Raudsepp, M., and Francis, C.A. (2011) The crystal structure of stichtite, re-examination of barbertonite, and the nature of polytypism in MgCr hydrotalcites. *American Mineralogist*, 96(1), 179-187.

- Mineralcarbonation.com. (2018) MCI – A large scale permanent and safe technology for storing and utilising CO<sub>2</sub> in building products. Mineral Carbonation International, <http://mineralcarbonation.com/>, 12/03/2018, GoDaddy.com LLC.
- Miyata, S. (1975) The Syntheses of Hydrotalcite-Like Compounds and Their Structures and Physico-Chemical Properties -1: The Systems Mg<sup>2+</sup>-Al<sup>3+</sup>-NO<sub>3</sub><sup>-</sup>, Mg<sup>2+</sup>-Al<sup>3+</sup>-Cl<sup>-</sup>, Mg<sup>2+</sup>-Al<sup>3+</sup>-ClO<sub>4</sub><sup>-</sup>, Ni<sup>2+</sup>-Al<sup>3+</sup>-Cl<sup>-</sup>, AND Zn<sup>2+</sup>-Al<sup>3+</sup>-Cl<sup>-</sup>. *Clays and Clay Minerals*, 23(5), 369-375.
- Miyata, S. (1983) Anion-exchange properties of hydrotalcite-like compounds. *Clays and Clay Minerals*, 31(4), 305-311.
- Miyata, S., and Okada, A. (1977) Synthesis of Hydrotalcite-like compounds and their physico-chemical properties - the systems Mg<sup>2+</sup>-Al<sup>3+</sup>-SO<sub>4</sub><sup>2-</sup> and Mg<sup>2+</sup>-Al<sup>3+</sup>-CrO<sub>4</sub><sup>2-</sup>. *Clays and Clay Minerals*, 25, 14-18.
- Mumpton, F.A., Jaffe, H.W., and S., T.C. (1965) Coalingite, a new mineral from the New Idria Serpentinite, Fresno and San Benito counties, California. *The American Mineralogist*, 50, 1893-1913.
- Mumpton, F.A., and Thompson, C.S. (1966) The Stability of Brucite in the Weathering Zone of the New Idria Serpentinite. *Clays and Clay Minerals*, 14(1), 249-257.
- Nam, S.-Y., Seo, J., Thriveni, T., and Ahn, J.-W. (2012) Accelerated carbonation of municipal solid waste incineration bottom ash for CO<sub>2</sub> sequestration. *Geosystem Engineering*, 15(4), 305-311.
- O'Connor, W.K., Dahlin, D.C., Dahlin, C.L., and Collins, W.K. (2002) Carbon Dioxide Sequestration by Direct Mineralogy Carbonation: Process Mineralogy of Feed and Products. *Minerals & metallurgical processing*, 19(2), 95-101.

- O'Neil, J.R., and Barnes, I. (1971) C13 and O18 compositions in some fresh-water carbonates associated with ultramafic rocks and serpentinites; western United States. *Geochimica et Cosmochimica Acta*, 35, 687-697.
- Oelkers, E.H., Berninger, U.-N., Pérez-Fernández, A., Chmieleff, J., and Mavromatis, V. (2018) The temporal evolution of magnesium isotope fractionation during hydromagnesite dissolution, precipitation, and at equilibrium. *Geochimica et Cosmochimica Acta*, 226, 36-49.
- Oelkers, E.H., Gislason, S.R., and Matter, J. (2008) Mineral Carbonation of CO<sub>2</sub>. *Elements*, 4, 333-337.
- Offler, R., Glen, R.A., Hyodo, H., and Jiang, Z. (2004) Subduction of arc basaltic andesite: Implications for the tectonic history of the southern New England Fold Belt. *Australian Journal of Earth Sciences*, 51(6), 819-830.
- Offler, R., O'Hanley, D.S., and Lennox, P.G. (1997) Tectonic significance of veins and associated structures at Woodsreef, New South Wales. *Special Publication - Geological Society of Australia*, 19, 226-241.
- Offler, R., and Shaw, S. (2006) Horneblende Gabbro Block in Serpentinite Melange, Peel-Manning Fault System, New South Wales, Australia: Lu-Hf and U-Pb Isotopic Evidence for Mantle-Derived, Late Ordovician Igneous Activity. *The Journal of Geology*, 114(2), 211-230.
- Oskierski, H.C., Dlugogorski, B.Z., and Jacobsen, G. (2013) Sequestration of atmospheric CO<sub>2</sub> in chrysotile mine tailings of the Woodsreef Asbestos Mine, Australia: Quantitative Mineralogy, isotopic fingerprinting and carbonation rates. *Chemical Geology*.
- Pacala, S., and Socolow, R. (2004) Stabilization Wedges: Solving the Climate Problem for the Next 50 Years with Current Technologies. *Science*, 305.

- Parello, M.L., Rojas, R., and Giacomelli, C.E. (2010) Dissolution kinetics and mechanism of Mg–Al layered double hydroxides: A simple approach to describe drug release in acid media. *Journal of Colloid and Interface Science*, 351(1), 134-139.
- Park, A.A., and Fan, L.S. (2004) CO<sub>2</sub> mineral sequestration: physically activated dissolution of serpentine and pH swing process. *Chemical Engineering Science*, 59, 5241-5247.
- Perez-Lopez, R., Montes-Hernandez, G., Nieto, J.M., Renard, F., and Charlet, L. (2008) Carbonation of alkaline paper mill waste to reduce CO<sub>2</sub> greenhouse gas emissions into the atmosphere. *Applied Geochemistry*, 23(8), 2292-2300.
- Petterd, W.F., Ward, L.K., Hezner, L., and Himmelbauer, A. (1914) Stichtite A New Tasmanian Mineral. In W.H. Twelvetrees, Ed. Tasmania Department of Mines, John Vail. Government Printer Hobart.
- Pevzner, R., Shulakova, V., Kepic, A., and Urosevic, M. (2011) Repeatability analysis of land time-lapse seismic data: CO<sub>2</sub>CRC Otway pilot project case study. *Geophysical Prospecting*, 59(1), 66-77.
- Portner, H.O., Langenbuch, M., and Reipschlager, A. (2004) Biological Impact of Elevated Ocean CO<sub>2</sub> Concentrations: Lessons from Animal Physiology and Earth History. *Journal of Oceanography*, 60, 705-718.
- Power, I.M., Wilson, S.A., and Dipple, G.M. (2013) Serpentinite Carbonation for CO<sub>2</sub> Sequestration. *Elements*, 9, 115-121.
- Pronost, J., Beaudoin, G., Lemieux, J.M., Hebert, R., Constantin, M., Marcouiller, S., Klein, M., Duchesne, J., Molson, J.W., Larachi, F., and Maldague, X. (2012) CO<sub>2</sub>-depleted warm air venting from chrysotile milling waste (Thetford Mines, Canada): Evidence for in-situ carbon capture from the atmosphere. *Geology*, 40(3), 275-278.
- Reichle, W.T. (1986) Synthesis of anionic clay minerals (mixed metal hydroxides, hydrotalcite). *Solid State Ionics*, 22(1), 135-141.

- Reid, M. (1925) The Dundas Mineral Field. In D.o. Mines, Ed, John Vail, Government Printer, Hobart.
- Rubin, E.S., Chen, C., and Rao, A.B. (2007) Cost and performance of fossil fuel power plants with CO<sub>2</sub> capture and storage. *Energy Policy*, 35(9), 4444-4454.
- Sahu, R.C., Patel, R.K., and Ray, B.C. (2010) Neutralization of red mud using CO<sub>2</sub> sequestration cycle. *Journal of Hazardous Materials*, 179(1–3), 28-34.
- Schellenger, A.E., and Larese-Casanova, P. (2013) Oxygen isotope indicators of selenate reaction with Fe(II) and Fe(III) hydroxides. *Environ Sci Technol*, 47(12), 6254-62.
- Seifritz, W. (1990) CO<sub>2</sub> disposal by means of silicates *Nature*, 345.
- Seymour, D.B., and McMclenaghan, M.P. (2003) Dundas. Digital Geological Atlas 1:25 00 Scale Series 3636.
- Shulakova, V., Pevzner, R., Christian Dupuis, J., Urosevic, M., Tertyshnikov, K., Lumley, D.E., and Gurevich, B. (2015) Burying receivers for improved time-lapse seismic repeatability: CO<sub>2</sub>CRC Otway field experiment. *Geophysical Prospecting*, 63(1), 55-69.
- Sittinger, R., and Sittinger, C. (2008) July 2008 Mineral of the Month: Stichtite. Mineral of the Month. Mineral of the Month Club, 1770 Orville Avenue Cambria, CA.
- Snæbjörnsdóttir, S.Ó., Wiese, F., Fridriksson, T., Armansson, H., Einarsson, G.M., and Gislason, S.R. (2014) CO<sub>2</sub> storage potential of basaltic rocks in Iceland and the oceanic ridges. *Energy Procedia*, 63, 4585-4600.
- Stewart, C., and hessami, M.-A. (2005) A study of methods of carbon dioxide capture and sequestration-the sustainability of a photosynthetic bioreactor approach. *Energy Conversion and Management*, 46, 403-420.

- Tamburri, M.N., Peltzer, E.T., Friederich, G.E., Aya, I., Yamane, K., and Brewer, P.G. (2000) A field study of the effects of CO<sub>2</sub> ocean disposal on mobile deep-sea animals. *Marine Chemistry*, 72(2–4), 95-101.
- Teir, S., Kuusik, R., Fogelholm, C.-J., and Zevenhoven, R. (2007) Production of magnesium carbonates from serpentinite for long-term storage of CO<sub>2</sub>. *International Journal of Mineral Processing*, 85(1–3), 1-15.
- Turvey, C.C., Wilson, S.A., Hamilton, J.L., and Southam, G. (2017) Field-based accounting of CO<sub>2</sub> sequestration in ultramafic mine wastes using portable X-ray diffraction. *American Mineralogist*.
- Uibu, M., Velts, O., and Kuusik, R. (2010) Developments in CO<sub>2</sub> mineral carbonation of oil shale ash. *Journal of Hazardous Materials*, 174(1–3), 209-214.
- Vaccari, A. (1998) Preparation and catalytic properties of cationic and anionic clays. *Catalysis Today*, 41(1–3), 53-71.
- Van der Zwaan, B., and Smekens, K. (2009) CO<sub>2</sub> Capture and Storage with Leakage in an Energy-Climate Model. *Environmental Modeling & Assessment*, 14(2), 135-148.
- Wilson, S.A., Barker, S.L.L., Dipple, G.M., and Atudorei, V. (2010) Isotopic Disequilibrium during uptake of Atmospheric CO<sub>2</sub> into Mine Process Waters: Implications for CO<sub>2</sub> Sequestration. *Environmental Science & Technology*, 44, 9522-9529.
- Wilson, S.A., Dipple, G.M., Power, I.M., Thom, J.M., Anderson, R.G., Raudsepp, M., Gabites, J.E., and Southam, G. (2009a) Carbon Dioxide Fixation within Mine Wastes of Ultramafic-Hosted Ore Deposits: Examples from the Clinton Creek and Cassiar Chrysotile Deposits, Canada. *Economic geology*, 104, 95–112.
- Wilson, S.A., Harrison, A.L., Dipple, G.M., Power, I.M., Barker, S.L.L., Mayer, K.U., Fallon, S.J., Raudsepp, M., and Southam, G. (2014) Offsetting of CO<sub>2</sub> emissions by air capture in mine tailings at the Mount Keith Nickel mine, Western Australia: Rates,

controls and prospects for carbon neutral mining. *International Journal of Greenhouse Gas Control*, 25, 121-140.

Wilson, S.A., Raudsepp, M., and Dipple, G.M. (2006) Verifying and quantifying carbon fixation in minerals from serpentine-rich mine tailings using the Rietveld method with X-ray powder diffraction data. *American Mineralogist*, 91(8-9), 1331-1341.

Wilson, S.A., Raudsepp, M., and Dipple, G.M. (2009b) Quantifying carbon fixation in trace minerals from processed kimberlite; a comparative study of quantitative methods using X-ray powder diffraction data with applications to the Diavik diamond mine, Northwest Territories, Canada. *Applied Geochemistry*, 24(12), 2312-2331.

Woodhouse, J. (2006) The characterization of hydrotalcite-group minerals and their anion exchange capabilities at mount keith nickel mine, Western Australia. Unpublished masters thesis.

Xu, Z.P., Zeng, Q.H., Lu, G.Q., and Yu, A.B. (2006) Inorganic nanoparticles as carriers for efficient cellular delivery. *Chemical Engineering Science*, 61(1027-1040).

Yadav, V.S., Prasad, M., Khan, J., Amritphale, S.S., Singh, M., and Raju, C.B. (2010) Sequestration of carbon dioxide (CO<sub>2</sub>) using red mud. *Journal of Hazardous Materials*, 176(1–3), 1044-1050.

Yang, H., Xu, Z., Fan, M., Gupta, R., Slimane, R.B., Bland, A.E., and Wright, I. (2008) Progress in carbon dioxide separation and capture: A review. *Journal of Environmental Sciences*, 20, 14-27.

Zarandi, A.E., Larachi, F., Beaudoin, G., Plante, B., and Sciortino, M. (2017) Ambient mineral carbonation of different lithologies of mafic to ultramafic mining wastes/tailings – A comparative study. *International Journal of Greenhouse Gas Control*, 63, 392-400.

Zoback, M.D., and Gorelick, S.M. (2012) Earthquake triggering and large-scale geologic storage of carbon dioxide. *Proceedings of the National Academy of Sciences*, 109(26), 10164-10168.



## Declaration for Thesis Chapter 3

Declaration by candidate

In the case of Chapter 3, the nature and extent of my contribution is as follows:

Nature of Contribution	Extent of contribution (%)
Concept, experimental design, conducted experiments, collected and analysed data, writing and editing.	75%

The following co-authors contributed to the work. If co-authors are students at Monash University, the extent of their contribution in percentage terms must be stated:

Name	Nature of contribution	Extent of Contribution (%)
Sasha A. Wilson	Supervisory role, concept, assisted with data analysis and had input into the manuscript	20%
Jessica L. Hamilton	Experimental design and data analysis	5%

The undersigned hereby certify that the above declaration correctly reflects the nature and extent of the candidate's and co-authors contributions to this work\*.

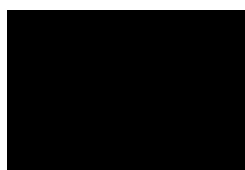
Candidate's signature:



Date:

22/03/2018

Main supervisor's signature:



Date: 22/03/2018

\* Note: Where the responsible author is not the candidate's main supervisor, the main supervisor should consult with the responsible author to agree on the respective contributions of the authors.

## Chapter 3

### **Comparison of Rietveld-compatible structureless fitting analysis methods for accurate quantification of carbon dioxide fixation in ultramafic mine tailings**

Connor C. Turvey<sup>1\*</sup>, Jessica L. Hamilton<sup>1,2a</sup> and Siobhan A. Wilson<sup>1,3a</sup>

<sup>1</sup>School of Earth, Atmosphere & Environment, Monash University, Clayton, Melbourne, Victoria 3800, Australia

<sup>2</sup>School of Earth and Environmental Sciences, The University of Queensland, St Lucia, QLD 4072, Australia

<sup>3</sup>Department of Earth and Atmospheric Sciences, University of Alberta, Edmonton, Alberta, T6G 2E3, Canada

<sup>a</sup> Current Address

Submitted to *American Mineralogist* 21/2/2018

### 3.0 Abstract

The carbonation of ultramafic rocks, including tailings from ultramafic-hosted ore deposits, can be used to remove CO<sub>2</sub> from the atmosphere and store it safely within minerals over geologic time scales. Quantitative X-ray diffraction (XRD) using the Rietveld method can be employed to estimate the amount of carbon sequestered by carbonate minerals that form as a result of weathering of ultramafic rocks. However, the presence of structurally disordered phases such as serpentine minerals, which are common in ultramafic ore bodies such as at the Woodsreef chrysotile mine (NSW, Australia), results in samples that cannot be analysed using typical Rietveld refinement strategies. Previous investigations of carbon sequestration at Woodsreef and other ultramafic mine sites typically used modified Rietveld refinement methods that apply structureless pattern fitting for disordered phases; however, no detailed comparison of the accuracy (or precision) of these methods for carbon accounting has yet been done, making it difficult to determine the most appropriate analysis method. Such an analysis would need to test whether some methods more accurately quantify the abundances of certain minerals, such as pyroaurite [Mg<sub>6</sub>Fe<sup>3+</sup><sub>2</sub>(CO<sub>3</sub>)(OH)<sub>16</sub>·4H<sub>2</sub>O] and other hydrotalcite group minerals, which suffer from severe preferred orientation and may play an important role in carbon sequestration at some mines. Here, we assess and compare the accuracy, and to a lesser extent the precision, of three different non-traditional Rietveld refinement methods for carbon accounting: (1) the PONKCS method, (2) the combined use of a Pawley fit for serpentine minerals and an internal standard (Pawley/internal standard method) and (3) the combined use of PONKCS and Pawley/internal standard methods. We examine which of these approaches represents the most accurate way to quantify the abundances of serpentine, pyroaurite and other carbonate-bearing phases in a given sample. We demonstrate that by combining the PONKCS and Pawley/internal standard methods it is possible to quantify the abundances of disordered phases in a sample and to obtain an

estimate of the amorphous content and any unaccounted intensity in an XRD pattern. Eight artificial tailings samples with known mineralogical compositions were prepared to reflect the natural variation found within the tailings at the Woodsreef chrysotile mine. Rietveld refinement results for the three methods were compared with the known compositions of each sample to calculate absolute and relative error values and to evaluate the accuracy of the three methods, including whether they produce systematic under- or overestimates of mineral abundance. Estimated standard deviations were also calculated during refinements; these values, which are a measure of precision, were not strongly affected by the choice of refinement method. The abundance of serpentine minerals is, however, systematically overestimated when using the PONKCS and Pawley/internal standard methods, and the abundances of minor phases (< 10 wt%) are systematically underestimated using all three methods. Refined abundances for pyroaurite were found to be increasingly susceptible to error with increasing abundance, with an underestimation of 6.6 wt% absolute (60.6 % relative) for a sample containing 10.9 wt% pyroaurite. These significant errors are due to difficulties in mitigating preferred orientation of hydrotalcite minerals during sample preparation as well as modelling its effects on XRD patterns. The abundances of hydromagnesite [ $\text{Mg}_5(\text{CO}_3)_4(\text{OH})_2 \cdot 4\text{H}_2\text{O}$ ], another important host for atmospheric  $\text{CO}_2$  during weathering of ultramafic rocks, was consistently underestimated by all three methods, with the highest underestimation being 3.7 wt% absolute (or 25 % relative) for a sample containing 15 wt% hydromagnesite. Overall, the Pawley/internal standard method produced more accurate results than the PONKCS method, with an average bias per refinement of 6.7 wt%, compared with 10.3 wt% using PONKCS and 12.9 wt% for the combined PONKCS-Pawley/internal standard method. Furthermore, the values for refined abundance of hydromagnesite obtained from refinements using the Pawley/internal standard method were significantly more accurate than those for refinements done with the PONKCS method, with

relative errors typically less than 25 % for hydromagnesite abundances between 5 and 15 wt%. The simpler and faster sample preparation makes the PONKCS method well-suited for rapid carbon accounting, for instance in the field using a portable XRD; however, the superior accuracy gained when using an internal standard make the Pawley/internal standard method the preferable means of undertaking a detailed laboratory-based study. As all three methods displayed an underestimation of carbonate phases, applying these methods to natural samples will likely produce an underestimate of hydromagnesite and hydrotalcite group mineral abundances. As such, crystallographic accounting strategies that use modified Rietveld refinement methods produce a conservative estimate of the carbon sequestered in minerals.

**Keywords:** carbon accounting, X-ray diffraction, Rietveld analysis, PONKCS method, Pawley/internal standard method, serpentine, amorphous material, pyroaurite, hydromagnesite

### 3.1 Introduction

The release of anthropogenic CO<sub>2</sub> and other greenhouse gases into the atmosphere is causing potentially irreparable damage to the Earth's climate, with global temperature rises of between 1.5 and 2°C predicted before the end of the 21<sup>st</sup> century (Houghton et al., 2001; IPCC, 2005; IPCC, 2013; IPCC, 2014; Millar et al., 2017). This has led to the development of multiple strategies to combat the adverse impacts of anthropogenic climate change upon the planet, including the reduction of both deforestation and our reliance on fossil fuels, adoption of market controls on greenhouse gas emissions, increased use of renewable energy, and the use of carbon sequestration technologies (Cleugh et al., 2011; IPCC, 2013; IPCC, 2014; Pacala and Socolow, 2004). Carbon mineralisation is a carbon sequestration strategy that traps CO<sub>2</sub> within the crystal structures of minerals (Lackner, 2003; Lackner et al., 1995;

Seifritz, 1990). Carbon mineralisation has been proposed for capturing carbon from waste streams of power plants as well as capturing it directly from the atmosphere through passive or accelerated carbonation of mine tailings and alkaline wastes (as reviewed by Bobicki et al., 2012; Chang et al., 2011; Cleugh et al., 2011; Lackner, 2002; Leung et al., 2014; Oelkers., 2008; Power et al., 2013a; Power et al., 2013b). It has been predicted that over a timescale of  $10^6$  years, carbonate minerals will likely be the primary as sink for all anthropogenic  $\text{CO}_2$  (Kump et al., 2000); however, carbon mineralisation reactions need to be accelerated to curb net greenhouse gas emissions on a socially relevant timescale.

Ultramafic rocks, and mine tailings in particular, are of great interest for use in enhanced passive carbonation (i.e., carbonation of rocks by reaction with atmospheric  $\text{CO}_2$  at an enhanced rate) because they provide an ideal feedstock for the formation of carbonate minerals. Mg- and Ca-rich silicate and hydroxide minerals weather quickly when exposed to meteoric precipitation and atmospheric  $\text{CO}_2$ , releasing  $\text{Mg}^{2+}$  and  $\text{Ca}^{2+}$  into solution, where they react with aqueous carbonate anions to form hydrated carbonate minerals (Berner, 1990; Lackner, 2002; Oelkers et al., 2008; Power et al., 2013a). Furthermore, the mineral processing that tailings have undergone reduces grain size thereby increasing surface area and reactivity, ensuring that mineral dissolution and carbonation reactions occur over rapid time scales (Wilson et al., 2009a; Wilson et al., 2014). Previous research in this field has investigated the passive carbonation reactions that are occurring within the tailings material of several ultramafic mines in Australia, Canada and Norway (e.g., Assima et al., 2012; Bea et al., 2012; Beinlich and Austrheim, 2012; Hamilton et al., 2018; Hamilton et al., 2016; Hitch et al., 2010; Lechat et al., 2016; McCutcheon et al., 2015; McCutcheon et al., 2017; McCutcheon et al., 2016; Oskierski et al., 2013; Pronost et al., 2012; Pronost et al., 2011; Turvey et al., 2017; Wilson et al., 2009a; Wilson et al., 2014; Wilson et al., 2006; Wilson et al., 2009b). Laboratory and field trials are underway using abiotic and biological means of

enhancing these reaction rates to maximize carbon sequestration in mine wastes (e.g., Assima et al., 2013a; Assima et al., 2014a; Assima et al., 2014b; Assima et al., 2012; Beaudoin et al., 2017; Harrison et al., 2015; Harrison et al., 2013; McCutcheon et al., 2017; McCutcheon et al., 2016).

Quantifying the amount of atmospheric CO<sub>2</sub> that has been trapped within tailings storage facilities is an important first step in understanding their carbon sequestration potential and how much atmospheric CO<sub>2</sub> has already been sequestered (Wilson et al., 2009a; Wilson et al., 2014; Wilson et al., 2006). There are multiple methods for quantifying carbon fixation in minerals, which work best when used in combination. Typical bulk geochemical analyses can be used to quantify the amount of carbon stored within minerals in tailings but they cannot be used to differentiate between different carbonate-bearing phases, nor can they be used to distinguish between bedrock carbonate minerals and secondary carbonate minerals that have formed via passive capture of CO<sub>2</sub> from air. Stable and radiogenic isotopic fingerprinting can be used to trace the source of carbon in minerals but cannot be used to give a quantitative assessment of the amount CO<sub>2</sub> stored within a sample of tailings (Oskierski et al., 2013; Wilson et al., 2009a; Wilson et al., 2014). Textural observations, using microscopy, and isotopic analyses can be used in combination to determine the origin of each carbon-bearing mineral species, either as gangue minerals inherited from the ore or as an alteration phase derived from an atmospheric source of carbon (Oskierski et al., 2013; Wilson et al., 2009a; Wilson et al., 2014). Quantitative XRD can be used to provide an estimate of the weight-percent contribution of each gangue and secondary carbonate mineral in a sample of tailings, which can then be used in combination with textural and isotopic data to estimate the amount of atmospheric CO<sub>2</sub> sequestered in the tailings from stoichiometry (Wilson et al., 2006; Wilson et al., 2009a).

Performing quantitative XRD upon samples of ultramafic tailings is often challenging owing to the presence of serpentine minerals, other disordered minerals such as smectites, and amorphous phases (e.g., Mervine et al., in review; Turvey et al., 2017). Like many clay minerals, the serpentine polymorphs chrysotile, antigorite and lizardite, are affected by turbostratic stacking disorder and thus do not have well-defined crystal structures (Wicks and Whittaker, 1975). Amorphous silica and/or amorphous hydrated carbonate phases are also products of carbon mineralisation reactions that have been identified in previous studies of passive and enhanced tailings carbonation both in the laboratory (Harrison et al., 2015) and in the field at Woodsreef (McCutcheon et al., 2017; Oskierski et al., 2013). Owing to the mineralogical complexity of ultramafic rocks, traditional Rietveld refinements using powder XRD data cannot be used for quantitative phase analysis. The original Rietveld method typically requires that all phases in a mixture have well-defined and well-ordered crystal structures (Bish and Howard, 1988; Hill and Howard, 1987; Rietveld, 1969). This has been overcome in previous studies by using alternative quantitative XRD methods or by using modified Rietveld refinement methods. Wilson et al. (2009b) and Oskierski et al. (2013) used the internal standard method of Alexander and Klug (1948) and the reference intensity ratio method (Chung, 1974) to quantify individual carbon-bearing alteration minerals in serpentinite mine tailings. Although the internal standard method and reference intensity ratio method can yield more accurate quantitative estimates of low-abundance carbonate minerals (Wilson et al., 2009b), these methods are laborious to calibrate; Rietveld refinement offers the advantage of simultaneous, complete quantification of all detectable phases in sample. Previous studies such Turvey et al. (2017) and Wilson et al. (2006) have instead used modified Rietveld methods, aiming to keep the advantages of the Rietveld method while introducing structureless pattern fitting to quantify disordered phases. Turvey et al. (2017) used the Partial Or No Known Crystal Structure (PONKCS; Scarlett & Madsen,

2006) method to model the peak profiles of serpentine minerals, whereas Wilson et al. (2006) applied structureless pattern fitting with the Pawley method (Pawley, 1981) and an internal standard so that serpentine minerals could be modelled and quantified as ‘amorphous phases’. These methods have begun to see adoption by the minerals industry for carbon accounting (e.g., Mervine et al., in review), but there has not previously been a direct comparison of the PONKCS and Pawley/internal standard methods and the accuracy and precision of the results that they produce. These methods also have the potential to be applied simultaneously to quantify multiple disordered phases and amorphous phases separately (the latter without the need to create a PONKCS model) or as an estimate of the misfit between an XRD pattern and Rietveld refinement model for a sample.

The purpose of this study is four-fold. The primary objective of this work is to optimize a reproducible refinement strategy using artificial samples of serpentinite tailings that span a range of mineralogical compositions, so that this method can be applied with a high degree of accuracy to natural samples of similar composition. The second objective is to provide a direct comparison between two quantitative XRD methods, the PONKCS method (Scarlett and Madsen, 2006) and the Pawley/internal standard method (Wilson et al., 2006), when working with serpentinite tailings. This is achieved by analysis of eight artificial serpentinite tailings samples with known mineralogical compositions. The accuracy of the two methods can be assessed by comparing the known and refined values for mineral abundances. Thirdly, this study aims to assess whether the two methods can be successfully applied together to simultaneously quantify (1) multiple poorly ordered phases using PONKCS models and (2) the presence of any amorphous content or misfits caused by unaccounted for intensity in the patterns using an internal standard. Here, rather than add a known amount of an amorphous material to our samples, we use this method as a measure of misfit between our models and observed results. The fourth objective is to assess the accuracy of the PONKCS method, the

Pawley/internal standard method and the combined use of these methods for quantifying the abundance of pyroaurite  $[\text{Mg}_6\text{Fe}^{3+}_2(\text{CO}_3)(\text{OH})_{16}\cdot 4\text{H}_2\text{O}]$ , the most common hydrotalcite supergroup mineral in serpentinite-hosted ore deposits and tailings storage facilities. Pyroaurite makes up a significant portion of the tailings material at Woodsreef, and it is likely to be trapping atmospheric  $\text{CO}_2$  (Oskierski et al., 2013), thus accurately quantifying the abundance of pyroaurite is essential for successful carbon accounting at this site and at many other mines.

## **3.2 Experimental method**

### **3.2.1 Synthetic tailings samples**

Eight synthetic tailings samples of known compositions were prepared to evaluate the accuracy of the three Rietveld refinement methods and to allow for the optimization of the refinement methods. The synthetic tailings were prepared to mimic the mineralogical variation found throughout the tailings storage facility of the Woodsreef chrysotile mine, a derelict mine in New South Wales, Australia, that is the subject of ongoing research for its carbonation potential. The tailings at the Woodsreef chrysotile mine have been undergoing passive carbon mineralisation by reaction with atmospheric  $\text{CO}_2$  since mine closure in 1983 (Oskierski et al., 2013). The Woodsreef mine was Australia's largest tonnage chrysotile mine, producing 500,000 t of long-fibre chrysotile as well as 24 Mt of tailings and 75 Mt of waste rock during operation (Laughton and Green, 2002; Merrill et al., 1980). Previous studies at Woodsreef have shown that multiple carbonate minerals are present in the tailings, including secondary pyroaurite and hydromagnesite  $[\text{Mg}_5(\text{CO}_3)_4(\text{OH})_2\cdot 4\text{H}_2\text{O}]$  as well as trace amounts of gangue calcite, magnesite and dolomite, and that the tailings mineralogy is dominated by the serpentine polymorphs, lizardite and chrysotile (McCutcheon et al., 2016; Oskierski et al., 2013; Turvey et al., 2017). The compositions of the artificial tailings samples were

chosen to cover the full range of mineral abundances reported in the tailings at Woodsreef by Oskierski et al. (2013) and Turvey et al. (2017). These previous studies found that hydromagnesite was present at abundances <15 wt% and that the abundance of pyroaurite varied from 1 to 11 wt%. Known amounts of pure mineral specimens were weighed and mixed to produce the eight samples of synthetic tailings. See Table 3.1 for the compositions of the synthetic tailings samples. Samples Artrock1–4 were originally prepared for a previous study, Turvey et al. (2017), which investigated the potential use of portable XRD instruments and the PONKCS method for rapid, field-based carbon accounting. No results are replicated between this study and Turvey et al. (2017) as different Rietveld refinement strategies were used here.

**Table 3.1** Weighed composition of artificial tailings samples

		Artrock1	Artrock2	Artrock3	Artrock4	Artrock5	Artrock6	Artrock7	Artrock8
Pyroaurite	(wt%)	1.9	3.2	3.2	3.3	1.3	5.4	7.6	10.9
Magnetite	(wt%)	7.1	5.0	5.0	5.0	5.0	5.0	5.1	3.0
Brucite	(wt%)	1.1	1.8	1.8	1.8	0.2	1.1	1.5	2.2
Hydromagnesite	(wt%)	1.0	5.0	10	15	3.6	5.0	5.0	5.0
Serpentine	(wt%)	88.9	85	80	74.9	89.9	83.5	80.8	78.9
Total <sup>a</sup>	(wt%)	100.0	100.0	100.0	100.0	100.0	100.0	100.0	100.0

<sup>a</sup> Total mass of each sample was 100 g.

Several specimens of serpentine were used as components within the synthetic tailings samples, Artrock1–8. The purity of the serpentine specimens was confirmed using X-ray powder diffraction and Raman spectroscopy. The dominant polymorph of serpentine within each sample was determined using XRD patterns and Raman spectra following the recommendations of Wicks (2000) and Rinaudo et al. (2003). The serpentine specimen used to make samples Artrock1–4 is a picrolite (chrysotile) taken from the Clinton Creek mine, Yukon, Canada (previously characterized by Wilson et al. 2006). The serpentine component of Artrocks5–8 consisted of lizardite [previously described by Wilson et al. (2009b)], sourced from the mineral collection of The University of British Columbia (original locality

unknown). The hydromagnesite standard was taken from a carbonate playa near Atlin, British Columbia, Canada (07AT7-3; Power et al. 2014). The pyroaurite standard was produced by placing a natural sample of pulverized iowaite [ $\text{Mg}_6\text{Fe}^{3+}_2\text{Cl}_2(\text{OH})_{16}\cdot 4\text{H}_2\text{O}$ ] from the Mount Keith nickel mine, Western Australia in excess deionized water which was vigorously stirred for 48 hours. This method converts iowaite to pyroaurite through an anion exchange reaction using dissolved atmospheric  $\text{CO}_2$  [adapted from the work of Bish (1980) and Miyata (1983)]. Following the exchange reaction Rietveld refinement indicated that the powder contained pyroaurite-3R (92.4 wt%), and minor amounts of brucite (2.2 wt%) and residual iowaite (5.4 wt%, also a 3R polytype). The magnetite standard sourced from the mineral collection at Monash University was found to be 94.4% pure by Rietveld refinement, with minor hematite (5.6 wt%) contamination.

All artificial tailings samples were milled for seven minutes under anhydrous ethanol using a McCrone micronizing mill to reduce the mean particle size and to ensure homogenization of the samples. Samples were dried at room temperature and disaggregated with an agate mortar and pestle prior to XRD analysis. A subsample of each micronized synthetic tailings sample was spiked using 10 wt% of an in-house fluorite standard for refinements using the Pawley/internal standard method and combined use of the PONKCS and Pawley/internal standard methods. The fluorite standard was determined to be  $98.8 \pm 3.3\%$  crystalline by refinement of a 50:50 mixture by weight of the fluorite and NIST 676a  $\alpha\text{-Al}_2\text{O}_3$ . Fluorite was used as an internal standard instead of corundum in order to minimise peak overlap between the internal standard and the sample. The 0 -1 4 corundum peak at  $35.1^\circ 2\theta$  and, to a lesser extent, the 0 1 2 ( $25.5^\circ 2\theta$ ) and -1 -1 0 ( $37.8^\circ 2\theta$ ) peaks of corundum overlap with major peaks of serpentine minerals and magnetite. The diagnostic 1 1 1 and 2 0 2 fluorite peaks (at  $28.3^\circ 2\theta$  and  $47.0^\circ 2\theta$ , respectively) do not overlap with any peaks belonging to

phases that are typically found in serpentinite mine tailings (the composition of which was used as the basis for the synthetic tailings samples).

### **3.2.2 Instrument details**

XRD patterns of the synthetic tailings were collected using a Bruker D8 Advance X-ray diffractometer in the Monash X-ray Platform. Patterns were collected using a Cu X-ray tube operating at 40 kV and 40 mA, and a LynxEye 1D position sensitive detector operating over a  $2\theta$  range of  $3\text{--}80^\circ$  with a step size  $0.02^\circ$  and a dwell time of 1s/step. Samples were loaded into back loading cavity mounts against a frosted glass slide or 400 grit sandpaper to reduce preferred orientation of crystallites. Qualitative identification of minerals in the XRD patterns was performed using DIFFRAC.EVA V.2 (Bruker AXS) with reference to standard patterns from the ICDD PDF-2 database and Crystallography Open Database.

The contribution of instrumental peak broadening to XRD patterns collected from experimental samples was modelled using an instrument profile refined from a pattern of NIST SRM 660b  $\text{LaB}_6$ . Refinement of the  $\text{LaB}_6$  pattern was done using the fundamental parameters approach (Cheary and Coelho, 1992), which takes machine geometry into account, permitting an estimate of crystallite size and strain for specific minerals from refinements using XRD patterns collected from experimental samples.

### **3.2.3 Rietveld refinement strategy**

Quantitative phase analysis was performed on the artificial tailings samples using the Rietveld method (Bish and Howard, 1988; Hill and Howard, 1987; Rietveld, 1969). Three modified approaches to the Rietveld method were employed: the PONKCS method (Scarlett and Madsen, 2006), the Pawley/internal standard method (Wilson et al., 2006) and a combined PONKCS Pawley/internal standard method. Rietveld refinements typically require that all phases in a mixture be well-ordered and have well-known crystal structures,

as the mass and volume of the unit cell are used to derive a calibration factor that is used to quantify each phase (Bish and Howard, 1988). This makes quantifying mineral abundances in serpentinite tailings, such as those found at Woodsreef, and in the synthetic tailings, difficult because they are typically dominated by the presence of the serpentine polymorphs chrysotile and lizardite. Serpentine minerals, like many clay minerals, are affected by turbostratic stacking disorder, which leads to anisotropic peak broadening in XRD patterns and peaks that cannot be accurately modelled using traditional Rietveld refinements. These problems have previously been overcome by spiking the sample with an internal standard (Wilson et al., 2014; Wilson et al., 2006; Wilson et al., 2009b) and then using the Pawley method for structureless pattern fitting (Pawley, 1981), or by using the PONKCS method of Scarlett and Madsen (2006) as implemented for carbon accounting by Turvey et al. (2017).

**Table 3.2** Sources of crystal-structure data for Rietveld refinement

Mineral	Source
Pyroaurite	Olowe (1995)
Magnetite	Tsukimura et al. (1997)
Brucite	Catti et al. (1995)
Hydromagnesite	Akao and Iwai (1977)
Chrysotile	Falini et al. (2004)
Lizardite	Mellini and Viti (1994)

Quantitative phase analysis via Rietveld refinement was performed using the XRD patterns of the synthetic tailings with DIFFRAC.TOPAS v.5 (Bruker AXS), using the fundamental parameters approach (Cheary and Coelho, 1992). Background was modelled using fourth-order Chebychev polynomials with an additional  $1/x$  function. A default Brindley radius of 0.00025 mm and a packing density of 0.4 were used to correct for microabsorption contrast amongst all phases (Brindley, 1945). The sources of crystal structure information for all phases are shown in Table 3.2. The chrysotile and lizardite structures listed in Table 3.2 were then heavily modified, as described below, for implementation of the three refinement

methods to allow for quantification of the serpentine minerals within the artificial tailings samples.

**3.2.3.1 PONKCS method.** The PONKCS method can be used to quantify the abundances of multiple disordered phases, such as serpentine minerals, without the addition of an internal standard into every sample. It is an external standard method in which one or more poorly crystalline phases are modelled using structureless profile fitting. The Rietveld refinement parameters  $Z$ ,  $M$  and  $V$  are calibrated against those of an ordered, well-characterized phase, where  $Z$ =the number of formula units in the unit cell,  $M$ =the molecular mass of the formula unit and  $V$ =the unit cell volume (Scarlett and Madsen, 2006).

Two mixtures were made to create the PONKCS models for the two serpentine standards: a 50:50 wt% mix of NIST 676a  $\alpha$ -Al<sub>2</sub>O<sub>3</sub> corundum and chrysotile (from Clinton Creek, Yukon, Canada) and a 50:50 mix of NIST 676a  $\alpha$ -Al<sub>2</sub>O<sub>3</sub> and lizardite (sourced from The University of British Columbia). The space groups and unit cell parameters for lizardite and chrysotile were taken from Mellini and Viti (1994) and Falini et al. (2004), respectively. Calibrated mass ( $M$ ) values for the unit cell of each disordered serpentine phase were obtained by Rietveld refinement for the two mixtures in DIFFRAC.TOPAS v.3 (Bruker AXS) using the Pawley method for structureless pattern fitting (Pawley, 1981). Anisotropic peak shape exhibited by the serpentine minerals was modelled using the spherical harmonics approach of Stephens (1999). These refinements were used to generate  $Z$  and  $V$  values for the serpentine minerals, using Equation 1 below, where  $Z$ =the number of formula units in the unit cell,  $M$ =the molecular mass of the formula unit,  $V$ =the unit cell volume,  $S$ =the Rietveld scale factor and  $W$ =the weight fraction of the standard  $s$  and amorphous phase  $\alpha$ . Combined with the Pawley method for structureless pattern fitting this created two PONKCS

models that can be used in a similar manner to crystal structures when performing Rietveld refinements.

$$(ZV)_\alpha = \frac{W_\alpha}{W_s} \cdot \frac{S_s}{S_\alpha} \cdot \frac{(ZMV)_s}{M_\alpha} \quad (1)$$

Refinements were completed in a single step when using the PONKCS method for quantifying phases in serpentine-rich samples. Although PONKCS models were used for both lizardite and chrysotile, the refined abundances of these two phases was always summed to give a total abundance for serpentine minerals in line with the procedure that was employed in Turvey et al. (2017). Refinements were attempted using lizardite and chrysotile models individually but they were ultimately not used as they produced a worse fit (see below). The scale factors and unit cell parameters were allowed to refine for all phases. The Lorentzian crystallite size and strain values for pyroaurite, magnetite and hydromagnesite were allowed to refine from starting values of 1000 nm and 0.1, respectively. Crystallite size and strain were not refined for brucite as this phase was present at very low abundance and refining these values tended to lead to unrealistic peak broadening and unrealistically high refined abundances. A March-Dollase preferred orientation correction was used for the 0 0 3 peak of pyroaurite, 0 0 1 peak of brucite and 1 0 0 peak of hydromagnesite (using soft constraints to refine between values of 0.6 and 1). Asymmetrical peak shapes for the hydromagnesite were accounted for using a Thompson-Cox-Hasting pseudo-Voigt profile.

**3.2.3.2 Pawley/internal standard method.** Measuring the amorphous content of a sample by adding an internal standard and then performing Rietveld refinements was first proposed by (Bish and Howard, 1988). Gualtieri (2000) used the method to quantify the (amorphous) glass content of pyroclastic flows and Wilson et al. (2006) adapted the method to include structureless pattern fitting to treat disordered phases as though they were ‘amorphous’ for quantification of serpentine minerals. We used a 10 wt% spike of a well-ordered standard

(an in-house fluorite standard) to quantify the amount of the disordered phases(s) in our samples. The amount of ‘amorphous’ material,  $X_a$ , can be calculated directly from the refined and known weights of the internal standard:

$$X_a = \left(\frac{100}{90}\right) \left[1 - \left(\frac{X_s}{X_{s,c}}\right)\right] \quad (2)$$

where  $X_s$  is the measured weight of the internal standard and  $X_{s,c}$  is the refined weight of the internal standard (Gualtieri, 2000). The Pawley method (Pawley, 1981) was used to extract peak intensities independently of the scattering structure model from powder diffraction patterns of pure chrysotile and lizardite samples. The extracted intensities with appropriate space groups and unit cell dimensions of chrysotile and lizardite were used to fit the serpentine component in the patterns for the artificial tailings samples as a peaks phase as used in Wilson et al. (2006).

A similar refinement strategy was used for the Pawley/internal standard method as for the PONKCS method. A chrysotile peaks phase was used to fit the peaks of all serpentine minerals present in all of the samples (see below). Refinements were attempted using both lizardite and chrysotile peaks phases but these results were ultimately not used as they produced a worse fit. Serpentine mineral abundance was calculated using Eq.2 based on the addition of 10 wt% fluorite. Scale factors and unit-cell parameters were refined for all phases in the sample. The Lorentzian crystallite size and strain values for pyroaurite, brucite, magnetite and hydromagnesite were allowed to refine from starting values of 1000 nm and 0.1 respectively (refining to values of between 60 and 10000 nm, and 0.001–0.2 respectively). The Lorentzian crystallite size and strain values for the fluorite spike were held constant at 1000 nm and 0.1. A March-Dollase preferred orientation correction was used for the 0 0 3 peak of pyroaurite, 0 0 1 peak of brucite and 1 0 0 peak of hydromagnesite

(refining between values of 0.6 and 1). Asymmetrical peak shapes for hydromagnesite were accounted for using a Thompson-Cox-Hasting pseudo-Voigt profile.

**3.2.3.3 PONKCS Pawley/internal standard method.** We used the PONKCS method to quantify the abundances of serpentine minerals while also including a 10 wt% fluorite internal standard to measure the abundance of any amorphous material in the synthetic tailings samples and estimate the misfit between unaccounted for intensity and the refinement. The Pawley/internal standard method can be used to quantify the abundances of any number of disordered or amorphous phases or can be used to give an estimate for unaccounted for intensity in the pattern; however, all these abundances are amalgamated and reported together only as ‘amorphous content’, it cannot be used to separate the individual abundances of multiple amorphous phases, and it cannot provide a separate estimate of how much material is unaccounted for in the model (Wilson et al., 2006). Low-abundance amorphous phases that do not produce Bragg peaks can be quantified using an internal standard without applying a peak fitting procedure (Bish and Howard, 1988; Gualtieri, 2000). The PONKCS method allows for individual disordered phases to be quantified in a sample but requires that a high-purity sample of the material exists that can be used to produce a suitable peaks phase and calibrated values of Z, M, and V (Scarlett and Madsen, 2006). Combining the method of Bish and Howard (1988) and Gualtieri (2000) with that of Scarlett and Madsen (2006) has the potential to overcome some of the shortcomings associated with each method and could be used to estimate how much crystalline and amorphous material remains unaccounted for in a refinement. It could also potentially be used to quantify multiple separate disordered phases in cases where it is difficult to produce a PONKCS model for all such phases.

XRD patterns were collected from subsamples of the synthetic tailings that contained 10 wt% fluorite. No amorphous material was added to these samples. Instead, the estimate provided for 'amorphous' content using Eq.2 was used to test whether this method can be (1) used to accurately determine whether a sample contains no or a low amount of amorphous material and (2) used as a measure of goodness of fit in refinements employing PONKCS models. Rietveld refinements were performed in Topas.V5 using the structures outlined in Table 3.2, including chrysotile and lizardite structures that were used to produce structureless PONKCS models (see above). The fluorite internal standard was modelled using the same method as in the Pawley/internal standard method (see above), with the refined abundance of the internal standard was normalized to 10 wt%. Most of the phases in the artificial tailings (pyroaurite, magnetite, fluorite, brucite and hydromagnesite) were modelled using a standard Rietveld approach that relies upon structural information, whereas the peaks of the serpentine minerals (chrysotile and lizardite) were fitted using PONKCS models, and the abundance of 'amorphous' material was estimated using Eq.2.

PONKCS models were used for lizardite and chrysotile and the refined abundances for these two phases were summed to give a serpentine abundance (see section below). The crystallite size and strain values for the fluorite spike were kept constant at 1000 nm and 0.1 (as with the Pawley/internal standard method above) and a split-Pearson VII function was used to model the peak shape because it gave an improved fit compared with the fundamental parameters approach. All other refinement parameters were the same as those used in the PONKCS and Pawley/internal standard methods as outlined above, including refining scale factors and unit cell parameters, and Lorentzian size and strain for most phases; the use of a Thompson-Cox-Hastings pseudo-Voigt profile for modelling asymmetrical peak shape in hydromagnesite; and the use of a March-Dollase preferred orientation correction for pyroaurite, brucite and hydromagnesite.

**3.3.2.4 Serpentine structures.** Multiple refinement approaches were tested with all three methodologies to quantify the abundances of serpentine minerals within the artificial tailings. Refinements were done using structureless fitting models for (1) chrysotile, (2) lizardite and (3) both chrysotile and lizardite, with the individual abundances summed to model the overall serpentine abundance in the latter case, in order to determine whether the use of one or more of these models improved the accuracy of estimates for serpentine abundance. Ultimately, it was found that using both chrysotile and lizardite models produced more accurate estimates of mineral abundance and better fits when applying the PONKCS method (and combined PONKCS Pawley/internal standard method), even in cases where only one of these minerals was present in a sample. Using only the structureless model for chrysotile with the Pawley/internal standard method gave more accurate mineral abundance results than the combined use of both structureless models, including for Artrocks 5–8, which contained only lizardite. This indifference to the serpentine model that is used most likely occurs because the structureless pattern fitting procedure used here, which employs a spherical harmonics model for anisotropic peak shape (Stephens, 1999), is intended to be able to fit almost any peak shape. Lizardite and chrysotile (but not the third polymorph, antigorite) produce XRD patterns that are very similar with almost complete overlap of all major reflections (Wicks, 2000). This means that either the structureless model for lizardite or chrysotile can be used to fit the patterns produced by each of these serpentine polymorphs.

**3.3.2.5 Preferred orientation.** In addition to the serpentine minerals, the abundances of several other minerals found in ultramafic rocks are also challenging to quantify accurately because these minerals suffer from severe preferred orientation. These phases include pyroaurite, iowaite and brucite. Preferred orientation occurs where platy or fibrous minerals preferentially align along certain crystallographic directions. This can lead to a drastic increase in the intensity of some reflections for a given zone or zones, with similar decreases

in other reflections, which can result in over- or under-reporting of mineral abundances when using Rietveld refinement. Various preferred orientation corrections have been developed to account for this phenomenon including the March-Dollase correction (Dollase, 1986; Leventouri, 1997; March, 1932) and a spherical harmonics correction (Von Dreele, 1997). Back- or side-mounting techniques can also be employed during sample preparation to reduce the effects of preferred orientation. In this case, we re-collected patterns for the artificial tailings samples that exhibited the most severe preferred orientation by back-loading them against 400 grit sand paper rather than back-loading against frosted glass (which was used for samples that displayed a lesser degree of preferred orientation). This was deemed necessary even though it can introduce more complications in the form of surface roughness which can affect microabsorption.

**Figure 3.1**

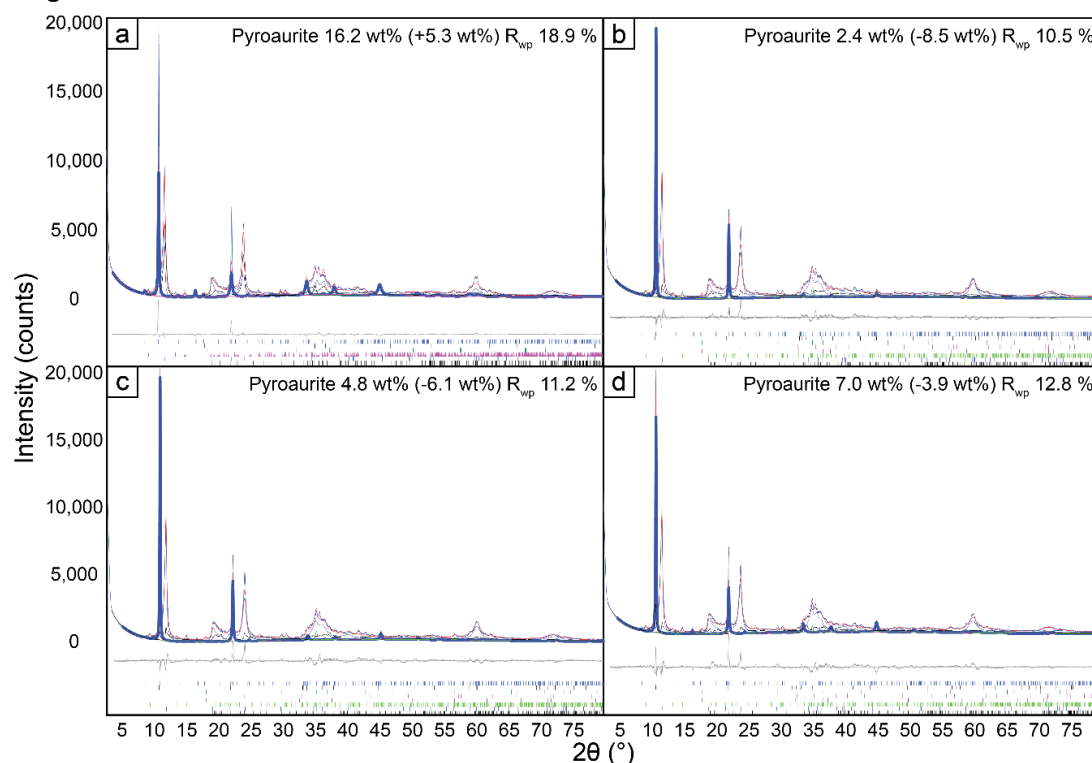


**Figure 3.1** Modelling pyroaurite using with the PONKCS method and **a)** no March-Dollase preferred orientation, and a March-Dollase correction with **b)** no minimum value **c)** a minimum of 0.6 and **d)** a minimum of 0.75. Refined pyroaurite abundance (absolute error) and  $R_{wp}$  is reported for each of the conditions.

For the purposes of this study, both the March-Dollase correction and a spherical harmonics correction were tested as methods to overcome the issues associated with quantifying the abundance of minerals that exhibited preferred orientation. Refinements using a spherical harmonics correction for preferred orientation tended to produce physically impossible results such as negative intensities, an undesirable occurrence that has been previously documented (Whitfield, 2008), as such the spherical harmonics correction for preferred orientation was ultimately discarded in favour of using the March-Dollase correction. Applying the March-Dollase correction on the  $0\ 0\ 3l$  peaks for pyroaurite and iowaite (where present at trace abundance), the  $0\ 0\ l$  peaks for brucite and the  $h\ 0\ 0$  peaks for hydromagnesite, gave the best results. The degree of preferred orientation exhibited by the  $0\ 0\ 3$  pyroaurite peak and its higher orders reflections was most pronounced in the artificial samples with the highest weighed abundances for pyroaurite (e.g., 10.9 wt% pyroaurite in Artrock8). In these cases, the March-Dollase preferred orientation correction could be used to fit the peak intensities but the degree of correction necessary to achieve a very good fit to the  $0\ 0\ 3$  peak resulted in drastic underreporting of the pyroaurite abundance: in one case by up to 8.5 wt% (78.0 % relative error, as seen in Figure 3.1). Placing limits on the minimum and maximum values for the March-Dollase correction yielded more accurate refined abundances of pyroaurite but it led to a worse fit between the model and the observed intensities of the pyroaurite peaks, and a worse fit to the XRD pattern overall. Several variations were tested both for the PONKCS method and the Pawley/internal standard method, including using the March-Dollase correction with different lower limits used (e.g., a maximum value of 1 with a minimum of 0.6; a maximum value of 1 with a minimum value of 0.75). Figures 3.1 and 3.2 compare the resulting  $R_{wp}$  and refined pyroaurite abundances obtained using both methods and the different lower bounds for the March-Dollase correction. The refined value for the March-Dollase correction used on the  $0\ 0\ 3l$  reflections of pyroaurite consistently

reached the minimum value of 0.6 whenever minimum limits were set. When minimum values were not set, the refined values reached lower limits of 0.53 (when using the Pawley/internal standard method) and 0.47 (when using the PONKCS method). Ultimately, a minimum value of 0.6 provided a suitable compromise between (1) a good fit between the model and data and (2) the accuracy of the reported abundances for hydrotalcite minerals.

**Figure 3.2**

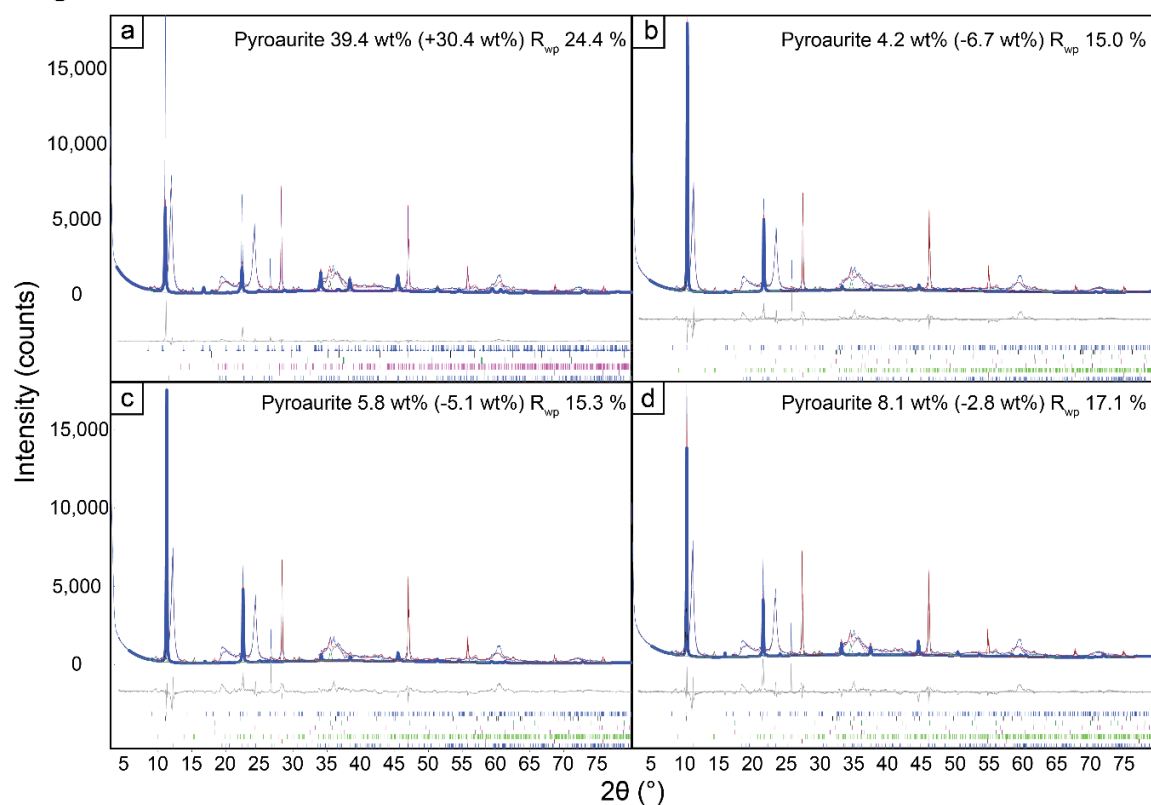


**Figure 3.2** Modelling pyroaurite using with the Pawley/internal standard method and **a**) no March-Dollase preferred orientation, and a March-Dollase correction with **b**) no minimum value **c**) a minimum of 0.6 and **d**) a minimum of 0.75. Refined pyroaurite abundance (absolute error) and  $R_{wp}$  is reported for each of the conditions.

The McCrone micronizing mill that we used had been kept in good repair (with the rubber “mounts” having been recently replaced before sample preparation). It is likely that the milling was insufficient to reduce the grain size of all minerals. This effect has been previously reported for platy minerals in other studies such as Wilson et al., (2009b) where

large (~50  $\mu$ m) phlogopite sheets (size confirmed by SEM imaging) remained after 10 minutes of milling in a McCrone mill. Alternative methods for reducing preferred orientation could be employed in future studies. For instance, the use of side-loading cavity mounts or spray drying of the samples (Hillier, 1999) could be employed to mitigate the effects of preferred orientation. However, it remains to be seen whether these more involved methods for sample preparation are practicable for the large numbers of samples that need to be analysed during carbon sequestration studies, and there are likely to be OH&S considerations that must be addressed before aerosolising serpentinite samples that commonly contain chrysotile.

### **3.3 Results and discussion**

#### **3.3.1 Comparison of results from the three refinement methods**

The results of using all three Rietveld refinement methods are shown in Tables 3.3, 3.4 & 3.5. These tables report the refined abundances for each phase, the estimated standard deviation (ESD, as reported in Topas V.5) and the difference between refined abundance and known abundance for each phase in every sample. Refined abundances obtained using the three methods are plotted against known abundances for each phase in Figure 3.3, where deviation from the ideal 1:1 trend indicates an over or underestimate. The absolute and relative errors on the refined values for all phases and all three methods are compared in Figure 3.4.

For the PONCKS and Pawley/internal standard methods, the largest source of error results from overestimation of serpentine mineral abundance (an average error of 4.6 wt% absolute and 6.0% relative) and the resulting systematic underestimation of the abundances of all minor phases. This can be seen in Figure 3.3e where the majority of data points lie above the 1:1 line, indicating the refined abundance is greater than the measured abundance.

**Table 3.3** Refinement results for PONKCS method

Sample	Abundance	Pyroaurite	Magnetite	Brucite	Hydromagnesite	Serpentine	Total	R <sub>wp</sub> <sup>a</sup>	χ <sup>2</sup> <sup>b</sup>	d <sup>c</sup>	Total bias <sup>d</sup>
Artrock1	weighed (%)	1.9	7.1	1.1	1.0	88.9	100.0				
	refined (ESD <sup>e</sup> )	2.7 (0.2)	3.6 (0.1)	2.6 (0.1)	1.0 (0.4)	90.1 (1.5)	100.0	15.4	4.4	0.2	
	difference	+0.8	-3.5	+1.5	+0.0	+1.2					7.0
Artrock2	weighed (%)	3.2	5.0	1.8	5.0	85	100.0				
	refined (ESD <sup>e</sup> )	4.3 (0.1)	3 (0.1)	1.1 (0.1)	4.4 (0.5)	87.1 (1.4)	100.0	11.9	3.5	0.2	
	difference	+1.1	-2.0	-0.7	-0.6	+2.1					6.5
Artrock3	weighed (%)	3.2	5.0	1.8	10.0	80	100.0				
	refined (ESD <sup>e</sup> )	4.4 (0.1)	2.6 (0.1)	1.3 (0.1)	8 (0.3)	83.6 (1.0)	100.0	11.2	3.8	0.2	
	difference	+1.2	-2.4	-0.5	-2.0	+3.6					9.7
Artrock4	weighed (%)	3.3	5.0	1.8	15.0	74.9	100.0				
	refined (ESD <sup>e</sup> )	4.7 (0.1)	3 (0.1)	1.3 (0.1)	11.3 (0.4)	79.7 (1.0)	100.0	11.1	3.6	0.2	
	difference	+1.4	-2.0	-0.5	-3.7	+4.8					12.3
Artrock5	weighed (%)	1.3	5.0	0.2	3.6	89.9	100.0				
	refined (ESD <sup>e</sup> )	3.1 (0.2)	5.4 (0.2)	0.7 (0.1)	5 (0.5)	85.7 (1.6)	100.0	10.4	2.6	0.3	
	difference	+1.8	+0.4	+0.5	+1.4	-4.2					8.3
Artrock6	weighed (%)	5.4	5.0	1.1	5.0	83.5	100.0				
	refined (ESD <sup>e</sup> )	3.9 (0.2)	6.6 (0.2)	0.3 (0.1)	4.8 (0.5)	84.5 (1.9)	100.0	11.2	2.7	0.3	
	difference	+1.5	+1.6	-0.8	-0.2	+1.0					5.1
Artrock7	weighed (%)	7.6	5.1	1.5	5.0	80.8	100.0				
	refined (ESD <sup>e</sup> )	3.7 (0.2)	6.1 (0.2)	0.3 (0.1)	5.5 (0.4)	84.5 (1.9)	100.0	11.6	2.8	0.3	
	difference	-3.9	+1.0	-1.2	+0.5	+3.7					10.3
Artrock8	weighed (%)	10.9	3.0	2.2	5.0	78.9	100.0				
	refined (ESD <sup>e</sup> )	4.3 (0.2)	2.5 (0.1)	0.2 (0.1)	2.5 (0.3)	90.5 (3.0)	100.0	11.4	3.0	0.3	
	difference	-6.3	-0.5	-2.0	-2.5	+11.6					23.2

<sup>a</sup> Weighted pattern residual, a function of the least-squares residual (%).

<sup>b</sup> Reduced chi-squared statistic for the least-squares fit.

<sup>c</sup> Weighted Durbin-Watson statistic.

<sup>d</sup> Total bias ( $\Delta$ ) =  $\sum \text{abs}(W_{i, \text{actual}} - W_{i, \text{reported}})$ ,  $W_i$  is the weight% of the  $i^{\text{th}}$  mineral. (Omotoso et al., 2006).

<sup>e</sup> Estimated Standard Deviation, calculated using the Topaz V.5 "do\_errors" macro.

As a consequence of the overestimation of the serpentine abundance, the minor phases (all phases other than serpentine) tend to be underestimated, lying below the 1:1 line in most cases. This is not the case with the combined PONCKS-Pawley/internal standard method, which produced several instances of severe underestimates of serpentine abundance in the artificial tailings samples. This underestimation is likely occurring for the combined method because the abundance of serpentine and the abundance of amorphous material are being considered separately. Because these samples lack significant amorphous material (i.e., no

amorphous phase was deliberately added), the amorphous content calculation represents more of a measure of the goodness of fit than an estimate of the amount of amorphous material in the samples. Asymmetry and peak broadening make fitting serpentine peaks difficult, making this the largest source of error when it comes to pattern fitting using a PONKCS phase. For samples with severely underestimated serpentine abundances, the unaccounted for intensity, which results in an overestimate of fluorite abundance, is then reported as ‘amorphous’ content.

**Figure 3.3**

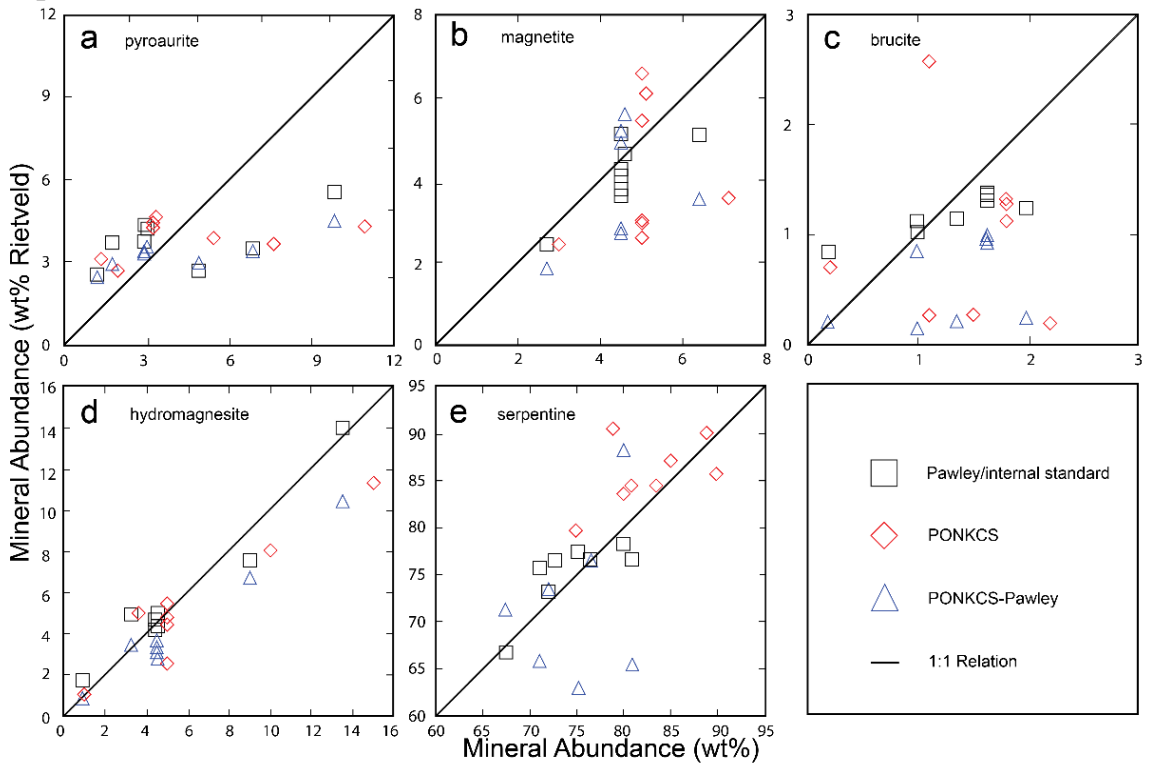


**Figure 3.3** Results of Rietveld refinements for each mineral phase in the synthetic tailings using both the PONKCS and Rietveld spike method.

**Table 3.4** Refinement results for Pawley/internal standard method

Sample	Abundance	Pyroaurite	Magnetite	Brucite	Hydromagnesite	Fluorite	Serpentine	Total	R <sub>wp</sub> <sup>a</sup>	χ <sup>2b</sup>	d <sup>c</sup>	Total bias <sup>d</sup>
Artrock1	weighed (%)	1.7	6.4	1.0	0.9	10.0	80.0	100.0				
	refined (ESD <sup>e</sup> )	3.7 (0.2)	5.1 (0.2)	1.1 (0.1)	1.8 (0.6)	10.0 (0.0)	78.3 (0.6)	100.0	13.9	3.9	0.1	
	difference	+2.0	-1.3	+0.1	+0.9	+0.0	+1.7					6.6
Artrock2	weighed (%)	2.9	4.5	1.6	4.5	10.0	76.5	100.0				
	refined (ESD <sup>e</sup> )	4.3 (0.2)	3.6 (0.2)	1.4 (0.1)	4.1 (0.6)	10.0 (0.0)	76.5 (0.7)	100.0	14.7	4.3	0.1	
	difference	+1.4	-0.9	-0.2	-0.4	+0.0	+0.0					3.3
Artrock3	weighed (%)	2.9	4.5	1.6	9.0	10.0	72.0	100.0				
	refined (ESD <sup>e</sup> )	3.8 (0.1)	4.1 (0.1)	1.4 (0.1)	7.6 (0.4)	10.0 (0.0)	73.2 (0.5)	100.0	13.1	3.5	0.2	
	difference	+0.9	-0.4	-0.2	-1.4	+0.0	+1.2					4.6
Artrock4	weighed (%)	3.0	4.5	1.6	13.5	10.0	67.4	100.0				
	refined (ESD <sup>e</sup> )	4.2 (0.2)	3.8 (0.2)	1.3 (0.2)	14.0 (0.8)	10.0 (0.0)	66.7 (0.9)	100.0	15.5	3.1	0.3	
	difference	+1.2	-0.7	-0.3	+0.5	+0.0	-0.7					3.9
Artrock5	weighed (%)	1.2	4.5	0.2	3.2	10	80.9	100.0				
	refined (ESD <sup>e</sup> )	2.5 (0.3)	5.1 (0.2)	0.8 (0.3)	4.9 (1.0)	10.0 (0.0)	76.6 (1.1)	100.0	17.1	3.9	0.1	
	difference	+1.3	+0.6	+0.6	+1.7	+0.0	-4.3					9.6
Artrock6	weighed (%)	4.9	4.5	1.0	4.5	10	75.2	100.0				
	refined (ESD <sup>e</sup> )	2.7 (0.2)	4.3 (0.2)	1.0 (0.2)	4.6 (0.6)	10.0 (0.0)	77.4 (0.7)	100.0	15.1	6.2	0.2	
	difference	-2.2	-0.2	+0.0	+0.1	+0.0	+2.2					5.3
Artrock7	weighed (%)	6.8	4.6	1.4	4.5	10.0	72.7	100.0				
	refined (ESD <sup>e</sup> )	3.5 (0.2)	4.6 (0.2)	1.1 (0.2)	4.3 (0.5)	10.0 (0.0)	76.5 (0.6)	100.0	15.4	3.8	0.2	
	difference	-3.3	+0.0	-0.3	-0.2	+0.0	+3.8					8.6
Artrock8	weighed (%)	9.8	2.7	2.0	4.5	10.0	71.0	100.0				
	refined (ESD <sup>e</sup> )	5.6 (0.2)	2.4 (0.2)	1.2 (0.3)	5.0 (0.6)	10.0 (0.0)	75.7 (0.8)	100.0	16.3	4.1	0.2	
	difference	-4.2	-0.3	-0.8	+0.5	+0.0	+4.7					11.9

<sup>a</sup> Weighted pattern residual, a function of the least-squares residual (%).

<sup>b</sup> Reduced chi-squared statistic for the least-squares fit.

<sup>c</sup> Weighted Durbin-Watson statistic.

<sup>d</sup> Total bias ( $\Delta$ ) =  $\sum \text{abs}(W_{i, \text{actual}} - W_{i, \text{reported}})$ ,  $W_i$  is the weight% of the  $i^{\text{th}}$  mineral. (Omotoso et al., 2006).

<sup>e</sup> Estimated Standard Deviation, calculated using the Topaz V.5 “do\_errors” macro.

**Table 3.5** Refinement results for combined PONKCS-Pawley/internal standard method

Sample	Abundance	Pyroaurite	Magnetite	Brucite	Hydromagnesite	Fluorite	Serpentine	'Amorphous'	Total	R <sub>wp</sub> <sup>a</sup>	χ <sup>2</sup> <sup>b</sup>	d <sup>c</sup>	Total bias <sup>d</sup>
Artrock1	weighed (%)	1.7	6.4	1.0	0.9	10.0	80.0		100.0				
	refined (ESD <sup>e</sup> )	2.8 (0.1)	3.5 (0.1)	0.8 (0.0)	0.8 (0.3)	10.0 (0.0)	88 (2.0)	-5.9 (1.8)	100.0	10.5	2.9	0.3	
	difference	+1.1	-2.9	-0.2	-0.1	+0.0	+8.0						12.3
Artrock2	weighed (%)	2.9	4.5	1.6	4.5	10.0	76.5		100.0				
	refined (ESD <sup>e</sup> )	3.3 (0.1)	2.7 (0.1)	0.9 (0.1)	3.0 (0.3)	10.0 (0.0)	76.3 (1.9)	3.8 (1.9)	100.0	10.6	3.1	0.3	
	difference	+0.4	-1.8	-0.7	-1.5	+0.0	-0.2						4.6
Artrock3	weighed (%)	2.9	4.5	1.6	9.0	10.0	72.0		100.0				
	refined (ESD <sup>e</sup> )	3.3 (0.1)	2.7 (0.1)	1 (0.1)	6.6 (0.4)	10.0 (0.0)	73.3 (1.6)	3.2 (1.6)	100.0	11.2	3	0.3	
	difference	+0.4	-1.8	-0.6	-2.4	+0.0	+1.3						6.5
Artrock4	weighed (%)	3	4.5	1.6	13.5	10.0	67.4		100.0				
	refined (ESD <sup>e</sup> )	3.5 (0.2)	2.8 (0.1)	0.9 (0.1)	10.3 (0.5)	10.0 (0.0)	71.1 (1.7)	1.4 (1.7)	100.0	11.5	2.3	0.4	
	difference	+0.5	-1.7	-0.7	-3.2	+0.0	-3.7						9.8
Artrock5	weighed (%)	1.2	4.5	0.2	3.2	10.0	80.9		100.0				
	refined (ESD <sup>e</sup> )	2.4 (0.3)	4.9 (0.2)	0.2 (0.1)	3.4 (0.4)	10.0 (0.0)	65.3 (2.0)	14.0 (1.7)	100.0	11	2.5	0.3	
	difference	+1.2	+0.4	+0.0	+0.2	+0.0	-15.6						17.4
Artrock6	weighed (%)	4.9	4.5	1.0	4.5	10.0	75.2		100.0				
	refined (ESD <sup>e</sup> )	2.9 (0.2)	5.2 (0.2)	0.1 (0.1)	3.6 (0.3)	10.0 (0.0)	62.8 (1.7)	15.5 (1.4)	100.0	10.6	2.5	0.3	
	difference	-2.0	+0.7	-0.9	-0.9	+0.0	-12.4						16.9
Artrock7	weighed (%)	6.8	4.6	1.4	4.5	10.0	72.7		100.0				
	refined (ESD <sup>e</sup> )	3.3 (0.2)	5.6 (0.2)	0.2 (0.1)	3.2 (0.4)	10.0 (0.0)	59.7 (2.1)	18.0 (1.7)	100.0	10.9	2.7	0.3	
	difference	-3.5	+1.0	-1.2	-1.3	+0.0	-13.0						20
Artrock8	weighed (%)	9.8	2.7	2.0	4.5	10.0	71.0		100.0				
	refined (ESD <sup>e</sup> )	4.4 (0.2)	1.8 (0.1)	(0.1)	2.7 (0.3)	10.0 (0.0)	65.6 (1.9)	15.2 (1.7)	100.0	12.63	3.2	0.3	
	difference	-5.4	-0.9	-1.8	-1.8	+0.0	-5.4						15.3

<sup>a</sup> Weighted pattern residual, a function of the least-squares residual (%).<sup>b</sup> Reduced chi-squared statistic for the least-squares fit.<sup>c</sup> Weighted Durbin-Watson statistic.<sup>d</sup> Total bias ( $\Delta$ ) =  $\sum \text{abs}(W_{i, \text{actual}} - W_{i, \text{reported}})$ ,  $W_i$  is the weight% of the  $i^{\text{th}}$  mineral. (Omotoso et al., 2006).<sup>e</sup> Estimated Standard Deviation, calculated using the Topaz V.5 "do\_errors" macro.

Magnetite and hydromagnesite abundances tend to be underestimated using all three methods, and underestimates tend to be greater in samples with high abundances of these phases. The largest underestimate of magnetite abundance occurs for Artrock1 when using the PONKCS method (3.6 wt% refined, 7.1 wt% weighed) and the largest underestimate of hydromagnesite occurs for Artrock4 when using the PONKCS method (11.3 wt% refined, 15.0 wt% weighed). Preferred orientation issues could have led either to overestimations of refined abundances due to uncharacteristically high peak heights or underestimations if preferred orientation corrections were used (as detailed above). However, the lack of

appreciable preferred orientation displayed by hydromagnesite and magnetite makes either of these cases unlikely. The systematic underestimation of magnetite abundance may be related to microabsorption contrast given the relatively high linear absorption coefficient of magnetite compared to those of the silicate, hydroxide and carbonate minerals in the synthetic tailings samples. This underestimation may also stem in part from assumptions about particle size and shape that must be made in order to use of the Brindley correction for microabsorption contrast (e.g., Scarlett et al, 2002, Pederson et al., 2004). Underestimation of hydromagnesite abundance could be related to the asymmetric peak shapes observed for this phase. This asymmetry in the low angle peaks of hydromagnesite, which was modelled using a Thompson-Cox-Hastings pseudo-Voight profile, commonly occurs in naturally-occurring samples, such as this one, that have formed via decomposition of dypingite  $[\text{Mg}_5(\text{CO}_3)_4(\text{OH})_2 \cdot \sim 5\text{H}_2\text{O}]$  to hydromagnesite (Wilson et al., 2010; Power et al., 2014). The systematic underestimation of these two minor phases could also be due to peak overlap with the serpentine minerals since the use of structureless pattern fitting methods tends to overestimate major phases, such as the lizardite and chrysotile that are modelled using this approach.

Pyroaurite and brucite show a different tendency to be overestimated at low abundances but then underestimated at higher abundances. The pyroaurite abundance for samples containing <4 wt% of this phase tended to be overestimated, whereas samples with >4 wt% pyroaurite produced underestimates of up to 6.3 wt% absolute (in sample Artrock8, which has a known pyroaurite abundance of 10.9 wt%). A similar, but less distinct trend occurs for brucite, with brucite abundances of <1 wt% tending to be overestimated and samples with >1 wt% tending to be underestimated. This likely occurs due to the difficulty in modelling severe preferred orientation for platy minerals such as pyroaurite and brucite. The March-Dollase preferred orientation correction that was used may be overcompensating in samples with high

abundances of platy minerals, leading to significantly lower refined abundances than those in which they are actually present. This switch from an overestimate to an underestimate is important to consider for carbon accounting purposes as it is more convoluted than if the phases were being consistently over- or underestimated.

**Figure 3.4**

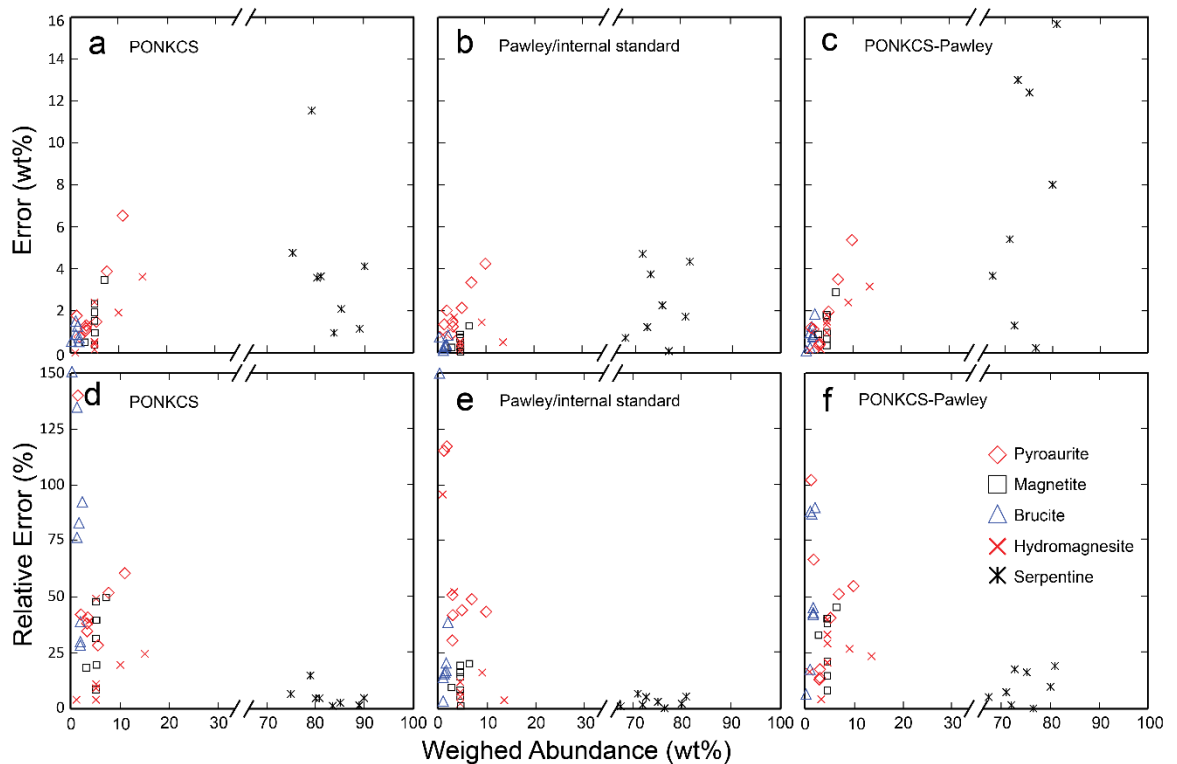


**Figure 3.4** Relative and absolute error values between the weighed compositions of the artificial tailings samples and the compositions calculated via Rietveld refinement for **a)** absolute error values for PONKCS method **b)** relative error values for PONKCS method **c)** absolute error values for Rietveld spike method **d)** relative error values for Rietveld spike method.

The use of structureless pattern fitting is known to produce overestimates for those phases modelled using the approach, while producing systematic underestimates of other phases. Wilson et al. (2006) observed that these underestimates tend to be greatest for phases that are present at less than 5 wt% abundance. These observations have been reproduced by Wilson et al. (2009b) and Turvey et al. (2017). Underestimates on the abundances of minor

phases are due to limitations in fitting anisotropic peaks using the fundamental parameters approach, difficulties in modelling preferred orientation (particularly for minerals that have a platy, fibrous or bladed morphology), and the tendency of refinements that include PONKCS models to incorrectly attribute the intensity of overlapping or adjacent reflections from other phases to the phase being modelled using the PONKCS method (Turvey et al., 2017; Wilson et al., 2009b).

The relative error on refined mineral abundances is typically less than 50% for phases present at > 10 wt% abundance using all three methods (Figure 3.4). Relative error values tend to increase dramatically for phases present at < 2 wt% abundance. This increase in relative error at very low abundances has been seen in similar studies (Dipple et al., 2002 ; Raudsepp et al., 1999; Turvey et al., 2017; Wilson et al., 2006; Wilson et al., 2009b). However, even though the relative error increases substantially, because of the very low abundances of these phases, the corresponding absolute errors are still comparatively low. All three methods tend to give relative errors in excess of 50% for low-abundance phases (<2 wt%) and, in several cases, the relative error values are in excess of 100% (Figure 3.4). The absolute error values for these phases, however, are still some of the lowest reported (Tables 3.3–3.5), and all are within 2 wt% of the actual known values (Figure 3.3 and 3.4). Thus, even though refined abundances for the minor phases such as the carbonate-bearing minerals, pyroaurite and hydromagnesite, suffer the largest relative error values at low abundances they are close to the actual known values.

Refinements using the PONKCS method produced greater values for the overall relative and absolute error compared with the Pawley/internal standard method with an average refinement bias (as defined by Omotoso et al., 2006) per sample of 10.3 wt%. Absolute error values for the minor (non-serpentine) phases gradually increased from <2 wt% at weighed

abundances of <5 wt% to 2.0–6.6 wt% for phases at weighed abundances between 10 and 20 wt%. The relative error values are inversely proportional to the weighed abundances of a phase. Brucite was heavily underestimated with relative errors >50%, and the highest relative error value produced in the PONKCS refinements was for brucite: a 250% relative error was obtained for brucite in Artrock 5 (0.5 wt%), actual abundance 0.2 wt%.

The Pawley/internal standard method generally produced more accurate results than the PONKCS method, with an average refinement bias per sample of 6.7 wt%. Phases known to be present at <20 wt% abundance typically had absolute error values <2 wt% with the exception of the pyroaurite in samples Artrock6, 7 and 8, which contained the highest abundances of pyroaurite (4.9–9.8 wt%) and had absolute errors of 2.2–4.2 wt%. Although the relative error values for the Pawley/internal standard method are typically lower than those obtained using the PONKCS method, this approach produced the highest single relative error value in the study. Phases with <10 wt% abundance typically gave relative errors <50 %; however, a relative error of 367% for brucite abundance was recorded using this method, again for Artrock5, where a refined abundance of 0.9 wt% was obtained compared with the known value of 0.2 wt%. However, this is not unexpected given that the abundance of brucite in this particular sample is close to the detection limit of ~0.1 wt% for this phase under the conditions used to collect XRD patterns during this study. Refined abundances for serpentine minerals using the Pawley/internal standard method were also more accurate than those obtained using the PONKCS method, with all serpentine abundances being within 5 wt% absolute and 6 % relative error. This is a minor improvement on results obtained using the PONKCS method in Turvey et al. (2017) (where serpentine was within 6 wt% absolute and 8% relative error) and using the Pawley/internal standard method in Wilson et al. (2006) and Wilson et al. (2009b) (where serpentine was within 5 wt% absolute and 11 % relative error).

The combined PONKCS Pawley/internal standard method produced results similar to those obtained using the PONKCS method, with an average refinement bias per sample of 12.9 wt%. Phases known to be present at <5 wt% abundance typically had absolute error values <2 wt% on refined abundances whereas phases present at between 5 and 15 wt% yielded absolute errors of between 2 and 6 wt%, similar to the results obtained using only the PONKCS method. Relative error values were typically <50% except for phases present at very low abundances (i.e., pyroaurite and brucite, where present at <2 wt%). Interestingly, the PONKCS Pawley/internal standard method produced relatively accurate results for phases present at very low abundances with relative errors all below 102% even for phases present at <2 wt% abundance (unlike the PONKCS and Pawley/internal standard methods which yielded extreme relative errors in some cases). One obvious weakness of the PONKCS Pawley/internal standard method is the poor accuracy of the refined abundances for the serpentine minerals, which is noticeably worse than using either the PONKCS or the Pawley/internal standard method alone. Absolute error values of 0.2–15.6 wt% were reported for serpentine when using the combined method (up to 19.3 % relative error), greater than errors of 1.0–11.6 wt% for the PONKCS method (up to 14.7 % relative error) and significantly greater than errors obtained when estimating the serpentine abundance using the Pawley/internal standard method (0.0–4.7 wt%, up to 6.6% relative error).

The ESD values reported in Tables 3.3–3.5, give an indication of the precision with which each mineral phase is measured using the three refinement methods that were tested. Refined abundances for pyroaurite, magnetite and brucite have similar ESD values of 0.1–0.3 wt%. Hydromagnesite and serpentine abundances have larger ESD values: 0.3–1.0 wt% for hydromagnesite and 0.5–3.0 at% for serpentine. The three different refinement methods used in this study do not give significantly different ESD values for pyroaurite, magnetite and brucite for a given. However, which refinement method is used does appear to affect ESD

values for hydromagnesite and serpentine, with the Pawley/internal standard method having the largest ESD values for hydromagnesite (0.4–1.0 wt%) but the lowest values for serpentine (0.5–1.1 wt%). For pyroaurite, magnetite and serpentine, the values for refined mineral abundance are significantly larger than the corresponding ESD values. The ESD values for these three phases are typically smaller in magnitude than the over- and underestimates between modelled abundance and known abundance observed for each mineral. However the ESD values for brucite and hydromagnesite are of a similar to the differences observed between the refined and known abundances. This indicates that the errors on refined abundances for these two minerals may largely be driven by the precision of the measurements rather than systematic over- or underestimation.

### **3.3.2 Carbon sequestration and carbonation potential estimates**

Table 3.6 and Figure 3.5 show estimates of the carbon sequestered and the carbonation potential of each of the artificial tailings samples according to their weighed and refined abundances of carbonate minerals and brucite, respectively. The carbon sequestered in the tailings samples is reported here as the amount of CO<sub>2</sub> contained in the hydromagnesite and pyroaurite in a sample, and the carbonation potential is an estimate of the amount of CO<sub>2</sub> that could be sequestered assuming brucite is altered to either pyroaurite or hydromagnesite. Hydromagnesite and pyroaurite have been reported to sequester atmospheric CO<sub>2</sub> in previous studies of carbonation reactions in mine tailings (e.g., Oskierski et al., 2013; Wilson et al., 2014), they represent the amount of atmospheric CO<sub>2</sub> that has already been sequestered in a tailings sample. Brucite is reported as the primary Mg source for passive carbonation of mine tailings at many sites (e.g., Oskierski et al., 2013; Wilson et al., 2014), where it can be replaced by hydromagnesite, dypingite, nesquehonite (MgCO<sub>3</sub>·3H<sub>2</sub>O) or pyroaurite (Harrison et al., 2015; Harrison et al., 2013; Oskierski et al., 2013; Wilson et al., 2010;

Wilson et al., 2014), where dypingite and nesquehonite are more likely to form and persist in colder climates than that of New South Wales. Thus the brucite abundance in tailings samples can be considered analogous to the amount of future carbonation potential possible for the sample (Wilson et al., 2014). Whether brucite is altered to hydromagnesite or pyroaurite at Woodsreef will largely determine the amount of CO<sub>2</sub> that could be sequestered at this and other mine sites. Assuming that brucite can produce either a high-C phase (hydromagnesite, which is 37.6 % CO<sub>2</sub> by weight) or a low-C phase (pyroaurite, which is 6.7 % CO<sub>2</sub> by weight) provides an upper and lower estimate for the carbonation potential of brucite and both scenarios are considered in Table 3.6 and Figure 3.5. Figure 3.5 compares (1) the amount of CO<sub>2</sub> currently sequestered in each of the tailings samples (calculated using the abundances of pyroaurite and hydromagnesite and their stoichiometric CO<sub>2</sub> content) and (2) the potential amount of future carbon sequestration (calculated using the abundance of brucite and the stoichiometric CO<sub>2</sub> content of hydromagnesite or pyroaurite) obtained using the three Rietveld refinement methods. The results in Figure 3.5 demonstrate that all three refinement methods result in systematic underestimates of the known extents of carbon sequestration and carbonation potential of the artificial tailings samples, except for Artrock1 and Artrock5. Of the three methods, the Pawley/internal standard produced the most consistently accurate results, giving the closest estimate to the known values for carbon content of the artificial tailings samples, with an average absolute error of 0.6 g CO<sub>2</sub> (25.4 % relative error). The PONKCS and Pawley/internal standard methods are typically quite similar in terms of the accuracy with which they estimate C content; however, in the case of Artrock4 and Artrock8, the Pawley/internal standard method offers significantly better results (8.0 % relative error compared with 22.9 % error for Artrock4 and 21.5 % relative error compared with 63.0 % error for Artrock8). The combined PONKCS Pawley/internal standard method consistently produced the least accurate results, with an average absolute

error of 1.2 g of CO<sub>2</sub> per sample, compared with 0.9 g of CO<sub>2</sub> for the PONKCS method and 0.6 g of CO<sub>2</sub> for the Pawley/internal standard method (relative errors of 34.4 %, 36.2 % and 25.4 % respectively). However, the PONKCS Pawley/internal standard method did yield more accurate results for wt% CO<sub>2</sub> content of Artrock1 and Artrock5, whereas the other two methods yielded significant overestimates for the known amount of sequestered CO<sub>2</sub>.

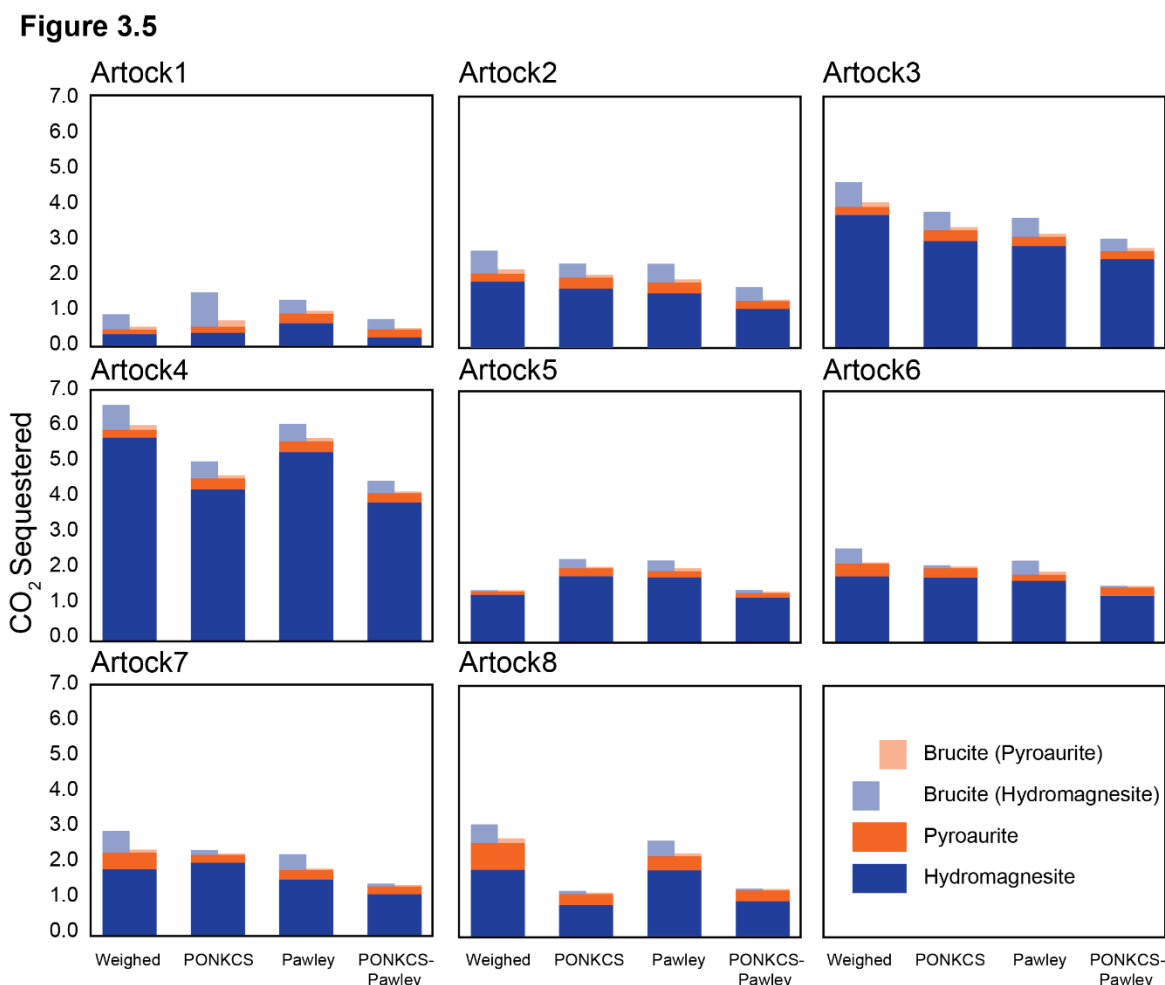


**Figure 3.5** Estimates for carbon sequestration and remaining carbonation potential of the artificial tailings based on the abundance of (1) hydromagnesite and pyroaurite and (2) brucite, respectively according to their weighed and refined abundances. Two values are included for brucite to represent the potential for it to form hydromagnesite (high C) or pyroaurite (low C).

Hydromagnesite abundance is the greater contributor to the carbon sequestration and carbonation potential of most of the tailings samples owing to its high stoichiometric CO<sub>2</sub>

content. The results in Figure 3.5 indicate that the large errors that occur in estimating the abundances of carbonate minerals in the synthetic tailings have a significant effect on estimates of carbon sequestration and carbonation potential. These errors result in consistent underestimation of the amount of CO<sub>2</sub> sequestered in the samples as well as their potential to sequester additional CO<sub>2</sub> by carbonation of unreacted brucite. This is particularly noticeable when considering the mass of CO<sub>2</sub> sequestered in pyroaurite and the carbonation potential of brucite, both of which minerals suffer from severe preferred orientation. At high abundances of pyroaurite and brucite, the use of the PONKCS and the PONKCS-Pawley/internal standard methods in particular leads to significant underestimates of the abundances of these minerals (as seen in Figure 3.3). Underestimates of the abundances of pyroaurite and brucite result in a corresponding underestimation of the amount of CO<sub>2</sub> sequestered in the pyroaurite and the carbonation potential of brucite in a given sample. This is most apparent for Artock8, where the high pyroaurite abundance (10.9 wt%) was underestimated using all three methods (i.e., underestimates of 5.6 wt% using the Pawley/internal standard method, 4.3 wt% using the PONKCS method and 4.4 wt% using the combined PONKCS-Pawley/internal standard method), leading to a large discrepancy between the amount of CO<sub>2</sub> sequestered in pyroaurite (0.72 g CO<sub>2</sub>) and the amount that is estimated using the various refinement methods (estimated at 0.37 g CO<sub>2</sub> using the Pawley/internal standard method, 0.29 g CO<sub>2</sub> using the PONKCS method and 0.29 g CO<sub>2</sub> using the combined PONKCS-Pawley/internal standard method).

**Table 3.6** Estimated carbon sequestration plus carbonation potential (from brucite only) of artificial tailings

Sample	Method	Carbon sequestration potential (g CO <sub>2</sub> ) <sup>a</sup>				Total
		Hydrom- agnesite	Pyro- aurite	Brucite (Hydro)	Brucite (Pyro)	
Artrock1	Weighed	0.4	0.1	0.4	0.1	1.0
	PONKCS	0.4	0.2	1.0	0.2	1.7
	Pawley	0.7	0.2	0.4	0.1	1.4
	PONKCS-Pawley	0.3	0.2	0.3	0.1	0.8
Artrock2	Weighed	1.9	0.2	0.7	0.1	2.9
	PONKCS	1.7	0.3	0.4	0.1	2.5
	Pawley	1.5	0.3	0.5	0.1	2.4
	PONKCS-Pawley	1.1	0.2	0.4	0.1	1.8
Artrock3	Weighed	3.8	0.2	0.7	0.1	4.8
	PONKCS	3.0	0.3	0.5	0.1	3.9
	Pawley	2.8	0.2	0.5	0.1	3.7
	PONKCS-Pawley	2.5	0.2	0.4	0.1	3.1
Artrock4	Weighed	5.6	0.2	0.7	0.1	6.7
	PONKCS	4.3	0.3	0.5	0.1	5.1
	Pawley	5.3	0.3	0.5	0.1	6.1
	PONKCS-Pawley	3.9	0.2	0.3	0.1	4.5
Artrock5	Weighed	1.4	0.1	0.1	0.0	1.5
	PONKCS	1.9	0.2	0.3	0.0	2.4
	Pawley	1.9	0.2	0.3	0.1	2.4
	PONKCS-Pawley	1.3	0.2	0.1	0.0	1.5
Artrock6	Weighed	1.9	0.4	0.4	0.1	2.7
	PONKCS	1.8	0.3	0.1	0.0	2.2
	Pawley	1.7	0.2	0.4	0.1	2.4
	PONKCS-Pawley	1.3	0.2	0.0	0.0	1.6
Artrock7	Weighed	1.9	0.5	0.6	0.1	3.1
	PONKCS	2.1	0.2	0.1	0.0	2.4
	Pawley	1.6	0.2	0.4	0.1	2.3
	PONKCS-Pawley	1.2	0.2	0.1	0.0	1.5
Artrock8	Weighed	1.9	0.7	0.8	0.1	3.6
	PONKCS	1.0	0.3	0.1	0.0	1.3
	Pawley	1.9	0.4	0.5	0.1	2.8
	PONKCS-Pawley	1.0	0.3	0.1	0.0	1.4

<sup>a</sup> Total mass of each sample was 100 g.

The use of all three refinement methods tends to result in underestimates for all minor phases, including carbonate-bearing phases. These refinement methods also cannot be used to quantify the amount of amorphous carbonate in a sample independently from other amorphous phases, thus it is likely that the use of Rietveld refinement methods for carbon accounting leads to underestimates of the amount of CO<sub>2</sub> sequestered in a sample. Thus carbon accounting XRD likely provides a conservative estimate of the amount of CO<sub>2</sub> sequestered in mine tailings. Understanding the advantages and disadvantages of XRD-based methods for carbon accounting allows for improved comparison with other methods.

Elemental C analysis can be used to provide a more accurate and direct estimate of the amount of CO<sub>2</sub> sequestered in a sample, but it cannot be used to differentiate between atmospheric carbon and carbon from other sources nor can it quantify the relative amounts of atmospheric and bedrock carbon in specific minerals. Thermal decomposition of brucite can provide a very accurate estimate of the amount of this highly reactive mineral in a sample (Assima et al., 2013b), making it appropriate for estimating the carbonation potential of a sample; however, complementary methods should be used to estimate the amount of CO<sub>2</sub> sequestration that has already occurred.

### **3.3.3 Method comparison**

The PONKCS method has several advantages over other Rietveld refinement methods for dealing with structurally disordered phases such as serpentine minerals. It does not require (1) the addition of an internal standard to the samples; (2) experimental reference patterns for all minerals in a given sample or (3) specialized and labour-intensive preparation of specimens (Scarlett and Madsen, 2006; Turvey et al., 2017). However, these advantages must be weighed against the superior accuracy obtained using the Pawley/internal standard method. The accuracy with which the abundances of carbonate-bearing minerals can be estimated is the most important factor when using X-ray diffraction to estimate the amount of CO<sub>2</sub> sequestered in tailings or similar materials. Accurate measurements of the abundances of brucite, in particular, and also of serpentine minerals are most important for estimating future carbonation potential. The Pawley/internal standard method produces more accurate estimates for pyroaurite and hydromagnesite abundances in the artificial tailings samples (Table 3.4, Figure 3.3). The absolute error values for the hydromagnesite abundances obtained using the Pawley/internal standard method were typically <1 wt% for abundances of 0.9–13.5 wt%. This also resulted in relative error values of <20%. Estimates

of pyroaurite abundance were not as accurate, with absolute errors of 2 wt% being typical for samples with <5 wt% pyroaurite and absolute errors of up to 4 wt% for abundances between 5 and 10 wt%. Therefore, we recommended that an internal standard be used with structureless pattern fitting of XRD data in order to more accurately estimate CO<sub>2</sub> fixation in mine tailings. However, the PONKCS method has the distinct advantage that it can be applied in the field alongside portable XRD instruments, where quickly generating usable data is more important than maximising the accuracy of the analyses (Turvey et al., 2017).

Although the combined PONKCS-Pawley/internal standard method produced less accurate results than either the PONKCS or Pawley/internal standard methods, it does offer a feature not permitted by either of the other methods: the possibility to independently quantify multiple disordered phases using PONKCS models while measuring amorphous material using an internal standard, without have to calibrate a PONKCS phase for each amorphous component. Use of this combined method could make it possible to quantify the various disordered and amorphous phases in a sample without necessarily having to calibrate PONKCS models for all of them. In samples that do not contain detectable levels of amorphous material, such as the artificial tailings samples that were studied here, the refined abundance for ‘amorphous’ content could also potentially be used as a test of the ‘goodness of fit’ for refinements that include PONKCS phases, because unaccounted for intensity will contribute to the refined value for ‘amorphous’ content. It is important to consider that amorphous material is typically not visible (as broad peaks) in XRD patterns when present at abundances below 20 or 30 wt%. As such, this method should only be applied when amorphous material is known to be present in a sample, for instance should it be present at a sufficiently high abundance to be detectable from an XRD pattern. It should not be used in those cases where amorphous content does not produce any detectable peaks in an XRD pattern. This method could also potentially be used to distinguish between various disordered

phases such as the polymorphs of serpentine, lizardite and chrysotile, which are difficult to discriminate in XRD patterns of multiphase materials. It was found that the refined values for ‘amorphous’ content for Artrock1–4 were relatively low <4 wt% whereas those for Artrock5–8 were significantly higher, 14–18 wt%. It should be noted that a physically impossible refined value of -5.9 wt% ‘amorphous’ content was obtained for Artrock1 as an artefact of refined fluorite abundance being less than the known value of 10 wt%. The difference in the estimated abundance of ‘amorphous’ content for the two groups of Artrock samples can be explained by the use of two different serpentine minerals to make Artrock samples, with a sample of picrolite (chrysotile) being used for Artrock1–4 and a sample of lizardite being used in Artrock5–8. The two different mineral standards may have differing levels of amorphous material which could lead to the differences in refined ‘amorphous’ content. However, it is more likely that the use of a single chrysotile PONKCS model for evaluating the serpentine content in all of the samples, rather than chrysotile for Artrocks1–4 and lizardite for Artrocks5–8, resulted in this inaccurate estimate in samples that do not contain appreciable amorphous material but do contain a different polymorph of serpentine (i.e., lizardite). While the combined method does offer a way to separately quantify multiple disordered or amorphous phases and may provide an estimate of the goodness of fit, care must be used when applying it as use of the method can give rise to non-physical values for amorphous content in cases where there is no or very little amorphous material and the refined abundance for the fluorite spike (before normalization using Eq.2) is lower than the actual abundance of the internal standard. In this scenario a negative abundance for amorphous content will be reported (this occurred for Artrock1). As such, it is important to carefully apply the combined PONKCS Pawley/internal standard method to avoid unphysical results and overestimates of amorphous material.

### 3.4 Implications

When performing quantitative phase analysis of samples that include structurally disordered phases, such as serpentine minerals, it is important to choose a Rietveld refinement approach that gives the most accurate possible results. We have found that of the three methods tested here, the most accurate results were produced by the Pawley/internal standard method, justifying the addition of an internal standard to each sample. The more flexible PONKCS method is more suitable for obtaining geochemically useful quantitative results quickly in the course of fieldwork with a portable XRD (Turvey et al., 2017). But if a more robust accounting of carbon fixation in tailings material is required, an internal standard should be added to each sample. The combined PONKCS-Pawley/internal standard method, although less accurate than either the Pawley/internal standard method or the PONKCS method, could potentially be of use when analysing samples such as tailing material from ultramafic mines that may contain amorphous carbonate and silica phases. The ability to independently quantify multiple disordered phases could be necessary when investigating carbon sequestration and carbonation potential because carbonation reaction can produce amorphous hydrated carbonated phases as well as well-ordered minerals such as pyroaurite, and hydromagnesite (e.g., Harrison et al., 2015).

By optimizing and assessing the accuracy of both the PONKCS and Pawley/internal standard methods, we are laying the groundwork for further crystallographic carbon accounting at Woodsreef and similar mine sites. Previous XRD studies at Woodsreef used small sample sets to estimate the amount of CO<sub>2</sub> stored in mine tailings: Oskierski et al. (2013) investigated eight samples from the tailings at Woodsreef and Turvey et al. (2017) used another six. A large-scale XRD study could be used to refine previous estimates for CO<sub>2</sub> sequestration at Woodsreef, which vary from 1400 t to 70,000 t of CO<sub>2</sub> sequestered in the

tailings pile (Oskierski et al., 2013). Such a study should use samples from many locations and from different depths below the surface of the tailings storage facility at Woodsreef to improve the accuracy of estimations of CO<sub>2</sub> sequestration at this locality. This work has determined the optimal Rietveld refinement strategy for tailings from the Woodsreef mine and samples from mineralogically similar mines. It has also resulted in a systematic analysis of which mineral abundances are under- and overestimated during Rietveld refinement, making it possible to predict that minor phases including carbonate-bearing phases will likely be underestimated using XRD data for carbon accounting.

With a firm understanding of the limitations and advantages of the various methods and their application to carbon accounting, quantitative XRD can be used more effectively to quantify carbon sequestration within ultramafic tailings and natural landscapes. Although the use of Rietveld-based methods tends to underestimate minor phases, and thus is likely to result in underestimates of the current carbon sequestration and future carbonation potential of a mine site, these methods can be used to determine an effective baseline of the amount of CO<sub>2</sub> that is being sequestered in mineralogically complex tailings. Crystallographic carbon accounting methods are also unlikely to result in gross overestimates of CO<sub>2</sub> sequestration in minerals and the carbonation potential of mineral wastes and rocks, both which are likely to become important in situations where regulatory monitoring of carbon sequestration is introduced.

### **3.5 Acknowledgements**

We would like to thank Jenine McCutcheon and Gordon Southam for their invaluable assistance in the field. We would like to acknowledge the financial assistance of Carbon Management Canada and the New South Wales Department of Industry. We would also like to thank Kate Maddison, Nick Staheyeff, Catherine Karpel and Brad Mullard at the NSW

Department of Industry for granting us access to the field site and for their support of our work at Woodsreef. We thank Ben Grguric for providing a sample of iowaite from the Mount Keith nickel mine. Work by C.C. Turvey and J.L. Hamilton was supported by Australian Postgraduate Awards. We are grateful to David Bish and an anonymous reviewer for their constructive advice that has helped us to improve our work. Our thanks go to Warren Huff for editorial handling of this manuscript.

### 3.6 References

- Akao, M., and Iwai, S. (1977) The hydrogen bonding of hydromagnesite. *Acta Crystallographica Section B*, 33 (4), 1273-1275.
- Alexander, L., and Klug, H.P. (1948) Basic aspects of X-ray absorption in quantitative diffraction analysis of powder mixtures. *Analytical Chemistry*, 20 (10), 886-889.
- Assima, G.P., Larachi, F., Beaudoin, G., and Molson, J. (2013a) Dynamics of carbon dioxide uptake in chrysotile mining residues – Effect of mineralogy and liquid saturation. *International Journal of Greenhouse Gas Control*, 12, 124-135.
- Assima, G.P., Larachi, F., Molson, J., and Beaudoin, G. (2013b) Accurate and direct quantification of native brucite in serpentine ores—New methodology and implications for CO<sub>2</sub> sequestration by mining residues. *Thermochimica Acta*, 566, 281-291.
- Assima, G.P., Larachi, F., Molson, J., and Beaudoin, G. (2014a) Emulation of ambient carbon dioxide diffusion and carbonation within nickel mining residues. *Minerals Engineering*, 59, 39-44.
- Assima, G.P., Larachi, F., Molson, J., and Beaudoin, G. (2014b) New tools for stimulating dissolution and carbonation of ultramafic mining residues. *The Canadian Journal of Chemical Engineering*, 92 (12), 2029-2038.

- Assima, P.G., Larachi, F., Beaudoin, G., and Molson, J.W. (2012) CO<sub>2</sub> sequestration in chrysotile mining residues - Implication of watering and passivation under environmental conditions. *Industrial & Engineering Chemistry Research*, 51 (26), 8726-8734.
- Bea, S.A., Wilson, S.A., Mayer, K.U., Dipple, G.M., Power, I.M., and Gamazo, P. (2012) Reactive transport modeling of natural carbon sequestration in ultramafic mine tailings. *Vadose Zone Journal*, 11(2).
- Beaudoin, G., Nowamooz, A., Assima, G.P., Lechat, K., Gras, A., Entezari, A., Kandji, E.H.B., Awoh, A.-S., Horswill, M., Turcotte, S., Larachi, F., Dupuis, C., Molson, J., Lemieux, J.-M., Maldague, X., Plante, B., Bussière, B., Constantin, M., Duchesne, J., Therrien, R., and Fortier, R. (2017) Passive mineral carbonation of Mg-rich mine wastes by atmospheric CO<sub>2</sub>. *Energy Procedia*, 114, 6083-6086.
- Beinlich, A., and Austrheim, H. (2012) In situ sequestration of atmospheric CO<sub>2</sub> at low temperature and surface cracking of serpentinized peridotite in mine shafts. *Chemical Geology*, 332–333, 32-44.
- Berner, R.A. (1990) Atmospheric carbon dioxide levels over phanerozoic time. *Science*, 249 (4975), 1382-1386.
- Bish, D.L. (1980) Anion-exchange in takovite: applications to other hydrotalcite minerals. *Bulletin Mineralogie*, 103, 170-175.
- Bish, D.L., and Howard, S.A. (1988) Quantitative phase analysis using the Rietveld method. *Journal of Applied Crystallography*, 21(2), 86-91.
- Bobicki, E.R., Liu, Q., Xu, Z., and Zeng, H. (2012) Carbon capture and storage using alkaline industrial wastes. *Progress in Energy and Combustion Science*, 38(2), 302-320.

- Brindley, G.W. (1945) XLV. The effect of grain or particle size on x-ray reflections from mixed powders and alloys, considered in relation to the quantitative determination of crystalline substances by x-ray methods. *Philosophical Magazine Series 7*, 36(256), 347-369.
- Catti, M., Ferraris, G., Hull, S., and Pavese, A. (1995) Static compression and H disorder in brucite,  $\text{Mg}(\text{OH})_2$ , to 11 Gpa: a powder neutron diffraction study. *Physics and Chemistry of Minerals*, 22, 200-206.
- Chang, E.E., Chen, C.H., Chen, Y.H., Pan, S.Y., and Chiang, P.C. (2011) Performance evaluation for carbonation of steel-making slags in a slurry reactor. *J Hazard Mater*, 186(1), 558-64.
- Cheary, R.W., and Coelho, A. (1992) A fundamental parameters approach to X-ray line-profile fitting. *Journal of Applied Crystallography*, 25(2), 109-121.
- Chung, F.H. (1974) Quantitative interpretation of X-ray diffraction patterns of mixtures 1. Matrix-flushing method for quantitative multicomponent analysis. *Journal of Applied Crystallography*, 7(6).
- Cleugh, H., Smith, M.S., Battaglia, M., and Graham, P. (2011) *Climate change science and solutions for Australia*. CSIRO Publishing, 150 Oxford Street Collingwood VIC Australia.
- Dipple, G.M., Raudsepp, M., and Gordon, T.M. (2002) Assaying wollastonite in skarn. In *Industrial Minerals in Canada*, Canadian Institute of Mining Metallurgy and Petroleum Special Volume, 53, 303-312.
- Dollase, W. (1986) Correction of intensities for preferred orientation in powder diffractometry: application of the March model. *Journal of Applied Crystallography*, 19(4), 267-272.

- Falini, G., Foresti, E., Gazzano, M., Gualtieri, A.F., Leoni, M., Lesci, I.G., and Roveri, N. (2004) Tubular-shaped stoichiometric chrysotile nanocrystals. *Chemistry*, 10(12), 3043-3049.
- Gualtieri, A.F. (2000) Accuracy of XRPD QPA using the combined Rietveld-RIR method. *Journal of Applied Crystallography*, 33(2), 267-278.
- Hamilton, J.L., Wilson, S.A., Morgan, B., Turvey, C.C., Paterson, D.J., Jowitt, S., McCutcheon, J., and Southam, C. (2018) Fate of transition metals during passive carbonation of ultramafic mine tailings via air capture with potentials for metal resource recovery. *International Journal of Greenhouse Gas Control*, In Press.
- Hamilton, J.L., Wilson, S.A., Morgan, B., Turvey, C.C., Paterson, D.J., MacRae, C., McCutcheon, J., and Southam, G. (2016) Nesquehonite sequesters transition metals and CO<sub>2</sub> during accelerated carbon mineralisation. *International Journal of Greenhouse Gas Control*, 55, 73-81.
- Harrison, A.L., Dipple, G.M., Power, I.M., and Mayer, K.U. (2015) Influence of surface passivation and water content on mineral reactions in unsaturated porous media: Implications for brucite carbonation and CO<sub>2</sub> sequestration. *Geochimica et Cosmochimica Acta*, 148, 477-495.
- Harrison, A.L., Power, I.M., and Dipple, G.M. (2013) Accelerated carbonation of brucite in mine tailings for carbon sequestration. *Environmental Science and Technology*, 47(1), 126-134.
- Hill, R.J., and Howard, C.J. (1987) Quantitative phase analysis from neutron powder diffraction data using the Rietveld method. *Journal of Applied Crystallography*, 20(6), 467-474.
- Hillier, S. (1999) Use of an air brush to spray dry samples for X-ray powder diffraction. *Clay Minerals*, 34, 127–135.

- Hitch, M., Ballantyne, S.M., and Hindle, S.R. (2010) Revaluing mine waste rock for carbon capture and storage. *International Journal of Mining, Reclamation and Environment*, 24(1), 64-79.
- Houghton, J.T., Ding, Y., Griggs, D.J., Noguera, M., van der Linden, P.J., Dai, X., Maskell, K., and Johnson, C.A. (2001) *Climate Change 2001: The scientific basis: Contribution of Working Group 1 to the third assessment report of the Intergovernmental Panel on Climate Change*. Cambridge University Press, U.K.
- IPCC. (2005) *IPCC special report on carbon dioxide capture and storage*. In O.D. Bert Metz, Heleen de Coninck, Manuela Loos, Leo Meyer, Ed, p. 442. Cambridge University Press, 40 West 20th Street, New York, NY 10011-4211, USA.
- IPCC. (2013) *Climate Change 2013: The physical science basis*. In IPCC, Ed. IPCC Working Group 1.
- IPCC. (2014) *Climate Change 2014: Mitigation of climate change*. In IPCC, Ed. IPCC Working Group 3.
- Kump, L.R., Brantley, S.L., and Arthur, M.A. (2000) Chemical weathering, atmospheric CO<sub>2</sub> and climate. *Annual Review of Earth and Planetary Sciences*, 28, 611-67.
- Lackner, K.S. (2002) Carbonate chemistry for sequestering fossil carbon. *Annual review of energy and the environment*, 27(1), 193-232.
- Lackner, K.S. (2003) A guide to CO<sub>2</sub> sequestration. *Science*, 300, 1677-1678.
- Lackner, K.S., Wendt, C.H., Butt, D.P., Joyce Jr, E.L., and Sharp, D.H. (1995) Carbon dioxide disposal in carbonate minerals. *Energy*, 20(11), 1153-1170.
- Laughton, C.A., and Green, N. (2002) Woodsreef magnesium project: An example of sustainable mineral waste processing from mined ore and its utilisation to produce refined metal products. *Green Processing 2002*. New South Wales Department of Mineral Resources, St Leonards, N.S.W., Australia, Cairns, QLD.

- Lechat, K., Lemieux, J.M., Molson, J.W., Beaudoin, G., and Hebert, R. (2016) Field evidence of CO<sub>2</sub> sequestration by mineral carbonation in ultramafic milling wastes, Thetford Mines, Canada. *International Journal of Greenhouse Gas Control*, 47, 110-121.
- Leung, D.Y.C., Caramanna, G., and Maroto-Valer, M.M. (2014) An overview of current status of carbon dioxide capture and storage technologies. *Renewable and Sustainable Energy Reviews*, 39, 426-443.
- Leventouri, T. (1997) A new method for measuring the degree of preferred orientation in bulk textured YBa<sub>2</sub>Cu<sub>3</sub>O<sub>x</sub>. *Physica C: Superconductivity*, 277(1-2), 82-86.
- March, A. (1932) Mathematische theorie der regelung nach der korn gestalt bei affiner deformation. *Zeitschrift für Kristallographie* 81, 285-297.
- McCutcheon, J., Dipple, G.M., Wilson, S.A., and Southam, G. (2015) Production of magnesium-rich solutions by acid leaching of chrysotile: A precursor to field-scale deployment of microbially enabled carbonate mineral precipitation. *Chemical Geology*, 413, 119-131.
- McCutcheon, J., Turvey, C.C., Wilson, S.A., Hamilton, J.L., and Southam, G. (2017) Mine site deployment of microbial carbonation for the stabilization of asbestos mine tailings. *Geochimica et Cosmochimica Acta*, Accepted in Press.
- McCutcheon, J., Wilson, S.A., and Southam, G. (2016) Microbially accelerated carbonate mineral precipitation as a strategy for in situ carbon sequestration and rehabilitation of asbestos mine sites. *Environmental Science & Technology*, 50(3), 1419-1427.
- Mellini, M., and Viti, C. (1994) Crystal structure of lizardite-1T from Elba, Italy. *American Mineralogist*, 79(11-12), 1194-1198.
- Merril, R.J., Butt, B.C., Forrest, V.C., Purdon, G., and Bramley-Moore, R.A. (1980) Asbestos production at Chrysotile Corporation of Australia Pty. Limited, Barraba,

- N.S.W. In J.T. Woodcock, Ed. Mining and metallurgical practices in Australasia, 10, p. 669-673. The Australasian Institute of Mining and Metallurgy, Clunies Ross House, 191 Royal Parade, Parkville, Victoria, Australia 3052.
- Millar, R.J., Fuglestedt, J.S., Friedlingstein, P., Rogelj, J., Grubb, M.J., Matthews, H.D., Skeie, R.B., Forster, P.M., Frame, D.J., and Allen, M.J. (2017) Emission budgets and pathways consistent with limiting warming to 1.5°C. *Nature Geoscience*, 10, 741-748.
- Miyata, S. (1983) Anion-exchange properties of hydrotalcite-like compounds. *Clays and Clay Minerals*, 31(4), 305-311.
- Oelkers, E.H., Gislason, S.R., and Matter, J. (2008) Mineral carbonation of CO<sub>2</sub>. *Elements*, 4, 333-337.
- Olowe, A. (1995) Crystal structures of pyroaurite and sjoegrenite. *Advances in X-ray Analysis*, 38, 749-755.
- Omotoso, O., McCarty, D.K., Hillier, S., and Kleeberg, R. (2006) Some successful approaches to quantitative mineral analysis as revealed by the 3<sup>rd</sup> Reynolds Cup contest. *Clays and Clay Minerals*, 54(6), 748-760.
- Oskierski, H.C., Dlugogorski, B.Z., and Jacobsen, G. (2013) Sequestration of atmospheric CO<sub>2</sub> in chrysotile mine tailings of the Woodsreef asbestos mine, Australia: quantitative mineralogy, isotopic fingerprinting and carbonation rates. *Chemical Geology*.
- Pacala, S., and Socolow, R. (2004) Stabilization wedges: Solving the climate problem for the next 50 years with current technologies. *Science*, 305.
- Pawley, G. (1981) Unit-cell refinement from powder diffraction scans. *Journal of Applied Crystallography*, 14(6), 357-361.

- Pederson, B.M., Schaible, K.J., and Winburn, R.S. (2004) Minimization of errors due to microabsorption or absorption contrast. *Advances in X-ray Analysis*, 47, 200-205.
- Power, I.M., Harrison, A.L., Dipple, G.M., Wilson, S.A., Kelemen, P.B., Hitch, M., and Southam, G. (2013a) Carbon mineralization: From natural analogues to engineered systems. *Reviews in Mineralogy & Geochemistry*, 77, 305-360.
- Power, I.M., Wilson, S.A., and Dipple, G.M. (2013b) Serpentinite carbonation for CO<sub>2</sub> sequestration. *Elements*, 9, 115-121.
- Power, I.M., Wilson, S.A., Harrison, A.L., Dipple, G.M., McCutcheon, J., Southam, G., and Kenward, P.A. (2014) A depositional model for hydromagnesite–magnesite playas near Atlin, British Columbia, Canada. *Sedimentology*, 61(6), 1701-1733.
- Pronost, J., Beaudoin, G., Lemieux, J.M., Hebert, R., Constantin, M., Marcouiller, S., Klein, M., Duchesne, J., Molson, J.W., Larachi, F., and Maldague, X. (2012) CO<sub>2</sub>-depleted warm air venting from chrysotile milling waste (Thetford Mines, Canada): Evidence for in-situ carbon capture from the atmosphere. *Geology*, 40(3), 275-278.
- Pronost, J., Beaudoin, G., Tremblay, J., Larachi, F., Duchesne, J., Hebert, R., and Constantin, M. (2011) Carbon sequestration kinetic and storage capacity of ultramafic mining waste. *Environ Sci Technol*, 45(21), 9413-20.
- Raudsepp, M., Pani, E., and Dipple, G.M. (1999) Measuring mineral abundance in skarn. I. The Rietveld method using X-ray powder-diffraction data. *The Canadian Mineralogist*, 13 (1-15).
- Rietveld, H. (1969) A profile refinement method for nuclear and magnetic structures. *Journal of Applied Crystallography*, 2(2), 65-71.
- Rinaudo, C., Gastaldi, D., and Bulluso, E. (2003) Characterization of chrysotile, antigorite and lizardite by FT-Raman spectroscopy. *Canadian Mineralogist*, 41, 883–890.

- Scarlett, N.V.Y., and Madsen, I.C. (2006) Quantification of phases with partial or no known crystal structures. *Powder Diffraction*, 21(4), 278-284.
- Scarlett, N.V.Y., Madsen, I.C., Cranswick, L.M.D., Lwin, T., Groleau, E., Stephenson, G., Aylmore, M., and Agron-Olshina, N. (2002) Outcomes of the International Union of Crystallography Commission on Powder Diffraction Round Robin on Quantitative Phase Analysis: samples 2, 3, 4, synthetic bauxite, natural granodiorite and pharmaceuticals. *Journal of Applied Crystallography*, 35, 383-400.
- Seifritz, W. (1990) CO<sub>2</sub> disposal by means of silicates. *Nature*, 345.
- Stephens, P.W. (1999) Phenomenological model of anisotropic peak broadening in powder diffraction. *Journal of Applied Crystallography*, 32, 281-289.
- Tsukimura, K., Sasaki, S., and Kimizuka, N. (1997) Cation distributions in nickel ferrites. *Japanese Journal of Applied Physics*, 36(6R), 3609.
- Turvey, C.C., Wilson, S.A., Hamilton, J.L., and Southam, G. (2017) Field-based accounting of CO<sub>2</sub> sequestration in ultramafic mine wastes using portable X-ray diffraction. *American Mineralogist*.
- Von Dreele, R.B. (1997) Quantitative texture analysis by Rietveld refinement. *Journal of Applied Crystallography*, 30(4), 517-525.
- Whitfield, P.S. (2008) Spherical harmonics preferential orientation corrections and structure solution from powder diffraction data - a possible avenue of last resort. *Journal of Applied Crystallography*, 42, 134-136.
- Wicks, F.J. (2000) Status of the reference X-ray powder-diffraction patterns for the serpentine minerals in the PDF database – 1997. *Powder Diffraction*, 15, 42–50.
- Wicks, F.J., and Whittaker, E.J.W. (1975) A reappraisal of the structures of the serpentine minerals *Canadian Mineralogist*, 13, 227-243.

- Wilson, S.A., Harrison, A.L., Dipple, G.M., Power, I.M., Barker, S.L.L., Mayer, K.U., Fallon, S.J., Raudsepp, M., and Southam, G. (2014) Offsetting of CO<sub>2</sub> emissions by air capture in mine tailings at the Mount Keith Nickel mine, Western Australia: Rates, controls and prospects for carbon neutral mining. *International Journal of Greenhouse Gas Control*, 25, 121-140.
- Wilson, S.A., Barker, S.L.L., Dipple, G.M., Atudorei, V. (2010) Isotopic disequilibrium during uptake of atmospheric CO<sub>2</sub> into mine process waters: implications for CO<sub>2</sub> sequestration. *Environmental Science & Technology*, 44, 9522–9529.
- Wilson, S.A., Dipple, G.M., Power, I.M., Thom, J.M., Anderson, R.G., Raudsepp, M., Gabites, J.E., and Southam, G. (2009a) Carbon dioxide fixation within mine wastes of ultramafic-hosted ore deposits: Examples from the Clinton Creek and Cassiar chrysotile deposits, Canada. *Economic geology*, 104, 95–112.
- Wilson, S.A., Raudsepp, M., and Dipple, G.M. (2009b) Quantifying carbon fixation in trace minerals from processed kimberlite; a comparative study of quantitative methods using X-ray powder diffraction data with applications to the Diavik diamond mine, Northwest Territories, Canada. *Applied Geochemistry*, 24(12), 2312-2331.
- Wilson, S.A., Raudsepp, M., and Dipple, G.M. (2006) Verifying and quantifying carbon fixation in minerals from serpentine-rich mine tailings using the Rietveld method with X-ray powder diffraction data. *American Mineralogist*, 91(8-9), 1331-1341.





## Declaration for Thesis Chapter 4

Declaration by candidate

In the case of Chapter 4, the nature and extent of my contribution is as follows:

<b>Nature of Contribution</b>	<b>Extent of contribution (%)</b>
Concept, conducted fieldwork, experimental design, conducted experiments, collected and analysed data, writing and editing.	60%

The following co-authors contributed to the work. If co-authors are students at Monash University, the extent of their contribution in percentage terms must be stated:

<b>Name</b>	<b>Nature of contribution</b>	<b>Extent of Contribution (%)</b>
Sasha A. Wilson	Supervisory role, fieldwork, assisted with data analysis and had input into the manuscript	15%
Jessica L. Hamilton	Fieldwork, data analysis	10%
Alastair W. Tait	Fieldwork, data analysis	10%
Jenine McCutcheon	Fieldwork	1%
Andreas Beinlich	Data analysis	1%
Stewart J. Fallon	Data analysis	1%
Gregory M. Dipple	Supervisory role	1%
Gordon Southam	Supervisory role, fieldwork	1%

The undersigned hereby certify that the above declaration correctly reflects the nature and extent of the candidate's and co-authors contributions to this work\*.

Candidate's signature:



Date:

22/03/2018

Main supervisor's signature:



Date: 22/03/2018

\* Note: Where the responsible author is not the candidate's main supervisor, the main supervisor should consult with the responsible author to agree on the respective contributions of the authors.

## Chapter 4

### **Hydrotalcites and hydrated Mg-carbonates as carbon sinks in serpentinite mineral wastes from the Woodsreef Chrysotile Mine, New South Wales, Australia: CO<sub>2</sub> limitation controls mineralogy and efficiency of CO<sub>2</sub> air capture in mine tailings**

Connor C. Turvey<sup>1\*</sup>, Siobhan A. Wilson<sup>1,2</sup>, Jessica L. Hamilton<sup>1,3</sup>, Alastair W. Tait<sup>1</sup>, Jenine McCutcheon<sup>3,4</sup>, Andreas Beinlich<sup>5,6</sup>, Stewart J. Fallon<sup>7</sup>, Gregory M. Dipple<sup>6</sup> and Gordon Southam<sup>3</sup>

<sup>1</sup>School of Earth, Atmosphere & Environment, Monash University, Clayton, Melbourne, Victoria 3800, Australia

<sup>2</sup>Department of Earth and Atmospheric Sciences, University of Alberta, Edmonton, Alberta, T6G 2E3, Canada

<sup>3</sup>School of Earth & Environmental Sciences, The University of Queensland, St Lucia, QLD 4072, Australia

<sup>4</sup>School of Earth and Environment, The University of Leeds, Leeds, LS2 9JT, United Kingdom

<sup>5</sup>The Institute for Geoscience Research (TIGeR), Curtin University, 6845 Perth, Australia

<sup>6</sup>Mineral Deposit Research Unit, Department of Earth, Ocean and Atmospheric Sciences, The University of British Columbia, 2207 Main Mall, Vancouver, British Columbia V6T 1Z4, Canada

<sup>7</sup>Research School of Earth Sciences, The Australian National University, Canberra, Australian Capital Territory 0200, Australia

Submitted to *The International Journal for Greenhouse Gas Control* 18/04/2018

#### 4.0 Abstract

Carbon mineralisation of ultramafic mine tailings can reduce net emissions of anthropogenic carbon dioxide by reacting Mg-silicate and hydroxide minerals with atmospheric CO<sub>2</sub> to produce carbonate minerals. We investigate the controls on carbonate mineral formation at the derelict Woodsreef chrysotile mine (NSW, Australia). Quantitative XRD was used to understand how mineralogy changes with depth into the tailings pile, and shows that hydromagnesite [Mg<sub>5</sub>(CO<sub>3</sub>)<sub>4</sub>(OH)<sub>2</sub>·4H<sub>2</sub>O], is present in shallow tailings material (<40 cm), while coalingite [Mg<sub>10</sub>Fe<sup>3+</sup><sub>2</sub>(CO<sub>3</sub>)(OH)<sub>24</sub>·2H<sub>2</sub>O] and pyroaurite [Mg<sub>6</sub>Fe<sup>3+</sup><sub>2</sub>(CO<sub>3</sub>)(OH)<sub>16</sub>·4H<sub>2</sub>O] are forming deeper in the tailings material. This indicates that there may be two geochemical environments within the upper ~1 m of the tailings, with hydromagnesite forming within the shallow tailings via carbonation of brucite in CO<sub>2</sub>-rich conditions, and pyroaurite and coalingite forming under more carbon limited conditions at depth. Radiogenic isotope results indicate hydromagnesite and pyroaurite have a modern (F<sup>14</sup>C > 0.8) atmospheric CO<sub>2</sub> source. Laboratory-based anion exchange experiments, conducted to explore stable C isotope fractionation in pyroaurite, shows that pyroaurite δ<sup>13</sup>C values change with carbon availability, and <sup>13</sup>C-depleted signatures are typical of hydrotalcites in C-limited environments, such as the deep tailings at Woodsreef. Quantitative XRD and elemental C data estimates that Woodsreef absorbs between of 229.0–405.1 g CO<sub>2</sub> m<sup>-2</sup> y<sup>-1</sup>.

**Keywords:** carbon sequestration, hydrotalcites, brucite, hydromagnesite, carbon accounting, mine tailings

## 4.1 Introduction

The release of anthropogenic greenhouse gases into the atmosphere has been linked to alteration of the Earth's climate, with research estimating that global average surface temperature increases are likely to exceed 1.5°C by the end of the 21<sup>st</sup> Century, and potentially reach 2°C (Houghton et al., 2001; IPCC, 2005; IPCC, 2013; IPCC, 2014). Strategies are needed not only to reduce emissions but to actively capture greenhouse gases, chiefly CO<sub>2</sub>, from the atmosphere in order to mitigate the adverse effects of anthropogenic climate change. The adoption of market controls on greenhouse gas emissions, reducing deforestation, and increasing use of both renewable energy and carbon sequestration technologies are becoming necessary to limit the adverse effects of anthropogenic greenhouse gas release (Cleugh et al., 2011; IPCC, 2013; IPCC, 2014; Pacala and Socolow, 2004). Carbon sequestration is important to this effort as it provides a mechanism for both preventing emissions and lowering atmospheric CO<sub>2</sub> concentrations by capturing this greenhouse gas directly from air. Carbon mineralisation, whereby CO<sub>2</sub> is trapped and stored within carbonate minerals, uses the lithosphere as a long term sink for carbon (e.g., Kump et al., 2000; Lackner et al., 2003; Lackner et al., 1995; Matter et al., 2016; Seifritz, 1990). Carbon mineralisation reactions can be used to carbonate mine tailings and other alkaline wastes via reaction with either CO<sub>2</sub>-rich waste gas streams from power plants or with atmospheric CO<sub>2</sub> (as reviewed in Bobicki et al., 2012; Cleugh et al., 2011; Lackner, 2002; Leung et al., 2014; Oelkers et al., 2008; Power et al., 2013a).

Passive carbon mineralisation is a natural weathering process that occurs as silicate and hydroxide minerals react with atmospheric CO<sub>2</sub> under ambient conditions, to produce carbonate minerals (Brantley, 2003; Kump et al., 2000). It has been predicted that over a timescale of 10<sup>6</sup> years, carbonate minerals will ultimately act as the sink for all

anthropogenic CO<sub>2</sub> via natural silicate weathering (Kump et al., 2000). However, the rate of natural silicate weathering is typically orders of magnitude too slow to remove excess anthropogenic CO<sub>2</sub> from the atmosphere within the 21<sup>st</sup> century (the timescale on which this must be done to limit further changes to the climate). If carbon mineralisation is to play an effective role in climate change mitigation, then strategies must be developed to drastically increase the rates of silicate and hydroxide weathering, and precipitation of carbonate minerals. Ultramafic mine tailings are of great interest as feedstocks for *enhanced* passive carbonation reactions, as described by Power et al. (2013a), because they contain abundant Mg-rich silicate and hydroxide minerals and have a smaller grainsize and increased reactive surface area due to ore processing (Wilson et al., 2009a; Wilson et al., 2006). Passive carbonation, that which has not been accelerated intentionally, is known to occur at rapid rates within the tailings material of several ultramafic mines in Canada, Norway, South Africa and Australia (e.g., Bea et al., 2012; McCutcheon et al., 2015; Mervine et al., in review; Oskierski et al., 2013; Pronost et al., 2012; Turvey et al., 2017; Wilson et al., 2009a; Wilson et al., 2009b; Wilson et al., 2014). Laboratory and field studies are being conducted into how biotic and abiotic treatments may be used to increase carbonation rates within tailings even further (e.g., Gras et al., 2015; Gras et al., 2017; Hamilton et al., in prep-a; Harrison et al., 2013; Harrison et al., 2015; Lechat et al., 2016; McCutcheon et al., 2015; McCutcheon et al., 2016; McCutcheon et al., 2017; Power et al., 2010; Power et al., 2011; Zarandi et al., 2017). Increasing carbonation rates within mine tailings storage facilities has the potential to offset 100% or more of the emissions produced by many ultramafic mines, allowing for the possibility of carbon neutral mining practices (Hitch et al., 2010; Power et al., 2014; Wilson et al., 2014).

Much of the current research on tailings carbonation has focused on sequestration of CO<sub>2</sub> during the dissolution of brucite and Mg-silicate minerals and the precipitation of hydrated

Mg-carbonate minerals (e.g., Assima et al., 2013a; Assima et al., 2013b; Wilson et al., 2014; Wilson et al. 2009a). However, CO<sub>2</sub> may also be sequestered by (1) alteration of brucite to form carbonate-bearing hydrotalcite minerals (Oskierski et al., 2013; Turvey et al., 2017) or (2) anion exchange reactions by which Cl<sup>-</sup> or SO<sub>4</sub><sup>2-</sup>-bearing hydrotalcite minerals can be converted to their carbonate analogues (Mills et al., 2011; Woodhouse, 2006). Hydrotalcite supergroup minerals (hereafter ‘hydrotalcites’) are anionic clays that consist of positively charged hydroxide layers and negatively charged interlayer galleries that contain H<sub>2</sub>O molecules and various anions including CO<sub>3</sub><sup>2-</sup>, Cl<sup>-</sup> or SO<sub>4</sub><sup>2-</sup> (Cavani et al., 1991; Evans and Slade, 2006; Mills et al., 2012). Hydrotalcite minerals are commonly found in ultramafic rocks, and the tailings produced from ultramafic-hosted mineral deposits, thus, in some cases they may represent an additional carbon sink at mine sites provided that they are taking up a net quantity of atmospheric CO<sub>2</sub> (Mills et al., 2011; Oskierski et al., 2013; Turvey et al., 2017; Wilson et al., 2014; Woodhouse, 2006). Hydrotalcite minerals can form via high temperature carbonation of spinel minerals (e.g., Ashwal and Cairncross, 1997; Grguric, 2003, Grguric et al., 2001; Melchiorre et al., 2016; Melchiorre et al., 2018) and low temperature carbonation of brucite (e.g., Mumpton et al., 1965; Mumpton and Thompson, 1966). Hydrotalcite minerals can also undergo anion exchange with solutions, potentially sequestering carbonate anions from the local environment via exchange for interlayer chloride, sulfate and other common anions (Bish, 1980; Bish and Brindley, 1977; Miyata, 1983; Miyata and Okada, 1977). Hydrotalcites such as those in the pyroaurite–iowaite series [Mg<sub>6</sub>Fe<sup>3+</sup><sub>2</sub>(CO<sub>3</sub>)(OH)<sub>16</sub>·4H<sub>2</sub>O–Mg<sub>6</sub>Fe<sup>3+</sup><sub>2</sub>(Cl<sub>2</sub>)(OH)<sub>16</sub>·4H<sub>2</sub>O] and the stichtite–woodallite series [Mg<sub>6</sub>Cr<sup>3+</sup><sub>2</sub>(CO<sub>3</sub>)(OH)<sub>16</sub>·4H<sub>2</sub>O–Mg<sub>6</sub>Cr<sup>3+</sup><sub>2</sub>(Cl<sub>2</sub>)(OH)<sub>16</sub>·4H<sub>2</sub>O], as well as coalingite [Mg<sub>10</sub>Fe<sup>3+</sup><sub>2</sub>(CO<sub>3</sub>)(OH)<sub>24</sub>·2H<sub>2</sub>O], have previously been observed in the tailings at the Woodsreef chrysotile mine (Oskierski et al., 2013; Turvey et al., 2017) and the Mount Keith

nickel mine (Grguric, 2003; Grguric et al., 2001; Wilson et al., 2014) in Australia, and the Clinton Creek chrysotile mine in Canada (Wilson et al., 2009a; Wilson et al., 2006).

Various carbonate phases differ in terms of the efficiency with which they sequester CO<sub>2</sub> and what geochemical conditions are required to promote their formation (Power et al., 2013b). The efficiency with which they sequester CO<sub>2</sub> depends on the elemental composition of the carbonate phase, including the ratio of CO<sub>2</sub> to MgO, and the amount of H<sub>2</sub>O in the precipitating carbonate mineral. The CO<sub>2</sub> to MgO ratio dictates how much CO<sub>2</sub> can be sequestered with a given amount of aqueous Mg, while the hydration state of the carbonate mineral will determine (1) the water budget necessary for forming a given mineral (Power et al., 2013b) and (2) its temperature- and humidity-dependent stability (Davies and Bubela, 1973; Morgan et al., 2015). By understanding the geochemical relationships between different carbonate-bearing minerals, and quantifying the amount of CO<sub>2</sub> sequestered by each group of minerals at a given mine site, we can improve our ability to optimise carbon sequestration within mine tailings. It is important to determine which phases are sourcing carbon from the atmosphere in a mine tailings storage facility that contains multiple carbonate-bearing phases. Radiocarbon, and stable C and O isotopes can be used to fingerprint the origins of carbon within carbonate minerals for the purposes of carbon accounting in mine tailings (Gras et al., 2017; Oskierski et al., 2013; Wilson et al., 2011; Wilson et al., 2009a; Wilson et al., 2014). Elemental carbon analysis can be used to determine the total carbon content of a tailings sample; however, this technique cannot be used to differentiate between pools of carbon hosted within different minerals and it cannot be used to distinguish between the carbon sources from which minerals have formed (e.g., atmospheric CO<sub>2</sub> versus recycled bedrock carbon). Quantitative powder X-ray diffraction (XRD) and isotopic fingerprinting methods can be used together to quantify the abundance of each carbonate-bearing mineral phase that has a modern, atmospheric source of CO<sub>2</sub> in a

sample of mine tailings (Oskierski et al., 2013; Wilson et al., 2014; Wilson et al., 2006; Wilson et al., 2009b). By determining the modal mineralogy of a tailings sample, it becomes possible to not only estimate how much CO<sub>2</sub> has been sequestered but also to determine which carbonate-bearing minerals are sequestering the most atmospheric CO<sub>2</sub>. In this way, the efficiency of carbonation reactions can be assessed and enhanced passive carbonation schemes may be designed to favour formation of carbonate minerals with optimal Mg:CO<sub>2</sub> and Mg:H<sub>2</sub>O ratios (e.g., Power et al. 2013b).

The Woodsreef chrysotile mine was Australia's largest tonnage chrysotile mine, producing 24 Mt of tailings during operation from 1972–1983 (Laughton and Green, 2002; Merrill et al., 1980). Since closure of the mine in 1983, the tailings material at Woodsreef has been left exposed to the atmosphere and has not been disturbed, making it an ideal natural laboratory in which to observe carbon mineralisation reactions. Furthermore, previous carbon mineralisation studies at Woodsreef have shown that multiple carbonate minerals are present in the tailings including pyroaurite, coalingite, hydromagnesite and trace amounts of bedrock calcite, magnesite and dolomite (Hamilton et al., 2018; McCutcheon et al., 2017; McCutcheon et al., 2016; Oskierski et al., 2013; Turvey et al., 2017). This makes it an excellent study site to understand the geochemical conditions that favour formation of one carbonate alteration mineral versus another in the mine tailings environment and to determine how much CO<sub>2</sub> is sequestered by each of the hydrotalcite minerals and hydrated Mg-carbonate minerals.

The purpose of this study is to improve our understanding of the zonal distribution of hydromagnesite, pyroaurite and coalingite in the mine tailings pile at Woodsreef. Hydrotalcite phases are present in significant abundances at many ultramafic mine tailings storage facilities, but we currently lack knowledge regarding the role they play in

sequestering atmospheric CO<sub>2</sub>. Because little is known about stable isotope fractionation in hydrotalcite minerals, an anion exchange experiment was conducted as part of this study to determine how the stable C isotopic composition of hydrotalcites changes during the incorporation of atmospheric CO<sub>2</sub> into pyroaurite-iowaite. Understanding the different conditions under which hydrotalcites and hydrated Mg-carbonate minerals form within a mine tailings storage facility, can potentially lead to the alteration of geochemical conditions in the tailings as a means of enhancing the rate of carbon sequestration and encouraging the formation of optimal carbonate mineral products.

## **4.2 Material and methods**

### **4.2.1 Field site and sampling methods**

Samples were collected from the tailings pile and mine pit at the Woodsreef chrysotile mine, New South Wales, Australia (Figure 4.1) during field excursions in 2014, 2015 and 2016. Samples collected from Woodsreef include carbonate-rich surface crusts, cobbles of waste rock and unconsolidated tailings material (Figure 4.2). 77 samples of tailings material were collected from a series of 7 vertical profiles that were excavated using shovels and a gravel coring device. These profiles varied from between 20 cm and 120 cm in depth, with samples of tailings material collected every 10 cm to study the mineralogical and isotopic variation that occurs with depth into the tailings pile.

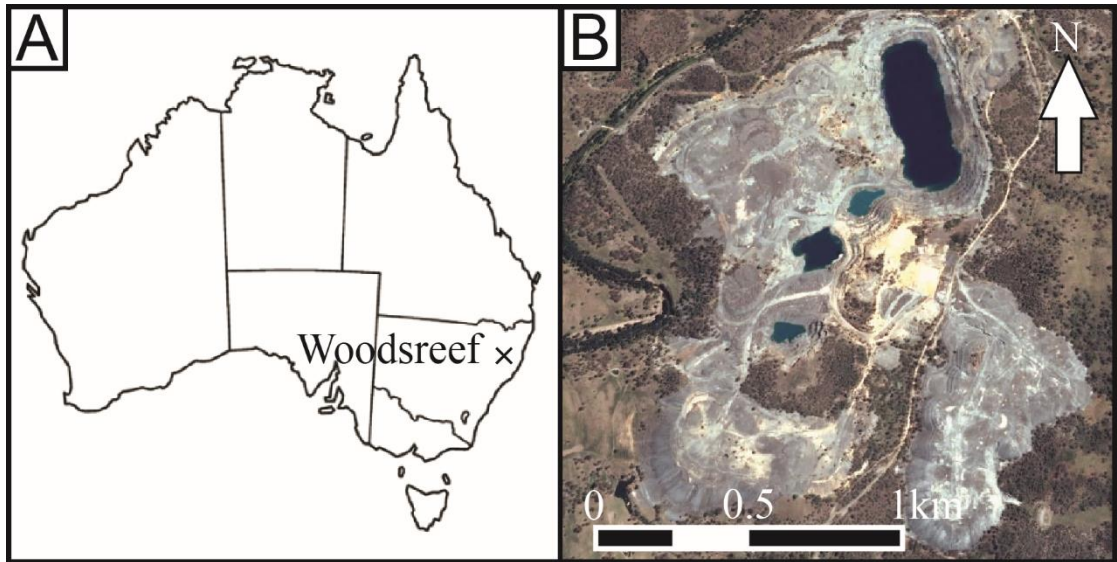


**Figure 4.1** (a) Map showing the location of the Woodsreef chrysotile mine. (b) Aerial photograph of the Woodsreef chrysotile mine.

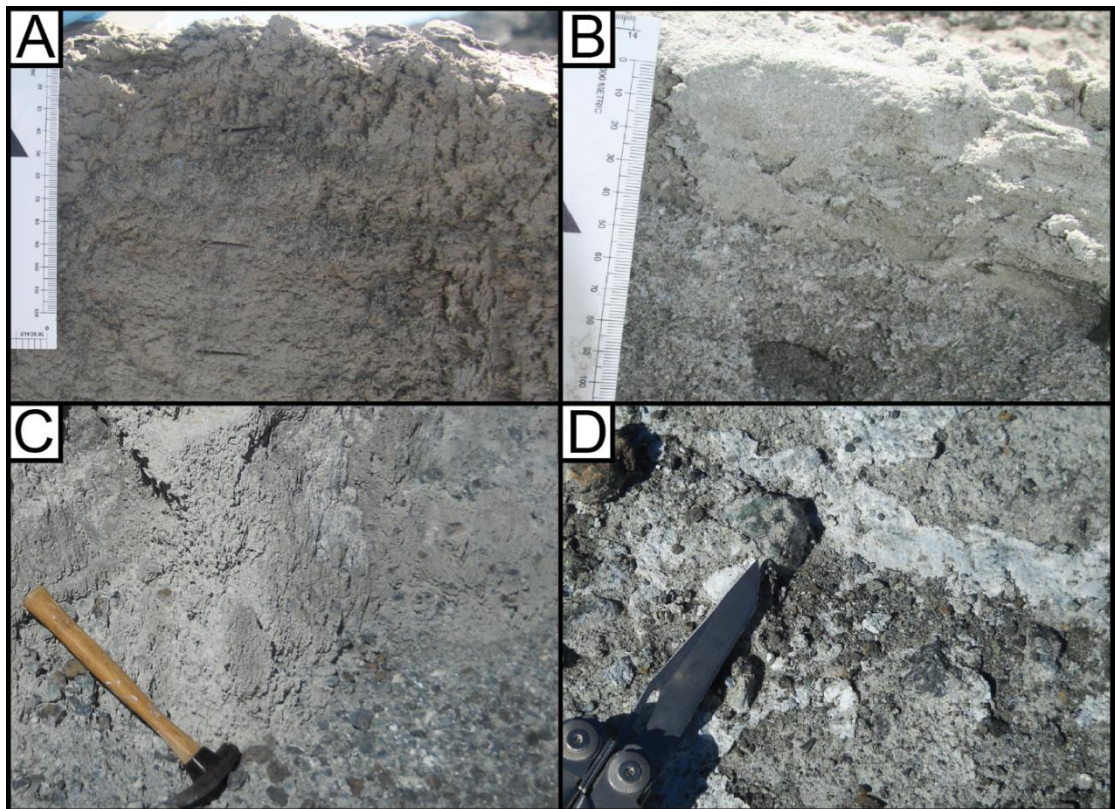


**Figure 4.2** Field photographs of (a) loose shallow tailings (14WRP-1, 15cm ruler for scale), (b) loose shallow tailings (14WRP-4, 15cm ruler for scale), (c) vertical crusts forming on the surface of the tailings (hammer for scale) and (d) horizontal crusts on the surface of the tailings (multi-tool for scale).

#### 4.2.2 X-ray diffraction methods

X-ray diffraction (XRD) is widely used to determine the composition of geological samples through qualitative phase identification and quantitative compositional analysis. However, quantification of mineral abundances using XRD data is complicated by the presence of serpentine minerals in the samples from Woodsreef. The serpentine polymorphs, chrysotile and lizardite, are the major components of the Woodsreef tailings, and both have crystal structures affected by turbostratic stacking disorder (Wicks and Whittaker, 1975). Rietveld refinements, which are typically used to obtain quantitative information from XRD data, require that all mineral phases in a sample have well defined crystal structures (Bish and Howard, 1988; Hill and Howard, 1987; Rietveld, 1969). This means that the mineralogical composition of samples that contain serpentine minerals cannot be quantified using normal Rietveld refinements. This challenge has been overcome in previous studies by using different quantitative XRD methods or by using modified Rietveld refinement methods. Wilson et al. (2009b) and Oskierski et al. (2013) used the internal standard method of Alexander and Klug (1948) and the reference intensity ratio (RIR) method of Chung (1974) to measure the abundances of carbonate-bearing minerals in serpentine rich tailings instead of employing Rietveld refinements. Wilson et al. (2006) developed a structureless fitting procedure that employs the use of a Pawley phase and a known amount of an internal standard to measure the abundance of one or more serpentine minerals using the Rietveld method. Turvey et al. (2017) trialled the use of the structureless Rietveld refinement procedure of Scarlett and Madsen (2006) for quantification of phases with Partial Or No Known Crystal Structure (PONKCS) in order to quantify carbonation of the mine tailings at Woodsreef using a portable X-ray diffractometer. Turvey et al. (in review)/Chapter 3 compared the accuracy of modal mineralogy results obtained using the PONKCS method and the Pawley/internal standard method by analysing artificial tailings samples with known

compositions. Turvey et al. (in review)/Chapter 3 found that the Pawley/internal standard method gave more accurate results for samples containing serpentine minerals, brucite, pyroaurite and hydromagnesite, the most important minerals that must be quantified to account for CO<sub>2</sub> sequestration and carbonation potential at Woodsreef and many other ultramafic mines. Following extensive calibration and optimisation for accuracy by Turvey et al. (2017, in review), these structureless fitting methods can now be applied more reliably to natural tailings samples of an unknown composition including those samples from Woodsreef.

**4.2.2.1 Instrument details.** XRD patterns of tailings samples were collected using a Bruker D8 Advance X-ray Diffractometer and a Bruker D8 Advance Eco X-ray Diffractometer located in the Monash X-ray Platform at Monash University. Patterns were collected on the D8 Advance using a Cu X-ray tube operating at 40 kV and 40 mA, and data were collected using a LynxEye 1D Position Sensitive Detector. The D8 Advance Eco, was operated using a Cu X-ray tube at 40 kV and 25 mA. All data were collected over a  $2\theta$  range of 3–80° with a step size of 0.02° and a dwell time of 1s/step. Samples were loaded into back loading cavity mounts against frosted glass slides or 400 grit sandpaper to reduce preferred orientation of crystallites. Qualitative identification of minerals from the XRD patterns was performed using DIFFRAC.EVA V.2 (Bruker AXS) with reference to standard patterns from the ICDD PDF-2 database and the Crystallography Open Database.

**4.2.2.2 Quantitative XRD.** Rietveld refinements using the Pawley/internal standard method were used to determine the modal mineralogy of the tailings samples. Refinements were performed with the software package DIFFRAC.TOPAS V.5 (Bruker AXS) using the fundamental parameters approach (Cheary and Coelho, 1992). A combination of the RIR method (Chung, 1974) and the Rietveld refinement procedure of Wilson et al. (2006) were

used to quantify the abundances of disordered, poorly crystalline or amorphous phases found within the tailings samples. The sources of crystal structure data that were used for Rietveld refinements are listed in Table 4.1.

**Table 4.1** Sources of crystal-structure data for Rietveld refinement

Mineral	Source
Pyroaurite	Olowe (1995)
Iowaite	Braithwaite (1994)
Magnetite	Tsukimura et al. (1997)
Hematite	Maslen et al. (1994)
Brucite	Catti et al. (1995)
Hydromagnesite	Akao and Iwai (1977)
Chrysotile	Falini et al. (2004)
Lizardite	Mellini and Viti (1994)

**4.2.2.3 Pawley/internal standard method.** The Pawley/internal standard method of Wilson et al. (2006) was used to analyse all XRD patterns collected in this study. The results of Turvey et al. (in review)/Chapter 3 indicate that this method produces more accurate quantitative mineralogical results for serpentinite mine tailings than the PONKCS method of Scarlett and Madsen (2006). A known amount (10 wt%) of an annealed, in-house fluorite ( $\text{CaF}_2$ ) standard was added to each sample prior to homogenisation and pulverisation under anhydrous ethanol in a McCrone Micronising Mill for 7 minutes. Samples were left to dry overnight at room temperature in a fume hood following milling. Once dry, each sample was disaggregated and homogenised using an agate mortar and pestle. The Pawley/internal standard method can be used to calculate the ‘amorphous’ content in a sample (in this case the serpentine content of the sample),  $X_a$  from the refined and known abundances of the internal fluorite standard using Eq.1:

$$X_a = \left(\frac{100}{90}\right) \left[1 - \left(\frac{X_s}{X_{s,c}}\right)\right] \quad (1)$$

where  $X_s$  is the measured weight of the internal standard and  $X_{s,c}$  is the refined weight of the internal standard (Gualtieri, 2000; Turvey et al., in review/Chapter 3; Wilson et al., 2006).

Refinements were done using the approach outlined by Turvey et al. (in review)/Chapter 3. Serpentine peaks were modelled using a peaks phase produced using the Pawley method (Pawley, 1981) to extract peak intensities independently of atomic scattering. Appropriate space groups and cell dimension were taken from Falini et al. (2004) for the chrysotile model and Mellini and Viti (1994) for the lizardite model (Table 4.1). The background was modelled using a fourth-order Chebychev polynomial with an additional  $1/x$  function. A default Brindley radius of 250 nm and a packing density of 0.4 were used to correct for microabsorption contrast amongst mineral phases (Brindley, 1945). Scale factors and unit cell parameters were allowed to refine for all phases. Lorentzian crystallite size and strain were permitted to refine from starting values of 1000 nm and 0.1 respectively (with minimum and maximum values of 60 to 10,000 nm for crystallite size and 0.0001 and 0.2 for strain). The March-Dollase correction (Dollase, 1986; March, 1932) was used to model the peak profiles of minerals that suffered from preferred orientation (refining between values of 0.6 and 1).

**4.2.2.4 Reference intensity ratio method.** Samples containing coalingite were analysed using the normalised Reference Intensity Ratio (RIR) method (Chung, 1974). The RIR method was used for this purpose because no suitable coalingite structure could be found for use in Rietveld refinements. The coalingite structure of Pastor-Rodriguez and Taylor (1971) did not correctly fit the positions of the (0 0 6) and (0 0 9) peaks for the coalingite in our samples. Although the coalingite pattern of Jambor (1969), which is found in the ICDD PDF database, gave the correct peak positions, there is no published crystal structure for this sample of coalingite.

The RIR used here to measure the abundance of coalingite is the ratio of the integrated intensities of the coalingite (0 0 9) reflection and the fluorite (1 1 1) reflection. Chung (1974)

presented a formula (Eq. 2) that allows the RIR to be used to estimate the weight fraction of any mineral phase in a sample that contained a known amount of a flushing agent:

$$X_i = X_f \left(\frac{k_f}{k_i}\right) \left(\frac{I_i}{I_f}\right) \quad (2)$$

where  $X_i$  and  $X_f$  are the weight fractions of the  $i^{\text{th}}$  mineral component of the sample and the flushing agent  $f$ ,  $k_f$  and  $k_i$  are the reference intensity ratios of the  $i^{\text{th}}$  component and the flushing agent and  $I_i$  and  $I_f$  are the intensities of the reference peak or peaks of the  $i^{\text{th}}$  component and the flushing agent. The 10 wt% fluorite standard was used as the flushing agent. The reference intensity ratios  $k_f$  and  $k_i$  were taken from the ICDD PDF database, and are calculated for the mineral in question and corundum  $k_f = 11.89$  (fluorite PDF 01-073-4219) and  $k_i = 5.67$  (coalingite PDF 00-034-0182).

The peak positions and integrated intensities of the fluorite (1 1 1) and coalingite (0 0 9) reference peaks were determined using the software package DIFFRAC.TOPAS V.5. Peaks were located manually and the integrated intensity of each reference peak was refined using the fundamental parameters approach (Cheary and Coelho, 1992). The average positions obtained using  $\text{CoK}\alpha$  radiation were  $20.9 \pm 0.1^\circ 2\theta$  for the coalingite (0 0 9) reflection and  $28.29 \pm 0.05^\circ 2\theta$  for the fluorite (1 1 1) reflection. Once the coalingite abundance had been estimated, the results of the Pawley/internal standard analyses were renormalised to take the abundance of coalingite into account.

### 4.2.3 Scanning electron microscopy

Scanning electron microscopy (SEM) was used to investigate the textural relationships between brucite, pyroaurite and coalingite in the deep tailings samples. Coarse grained (sand sized) pieces of the tailings were taken from a sample collected at a depth of 1 m from profile 15WR2-DC, mounted on aluminium stubs and secured using super glue, and then coated

with Ir for SEM analysis. Back scattered electron (BSE) and secondary electron micrographs (SE) were collected at the Monash Centre for Electron Microscopy (MCEM) using a JEOL 7001F FEG-SEM. SE-SEM and BSE-SEM was conducted in conjunction with elemental analysis using energy dispersive X-ray spectroscopy (EDS), using an accelerating voltage of 15 kV and working distance of 10 mm. Analysis of semi-qualitative EDS data and image processing were conducted using Oxford Instruments Aztec™ V3.3 analysis software.

#### **4.2.4 Stable carbon and oxygen isotope analysis**

Stable C and O isotope analysis of tailings samples and pure hydrotalcite samples was completed using a Los Gatos Research off-axis integrated cavity output spectrometer (OA-ICOS) located in the Department of Earth, Ocean and Atmospheric Sciences (The University of British Columbia). Detailed methods are described in Beinlich et al. (2017). Samples were placed into 3.7 mL borosilicate glass vials that were sealed with butyl rubber septa. CO<sub>2</sub> was released from the samples by reaction with ~0.2 mL H<sub>3</sub>PO<sub>4</sub> (85% pure) over approximately 1 hour at 72°C. Analysis of the CO<sub>2</sub> gas was performed using the OA-ICOS CO<sub>2</sub> isotope analyser in ‘batch’ mode (after Beinlich et al., 2017). Small sample volumes were flushed with CO<sub>2</sub> free ‘zero gas’. Isotopologue concentrations were measured before being converted to isotope ratio numbers (*R*). *R*(<sup>13</sup>C) and *R*(<sup>18</sup>O) values were converted to conventional  $\delta$  notation ( $\delta^{13}\text{C}_{\text{VPDB}}$ ,  $\delta^{18}\text{O}_{\text{VSMOW}}$ ) by the analysis of additional stable isotope reference materials of a known composition (Beinlich et al., 2017).

Stable C and O isotope ratios of additional tailings samples and solid samples collected from one of the anion exchange experiments (the high CO<sub>2</sub> experiment, see section 4.2.6) were measured at Monash University in the School of Earth, Atmosphere and Environment following the procedures outlined by Clark and Fritz (1997).  $\delta^{13}\text{C}_{\text{VPDB}}$  and  $\delta^{18}\text{O}_{\text{VSMOW}}$  values of carbonates were measured via acidification with phosphoric acid in sealed vials in a He

atmosphere using a Finnigan MAT Gas Bench coupled with a Thermo Delta Advanced mass spectrometer. Normalisation to the VPDB (carbon) and VSMOW (oxygen) scales was via analysis of the IAEA calcite standard CO-1. Precision is on the order of 0.1-0.2 ‰ for  $\delta^{13}\text{C}$  and 0.4-0.5 ‰ for  $\delta^{18}\text{O}$  values.

#### **4.2.5 Radiocarbon analysis**

Radiocarbon data and additional  $\delta^{13}\text{C}$  values were obtained in the Research School of Earth Sciences at The Australian National University using a Single Stage Accelerator Mass Spectrometer (SSAMS). The instrument is equipped with a gas/graphite hybrid ion source, allowing for direct analysis of  $\text{CO}_2$  as well as traditional graphite targets (Fallon et al., 2010).  $\delta^{13}\text{C}$  values are quoted from the SSAMS instrument for each of the samples that was analysed for radiocarbon content (including samples from the low  $\text{CO}_2$  anion exchange experiment, pure samples of hydrotalcite minerals and bulk tailings from Woodsreef). The precision of stable carbon isotope analyses on the SSAMS is lower than for IRMS and laser absorption spectrometry (LAS). Thus, results for the same sample obtained using SSAMS may differ from those collected using other techniques employed in this study. Radiocarbon concentration is reported as the fraction of modern carbon,  $F^{14}\text{C}$ . Values for conventional radiocarbon age, using the Libby half-life of 5568 years, are also provided following the conventions of Stuiver and Polach (1977). Sample preparation backgrounds were subtracted based on measurements of  $^{14}\text{C}$ -free  $\text{CO}_2$ .

#### **4.2.6 Anion exchange experiment**

Few studies report stable isotopic data for pure hydrotalcite minerals or samples containing hydrotalcite minerals (Johnson and Bullen, 2003; Melchiorre et al., 2016; Melchiorre et al., 2014; Oskierski et al., 2013; Schellenger and Larese-Casanova, 2013; Wilson et al., 2014) and no equilibrium stable isotopic fractionation factors have been determined for any

hydrotalcite mineral in any isotope system. Without an understanding of the kind of isotopic signatures that are expected for hydrotalcite minerals, and in the absence of known or calculated fractionation factors, it is difficult to interpret stable C and O isotope data for these minerals. We conducted two proof-of-concept anion exchange experiments using iowaite [ $\text{Mg}_6\text{Fe}^{3+}_2\text{Cl}_2(\text{OH})_{16}\cdot 4\text{H}_2\text{O}$ ] sourced from the Mount Keith nickel mine in order to better constrain the fractionation of stable C and O isotopes during uptake of dissolved inorganic carbon (DIC) into hydrotalcite minerals. Coalingite and pyroaurite at Woodsreef are potentially forming from brucite under carbon limited conditions within the tailings (Turvey et al., 2017), as has been seen within other serpentinites (Mumpton et al., 1965; Mumpton and Thompson, 1966). This makes an anion exchange experiment using a non-carbonate bearing hydrotalcite phase such as iowaite a closer analogue to the carbon-poor conditions that are expected to occur within the tailings, as opposed to a hydrotalcite synthesis experiment which would typically use concentrated carbonate salt (such as  $\text{Na}_2\text{CO}_3$ ) rather than the dissolution of atmospheric  $\text{CO}_2$  as a source of carbon.

Samples of iowaite were hand-picked using tweezers and ground using an agate mortar and pestle before being placed in stirred beakers containing an excess of MilliQ water ( $18.2 \text{ M}\Omega\cdot\text{cm}$ ) for 46 hours at room temperature ( $\sim 22^\circ\text{C}$ ). The only source of carbon, apart from any carbonate anions already present within the iowaite samples, was  $\text{CO}_2$  gas from the laboratory atmosphere ( $\sim 400 \text{ ppm}$ ). A stir bar was used to encourage dissolution of atmospheric  $\text{CO}_2$  into solution. Thus, the experiment was designed so that chlorine anions within the interlayer galleries of the iowaite structure would be replaced with carbonate ions sourced from the atmosphere, and introduced into solution by diffusion during the vigorous stirring of the water. Previous anion exchange experiments have shown that carbonate is preferentially incorporated into the interlayer galleries of hydrotalcite minerals over other common anions (Bish, 1980; Miyata, 1983). Two conditions were used, a low C condition

in which 50-100 mg of iowaite was placed in 100 mL of MilliQ water and gently agitated by the stir bar at 200 RPM and a high C condition in which 100 mg of iowaite was placed in 150 mL of water and vigorously agitated by the stir bar at 600 RPM. Subsamples of the solid phase were collected at multiple time points from both treatments and analysed for their stable carbon and oxygen isotopic composition using the methods described in the preceding sections.

#### **4.2.7 Total carbon analysis and carbon accounting**

Quantitative XRD data have previously been used to estimate the amount of CO<sub>2</sub> sequestered in tailings (Bea et al., 2012; McCutcheon et al., 2017; Oskierski et al., 2013; Turvey et al., 2017; Wilson et al., 2014; Wilson et al., 2006; Wilson et al., 2009b). This approach provides a stoichiometric estimate of the amount of atmospheric CO<sub>2</sub> stored within minerals, and can discriminate between carbon in primary gangue minerals and secondary alteration minerals (Wilson et al., 2006; Wilson et al., 2009b). For samples that contain relatively low abundances of gangue carbonate minerals, elemental carbon analysis can be used to provide a more direct estimate of the amount of carbon sequestered in a sample. The tailings at the Woodsreef mine contain only rare gangue carbonate minerals (e.g., calcite, dolomite and magnesite) which, where detected, are only present at low total abundances (<1 wt%) (McCutcheon et al., 2017; Oskierski et al., 2013; Turvey et al., 2017), making this locality an ideal setting in which to test the relative accuracy of quantitative XRD and elemental carbon analysis for carbon accounting in mine tailings. Total elemental C abundances were determined using a LECO instrument at SGS Australia (Newburn, Western Australia). Total carbon data provides a direct measurement of the amount of carbon (in wt%) within the tailings material, which can then be converted to the total inorganic carbon present by subtraction of the abundance of organic carbon. For samples in which the organic carbon

content was not specifically measured an average organic carbon value of 0.02 wt% C was assumed (Hamilton et al., in prep-b), where:

$$C_i = C_t - C_o \quad (3)$$

$C_i$ ,  $C_t$  and  $C_o$  are the inorganic, total and organic carbon contents of a given sample (in wt% carbon). The inorganic carbon content of a sample can be estimated using Equation 3, which allows the total amount of CO<sub>2</sub> sequestered within minerals to be calculated for a given mass of carbonated tailings.

Estimates of the amount of carbon sequestered in a given sample are calculated using the results of quantitative XRD data using Equation 4:

$$C_i = \sum(X_{p,h,c} \times C_{p,h,c}) \quad (4)$$

Where  $X$  is the abundance of either pyroaurite, hydromagnesite or coalingite (according to quantitative XRD) and  $C$  is the fractional mass of carbon in the same mineral (i.e., either pyroaurite, hydromagnesite and/or coalingite) according to stoichiometry.

## 4.3 Results

### 4.3.1 X-ray diffraction

**4.3.1.1 Qualitative XRD.** Qualitative XRD was used to identify the minerals present in Woodsreef tailings and to track any compositional changes that occur between (1) the waste rock, (2) carbonate-cemented crusts at the tailings surface and (3) the deeper, bulk tailings material (Table 4.2). Qualitative XRD results were then used to inform quantitative XRD work using Rietveld refinements and the RIR method. The tailings at Woodsreef have been well characterised during the course of previous carbon mineralisation studies (Hamilton et al., 2018; McCutcheon et al., 2017; Oskierski et al., 2013; Turvey et al., 2017). Serpentine minerals are the most abundant mineral phases at Woodsreef, with the polymorphs lizardite

and chrysotile both present within carbonate crusts, waste rock and tailings material. Magnetite and pyroaurite are present as minor phases throughout the tailings pile. Quartz, brucite, forsterite and chlorite are commonly present in trace amounts, at or near the detection limit under the conditions we used to collect XRD patterns. Hydromagnesite varies from a minor phase to a trace phase, being most abundant in the cemented carbonate crusts that are present at the tailings surface. Hydromagnesite is also present in some of the samples of loosely cemented tailings, down to a depth of 40 cm. Coalingite is present as a minor to trace phase in the tailings material with increasing amounts of coalingite found with greater frequency in the deeper tailings material.

**Table 4.2** Sample descriptions and qualitative XRD results for Woodsreef tailings and waste rock

Sample Name	Sample Description	Depth (cm)	Serp	Pyro	Mag	Qtz	Fors	Chlr	Bru	Hmgs	Coal	Amph
14WR1-2	Pyroaurite rich tailings	<10	XX	X	X			x	x		x	
14WR1-5	Vertical carbonate crust	2	XX	X	X	*		*	x	x		
14WR1-7	Vertical carbonate crust	2	XX	X	X	*		*	x	x		
14WR3-1	Unconsolidated bulk	<10	XX	X	X	*	*		x	x		
14WR3-2	Unconsolidated bulk	<10	XX	X	X	*	*	*	x	x		
14WR1-6	Layered mat of windblown	2–18	XX	X	X	x		x	x			
14WRP-1	1 m deep vertical tailings	10–100	XX	X	X	x	*	x	x	*	*	
14WRP-4	50 cm deep vertical tailings	10–50	XX	X	X	x	*	*	x	x		
14WRP-5	30 cm deep vertical tailings	10–30	XX	X	X	x	x	X	x	*	x	
15WR2-DC*	1 m deep vertical tailings	10–100	XX	X	X	*	x	X	x	*	x	*
15WR5-DC*	1.2 m deep vertical tailings	2–120	XX	X	X	*	*	X	x	*	x	
16WRP	90 cm deep vertical tailings	2–90	XX	X	X	*	x	*	x	*	x	

\*3 samples for the 10 cm, 20 cm and 30 cm material was collected for this profile

Serp – serpentine, Pyro – pyroaurite, Mag – magnetite, Qtz – quartz, Bru – brucite, Fors – forsterite, Coal – Coalingite, Chlr – chlorite, Cord – cordierite, Hmgs – Hydromagnesite, Amph – amphibole

XX – Major phase, X – Minor phase, x – Trace phase, \* - At detection limit

**4.3.1.2 Quantitative XRD of cemented crusts.** Quantitative XRD results illuminate distinct differences between waste rock and tailings collected from various depths at Woodsreef. The cemented surface crusts are dominated by the presence of serpentine minerals, and relatively high abundances of pyroaurite and hydromagnesite, whereas the deeper tailings contain significantly less hydromagnesite and pyroaurite, but see increased abundances of coalingite and brucite (Table 4.3). Serpentine minerals are the most abundant phases in both heavily

carbonated surface crusts and the deeper tailings, with all tailings and crust samples containing between 69.8 and 91.7 wt% serpentine. The most carbonate rich samples analysed are the vertical surface crusts 14WR1-5 and 14WR1-7 (see Table 4.3), with sample 14WR1-7, containing 13.2 wt% pyroaurite and 10.1 wt% hydromagnesite, the highest carbonate mineral abundances measured in a vertical crust sample in this study. This is a similar composition to that of the vertical crusts At Woodsreef described by Oskierski et al. (2013), which contain 4.5–7.9 wt% pyroaurite and 9.3–14.6 wt% hydromagnesite. The vertical crusts have a significantly higher proportion of carbonate minerals than horizontal surface crusts; horizontal surface crusts, which comprise the top 2 cm of vertical tailings profiles 14WR1-6, 15WR5-DC and 16WRP, contained no hydromagnesite and only a moderate amount of pyroaurite (1.0 to 7.0 wt%, see Table 4.3). Oskierski et al. (2013) found a similar composition within a horizontal surface crust from Woodsreef (i.e., a moderate pyroaurite abundance of 4.5 wt%, compared to vertical crusts, and no detectable hydromagnesite). However, Turvey et al. (2017) reported the presence of a horizontal crust that contained 12.5 wt% hydromagnesite. This discrepancy indicates that there may be a significant degree of heterogeneity occurring in the composition of the horizontal crusts, whereas the composition of vertical crusts is more consistent, with high pyroaurite (5.9–13.2 wt%) and hydromagnesite (6.8–10.1 wt%) abundances.

**Table 4.3** Quantitative XRD results for Woodsreef tailings and waste rock

Sample Name	Depth (cm)	Serp	Pyro	Mag	Qtz	Fors	Chlr	Bru	Hmgs	Coal	Total	R <sub>wp</sub> <sup>a</sup>	$\chi^2$ <sup>b</sup>	d <sup>c</sup>	Total C wt% (XRD)	Total C wt% (Elemental C)
14WR1-2	<10	80.9	1.5	5.9			3.9	2.4		5.8	100.0	19.8	0.1	5.3	0.11	
14WR1-5	2	81.0	5.9	2.0	0.1		4.3	0.0	6.8		100.0	13.1	0.2	3.7	0.81	
14WR1-7	2	69.9	13.2	4.3	0.1		1.1	1.3	10.1		100.0	12.5	0.2	3.4	1.28	
14WR3-1	<10	69.8	1.6	4.8	0.1	13.0	0.0	2.3	8.4		100.0	19.4	0.1	5.2	0.89	
14WR3-2	<10	75.3	4.6	2.8	0.2	8.5	3.0	1.9	3.7		100.0	14.6	0.2	4.0	0.47	
	2	86.8	7.0	1.4	0.4		4.0	0.4			100.0	13.8	0.2	4.0	0.13	
	4	85.6	7.9	1.5	0.3		4.3	0.3			100.0	10.0	0.1	4.6	0.14	
	6	87.8	7.4	1.3	0.3		3.1	0.4			100.0	14.6	0.1	4.2	0.13	
	8	87.5	7.0	0.8	0.2		4.1	0.4			100.0	13.6	0.2	3.9	0.13	
14WR1-6	10	87.5	7.2	1.8	0.3		2.8	0.5			100.0	14.7	0.2	4.0	0.13	
	12	86.4	7.4	1.6	0.5		3.6	0.5			100.0	14.8	0.1	4.0	0.13	
	14	88.1	6.6	1.2	0.5		3.3	0.4			100.0	13.6	0.2	3.8	0.12	
	16	85.2	8.2	0.6	0.2		5.6	0.2			100.0	10.7	0.3	3.0	0.15	
	18	85.2	4.8	1.2	0.2	2.9	5.4	0.3			100.0	14.4	0.2	4.1	0.09	
	10	82.8	7.3	1.4	0.3	3.8	4.4				100.0	14.5	0.1	4.0	0.13	0.54
	20	84.4	7.8	1.8	0.3		5.7				100.0	17.3	0.1	4.7	0.14	0.35
	30	88.0	7.9	0.8	0.1		2.1	1.2			100.0	13.4	0.2	3.8	0.14	0.33
14WRP-1	40	83.3	8.0	3.1	0.1		5.5				100.0	17.3	0.1	5.0	0.15	0.41
	50	85.6	6.2	2.7	0.1		2.2			3.3	100.0	17.4	0.1	5.0	0.16	0.36
	60	81.3	2.2	3.1	0.1	3.1	6.0	0.9		3.4	100.0	16.5	0.1	4.6	0.09	0.29
	70	85.1	1.1	1.4	0.1	2.6	4.3	1.7		3.9	100.0	14.0	0.2	3.9	0.07	0.24
	80	84.0	1.4	2.1	0.1	3.3	4.0	1.7		3.4	100.0	14.7	0.1	4.1	0.07	0.29
	90	86.8	1.7	2.0			3.1	2.4		4.3	100.0	14.2	0.1	4.1	0.09	0.23
	100	79.9	2.5	2.3	0.1	3.8	5.0	2.0		4.6	100.0	16.0	0.1	4.4	0.11	0.27
	10	90.5	3.4	2.7	0.3		3.1				100.0	15.2	0.1	4.1	0.06	
14WRP-4	20	85.4	7.9	2.0	0.1			1.2	4.3		100.0	12.8	0.2	3.7	0.57	
	30	79.6	2.5	2.6	0.1	3.6	5.0	1.0	5.6		100.0	14.3	0.2	4.1	0.63	
	40	77.6	5.7	2.8	0.1	5.0	3.1	1.6	4.1		100.0	15.1	0.1	4.2	0.53	
	50	91.7	7.4	0.7	0.2						100.0	13.6	0.2	4.0	0.13	
	10	79.9	4.4	4.4	0.1	4.8		2.2	4.3		100.0	17.4	0.1	4.6	0.52	
14WRP-5	20	72.9	2.5	5.3	0.1	6.8	5.1	3.0		4.5	100.0	15.5	0.1	4.4	0.11	
	30	80.9	1.4	3.9	0.1	4.5	5.0	2.1		2.2	100.0	16.6	0.1	4.7	0.06	
	10	77.2	3.7	2.4		4.0	2.4	1.3	6.5	2.5	100.0	13.8	0.2	3.3	0.77	0.33
	20	83.1	3.0	2.3		3.2	3.9	1.6		3.0	100.0	13.4	0.2	3.2	0.10	0.22
	30	84.3	2.7	2.6		2.7	2.9	1.8		3.1	100.0	13.3	0.2	3.2	0.09	0.24
	10	82.5	3.0	2.5		5.0	3.2	1.3	2.6	0.0	100.0	13.1	0.3	3.1	0.32	
	20	70.5	2.6	2.1		6.1	6.2	1.7	8.3	2.6	100.0	15.4	0.2	3.6	0.94	
	30	86.5	1.8	2.5		0.0	4.2	1.8		3.2	100.0	14.6	0.2	3.4	0.08	
	10	82.3	2.1	3.2		4.9	1.3	1.0	5.2	0.0	100.0	11.7	0.3	2.7	0.57	
15WR2-DC	20 <sup>d</sup>	79.27	1.7	1.6		3.4	8.6	1.8		2.9	100.0	13.7	0.2	3.1	0.08	
	30	86.3	0.9	1.8		3.1	2.7	2.0		3.3	100.0	10.9	0.4	2.5	0.06	
	40	82.9	2.7	2.3		3.4	3.2	2.3		3.4	100.0	13.3	0.2	3.1	0.10	0.19
	50	86.1	2.6	2.7		0.0	2.9	2.3		3.4	100.0	13.5	0.2	3.2	0.10	0.22
	60	79.7	1.7	2.2		7.5	2.9	2.5		3.7	100.0	13.1	0.2	3.2	0.08	0.16
	70	85.4	1.9	1.6		2.4	2.9	2.4		3.6	100.0	13.3	0.2	3.3	0.08	0.2
	80	88.2	1.6	1.8		0.0	3.0	2.4		3.0	100.0	14.9	0.2	3.8	0.07	0.18
	90	81.5	1.3	2.2		4.7	4.1	2.7		3.7	100.0	15.4	0.2	4.0	0.07	0.17
	100	83.0	1.6	2.0		4.8	2.9	2.5		3.3	100.0	14.8	0.2	3.8	0.07	0.22
	2	85.1	1.0	3.7	0.2	4.4	4.5	1.2			100.0	17.0	0.2	3.8	0.02	0.22
	10	80.5	3.7	2.9	0.2	3.9	4.7	1.3	2.6		100.0	13.8	0.3	3.0	0.34	0.29
	20	86.7	2.8	3.6			3.6	1.2	2.1		100.0	16.7	0.2	3.6	0.27	0.4
	30	83.0	3.2	3.2		6.1	2.9	1.7			100.0	15.2	0.2	3.3	0.06	0.34
	40	84.9	2.5	3.3			4.9	1.7		2.8	100.0	16.4	0.2	3.5	0.08	0.37
	50	85.2	2.3	4.2			5.8	2.6			100.0	13.9	0.3	3.0	0.04	0.42
15WR5-DC	60	85.6	1.6	3.9	5.1		1.3	1.3		2.5	100.0	17.0	0.2	3.7	0.06	0.39
	70	88.3	1.1	2.9			3.0	1.9		2.9	100.0	16.8	0.2	3.8	0.06	0.3
	80	81.0	1.8	2.6		4.8	5.3	2.0		2.6	100.0	14.9	0.2	3.4	0.07	0.25
	90	82.7	1.6	2.9		5.2	3.0	2.4		2.4	100.0	15.5	0.2	3.5	0.06	0.24
	100	78.0	2.1	2.5		4.3	8.2	2.8		2.3	100.0	14.6	0.3	3.3	0.07	0.24
	110	81.5	2.6	2.4		4.2	3.9	2.8		2.6	100.0	14.3	0.2	3.3	0.08	0.24
	120	85.1	1.0	3.7	0.2	4.4	4.5	1.2			100.0	12.1	0.3	2.7	0.03	0.27
	2	88.6	2.9	3.1			3.7	1.7			100.0	16.0	0.2	3.9	0.05	0.25
	10	69.0	2.1	1.9		8.6	5.0	1.3	12.1		100.0	14.4	0.2	3.6	1.28	1.14
	20	80.1	3.0	3.3	1.0	7.0		2.2	3.4		100.0	13.8	0.2	3.4	0.41	0.33
	30	84.1	2.6	2.1		5.7		2.4		3.2	100.0	15.0	0.2	3.6	0.09	0.24
16WRP	40	85.5	2.0	1.6		4.0		3.7		3.4	100.0	14.2	0.2	3.4	0.08	0.2
	50	84.1	2.5	2.1		5.4		2.4		3.6	100.0	14.8	0.2	3.5	0.09	0.22
	60	91.5	2.0	1.4		0.0		1.5		3.8	100.0	14.3	0.2	3.4	0.09	0.21
	70	79.0	1.4	1.7		3.8	8.7	1.8		3.8	100.0	16.4	0.1	3.8	0.08	0.24
	80	87.7	1.6	1.4		2.3		2.8		4.4	100.0	14.9	0.2	3.5	0.09	0.17
	90	86.8	1.9	2.6		3.0		2.6		3.2	100.0	12.4	0.3	2.8	0.08	0.18

Serp – serpentine, Pyro – pyroaurite, Mag – magnetite, Qtz – quartz, Bru – brucite, Fors – forsterite, Coal – coalingite, Chlr – chlorite, Cord – cordierite  
Hmgs – hydromagnesite

<sup>a</sup> Weighted pattern residual, a function of the least-squares residual (%)

<sup>b</sup> Reduced  $\chi^2$  statistic for the least squares fit.

<sup>c</sup> Weighted Durbin Watson statistic.

<sup>d</sup> Sample contains 0.81 wt% actinolite

**4.3.1.3 Quantitative XRD of vertical profiles.** Our quantitative XRD results for the 77 samples collected from the 7 vertical profiles taken across the tailings pile at Woodsreef (Table 4.3 and Figure 4.3) indicate that a significant change in mineralogical composition occurs within the tailings as a function of depth. Shallow tailings samples (<40 cm depth) have a similar composition to that of the vertical and horizontal crusts at the surface of the tailings storage facility. Hydromagnesite is found in 28 out of 40 samples of tailings from 0 to 40 cm depth. In the samples that contained detectable levels of hydromagnesite ( $> 3\sigma$  above the background intensity in XRD patterns), the abundance of this phase varies between 1.9 and 10.9 wt%. Pyroaurite is present at abundances between 0.9 and 8.2 wt% in all samples taken from a depth of 0 to 40 cm. Some vertical profiles display a lower pyroaurite abundance of between 0.9 and 3.7 wt%, while others are more enriched, exhibiting pyroaurite abundances of between 4.8 and 8.0 wt%. This appears to be the result of lateral spatial heterogeneity across the tailings pile, with profiles 14WR1-6, 14WRP-1 consistently having greater pyroaurite abundances in the shallow (<40 cm) tailings whereas profiles 15WR2-DC, 15WR5-DC and 16WRP contain lower pyroaurite abundances, and with profiles 14WRP-4 and 14WRP-5 plotting between the two groups. Below depths of 60 cm, the pyroaurite abundance becomes consistently less than 2.4 wt% across all 4 vertical profiles that were collected below 60 cm, varying between of 1.0 and 2.4 wt%.

Brucite is present as a trace or minor phase in almost all of the vertical profile samples. The brucite abundance increases with depth, being present at abundances between 0.4 and 1.6 wt% in the top 2 cm of tailings material and gradually increasing to between 1.9 and 2.6 wt% abundance for samples over 1 m in depth. Coalingite is present in 5 out of the 7 vertical profiles and follows a similar trend to that of brucite, where both phases are either absent or present at low abundance in the shallow tailings (<40 cm). At <40 cm coalingite is present in only 13 out of 40 samples and is present at abundances of between 2.2 and 4.5 wt%.

Coalingite becomes more abundant with increasing depth below the tailings surface, and is present in 11 out of the 12 samples taken from a depth of 80 to 120 cm at abundances of between 2.0 and 4.1 wt%.

Magnetite is consistently present at ~2 wt% abundance throughout the tailings pile at all depths that were sampled, with a larger variation in abundance closer to the tailings surface, between 0.6 and 5.0 wt%. Forsterite is found sporadically throughout the tailings from 2-90 cm depth. In samples where forsterite is detectable, it tends to be present at ~4 wt% abundance. As with magnetite, there is greater variation in the refined abundance of forsterite closer to the surface of the tailings with forsterite abundance varying from below the detection limit of our XRD data up to 8.6 wt% in a sample taken from the upper 20 cm of the tailings pile. The variability in forsterite and magnetite abundances within the shallow tailings likely occurs as a result of lateral heterogeneity within the tailings. They may also appear to be more common in the shallow tailings owing to sampling bias, since a larger number of samples taken were collected from the shallow tailings.

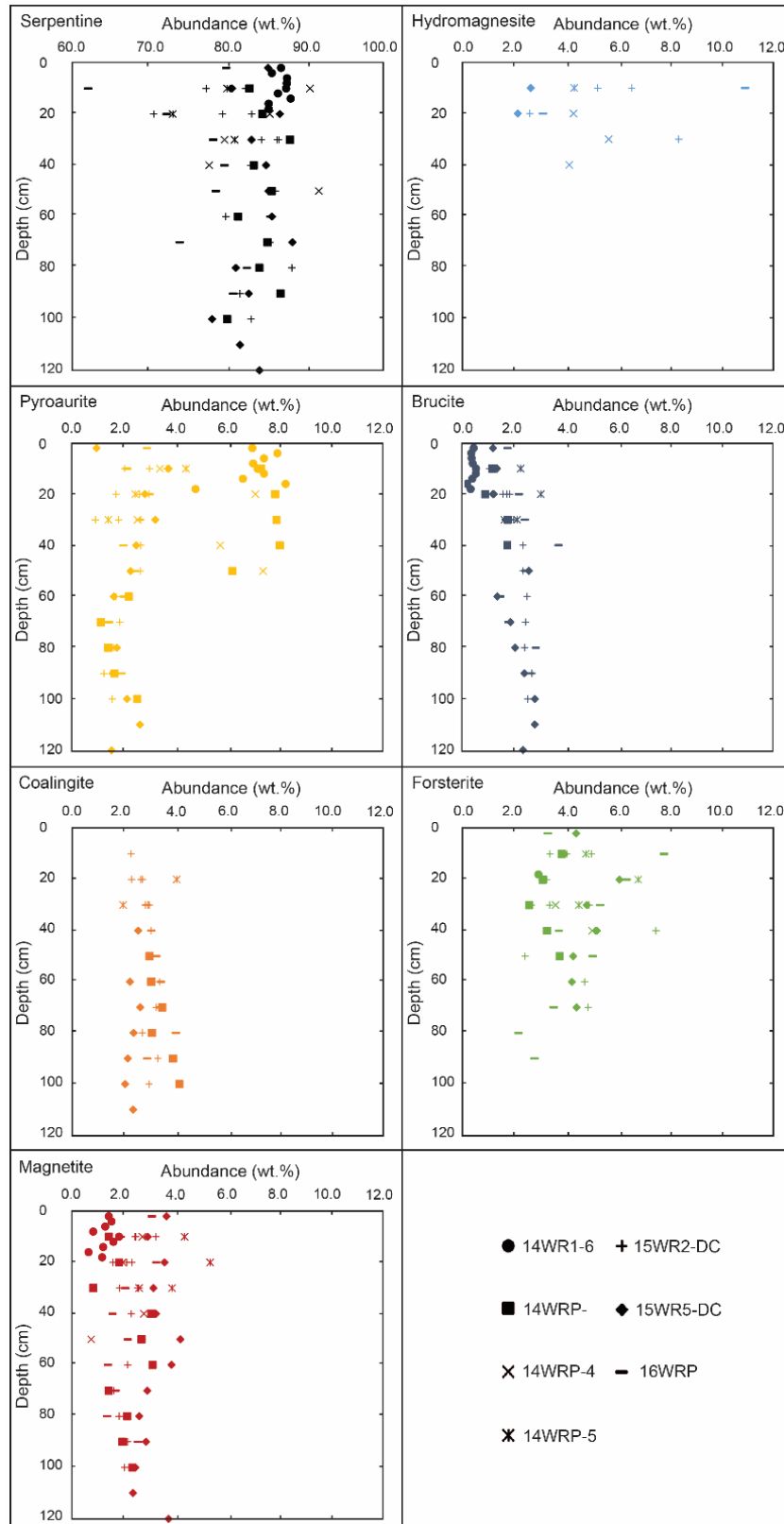


**Figure 4.3** Quantitative XRD results for the vertical tailings profiles, showing the abundance (wt%) of serpentine, hydromagnesite, pyroaurite, brucite, coalingite, forsterite and magnetite with depth below the tailings pile surface.

### 4.3.2 Scanning electron microscopy results

Electron micrographs and semi-quantitative EDS results for grains of tailings (collected at 100 cm depth from profile 15WR2-DC) are given in Figure 4.4. Figure 4.4a shows a magnetite grain (light-coloured, planar grain, a.1) surrounded by disarticulated chrysotile fibres (dark-coloured, fibrous grains, a.2) and covered by an amorphous phase indicated to be composed of Mg, Si and C-bearing material (a.3). EDS results are used to confirm that the chrysotile fibres contain Mg, Si and O and the magnetite grain contains Fe, Mg and O. Figure 4.4b shows a grain of brucite; localised dissolution and precipitation appears to be ongoing at the surface of the grain with deep fractures appearing perpendicular to  $[0\ 0\ 1]$  within the brucite grain. The precipitate replacing the brucite can be seen covering the surface of this grain, forming plates oriented approximately perpendicular to the  $[0\ 0\ 1]$  grain surface, and, in some instances, accreting into more massive surface coverings. EDS data for Figure 4.4b confirm that the large underlying grain is Fe-rich brucite (b.1), whereas the presence of C, O, Mg and Fe in the massive crystalline surficial precipitate (b.2) indicates it is either pyroaurite, coalingite or Fe-rich hydromagnesite. Figure 4.4c shows two Fe-rich brucite grains, one of which is largely unreacted (c.1), and the other that appears to be heavily altered (c.2), creating a cross-hatched network of fractures, similar to those observed in Figure 4.4b. EDS data for Figure 4.4c show that the two grains of brucite have a similar composition, containing Mg, Fe, C and O, with the grain that has undergone dissolution containing more C than the unreacted grain. Given the small regions that are being analysed, the uneven surface of the samples, and the use of energy-dispersive (rather than wavelength dispersive) X-ray spectroscopy, the values given for elemental abundances in Figure 4.4 should not be considered quantitative. Instead they provide an approximate indication of the relative abundances of elements present in the regions analysed.

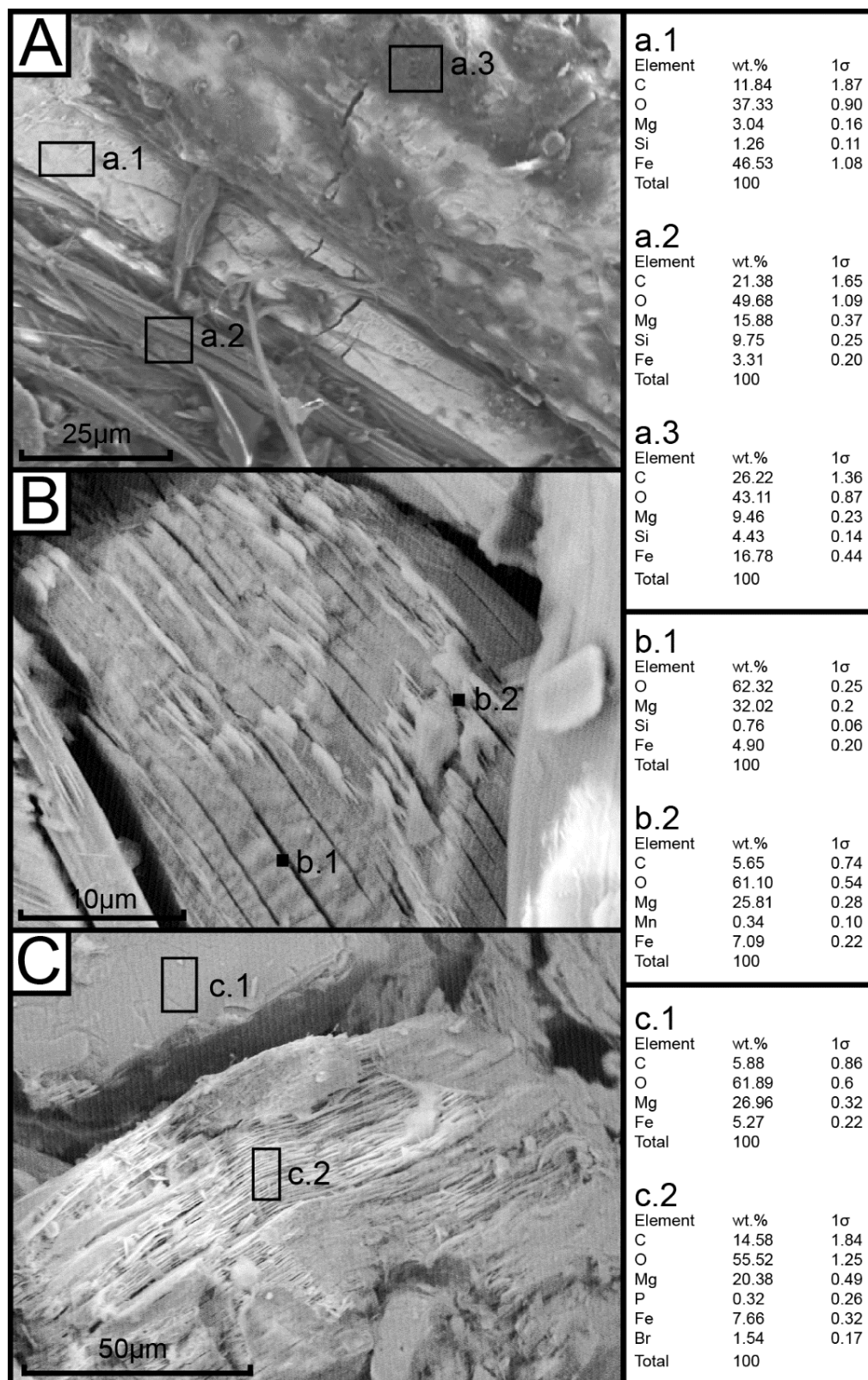


**Figure 4.4** SEM micrograph and EDS results for tailings samples showing (a) serpentine and magnetite grains and an amorphous Mg-Si carbonate, (b) carbonated brucite and pyroaurite grains and (c) heavily dissolved and carbonated brucite grains.

### 4.3.3 Radiocarbon and stable carbon and oxygen isotopes

**4.3.3.1 Radiocarbon.** Radiocarbon results indicate that the majority of the carbon stored in the tailings at Woodsreef has been sourced from the modern atmosphere (Table 4.4). Figure 4.5a plots radiocarbon content (as  $F^{14}C$ ) for bulk tailings and picked pyroaurite samples from the Woodsreef tailings against stable carbon isotope data. The atmospheric carbonate and bedrock carbonate fields in Figure 4.5a are replotted from Oskierski et al. (2013). All 10 samples analysed have  $F^{14}C$  values of between 0.80 and 1.00.  $\delta^{13}C$  values fall into two groups, the first group from -5 ‰ to -2 ‰, which fall between the atmospheric and bedrock derived carbonate fields, and the second group of samples with heavily  $^{13}C$ -depleted  $\delta^{13}C$  values of between -18 ‰ and -7 ‰ which are similar to those for bedrock carbonate, but with much greater values of  $F^{14}C$ . The pure samples of pyroaurite have relatively high  $F^{14}C$  values of 0.95 to 0.98, which are close to the composition of the modern atmosphere (i.e.,  $F^{14}C = 1.03$  in 2014; Turnbull et al. 2017, Graven et al., 2017).

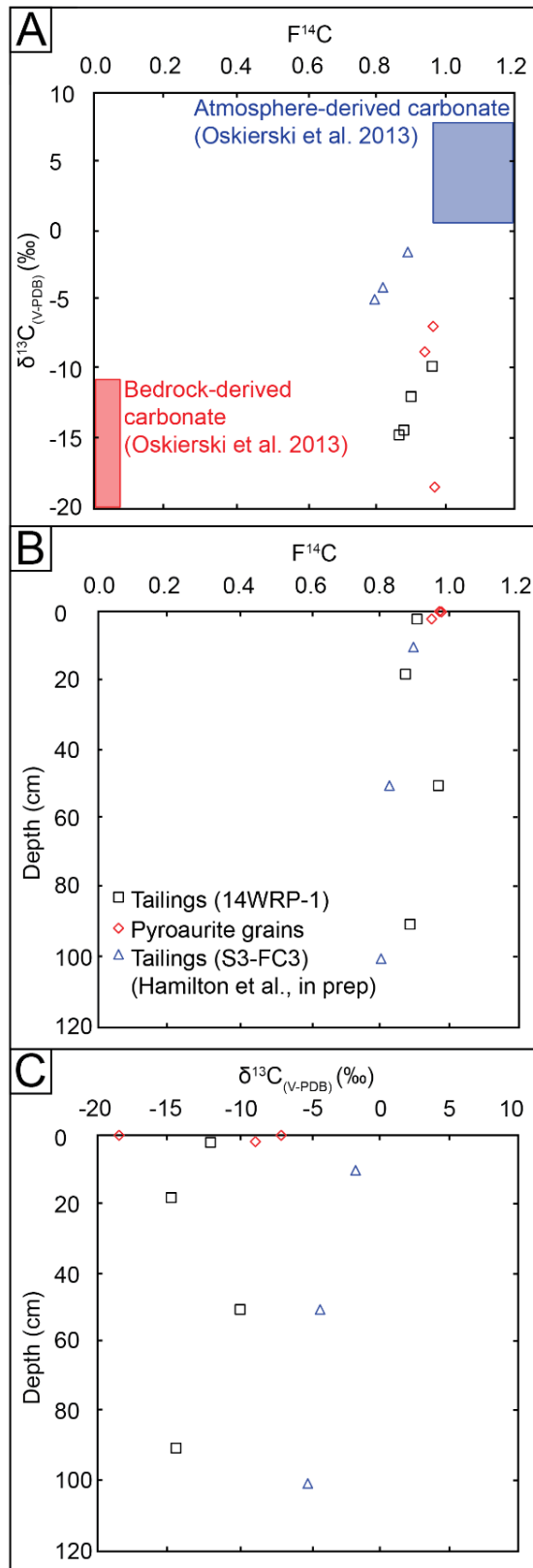


**Figure 4.5** Stable carbon and radiocarbon results of tailings material and pyroaurite grains showing (a)  $F^{14}C$  vs  $\delta^{13}C$  (bedrock and atmospheric carbonate fields are replotted from Oskierski et al. 2013), (b)  $F^{14}C$  vs depth and (c)  $\delta^{13}C$  vs depth. Tailings samples are replotted from Hamilton et al., in prep-b.

**Table 4.4** Radiocarbon and stable carbon values for Woodsreef tailings samples<sup>a</sup>

Experiment	Depth	$\delta^{13}\text{C}$	s.d. ( $2\sigma$ )	$F^{14}\text{C}$	s.d. ( $2\sigma$ )
14WR1-6	0	-12	1	0.91	0.01
	16	-15	1	0.87	0.01
14WRP1	50	-10	1	0.97	0.01
	90	-14	1	0.89	0.01
S3-FC3 <sup>b</sup>	10	-2	1	0.90	0.01
	50	-4	1	0.83	0.01
	100	-5	1	0.80	0.01
14WR1-2	2	-9	1	0.95	0.01
15WR-PYR-11	0	-7	1	0.97	0.01
15WR-PYR-11-2	0	-18	1	0.97	0.01

<sup>a</sup> Analysed using a SSAMS at The Australian national University

<sup>b</sup> Samples replicated from Hamilton et al. in prep-b

In Figure 4.5b,  $F^{14}\text{C}$  values are plotted against the depth at which the tailings sample were collected. Shallower samples taken from the vertical tailings profiles, and samples of pyroaurite collected from the surface tend to have the greatest  $F^{14}\text{C}$  values of up to 0.98, whereas samples taken from deeper in the tailings have lower values of  $F^{14}\text{C}$ , with the lowest value, 0.80, measured for a sample taken from 1 m depth. This indicates that there is a greater proportion of  $^{14}\text{C}$ -free carbon with increasing depth within the tailings, whereas an increasing proportion of  $^{14}\text{C}$ -enriched modern atmospheric carbon is present within carbonate minerals at the tailings surface.

**4.3.3.2 Stable carbon and oxygen isotopes.** Stable C and O isotopes results obtained using IRMS and laser isotope analysis are given in Table 4.5 and Figure 4.6.  $\delta^{13}\text{C}$  values range from -7.3 ‰ to 0.6 ‰ (VPDB), and  $\delta^{18}\text{O}$  values range from 11.3 ‰ to 26.3 ‰ (VSMOW). Fields for atmosphere-derived carbonate minerals and bedrock carbonate minerals are replotted from Oskierski et al. (2013) in Figure 4.6, as are stable isotope data for vertical and horizontal cements, surface crusts, deep cements and bedrock carbonate that were analysed as part of that study. Stable C and O isotope data for samples rich in hydromagnesite and pyroaurite plot in distinct regions of  $\delta^{18}\text{O}$ – $\delta^{13}\text{C}$  space. Samples of shallow unconsolidated tailings material have  $\delta^{13}\text{C}$  compositions between -5.8 ‰ and -3.6 ‰ and  $\delta^{18}\text{O}$  values of

between 23.2 ‰ and 26.8 ‰, placing them generally between the atmosphere and bedrock carbonate fields of Oskierski et al. (2013). Ten samples of pyroaurite were picked and purified from slickenside surfaces on cobbles of waste rock and from samples of the shallow (<10 cm) tailings for comparison with the stable C and O isotope results for the bulk tailings material. These purified pyroaurite samples have similar  $\delta^{13}\text{C}$  values to the bulk tailings material with values of  $-7.2 \text{ ‰} \leq \delta^{13}\text{C} \leq -3.4 \text{ ‰}$ . However, the pyroaurite has a distinct stable oxygen isotope signature of  $-6.5 \leq \delta^{18}\text{O} \leq -4.7 \text{ ‰}$ , indicating that samples of this phase are more depleted in  $^{18}\text{O}$  than the bulk carbonate minerals in the tailings.

**Table 4.5** Stable carbon and oxygen isotope results for Woodsreef tailings samples

Sample ID	Depth (cm)	Sample Description	Mineralogy	$\delta^{13}\text{C}$ (‰, VPDB)	s.d. (2 $\sigma$ )	$\delta^{18}\text{O}$ (‰, VSMOW)	s.d. (2 $\sigma$ )			
14WR1 <sup>a</sup>				-6.54	0.97	14.69	0.95			
14WR2 <sup>a</sup>				-5.06	0.97	17.14	0.95			
14WR3 <sup>a</sup>	<10	Pyroaurite collected from the shallow tailings	Pyro, Chrs, Liz	-6.03	0.97	18.74	0.95			
14WR4 <sup>a</sup>				-6.13	0.97	14.78	0.95			
14WR5 <sup>a</sup>				-3.42	0.97	17.23	0.95			
14WR1-1 <sup>a</sup>				0	Harzburgite cobbles with visible pyroaurite	Pyro, Chrs, Liz	-4.71	0.97	21.23	0.95
14WR2-6 <sup>a</sup>				0	Assorted pyroaurite from the pit	Pyro, Chrs, Liz, Mag	-3.71	0.97	16.58	0.95
14WR2-7 <sup>a</sup>	0	Pyroaurite taken from harzburgite boulder	Chrs, Liz, Pyro	0.63	0.97	24.54	0.95			
14WR2-9 <sup>a</sup>	0	Wasterock Serpentinite cobble	Chrs, Liz, Pyro, Mag, Qtz	-6.73	0.97	15.17	0.95			
14WR2-11 <sup>a</sup>	<10	Pyroaurite from the shallow tailings	Chrs, Liz, Pyro, Mag, Qtz	-7.15	0.97	19.92	0.95			
14WR1-6 <sup>b</sup>	0-2	Layered tailings mat from near the top of the profile	Chrs, Liz, Pyro, Mag, Qtz, Bru, Fors, Chlr	-4.35	0.05	26.76	0.04			
	4-6			-4.46	0.05	23.81	0.06			
	8-10			-7.34	0.58	11.30	0.19			
	16-18			-5.83	0.12	24.29	0.07			
14WRP1 <sup>b</sup>	10	Tailings sample taken from depth profile	Chrs, Liz, Pyro, Mag, Qtz, Bru, Fors, Nesq, Chlr	-3.73	0.03	25.85	0.07			
	30			-4.90	0.07	23.20	0.05			
	50			-3.66	0.02	23.85	0.10			
	70			-4.69	0.04	26.25	0.06			
	90			-4.41	0.05	23.97	0.04			

Chrs – chrysotile, Liz – lizardite, Pyro – pyroaurite, Mag – magnetite, Qtz – quartz, Bru – brucite, Fors – forsterite, Nesq – Nesquehonite, Chlr – chlorite

<sup>a</sup> Analysed using a Los Gatos OA-ICOS instrument at The University of British Columbia

<sup>b</sup> Analysed using a Thermo Delta Advanced mass spectrometer at Monash University

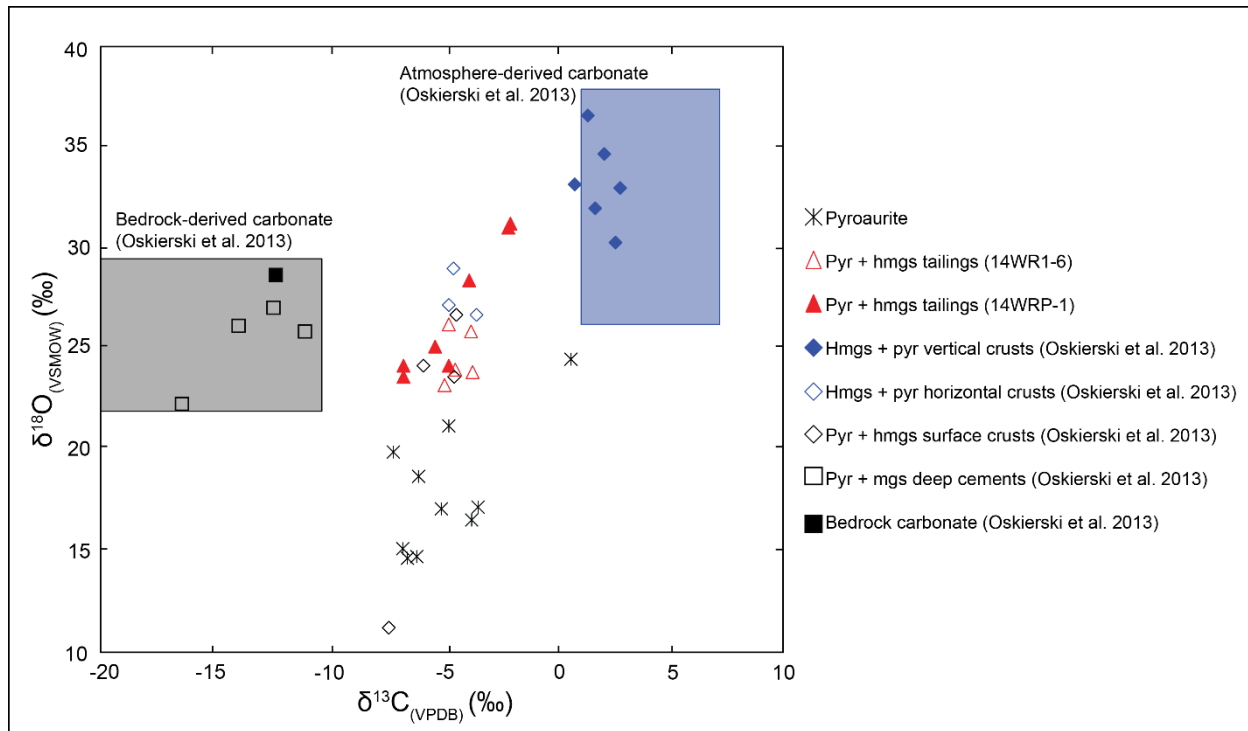


**Figure 4.6** Stable carbon ( $\delta^{13}\text{C}_{\text{VPDB}}$ ) and oxygen ( $\delta^{18}\text{O}_{\text{VSMOW}}$ ) results for pyroaurite, tailings and surface crusts from the Woodsreef tailings pile (bedrock and atmospheric carbonate fields and the bedrock carbonate, crusts and cements are taken from Oskierski et al. 2013). Pyr: pyroaurite, Hmgs: hydromagnesite.

#### 4.3.4 Anion exchange experiment

Figure 4.7 compares the XRD patterns of purified Mount Keith iowaite before the beginning of the anion exchange experiments and the resulting pyroaurite that was obtained after 46 hours in a reaction vessel that was left open to the atmosphere and stirred at 600 RPM. These patterns show the conversion of iowaite  $[\text{Mg}_6\text{Fe}^{3+}_2\text{Cl}_2(\text{OH})_{16}\cdot 4\text{H}_2\text{O}]$  into pyroaurite  $[\text{Mg}_6\text{Fe}^{3+}_2\text{CO}_3(\text{OH})_{16}\cdot 4\text{H}_2\text{O}]$  via anion exchange during exposure to atmosphere-derived dissolved inorganic carbon (DIC). There is an observable shift in the position of the (0 0 3) reflection from  $10.8^\circ$  to  $11.2^\circ$   $2\theta$  between the original iowaite and the resulting pyroaurite after 46 hours of exchange. This indicates the replacement of interlayer  $\text{Cl}^-$  by  $\text{CO}_3^{2-}$ , with the (0 0 3*l*) harmonic peaks shifting to higher  $2\theta$  positions due to the incorporation of the smaller anion into the hydrotalcite structure. Total carbon results for the 200 RPM

experiment illustrates this increase in carbon content (Table 4.6). The original iowaite sample contained 0.47 wt% C, indicating that it was not of pure endmember composition on the iowaite–pyroaurite solid solution (Table 4.6). After 46 hours of reaction the carbon content of the sample had increased to 2.63 wt%, which is slightly higher than expected for pyroaurite by stoichiometry (i.e., 1.82 wt% C; Table 4.6).

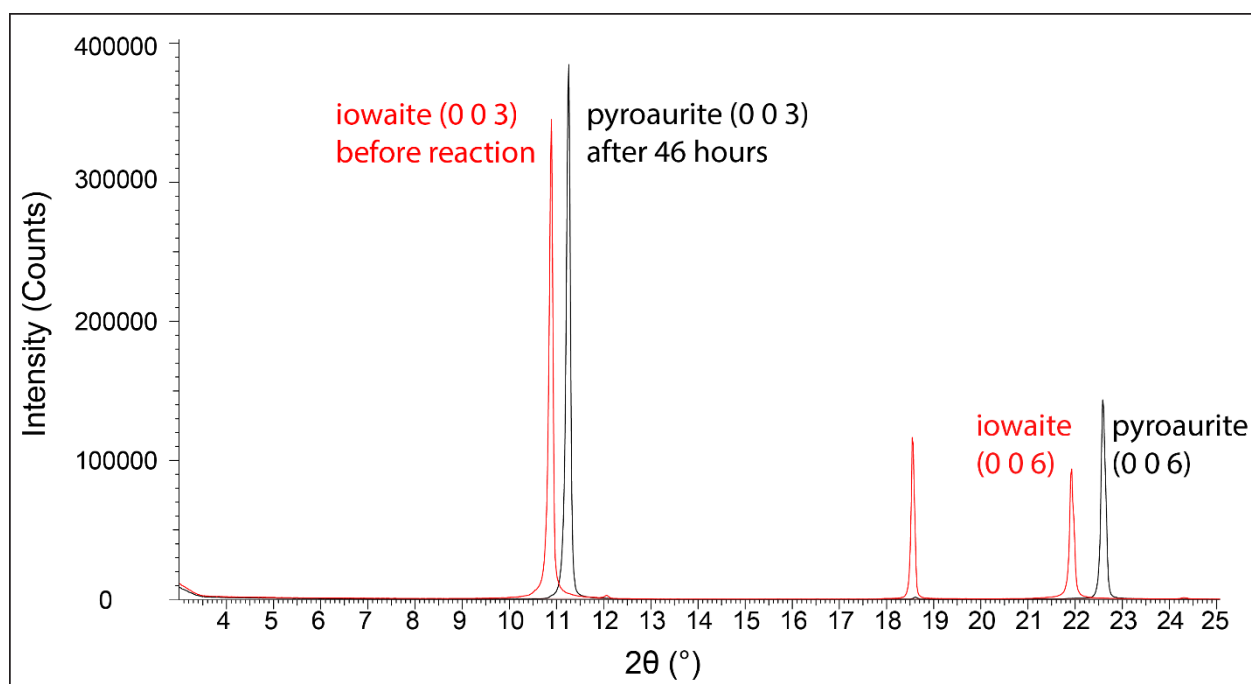


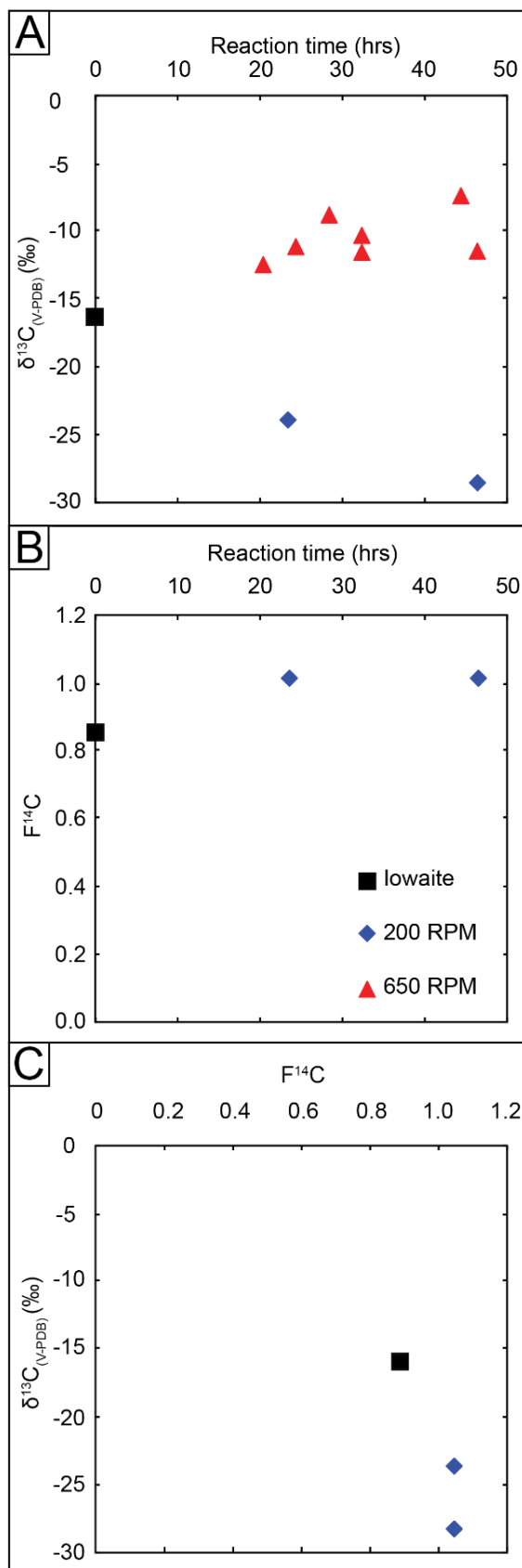
**Figure 4.7** XRD pattern showing the change in the 0 0 3 and 0 0 6 reflections that occurs during anion exchange from iowaite to pyroaurite after 46 hours in the high carbon treatment.

**Table 4.6** Radiocarbon, stable carbon and total carbon for anion exchange experiments

Experiment	Time	$\delta^{13}\text{C}$	s.d. ( $2\sigma$ )	pMC	s.d. ( $2\sigma$ )	F <sup>14</sup> C	s.d. ( $2\sigma$ )	%C
Iowaite <sup>a</sup>	0	-15.9	0.58	86.3	0.50	0.87	0.01	0.47
200 RPM <sup>a</sup>	24	-23.6	0.40	101.8	0.54	1.03	0.01	1.63
	46	-28.2	0.32	102	0.62	1.03	0.01	2.63
650 RPM <sup>b</sup>	20	-12.36	0.38					
	24	-11.05	0.06					
	28	-8.69	0.09					
	32	-11.43	0.26					
	32 (dup)	-10.22	0.57					
	44	-7.31	0.04					
	46	-11.33	0.32					

<sup>a</sup> Analysed using a SSAMS at The Australian national University

<sup>b</sup> Analysed using a Thermo Delta Advanced mass spectrometer at Monash University



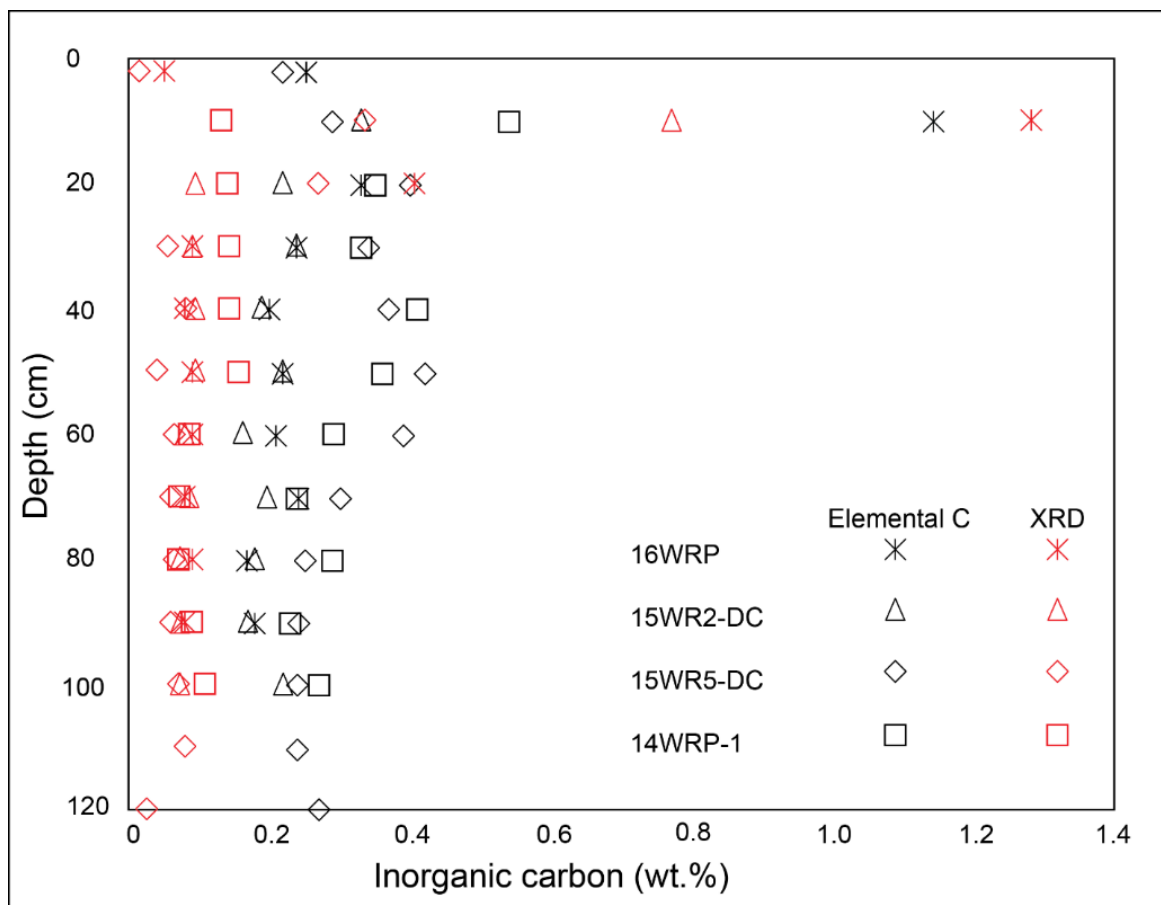
**Figure 4.8** Stable carbon and radiocarbon results for the anion exchange experiment indicating (a) the  $\delta^{13}\text{C}$  versus time exchanged; (b)  $F^{14}\text{C}$  versus time exchanged; and (c) the  $F^{14}\text{C}$  compared to  $\delta^{13}\text{C}$  results.

Table 4.6 and Figure 4.8 show the stable C and radiocarbon isotope results of the two anion exchange experiments over time. Figure 4.8a compares the  $\delta^{13}\text{C}$  composition of the iowaite–pyroaurite phase at various time points throughout the two experiments. The initial  $\delta^{13}\text{C}$  value of the unreacted iowaite was  $-15.94\text{‰}$  prior to experiments. However, when this sample was originally analysed by Wilson et al. (2014) in early 2007 following sampling in late 2006, it had a  $\delta^{13}\text{C}$  value of  $-2.83\text{‰}$  and a  $\delta^{18}\text{O}$  value of  $16.11\text{‰}$ , which is indistinguishable from the stable C and O isotope compositions of other hydrotalcite-rich samples at Mount Keith and other metamorphic carbonate minerals inherited from the ore, of which high purity samples had  $F^{14}\text{C} < 0.010$ . Stable carbon isotope results for the exchange experiment conducted at 600 RPM, which represents a reaction in an environment with more plentiful carbon, shows a general enrichment in  $^{13}\text{C}$  over time, reaching  $\delta^{13}\text{C}$  values of between  $-11.33\text{‰}$  and  $-7.31\text{‰}$  after 46 hours. The 200 RPM experiment, which represents reaction in a relatively carbon poor environment, instead shows a depletion of  $^{13}\text{C}$  over time, from the initial composition of  $-15.94\text{‰}$  to  $-28.24\text{‰}$  after 46 hours. Figure 4.8b plots  $F^{14}\text{C}$  against time for the 200 RPM experiment, showing an increase in the  $F^{14}\text{C}$  value over time from 0.87 at 0 hours, to 1.03 after 46 hours. Figure 4.8c plots  $\delta^{13}\text{C}$  against  $F^{14}\text{C}$  for the 200 RPM experiment, indicating that incorporation of  $^{14}\text{C}$ -rich atmospheric  $\text{CO}_2$  over time is linked to continued depletion in  $^{13}\text{C}$ .

#### **4.3.5 Total carbon**

Total inorganic carbon abundances for tailings samples are reported in Table 4.3. Two values are given for each sample: (1) a value calculated from carbonate mineral abundances refined from XRD data and (2) a value measured using elemental carbon analysis. Calculated carbon concentrations (XRD) are typically lower than the measured values. The average calculated C concentration is 0.17 wt% (ranging between values of 0.02 wt% and 1.28 wt%), compared

to the average measured C content of 0.28 wt% (ranging between values of 0.17 wt% and 1.14 wt%). Figure 4.9 shows the total inorganic carbon content (wt%) versus depth for samples taken from four of the vertical tailings profiles according to total carbon and quantitative XRD data. Total carbon varies between 0.22 wt% C and 1.14 wt% C in the top 10 cm of tailings material. For shallow tailings (10–40 cm), total C values range from between 0.17 wt% to 0.39 wt% C. The values continue to decrease from maximum values of ~0.4 wt% to ~0.2 wt% at 40–80 cm depth, below which they appear to stabilise in the deep tailings (80–120 cm) at between 0.15 wt% and 0.27 wt% C. Profiles 16WRP and 15WR2-DC appear to have relatively low amounts of C compared to the other profiles, with carbon contents of ~0.2 wt% C from 20 to 120 cm depth. Profiles 15WR5-DC and 14WRP-1 have higher C abundances, with carbon contents ~0.4 wt% C to a depth of 60 cm and lower values of ~0.25 wt% from 60–120 cm depth. Quantitative XRD data produces a lower estimate of the total inorganic carbon abundance in all profiles and at all depths, except 10 cm (16WRP, 15WR2-DC and 15WR5-DC) and 20 cm (16WRP, and 15WR5-DC) where they give higher estimates (Figure 4.9).



**Figure 4.9** Inorganic carbon content (wt%) versus depth for the vertical tailings profiles, as analysed by total carbon (LECO) and quantitative XRD analysis.

## 4.4 Discussion

### 4.4.1 Mineralogy as a function of depth in the tailings pile

The greatest mineralogical change that occurs within the tailings storage facility at Woodsreef is the formation of horizontal and vertical carbonate crusts at the surface of the tailings. These crusts were first described at this locality by Oskierski et al. (2013) and revisited by Turvey et al. (2017). The main mineralogical change that occurs in the shallow tailings is an increase in the abundances of hydromagnesite and pyroaurite relative to those measured at greater depths.

Samples 14WR1-5 and 14WR1-7 are both vertical crusts that were sampled from the surface of the tailings. They are characterised by relatively high abundances of pyroaurite (between 5.9 wt% and 13.2 wt%, Table 4.3) and hydromagnesite (6.8 wt% to 10.1 wt%, Table 4.3) compared to the average carbonate composition of the tailings samples from Woodsreef (3.7 wt% pyroaurite and 0.8 wt% hydromagnesite). These are comparable to the vertical crusts sampled by Oskierski et al. (2013) that contained 4.5–7.9 wt% pyroaurite and 9.3–14.6 wt% hydromagnesite, and the carbonating chrysotile vein described by Turvey et al. (2017) that contained 4.9 wt% pyroaurite and 13.6 wt% hydromagnesite. The consistently high concentrations of carbonate minerals separate the crust material from the rest of the tailings, which are less cemented by carbonate minerals and thus either loosely consolidated or unconsolidated. Samples from the shallow tailings (< 40 cm depth) commonly contain significant abundances of carbonate minerals, with 29 out of 42 shallow tailings samples containing either hydromagnesite (present at 2.1–12.1 wt% abundance) or > 3 wt% pyroaurite (Table 4.3). However, the remaining samples of shallow tailings and deeper tailings contain significantly less carbonate minerals, <3 wt% pyroaurite and no detectable hydromagnesite (detection limit is ~0.1 wt%). Turvey et al. (in review)/Chapter 3 showed that minor phases are typically underestimated when using Rietveld refinements to estimate mineral abundances in serpentinite samples. They found that pyroaurite tends to be underestimated where it is present at abundances > 3 wt% and overestimated at lower abundances, whereas the amount of hydromagnesite is consistently underestimated (by ~10 % relative) at abundances from 1–15 wt% (Turvey et al., in review/Chapter 3). This means that, for the range of pyroaurite and hydromagnesite abundances reported for the Woodsreef tailings, it is likely that the surface crusts and carbonate-rich shallow tailings samples contain more hydromagnesite and pyroaurite than is reported in the XRD results, consistent with the observed difference between calculated and measured carbon contents (Figure 4.9). These

results also mean that crusts formed by accelerated carbonation, such as those outlined in the *in situ* tailings carbonation experiment presented in McCutcheon et al. (2017), may have been underestimated. Contrastingly, the abundance of pyroaurite may be overestimated in the deeper tailings (>50 cm depth), which contain 1.1 wt% to 2.6 wt% pyroaurite.

A variety of mineralogical transitions occur within the tailings. The first is the disappearance of hydromagnesite with increasing depth below the tailings surface (Figure 4.3). The majority of the hydromagnesite found in the tailings is concentrated in the surface crusts which exist to a depth of approximately 2 cm. Hydromagnesite is also found sporadically within the shallow tailings material, at abundances between 2.1 wt% and 12.1 wt% from 2 and 40 cm depth (Table 3). Beyond a depth of 40 cm, hydromagnesite is absent from the tailings material or present below the detection limit of our XRD analyses (~0.1 wt% for most phases). The formation of hydrated Mg-carbonate minerals such as hydromagnesite has previously been linked primarily with the dissolution and carbonation of brucite and serpentine within tailings during field studies (Bea et al., 2012; Beinlich and Austrheim, 2012; Gras et al., 2017; Pronost et al., 2012; Wilson et al., 2014) and laboratory experiments (Assima et al., 2013a; Harrison et al., 2015; Harrison et al., 2016; Harrison et al., 2017; Pronost et al., 2011; Wilson et al., 2010). The formation of hydromagnesite only in the upper 40 cm of tailings indicates that the rate of brucite carbonation can be limited by pore water content, surface passivation and limited CO<sub>2</sub> concentration, although this may in part be offset by mechanical fracturing of waste rock or tailings, as has been observed in the Feragen ultramafic body (Norway) (Beinlich and Austrheim, 2012; Ulven et al., 2017).

A second mineralogical transition occurs in the tailings at Woodsreef and relates to the coexistence of brucite, coalingite and pyroaurite. Brucite is found in all samples of tailings that were analysed by XRD as part of this study and is commonly associated with pyroaurite

and coalingite. The abundance of brucite is lowest at the surface of the tailings, where it is typically below <2 wt%. The abundance of brucite gradually increases with depth, reaching values in the range of 1.9–2.6 wt% at depths of 80–120 cm. The abundance of pyroaurite is greatest in samples of surface crusts and shallow (<40 cm) tailings, up to 13.2 wt%; however this decreases significantly with depth, until it is present at  $\leq 2.6$  wt% abundance for samples collected from deeper than 60 cm. Coalingite is largely absent from the shallow tailings, first appearing at a depth of 10 cm in sample 15WR2-C1-1 (Table 4.3 and Figure 4.3). The occurrence of coalingite becomes more common and its abundance begins to increase below a depth of 10 cm until it is found at abundances between 2 and 4 wt% within almost all tailings samples taken from 60 cm depth or deeper (Table 4.3 and Figure 4.3). This transition that occurs with depth, from cemented tailings crusts at the surface that contain large amounts of pyroaurite + hydromagnesite  $\pm$  minor brucite, to shallow unconsolidated tailings containing pyroaurite + minor brucite  $\pm$  minor coalingite, to the deepest tailings that we sampled, which contained brucite + coalingite + minor pyroaurite, indicates that there is a depth-dependent environmental parameter that controls the alteration mineralogy of the tailings.

Coalingite and pyroaurite have previously been found to form at ambient conditions by carbonation of Fe-rich brucite in serpentinites (Hostetler et al., 1966; Mumpton et al., 1965). Mumpton and Thompson (1966) used laboratory experiments to demonstrate that Fe-rich brucite in samples of serpentinite oxidised and carbonated to form coalingite when in contact with the atmosphere, and that this phase can dissolve in water to later precipitate hydromagnesite. Pyroaurite has also been found to form from high temperature alteration of magnetite, where it exists as a complete solid solution with iowaite (Grguric, 2003). When formed at high temperature, pyroaurite exists as veinlets that link the rims of altered magnetite grains (Grguric, 2003). With two possible formation mechanisms, the origin of

pyroaurite in the tailings at Woodsreef must be identified, as secondary pyroaurite formed by sedimentary processes in the tailings would be doing so by sequestering atmospheric CO<sub>2</sub>, while pyroaurite with a metamorphic origin would have (at least originally) sourced CO<sub>2</sub> via hydrothermal fluids. Oskierski et al. (2013) argued that the pyroaurite at Woodsreef was forming as a secondary mineral within the tailings as a result of interactions with the atmosphere, but they also advocated for further investigation into the origin of pyroaurite at the mine site. Coalingite is structurally very similar to Fe-rich brucite, as it contains Mg-Fe hydroxide layers that lack long range ordering of the Fe<sup>3+</sup> cations (Mills et al., 2012). Coalingite has been described as the interstratification of pyroaurite and brucite, as only every second interlayer space contains CO<sub>3</sub> and H<sub>2</sub>O (Mills et al., 2012).

The quantitative XRD data of the vertical profiles supports *in situ* sedimentary formation for the hydromagnesite, pyroaurite, and coalingite at Woodsreef. The hydromagnesite is only found in the surface crusts and sporadically within the first 40 cm of tailings material. Similarly, the abundance of pyroaurite appears to be controlled by depth within the tailings material, being present at abundances up to 13.2 wt% in surface crusts, but the abundance falls with depth to ~2 wt% at 60–120 cm depth. Coalingite abundance is also controlled by depth, being entirely absent from the surface of the tailings but increasing in abundance to ~3 wt% at 100 cm depth. These results are consistent and repeatable in 4 vertical profiles taken from distances of up to 300 m apart within the tailings storage facility. If these minerals were of metamorphic origin, and had they been present as part of the original tailings mineralogy then they would not have had a consistent relationship with depth across multiple vertical profiles taken from across the tailings. The presence of carbonate-rich hydromagnesite and pyroaurite at the surface compared to carbon-poor coalingite and brucite at depth suggests that there are multiple reaction fronts occurring with depth into the tailings. With hydromagnesite forming via precipitation from Mg<sup>2+</sup> and CO<sub>3</sub><sup>2-</sup> rich fluids (sourced

from dissolution of brucite, serpentine, and Mg-bearing gangue minerals, and atmospheric CO<sub>2</sub>) or via direct replacement of brucite in the surface crusts and shallow tailings, whereas coalingite and pyroaurite form by the carbonation of brucite in the more carbon- and fluid-limited environment of the deeper tailings (Table 4.7).

**Table 4.7** Comparison of carbonate minerals and carbon sequestration estimate using XRD and elemental carbon data

	Mg:CO <sub>2</sub> (mol)	Mg+Fe:CO <sub>2</sub> (mol)	Mg:H <sub>2</sub> O + 2(OH) (mol)	Mg+Fe:H <sub>2</sub> O+2(OH) (mol)	Mg (wt%)	Fe (wt%)	C (wt%)	H <sub>2</sub> O (wt%)
hydromagnesite	1.25	1.25	1	1	25.99	0	10.27	19.26
pyroaurite	6	8	0.5	0.67	22.04	16.88	1.82	32.67
coalingite	10	12	0.71	0.86	28.3	13	1.4	29.36
brucite			0.5	0.5	41.68	0	0	30.89

The formation of multiple carbonate minerals is seen at other serpentinite-hosted ore deposits. For instance, Wilson et al. (2006) found that hydromagnesite and other more hydrated Mg-carbonate minerals form surface and vertical crusts, as well as cements the within deeper tailings, at the Clinton Creek chrysotile mine. At Clinton Creek, hydromagnesite is present at a low but significant abundance in bulk tailings (2.2 wt%) and vertical crusts (5.4–7.7 wt%), similar to what is seen at Woodsreef. Pyroaurite is also found at Clinton Creek (0.1–2.9 wt%); however, it has previously been considered to have a metamorphic origin and so is unlikely to be a net carbon sink, additionally minor unreacted abundances of brucite are found in some of the samples (0.9–1.0 wt%) (Wilson et al., 2006). Even if the pyroaurite at Clinton Creek was formed by low-temperature carbonation of brucite following mining, the relatively low abundances of brucite and pyroaurite at Clinton Creek make it unlikely that pyroaurite, would play as important a role in the carbon sequestration potential of Clinton Creek as it may at Woodsreef.

#### 4.4.2 Formation of coalingite and pyroaurite from brucite

Hydrotalcite minerals are known to form either during hydrothermal alteration of spinel minerals such as magnetite and chromite, during serpentinisation (Grguric, 2003; Grguric et al., 2001; Melchiorre et al., 2016) or from low temperature carbonation of brucite at the Earth's surface (Hostetler et al., 1966; Mumpton et al., 1965; Mumpton and Thompson, 1966). Figure 4.4a shows a magnetite grain from the tailings at Woodsreef (a.1) that is covered by chrysotile fibres (a.2) and a Mg-Si-C-bearing material (a.3). There are no obvious whorls of intergrown plates of pyroaurite or coalingite as are seen at other sites where hydrotalcite minerals have formed by replacement of spinels during hydrothermal alteration, such as at the Mount Keith nickel mine or the Dundas mineral field in Australia (Grguric, 2003; Grguric et al., 2001; Melchiorre et al., 2016). Figure 4.4b and Figure 4.4c show images of Fe-rich brucite grains undergoing dissolution and replacement by a new phase or phases. In Figure 4.4b, the brucite grain appears to be relatively unreacted, with dissolution localised to the (0 0 1) cleavage planes and orthogonal edges of individual plates of brucite. Accompanying the fractures, and oriented parallel to them, are plates of a newly formed mineral or minerals. In several locations, these plates begin to amass to form larger mineral growths on the surface of the brucite grain (b.1). Similar dissolution and formation textures have been observed for brucite previously by Hovelmann et al. (2012) who used atomic force microscopy (AFM) experiments to observe the formation of Mg-carbonates on the (0 0 1) cleavage surfaces of brucite under low temperatures (23–40 °C). EDS results indicate that these plates and growths contain Mg and O with minor abundances of C and Fe, as expected of pyroaurite or coalingite. Due to the uncertainty associated with analysing light elements, such as carbon using EDS, and the similar chemical compositions of pyroaurite, coalingite and hydromagnesite (that has undergone limited Fe substitution for Mg) it is unlikely that the three minerals can be differentiated using SEM (as seen in Hamilton et al., 2016, 2018).

However, quantitative XRD from the sample that was analysed using SEM (15WR5-DC, 100 cm) indicates that hydromagnesite is either completely absent from the sample or is present at abundances below the detection limit ( $<0.1$  wt%), while pyroaurite and coalingite are present at 1.6 wt% and 3.3 wt% respectively. These results indicate that it more likely that the platy minerals that are forming are pyroaurite or coalingite.

In Figure 4.4c, we see similar dissolution textures and elemental compositions to those in Figure 4.4b. However, the dissolution textures on the brucite grain in Figure 4.4c appear to be more extensive. In Figure 4.4b, the dissolution along the (0 0 1) cleavage surfaces was relatively isolated, running in parallel lines across the surface of the grain, whereas in Figure 4.4c they appear to be occurring as a cross hatch texture, with fractures meeting and intertwining with one another. It is likely that what is being observed is variation in the extent of the brucite carbonation reaction; when only limited amounts of carbon and water are available the carbonation reaction is more likely to be limited, with only some dissolution fractures forming and less evidence of pyroaurite and coalingite formation (Figure 4.4b). Over time, and with progressively more input of carbon and water, the brucite should continue to dissolve and form pyroaurite and coalingite until the texture of the grain changes to what is seen in Figure 4.4c. SEM images from McCutcheon et al. (2017) showed that when undergoing microbially mediated carbonation, the tailings at Woodsreef eventually formed masses of subhedral pyroaurite platelets. What we are observing is the most carbon limited version of this carbonation reaction, with minimal formation of pyroaurite in the deep tailings, while McCutcheon et al. (2017) observes the furthest extent of this reaction when conditions are altered to enhance carbonation.

The SEM and XRD results are consistent with formation of pyroaurite and coalingite *in situ* within the shallow and deep tailings at the expense of Fe-rich brucite as suggested by

Oskierski et al. (2013) and reiterated by Turvey et al. (2017), rather than being present in the tailings as gangue minerals that formed during the serpentinisation events that produced the Woodsreef Serpentinite. This is an important result because it suggests that pyroaurite at mineralogically similar serpentinite-hosted mineral deposits such as the Clinton Creek chrysotile mine (Wilson et al., 2006) and Dumont Nickel Project (Gras et al., 2017) may be sequestering atmospheric CO<sub>2</sub> via carbonation of Fe-rich brucite.

#### **4.4.3 Radiocarbon and stable carbon and oxygen isotope results reflect formation under carbon limited conditions**

**4.4.3.1 Woodsreef results.** Our radiocarbon results indicate that the tailings at Woodsreef are sequestering atmospheric CO<sub>2</sub>, a result that is in agreement with the conclusions of Oskierski et al. (2013). The radiocarbon values of  $0.80 < F^{14}C < 1.00$  (Figure 4.5) indicate that modern atmospheric carbon is present in the tailings alongside a lesser proportion of older, radiocarbon dead bedrock carbon. The Woodsreef Serpentinite formed through multiple serpentinisation events between the Early Permian and Tertiary periods (O'Hanley and Offler, 1992), meaning that whatever their carbon source, any carbonates that formed during the serpentinisation event would have an  $F^{14}C$  value of  $\sim 0$  today due to radioactive decay. Had all the carbon in the tailings pile been sourced from the atmosphere, the  $F^{14}C$  values would instead reflect an entirely modern carbon signature of  $F^{14}C > 1.00$ , reflecting exposure of the tailings to the atmosphere since the opening of the mine in 1972. The intermediate values that we observe of  $0.80 < F^{14}C < 1.00$  likely result from mechanical mixing of the small amount of bedrock carbonate minerals in the tailings with secondary alteration minerals that contain modern atmospheric carbon, thus lowering the  $F^{14}C$  values. Samples of pyroaurite that were picked by hand for radiocarbon analysis contain predominantly modern carbon, with values of  $0.95 \leq F^{14}C \leq 0.98$  (Table 4.4). This modern

atmospheric signature could occur either through (1) formation of pyroaurite *in situ* within the tailings by reaction of Fe-rich brucite with atmospheric CO<sub>2</sub> or (2) via the exchange of bedrock carbon housed within interlayer galleries of metamorphic pyroaurite for modern atmospheric carbon, similar to what has been observed during recrystallisation of hydrated Mg-carbonates under laboratory conditions (Mavromatis et al., 2015). The quantitative mineral abundance results for brucite, pyroaurite and coalingite (Figure 4.3) indicate that pyroaurite is more abundant towards the surface of the tailings, consistent with the formation of some or all of the hydrotalcite minerals through the *in situ* carbonation of brucite within the tailings, meaning that this radiocarbon signature is more likely to be due to reaction of brucite with atmospheric CO<sub>2</sub> post-mining rather than a result of gangue pyroaurite undergoing anion exchange. As such, the old carbon is likely sourced from the trace abundances of magnesite and calcite that have been reported within the tailings (Oskierski et al., 2013), whereas the modern carbon is contained within pyroaurite and hydromagnesite that is forming within the tailings. The small portion of <sup>14</sup>C-free carbon present in pure samples of pyroaurite could be sourced from limited dissolution of gangue magnesite and calcite or trace contamination of pyroaurite samples by these phases.

Samples taken from deeper within the tailings pile typically have lower F<sup>14</sup>C values than those taken from the surface (Figure 4.5). This observation is consistent with either the deeper carbonates having formed earlier, during the progressive placement of tailings during the mines operation or with mechanical mixing of two populations of carbonate minerals, with shallow tailings samples being dominated by atmosphere-derived carbonate minerals, whereas deeper tailings have a larger proportion of <sup>14</sup>C-free bedrock carbonate. The exception to this trend of decreasing F<sup>14</sup>C with depth is the 50 cm deep sample from profile 14WRP-1, which has a F<sup>14</sup>C value of 0.97. This is the highest F<sup>14</sup>C value for samples analysed from profile 14WRP-1, and it is significantly higher than the other sample from 50

cm depth (from profile S3-FC3), which has a  $F^{14}\text{C}$  value of 0.83. A  $F^{14}\text{C}$  value of 0.97 is more typical of samples taken from the surface of the tailings (the  $F^{14}\text{C}$  of the modern atmosphere in the southern hemisphere  $\sim 1.03$ ; Turnbull et al., 2017). This high  $F^{14}\text{C}$  value could potentially be attributed to the high abundance of  $^{14}\text{C}$ -rich pyroaurite in the sample (6.2 wt%), compared to other samples taken from a similar depth ( $\sim 2$  wt% pyroaurite), with the relatively high abundance of pyroaurite affecting the bulk  $F^{14}\text{C}$  composition of this sample. This abundance of pyroaurite could be due to the burial of older surface crusts by the addition of more recently deposited tailings, as suggested by Wilson et al. (2014) for the tailings storage facility at Mount Keith, or by deposition of wind-blown surface tailings, as 14WRP-1 was sampled from a slight depression in the tailings pile and was likely accumulating any fine wind-blown sediments of chrysotile, brucite and pyroaurite. The  $F^{14}\text{C}$  content of this buried crustal material ( $F^{14}\text{C} = 0.97$ ) demonstrates that carbonates that formed earlier *in situ* within the tailings still have a very high radiocarbon content, indicating that the more depleted samples ( $F^{14}\text{C} \leq 0.97$ ) are due to mechanical mixing of atmospheric derived carbonates and  $^{14}\text{C}$ -free bedrock carbonate, rather than radioactive decay of older atmospheric derived carbonates.

Stable carbon and oxygen isotopes have been used in previous carbon mineralisation studies to differentiate between carbon sinks within tailings material and to determine carbon sources (Gras et al., 2017; Oskierski et al., 2013; Wilson et al., 2011; Wilson et al., 2009a; Wilson et al., 2014). Oskierski et al. (2013) investigated the stable carbon and oxygen isotope compositions of carbonate crusts (hydromagnesite dominated), cements (pyroaurite dominated) and bedrock carbonate (magnesite and calcite) in the tailings at Woodsreef. When the results of Oskierski et al. (2013) are plotted with our new stable C and O isotope data for bulk tailings material and pure samples of pyroaurite, they create a more complete picture of the carbonation processes at Woodsreef (Figure 4.6). Our analyses of pure

pyroaurite samples show that pyroaurite is depleted in  $^{13}\text{C}$  and  $^{18}\text{O}$  relative to other pure carbonate minerals and sample types that have been analysed from Woodsreef as part of this study and by Oskierski et al. (2013). The 9 samples of pyroaurite that were analysed vary in composition between  $-7.2\text{‰} \leq \delta^{13}\text{C} \leq -3.4\text{‰}$  and  $14.7\text{‰} \leq \delta^{18}\text{O} \leq 21.2\text{‰}$ , with an average composition of  $-5.5\text{‰}$   $\delta^{13}\text{C}$  and  $17.3\text{‰}$   $\delta^{18}\text{O}$  (Table 4.5). Bulk samples of tailings material, which contain pyroaurite and trace hydromagnesite are typically more enriched in  $^{13}\text{C}$  and  $^{18}\text{O}$ , with 9 samples varying in composition between  $-5.8\text{‰} \leq \delta^{13}\text{C} \leq -3.7\text{‰}$  and  $23.2\text{‰} \leq \delta^{18}\text{O} \leq 26.8\text{‰}$ , with an average composition of  $-4.5\text{‰}$   $\delta^{13}\text{C}$  and  $24.5\text{‰}$   $\delta^{18}\text{O}$ . Stable C and O isotope data reported by Oskierski et al. (2013) show that vertical surface crusts at Woodsreef, which contained high abundances of hydromagnesite (i.e., 9.3–14.6 wt%), have significantly higher  $\delta^{13}\text{C}$  and  $\delta^{18}\text{O}$  values (i.e.,  $2.5\text{‰} \leq \delta^{13}\text{C} \leq 7.5\text{‰}$ ,  $26\text{‰} \leq \delta^{18}\text{O} \leq 40\text{‰}$ ), relative to those for samples of pyroaurite and bulk tailings. One possible explanation for the diversity of the observed  $\delta^{13}\text{C}$  and  $\delta^{18}\text{O}$  values, and the distribution of data in Figure 4.6, is that the majority of samples taken from the tailings pile have stable C and O isotope compositions that reflect mechanical mixing of various proportions of isotopically heavy hydromagnesite and isotopically light pyroaurite.

Stable carbon and oxygen isotope data can be used to elucidate the formation mechanisms of carbonate minerals in mine tailings (Gras et al., 2017; Oskierski et al., 2013; Wilson et al., 2010; Wilson et al., 2011; Wilson et al., 2014). Wilson et al. (2010) investigated the stable carbon and oxygen isotope signature of dypingite [ $\text{Mg}_5(\text{CO}_3)_4(\text{OH})_2 \cdot \sim 5\text{H}_2\text{O}$ ] that was precipitated from high-pH, saline solutions. They found that dypingite, which was produced by replacement of brucite, formed from a  $^{13}\text{C}$ -depleted pool of DIC ( $-20\text{‰} \leq \delta^{13}\text{C} \leq -16\text{‰}$ ), indicating kinetic fractionation of stable C isotopes occurred during the slow ingress of atmospheric  $\text{CO}_2$  into solution via diffusion (Wilson et al., 2010). The dypingite was enriched in  $^{13}\text{C}$  compared to the DIC from which it formed ( $\Delta^{13}\text{C}_{\text{dyp-DIC}} = +3.8\text{‰}$ ) and as the

carbonation reaction progressed, the  $\delta^{13}\text{C}$  of the remaining DIC pool became more depleted ( $\delta^{13}\text{C} < -20\text{‰}$ ) over time, indicating that the rate of  $\text{CO}_2$  uptake into solution was outpaced by the rate at which  $\text{CO}_2$  was fixed in the precipitate (Wilson et al., 2010). Similarly, previous field studies have found that Mg-carbonates forming in mine tailings, particularly those found at depth, rarely form in isotopic equilibrium with the atmosphere, and that they are typically more depleted in  $^{13}\text{C}$  and  $^{18}\text{O}$  than expected even though radiocarbon data indicate that they contain predominantly modern atmospheric-derived carbonate anions (Gras et al., 2017; Oskierski et al., 2013; Wilson et al., 2011; Wilson et al., 2014). The trend in the  $\delta^{18}\text{O}-\delta^{13}\text{C}$  results from Woodsreef likely reflects, at least in part a similar trend relating to a change in  $\text{CO}_2$  availability with depth (Figure 4.6). Our data and those of Oskierski et al. (2013) indicate that although the hydromagnesite-rich surface crusts appear to have formed in stable C isotopic equilibrium with atmospheric  $\text{CO}_2$ , the deeper hydromagnesite- and pyroaurite-bearing tailings and the pure pyroaurite samples are too depleted in  $^{13}\text{C}$  and  $^{18}\text{O}$  to have precipitated in equilibrium with atmospheric  $\text{CO}_2$  (Figure 4.6). The  $^{13}\text{C}$ - and  $^{18}\text{O}$ -depleted signature of the pyroaurite samples could indicate incorporation of  $^{13}\text{C}$ -depleted DIC from solution into the interlayers of these minerals, similar to what has been observed for other hydrated Mg-carbonates that have been investigated in carbon mineralisation studies (Gras et al., 2017; Harrison et al., 2013; Wilson et al., 2010; Wilson et al., 2014).

The stable C and O isotope results for pyroaurite cannot definitively indicate either the source of  $\text{CO}_2$  within pyroaurite or its formation mechanism at Woodsreef. Although both pyroaurite and hydromagnesite contain modern atmospheric carbon, our stable C and O isotope data for pyroaurite and the results of Oskierski et al. (2013) for hydromagnesite plot in distinct fields. Pyroaurite has an intermediate  $\delta^{13}\text{C}$  signature, between the atmosphere-derived carbonate and bedrock-derived carbonate fields determined by Oskierski et al. (2013). The  $\delta^{18}\text{O}$  values for pyroaurite show depletion in  $^{18}\text{O}$  compared to both atmosphere-

and bedrock-derived carbonate; this depleted signature is more typical of the  $\delta^{18}\text{O}$  values for metamorphic carbonate minerals in serpentinites (e.g., Wilson et al, 2009; Wilson et al., 2014). Part of the  $^{18}\text{O}$ -depleted signature in pyroaurite could have been inherited in part from the metamorphic brucite from which it forms; however, this relationship is not observed for hydromagnesite which can also form via replacement of brucite. Notably, pyroaurite abundances declines below a depth of 50 cm but it still persists at ~2 wt% abundance to at least 120 cm depth (the furthest extent that tailings profiles that were sampled, Figure 4.3). Thus, an alternative explanation could be that there are two populations of pyroaurite within the tailings: gangue pyroaurite, found at low abundance deeper into the tailings, and greater abundances of newly formed pyroaurite at the surface of the tailings. This could give rise to a mixed  $^{18}\text{O}$  signature, in which the metamorphic pyroaurite signature would become less dominant with decreasing depth below the tailings surface owing to the formation of atmosphere derived pyroaurite and hydromagnesite in the upper tailings. Another explanation may be that samples from deeper into the tailings experience less evaporative fractionation of stable oxygen isotopes, giving rise to an  $^{18}\text{O}$ -depleted signature relative to the tailings surface as seen in Gras et al. (2017). However, no stable C and O fractionation factors have been published for any hydrotalcite supergroup minerals, making a more detailed interpretation challenging. Furthermore, there is the possibility that the  $^{18}\text{O}$ -depleted stable O isotope signature of pyroaurite and coalingite could indeed reflect a metamorphic origin for these minerals, although our XRD and SEM results, and previous studies of coalingite stability (Mumpton et al., 1965; Mumpton and Thompson 1966), strongly support weathering derived *in situ* formation within the tailings pile. In this scenario, gangue hydrotalcite minerals might undergo continuous carbonate exchange, leading to continuous re-equilibration of stable C and O isotopes within interlayer carbonate groups, with the local environment, as seen for Mg-carbonates by Mavromatis et al. (2015). Because the stable O

isotope signature of hydrotalcite minerals will reflect the  $\delta^{18}\text{O}$  values of labile carbonate ions (3 O per formula unit; p.f.u), and interlayer  $\text{H}_2\text{O}$  molecules ( $\sim 4$  O p.f.u), but mostly structural OH groups (16 O p.f.u.), anion exchanged gangue pyroaurite should have  $\delta^{18}\text{O}$  values that mostly reflect formation from an  $^{18}\text{O}$ -depleted metamorphic fluid. As such, stable C and O isotope data and radiocarbon alone cannot be used to trace the origin of carbonate in hydrotalcite minerals. Alternative stable isotope systems, such as Mg may be more resistant to exchange than radiocarbon and stable C, as Mg is entirely held within the hydroxide layers of the hydrotalcite minerals, and so may be more resistant to re-equilibration than stable C isotopes and the stable O isotopes that are held in the interlayer spaces of the hydrotalcites.

**4.4.3.2 Exchange experiments.** The iowaite–pyroaurite anion exchange experiments were conducted to provide insight into how the stable C isotopic composition of hydrotalcite minerals evolves during sequestration of atmospheric  $\text{CO}_2$ . Hydrotalcite minerals are known to readily undergo anion exchange at ambient conditions and to have a strong preference for carbonate over other anions (Bish, 1980; Miyata, 1983), meaning that iowaite will exchange  $\text{Cl}^-$  for  $\text{CO}_3^{2-}$  when exposed to a source of aqueous  $\text{CO}_2$ , becoming pyroaurite (Figure 4.7). Previous stable isotope fractionation experiments have investigated the stable C and O isotope composition of dypingite that forms by replacement of brucite in high-pH, saline solution (Wilson et al., 2010) and precipitation of nesquehonite ( $\text{MgCO}_3 \cdot 3\text{H}_2\text{O}$ ) by replacement of brucite under variable  $p\text{CO}_2$  (Harrison et al., 2013). Wilson et al. (2010) precipitated dypingite from a high-pH, saline solution by introducing laboratory air bearing ambient concentrations of  $\text{CO}_2$  using a peristaltic pump. As mentioned previously, they found that the formation of Mg-carbonate minerals is kinetically inhibited by the rate at which  $\text{CO}_2$  diffuses from the atmosphere into solution, and that the slow diffusion of  $\text{CO}_2$  results in a  $^{13}\text{C}$ -depleted stable C isotope signature in DIC and the resulting dypingite (Wilson et al., 2010). Harrison et al. (2013) investigated the carbonation of brucite to

precipitate nesquehonite in solution with various partial pressures of CO<sub>2</sub>. They found that the nesquehonite was forming in equilibrium with the solution DIC; however, the DIC was not in equilibrium with the supply of CO<sub>2(g)</sub> and the divergence from equilibrium values was greatest for low *p*CO<sub>2</sub> conditions (Harrison et al., 2013). Similar to the results of Wilson et al. (2010), Harrison et al. (2013) determined that the rate of nesquehonite formation was limited by the slow kinetics of CO<sub>2</sub> ingress into solution.

Our anion exchange experiments used iowaite in contact with DIC sourced from the atmosphere to emulate the CO<sub>2</sub>-poor conditions that are known to dominate within mine tailings. Two solution conditions were created under which to observe the anion exchange reaction: a solution with carbon-limited conditions (made by a stir bar operating at 200 RPM), and a solution with a greater amount of carbon for anion exchange (600 RPM). Stable C isotope data were collected from the iowaite as it underwent exchange, and radiocarbon data were collected for the carbon-limited experiment. These experiments were meant to be demonstrative of process and no data for pH were collected, nor were the concentration or stable C isotopic compositions of DIC measured; thus a follow up experiment should be conducted to determine a stable C isotope fractionation factor between pyroaurite and DIC under these conditions and to monitor solution chemistry.

The two experimental conditions led to radically different trends in δ<sup>13</sup>C versus time as seen in Figure 4.8a. Before reaction, the starting iowaite had a δ<sup>13</sup>C value of -15.9 ‰ (Figure 4.8a). This value is significantly more depleted in <sup>13</sup>C relative to the value measured in 2007 by Wilson et al. (2014) for the same sample, indicating that the sample had likely been taking up atmospheric CO<sub>2</sub> since the time of sampling in 2006. The 200 RPM experiment shows a depletion of <sup>13</sup>C relative to the starting iowaite, reaching a δ<sup>13</sup>C value of -28.2 ‰ after 46 hours of exchange (Table 4.6), similar to the results from Wilson et al. (2010) and Harrison

et al. (2013). However, the 600 RPM experiment shows a gradual enrichment in  $\delta^{13}\text{C}$  relative to the starting iowaite (Figure 4.8a), reaching  $\delta^{13}\text{C}$  values between -11.3 ‰ and -7.3 ‰ after 44–46 hours (Table 4.6). The differences between the results of the two experiments could be explained by differences in the water–rock ratios used in the experiments as well as different amounts of carbon entering the system. The iowaite–pyroaurite sampled in the 200 RPM experiment, which represented carbon-limited conditions, exhibits similar behaviour to Mg-carbonates that are forming under low  $\text{CO}_2$  conditions as a result of kinetic limitations on  $\text{CO}_2$  dissolution. However, the 600 RPM, which we infer to have had more carbonate entering solution, exhibits a positive trend of  $^{13}\text{C}$  enrichment with time, which suggests that the mineral, which started with an initially low  $\delta^{13}\text{C}$  value is undergoing gradual exchange with a DIC pool that is approaching isotopic equilibrium with the atmosphere ( $\Delta^{13}\text{C}_{\text{DIC-CO}_2(\text{g})} \approx 0$  ‰). It appears that a hydrotalcite mineral undergoing anion exchange will develop a similar stable isotope signature to those that have previously been reported for Mg-carbonate minerals forming under  $\text{CO}_2$  limited conditions, and the magnitude of the kinetic fractionation is strongly tied to  $\text{CO}_2$  supply as seen by Harrison et al. (2013). The  $\text{F}^{14}\text{C}$  results (Figure 4.8b) show the incorporation of modern atmospheric carbon over time, starting from an  $\text{F}^{14}\text{C}$  value of 0.87 in the iowaite, indicating a significant radiocarbon uptake by the iowaite sample since sampling in 2006, to a value of  $\text{F}^{14}\text{C} = 1.03$  (Table 4.6), reflecting the composition of the current atmosphere (Graven et al., 2017; Turnbull et al., 2017). Under the carbon-limited conditions of the 200 RPM experiment, there is a correlation between decreasing value of  $\delta^{13}\text{C}$  and increasing  $\text{F}^{14}\text{C}$  (Figure 4.8c).

The results of this experiment could potentially explain the variability measured in the stable C isotope values of pyroaurite at Woodsreef. The large, negative  $\delta^{13}\text{C}$  values observed in the 200 RPM experiment most likely resulted from the limited diffusion of atmospheric  $\text{CO}_2$  into solution. However, the vigorous stirring of the 600 RPM experiment led to the

incorporation of far more CO<sub>2</sub> into solution (necessitating the measurement of solution DIC concentration and  $\delta^{13}\text{C}$  of DIC in future experiments). This may indicate that in carbon limited systems, such as the deeper tailings at Woodsreef, pyroaurite reflects a more depleted stable C isotope signature compared to pyroaurite  $\pm$  hydromagnesite forming at the top of the tailings, where atmospheric CO<sub>2</sub> can more easily ingress the tailings. Alternatively, the formation of <sup>13</sup>C-rich carbonates at the surface of the tailings could lead to depletion of the stable C isotope composition of the DIC, as observed by Wilson et al., (2010), such that pyroaurite and coalingite precipitating within deeper tailings form from a different DIC pool that is depleted in <sup>13</sup>C, relative to DIC in the fluids at the surface of the tailings. Other influences that dictates the composition of fluids within tailings wastes was explored in Gras et al. (2017) where the authors developed a conceptual model for isotope fractionation during carbonation of mine wastes from the Dumont nickel project (Abitibi, Québec). They describe the processes that influence the isotopic composition of the interstitial waters, including atmospheric CO<sub>2</sub> dissolution, bedrock carbonate dissolution, evaporation, oxidation and photosynthesis, and how each of these processes can fractionate stable C isotopes within DIC, before minerals precipitate from the DIC pool (Gras et al., 2017).

Few studies have published field or laboratory data on the stable isotopic compositions of hydrotalcites. Oskierski et al. (2013) attributed the isotopic C and O signature of pyroaurite at Woodsreef to either kinetic depletion of <sup>13</sup>C during uptake of atmospheric CO<sub>2</sub>, or formation from an organic carbon source; however, unlike other mine sites such as the Diavik diamond mine (Wilson et al., 2011) there is no readily available source of organic C to affect the composition pyroaurite at Woodsreef. Gras et al. (2017) investigated stable C and O isotopic compositions of minerals at the Dumont Nickel Project during passive carbon mineralisation. Similarly, they attribute the <sup>13</sup>C-depleted compositions of carbonate minerals to kinetic fractionation during slow diffusion of atmospheric CO<sub>2</sub> into solution. Gras et al.

(2017) found that hydrotalcite minerals had a similar  $\delta^{13}\text{C}$  compositions to those measured in the present study and by Oskierski et al. (2013) at Woodsreef, and concluded that the  $^{13}\text{C}$ -depleted signature in hydrotalcite minerals was due to formation in the carbon-limited tailings environment. The results of our exchange experiment also indicate that the stable carbon isotopic composition of hydrotalcites can be affected by anion exchange following precipitation. Our observation that the  $\delta^{13}\text{C}$  value of our iowaite sample changed between the time of sampling and the experiment also suggests that anion exchange may not require visible liquid  $\text{H}_2\text{O}$ . Rather, anion exchange in hydrotalcites could be mediated by atmospheric relative humidity, which is not surprising given the humidity dependent stability of many hydrated minerals, including the hydrated Mg-carbonates (Morgan et al., 2015). These observations potentially call into question some of the conclusions made by Melchiorre et al. (2016) who investigated the origins of Phanerozoic stichtite [ $\text{Mg}_6\text{Cr}_2(\text{OH})_{16}(\text{CO}_3)\cdot 4\text{H}_2\text{O}$ ] from various localities within the Dundas mineral field (Tasmania, Australia) and Tehuitzingo (Mexico) and Melchiorre et al. (2018) who investigated the origins of Archean stichtite from South Africa, Western Australia and Southern India. They concluded that the large, negative  $\delta^{13}\text{C}$  values (-29.4 ‰ to -6.4 ‰) in stichtite samples collected from the Earth's surface reflected marine kerogen and marine carbonate sources for C during the serpentinisation events that formed the stichtite (Melchiorre et al., 2016; Melchiorre et al., 2018). However preserving these isotopic signatures would require that no appreciable anion exchange had occurring between the stichtite and the local environment since formation. Our results, consistent with those of Oskierski et al. (2013) and Gras et al. (2017) suggest that this  $\delta^{13}\text{C}$  signature results from a kinetic diffusion fractionation during uptake of atmospheric  $\text{CO}_2$ , and that hydrotalcite minerals undergo anion exchange with the local environment. This possibility could be

investigated for the stichite samples of Melchiorre et al. (2016, 2018) by measuring their radiocarbon content.

The stable C and O isotope compositions of the Woodsreef tailings, combined with the trends observed in XRD data and textural evidence from SEM, indicate that the hydromagnesite and pyroaurite present at the site are forming due to interactions between the tailings and the atmosphere, with variable depletion in  $^{13}\text{C}$  and  $^{18}\text{O}$  occurring due to the slow diffusion of atmospheric  $\text{CO}_2$  into pore waters in the tailings. However, a lack of  $\delta^{13}\text{C}_{\text{DIC}}$  measurements for pore water samples from the tailings at Woodsreef, which are typically very dry, and a limited understanding of stable isotope fractionation between DIC and hydrotalcite minerals, hampers our ability to draw more detailed conclusions at this time. Despite this, the combination of radiocarbon and stable C and O isotopes indicates that hydromagnesite, pyroaurite and coalingite contain modern atmospheric  $\text{CO}_2$ , although XRD and SEM data are necessary to demonstrate *in situ* formation of the hydrotalcite minerals within tailings given how rapidly anion exchange occurs in these minerals.

#### **4.4.4 Differentiating metamorphic and sedimentary hydrotalcite minerals in mine tailings and natural environments**

The exchangeable nature of carbonate and  $\text{H}_2\text{O}$  make it difficult to determine the origin of hydrotalcites using stable C and O isotopes and radiocarbon. Thus, a multianalytical approach is needed to determine whether hydrotalcite minerals formed via low-temperature sedimentary processes or during metamorphism. For the formation of pyroaurite and coalingite at Woodsreef, the high abundance of pyroaurite (and hydromagnesite) in the shallow tailings, and the correspondingly low abundance of brucite, indicates *in situ* formation of these minerals at the interface with the atmosphere. SEM micrographs show the formation of Mg-Fe-carbonates perpendicular to the (0 0 1) cleavage planes of Fe-rich

brucite grains within the tailings (Figure 4.4); which is a texture more common to low-temperature formation of carbonate minerals (e.g., Hövelmann et al., 2012). Our radiocarbon results indicate the presence of modern atmospheric carbon in all of the pyroaurite samples analysed (Figure 4.5), and stable C and O isotope data are consistent with the formation of pyroaurite and coalingite under carbon limited conditions. However, the ambiguity in stable and radiogenic isotope signatures of hydrotalcite minerals means that determining their origins are less obvious and more open to a variety of possible interpretations at localities where other lines of evidence, such as XRD and SEM results, are less definitive.

Hydrotalcite minerals are present in the mineral wastes of other ultramafic mines in high abundances as either gangue minerals of metamorphic origin or as alteration minerals that have formed *in situ* within the tailings. At the Mount Keith nickel mine, Cl-rich hydrotalcites, such as the iowaite used in our anion exchange experiments, make up ~20 wt% of the ore and, thus, are present at similar abundance in the unaltered tailings material (Grguric, 2003; Grguric et al., 2001). Our experiments show uptake of atmosphere-derived DIC into iowaite is rapid (Table 4.6). Previous studies have speculated that exchange of Cl<sup>-</sup> for CO<sub>3</sub><sup>2-</sup> within Mount Keith iowaite and woodallite has the potential to sequester in excess of 40 kt of CO<sub>2</sub> per year (Mills et al., 2011; Wilson et al., 2014; Woodhouse, 2006); which would amount to a doubling of the carbonation rate at Mount Keith as estimated from CO<sub>2</sub> sequestration in hydromagnesite alone (for a total of ~80 kt CO<sub>2</sub>/year, Wilson et al., 2014). Furthermore, previous studies may have assumed that pyroaurite and other hydrotalcites were present in ultramafic tailings as gangue minerals, rather than having formed *in situ* within the tailings, meaning the CO<sub>2</sub> sequestration rates may be underestimated for some mines, e.g., Clinton Creek chrysotile mine (Wilson et al., 2006). Thus, improved estimates for CO<sub>2</sub> sequestration rates and carbon sequestration potential may be obtained by accounting for the contribution of hydrotalcite minerals (Gras et al., 2017; Oskierski et al., 2013).

Wilson et al. (2014) investigated the formation of carbonate minerals within the Mount Keith tailings storage facility. In addition to observing an increase in hydromagnesite abundance in the upper tailings, there is also a small increase in hydrotalcite-group minerals within the tailings over time, which increase from ~2.5 wt% in fresh tailings to ~5 wt% in tailings after 7–8 years of reaction with the atmosphere (Wilson et al., 2014). At first glance, these results mirror what is found at Woodsreef, with hydromagnesite forming in the shallow tailings where CO<sub>2</sub> rich fluids are more accessible and hydrotalcite-group minerals appearing to form in the deeper tailings under more CO<sub>2</sub> limited conditions. The quantitative XRD results of Wilson et al. (2014) could therefore be used to argue that hydrotalcites are forming from the carbonation of brucite at Mount Keith, similar to what we have observed at Woodsreef; however, there are various pieces of counter-evidence. Unlike at Woodsreef, the hydrotalcite minerals at Mount Keith are well-documented in ore samples and textural evidence from thin section and hand samples shows that they replace spinel minerals, indicating their hydrothermal origin (Grguric, 2003; Grguric et al., 2001). Shortly after sampling, and before it could exchange CO<sub>2</sub> with the atmosphere, the  $\delta^{13}\text{C}$  and  $\delta^{18}\text{O}$  values of the sample of iowaite that was analysed by Wilson et al. (2014) and used in our anion exchange experiments falls within the range of values expected for a metamorphic carbonate at Mount Keith ( $\delta^{13}\text{C}$  of ~ -3 ‰ and  $\delta^{18}\text{O}$  of ~ 16‰). Furthermore, quantitative XRD results from Bea et al. (2012), which describe the mineralogy of more heavily weathered 10-year old tailings, reveal that at Mount Keith there is a close correlation between the abundances of bedrock magnesite and hydrotalcite minerals with depth, with both phases being more abundant in the deeper tailings and less abundant at the tailings surface (i.e., abundance increases from ~1 wt% and ~2.5 wt% at the surface to ~4 wt% and ~7.5 wt% at 125 cm depth for the magnesite and hydrotalcites, respectively). As magnesite is not forming *in situ* within the tailings, and these minerals are part of the same alteration assemblage in ore, this variation

is almost certainly due to changing composition of the ore and gangue mineralogy of tailings over time during deposition, rather than changes in tailings mineralogy post-deposition. It is also possible that there are multiple populations of hydrotalcite minerals at Mount Keith, with primary (gangue) hydrotalcites that originally lacked modern interlayer  $\text{CO}_3^{2-}$ , but could undergo anion exchange, and secondary hydrotalcites that are forming *in situ* within the tailings.

The examples of Woodsreef and Mount Keith highlight some of the potential pitfalls in identifying the origin of hydrotalcite minerals. This is driven by a lack of stable isotope fractionation factors for hydrotalcites and their anion exchange behaviour, both of which complicate interpretation of stable C and O isotope data. One potential solution is to investigate the stable isotopic composition of elements held in the more stable brucite-like hydroxide layers of the hydrotalcites. For pyroaurite and coalingite, this would include stable Mg, Fe and O isotopes, although stable O isotope compositions will still be affected the presence of exchangeable  $\text{H}_2\text{O}$ ,  $\text{CO}_3^{2-}$  and  $\text{SO}_4^{2-}$ . Understanding stable Mg or Fe isotopic compositions of hydrotalcites may reveal more information about the formation mechanisms of these minerals, since these elements are more likely to preserve information about formation conditions that are lost when investigating stable C and O isotope compositions which are affected by anion exchange.

#### **4.4.5 $\text{CO}_2$ limitation controls mineralogy and capture of $\text{CO}_2$ from air in mine tailings**

Understanding the origins of carbonate minerals is essential when considering both the  $\text{CO}_2$  sequestration rate and capacity at a mine site such as Woodsreef. The formation of hydromagnesite at Woodsreef was studied extensively by Oskierski et al. (2013) who describe its precipitation from  $\text{Mg}^{2+}_{(\text{aq})}$ - and  $\text{CO}_3^{2-}_{(\text{aq})}$ -rich pore waters, forming cemented surface crusts across the tailings surface, comparable to the formation of hydrated Mg-

carbonate minerals including hydromagnesite, nesquehonite and dypingite studied at other ultramafic tailings storage facilities (Gras et al., 2017; Lechat et al., 2016; Wilson et al., 2011; Wilson et al., 2009a; Wilson et al., 2014; Wilson et al., 2006). As pyroaurite and coalingite make up a significant amount of the Woodsreef tailings, determining their origin is essential to understanding their role in passive carbon mineralisation.

Oskierski et al. (2013) previously investigated the origin of pyroaurite in the tailings but did not definitively conclude whether they came from an atmospheric- or bedrock-derived carbon source, or had a metamorphic or authigenic origin. Turvey et al. (2017) theorised that pyroaurite in the tailings is forming from carbonation of Fe-rich brucite by reaction with atmospheric CO<sub>2</sub> under carbon limited conditions that are not conducive to the formation of hydromagnesite. Stable C isotope results and radiocarbon data (Table 4.4, Figures 4.5–4.6) for the pyroaurite at Woodsreef give similar values to, (1) those observed in the limited literature regarding the formation of hydrotalcites under carbon-limited conditions (Gras et al., 2017; Oskierski et al., 2013) and (2) those obtained from our CO<sub>2</sub>-poor anion exchange experiments, (Table 4.6, Figure 4.8). Quantitative XRD data from the vertical profiles (Table 4.3 and Figure 4.3) at Woodsreef support the formation of hydromagnesite, pyroaurite and coalingite in at least the first 120 cm of tailings material. In shallow tailings, where C is plentiful, Fe-rich brucite is more likely to either undergo dissolution and precipitation to form hydromagnesite and Fe-oxyhydroxide minerals as observed by Hamilton et al. (2016; 2018) or may carbonate to form pyroaurite instead. Deeper in the tailings, where the availability of CO<sub>2</sub> is more limited, carbonation of brucite to form hydromagnesite is not possible; however, the limited amount of CO<sub>2</sub> present instead reacts with Fe-rich brucite to form coalingite and pyroaurite (Table 4.7).

#### 4.4.6 Carbon sequestration rate estimates

Previous studies have used either quantitative XRD (e.g., Oskierski et al., 2013b; Wilson et al., 2006; Wilson et al., 2009b) or elemental carbon data (Gras et al., 2017; Hamilton et al., in prep-b) to estimate the amount of carbon sequestered in tailings storage facilities. Here, the average inorganic carbon content measured using elemental C analysis (0.31 wt%) is approximately twice the carbon content estimated using XRD (0.15 wt%) for the 43 tailings samples that were analysed using both techniques (Table 4.3). A explanation for this discrepancy is that there is carbon in the samples that is unaccounted for when using quantitative XRD data, as (1) the Rietveld method has been found to underestimate the abundance of hydromagnesite and pyroaurite in artificial tailings samples of a known composition (Turvey et al., in review/Chapter 3) and (2) the quantitative XRD we employed can only be used to account for crystalline phases, meaning that any amorphous carbonate phases that form during carbonation such as those that have been seen in other studies (Hamilton et al., in prep-b; Harrison et al., 2015), cannot be accounted for using XRD data. Hamilton et al. (in prep-b) have documented formation of an amorphous carbonate phases in the tailings at Woodsreef, similar to what was observed in laboratory experiments by Harrison et al. (2015). Because the XRD results are underestimating the inorganic carbon content of the tailings, the total C values obtained using this technique represent a minimum estimate for the amount of carbon sequestered in the tailings at Woodsreef and other mines. The total elemental C data does not provide the mineralogical or isotopic context required to determine whether the C in a sample is stored in secondary carbonate minerals that have an atmospheric source of C, or within gangue carbonate minerals that have not sequestered atmospheric CO<sub>2</sub>, and do not account for the possibility that gangue hydrotalcite minerals may become isotopically indistinguishable from secondary hydrotalcites via anion exchange.

As such, the elemental C data are likely to represent the maximum estimate for the amount of C sequestered by the tailings.

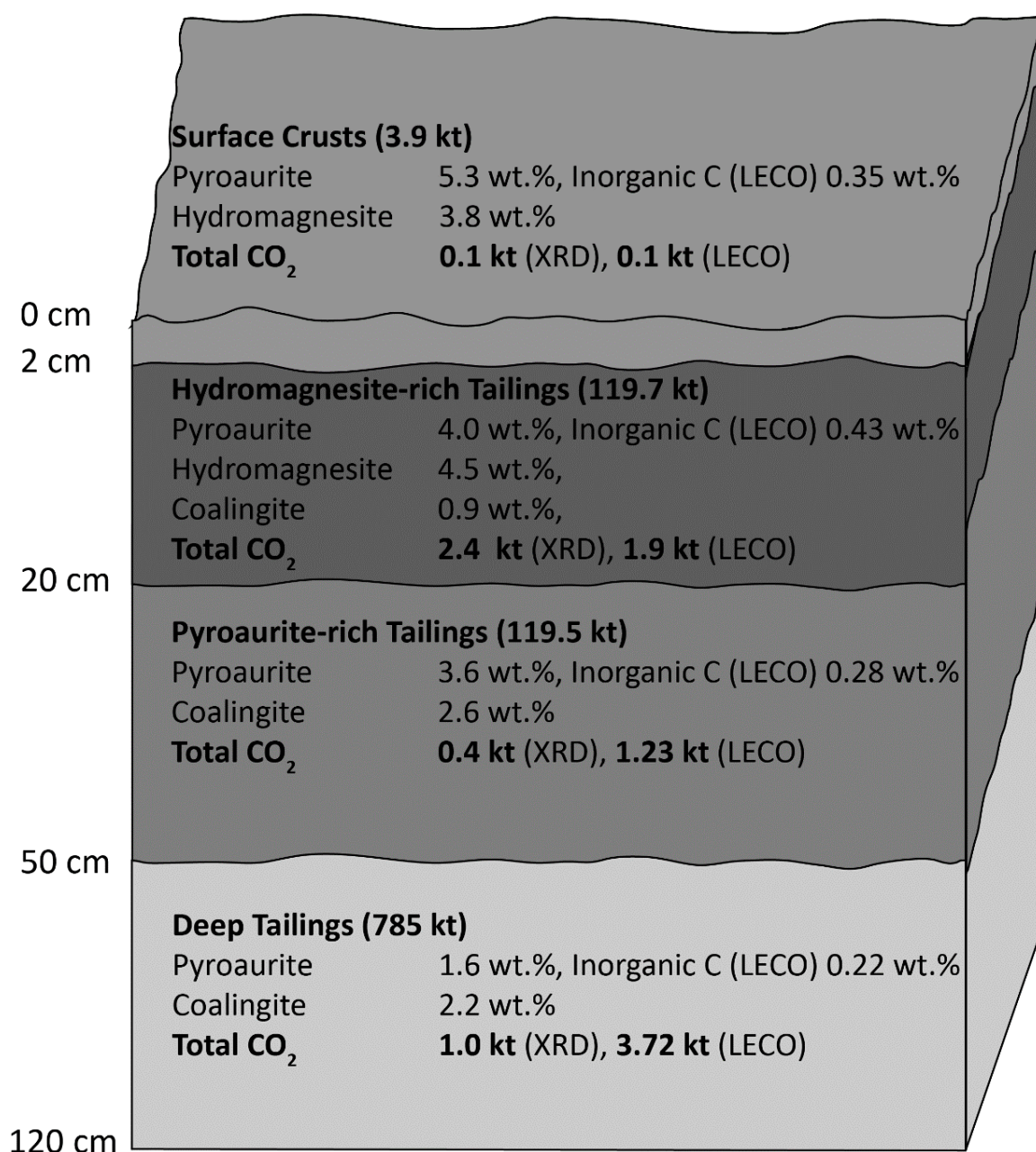
Estimates of the carbonation rate at Woodsreef have been made previously (Oskierski et al., 2013; Turvey et al., 2017). Oskierski et al. (2013) made two rate calculations of the amount of CO<sub>2</sub> sequestered at Woodsreef: the first assuming that pyroaurite was a primary gangue mineral and does not contribute to net CO<sub>2</sub> sequestration at Woodsreef and the second estimate assuming that the pyroaurite formed *in situ* within the tailings pile and is thus sequestering a net amount of atmospheric CO<sub>2</sub>. For the first estimate, Oskierski et al. (2013) calculated the average hydromagnesite content of vertical crust samples (12.9 wt%, estimated using quantitative XRD) and assumed that this average hydromagnesite content reflected the average composition of the top 2 cm of the entire tailings pile (which covers ~0.5 km<sup>2</sup>), leading to an estimate that there are 3,500 t of hydromagnesite at Woodsreef, sequestering 1,400 t of CO<sub>2</sub>. For the second estimate, in addition to the hydromagnesite in the surficial 2 cm, it was assumed that pyroaurite is a secondary mineral whose formation represents net sequestration of atmospheric CO<sub>2</sub>, and that it is present at an average abundance of 4.3 wt% throughout the entire depth of the tailings pile (Oskierski et al., 2013). This method was used to estimate that Woodsreef had sequestered 70,000 t of CO<sub>2</sub> within the hydromagnesite and pyroaurite between mine closure in 1983 and 2013. Oskierski et al. (2013) note that these methods likely represent the minimum and maximum amounts of CO<sub>2</sub> sequestered in the tailings at Woodsreef.

The results of the present study, particularly how the mineralogy of the tailings changes as a function of depth, and the origin of the pyroaurite, can be used to further refine the Woodsreef carbon sequestration estimates of Oskierski et al. (2013). Combined, the quantitative XRD and total C datasets can generate lower and upper bounds on the C content

of the tailings at different depths (Hamilton et al., in prep-b). XRD data illuminated the spatial mineralogical variability that occurs in the tailings pile, namely the formation of hydromagnesite in the shallowest 40 cm of tailings material, and the formation of coalingite and pyroaurite to a depth of at least 120 cm within the tailings. The depth relationship between hydromagnesite, pyroaurite, coalingite and brucite make it likely that carbonation of brucite is incomplete deeper in the tailings; however, this study did not sample deep enough into the tailings pile to determine the vertical extent of carbon ingress and pyroaurite/coalingite formation. The conceptual model of Lechat et al. (2016) describes carbonation occurring to a greater extent at the surfaces of tailings pile; but it is known to also occur on the exposed sides of tailings storage facilities. To create a conservative estimate of the carbon sequestration rate at Woodsreef it was assumed that carbonation is only occurring in the top 120 cm of tailings material, the limit to which we sampled and was observed in XRD in this study, across the ~0.5 km<sup>2</sup> tailings pile surface (after Oskierski et al., 2013). Table 4.8 summarises the assumptions that were made regarding the average hydromagnesite, pyroaurite and coalingite abundances of the tailings at different depths, and gives estimates of the amount of CO<sub>2</sub> sequestered in each part of the tailings, as calculated by XRD and total C data.

**Table 4.8** Comparison of atmospheric carbon sequestration rate estimates using XRD and total carbon (LECO) data

	Depth (cm)	Mass (kt)	Pyro (wt%)	Hydro (wt%)	Coal (wt%)	Inorganic C wt% (XRD)	CO <sub>2</sub> Sequestered kt (XRD)	Inorganic C wt% (LECO)	CO <sub>2</sub> Sequestered kt (LECO)
Surface Crusts	0-2	3.9	5.3	3.8		0.5	0.1	0.35	0.05
Hydromagnesite rich tailings	2-20	119.7	4.0	4.47	0.9	0.5	2.4	0.43	1.9
Pyroaurite rich tailings	20-50	119.5	3.6		2.6	0.1	0.4	0.28	1.2
Deep tailings	50-120	462	1.6		2.2	0.1	1.0	0.22	3.7
Total							3.9 kt		6.9 kt



**Total Mass: 785.1 kt**  
**Total CO<sub>2</sub>: 3.9 kt (XRD), 6.9 kt (LECO)**  
**Carbonation Rate: 229.0 g CO<sub>2</sub> m<sup>-2</sup> y<sup>-1</sup> (XRD) 405.1 g CO<sub>2</sub> m<sup>-2</sup> y<sup>-1</sup> (LECO)**

**Figure 4.10** Diagram comparing the quantity of atmospheric carbon sequestered in the tailings at various depths according to XRD and total carbon data.

Lower and upper limits for the average C composition of the surface crusts and tailings in the upper 120 cm of the tailings were determined from (1) the average abundances of hydromagnesite, pyroaurite and coalingite (according to quantitative XRD) and (2) the total elemental C data (see Figure 4.10). It was determined that 100% of the carbon in hydromagnesite was modern (hydromagnesite has a  $F^{14}C$  value of 1.07 according to Oskierski et al., 2013) and 96% of the carbon in the pyroaurite was modern (as pyroaurite has an average  $F^{14}C$  value of 0.96 according to the results of our study). Assuming that carbonation is occurring across the surface of the tailings pile ( $\sim 0.5 \text{ km}^2$ ), it is estimated that Woodsreef has sequestered between 3,900 t and 6,900 t of atmospheric  $\text{CO}_2$  within the hydromagnesite, pyroaurite and coalingite minerals found within the upper 120 cm of tailings at Woodsreef. The lower bound (3,900 t) was calculated using the tailings composition obtained with quantitative XRD to estimate the C content of the tailings, whereas the upper bound (6,900 t) was calculated using total elemental carbon data. These values fall within the range proposed by Oskierski et al. (2013) of 1,400-70,000 t. Their estimate assumed the pyroaurite abundance in the tailings is consistently high (4.3 wt% pyroaurite, Oskierski et al., 2013) throughout the depth of the entire tailings pile, which on further inspection has proven not to be the case. Our results indicate that at 120 cm depth the pyroaurite abundance had fallen to  $\sim 2 \text{ wt}\%$ . However, as we did not find the ‘end’ of the pyroaurite and coalingite in the tailings pile, it is possible it is present at  $\sim 2 \text{ wt}\%$  throughout the entire depth of the tailings pile. Improved accounting of  $\text{CO}_2$  sequestration at greater depth would require further detailed coring work and stable and radiogenic isotope investigations to assess the depth to which pyroaurite and coalingite are present and whether these minerals have also formed *in situ* within the tailings pile.

Rates of carbonation are typically reported based on the area of carbonating material, expressed as  $\text{g CO}_2 \text{ m}^{-2} \text{ y}^{-1}$  so that they may be compared with weathering rates in nearby

major river catchments (Wilson et al., 2011). For Woodsreef these rates are 229.0–405.1 g CO<sub>2</sub> m<sup>-2</sup> y<sup>-1</sup> (Figure 4.10). The rate is comparable to carbonation rates calculated for other ultramafic tailings storage sites and it is 3 orders of magnitude greater than the CO<sub>2</sub> fluxes associated with silicate weathering in the Australian Victorian Alps (0.15–0.47 g C m<sup>-2</sup> y<sup>-1</sup>, Hagedorn and Cartwright, 2009). Estimates for carbonation rates at other ultramafic tailings storage facilities range from 102–114 g CO<sub>2</sub> m<sup>-2</sup> y<sup>-1</sup> at the Diavik Diamond mine (Wilson et al. 2011), 162–270 g CO<sub>2</sub> m<sup>-2</sup> y<sup>-1</sup> at Mount Keith nickel mine TSF1 (Bea et al., 2012), up to 2400 g CO<sub>2</sub> m<sup>-2</sup> y<sup>-1</sup> at Mount Keith nickel mine TSF2 (Wilson et al., 2014) and as high as 6,200 g CO<sub>2</sub> m<sup>-2</sup> y<sup>-1</sup> for the Clinton Creek chrysotile mine (Wilson et al., 2009a). The rates for Mount Keith only consider CO<sub>2</sub> sequestration in hydrated Mg-carbonate minerals, and they are likely to be greater owing to CO<sub>2</sub> uptake in Cl-rich metamorphic hydrotalcites.

#### **4.5 Conclusions**

The presence of multiple mineral sinks for carbon at Woodsreef provides new insights into the environmental controls on carbon mineralisation. In the shallow tailings, where atmospheric CO<sub>2</sub> is abundant, hydromagnesite is forming by the dissolution and replacement of brucite, as has been seen at other tailings storage facilities (Gras et al., 2017; Lechat et al., 2016; Wilson et al., 2014). The carbonation of Fe-rich brucite into coalingite and pyroaurite occurs alongside the formation of hydromagnesite in the upper tailings, whereas coalingite and pyroaurite dominate within deeper tailings under more carbon limited conditions.

The limited understanding of the stability and isotopic compositions of hydrotalcites, combined with the exchangeable nature of their interlayer anions and H<sub>2</sub>O, means mineralogical and textural information, as well as isotope fractionation experiments, must currently be used to determine whether hydrotalcites are sourcing CO<sub>2</sub> from the atmosphere. At Woodsreef, the combination of XRD and SEM data shows the formation of pyroaurite

and coalingite at the expense of Fe-rich brucite in the upper 120 cm of the tailings, while stable and radiogenic isotope data indicate formation of hydrotalcites from a carbon-limited DIC pool. The origins of hydrotalcite minerals in mine tailings will be site specific. For instance at the Mount Keith nickel mine, hydrotalcites occur as abundant gangue minerals inherited from the ore; however, they are likely undergoing anion exchange with atmospheric CO<sub>2</sub> (overprinting the original metamorphic stable C isotope and radiocarbon signatures) and there may be new populations of secondary hydrotalcites forming in the tailings adding a layer of complexity to carbon accounting in hydrotalcites at Mount Keith. Tracing the origins of the hydrotalcites at a site like Mount Keith may require the use of stable isotope systems for elements that are less likely to undergo exchange, such as the Mg and Fe that are held in the brucite-like layers of hydrotalcites.

It is essential to have an accurate estimate of the amount of atmosphere-derived carbon stored in carbonate alteration minerals when estimating carbon sequestration rates. Thorough depth profiling in a tailings pile provides a more detailed picture of the carbonation process compared with just sampling at the surface. In terms of measuring passive carbonation rates, determining the depth relationships between secondary carbonate minerals enables a more nuanced estimate of the amount of carbon sequestered within a tailings pile. However, a comparison of the results of the quantitative XRD and total elemental carbon data demonstrates the potential shortcomings of both methods when used in isolation. There is a significant difference between the estimates for carbon content of the tailings obtained with XRD results and those obtained by direct measurement of elemental C, with the XRD data only accounting for half of the inorganic carbon content measured using elemental C analysis. This is likely due to error associated with Rietveld refinement of XRD patterns (Turvey et al., in review/Chapter 3; Turvey et al., 2017; Wilson et al., 2006) as well as the presence of

amorphous carbonate phases, which are known to occur at Woodsreef (Hamilton et al., in prep-b) and whose abundances are challenging to quantify using crystallographic methods.

Our results confirm that hydrotalcite minerals can form within ultramafic mine tailings piles, as originally put forth by (Oskierski et al., 2013), and that they contribute to sequestration of atmospheric CO<sub>2</sub> in this setting. At Woodsreef, atmospheric CO<sub>2</sub> is sequestered by multiple carbonate-bearing phases: including hydromagnesite, pyroaurite and coalingite, all of which form by carbonation of brucite. The formation of pyroaurite and coalingite under carbon limited conditions within the tailings pile at Woodsreef indicates that carbon sequestration can occur under more varied conditions than has been assumed by previous studies. This indicates that carbon sequestration estimates at some mines may need to be refined and that future modelling of carbon sequestration potential in mines will need to consider hydrotalcite minerals forming in carbon limited environments. Moreover, our results indicate that the increasingly limited supply of atmospheric CO<sub>2</sub> at depth within the tailings is a major control not only on carbonation rate but also on mineralogy and the efficiency of carbon sequestration in mine tailings. This observation offers hydrotalcites as a new mineralogical indicator of CO<sub>2</sub> limitation while providing an opportunity to increase the rate and efficiency of CO<sub>2</sub> sequestration in mine tailings. The formation of hydrotalcites in the carbon-limited deeper tailings indicates the potential of the tailings to sequester additional CO<sub>2</sub>. While the presence of hydromagnesite at the surface of the tailings shows how with sufficient CO<sub>2</sub> availability it is possible to promote the formation of highly efficient mineral sinks for CO<sub>2</sub>, which maximise the amount of CO<sub>2</sub> they sequester (for the available Mg) and minimise the volume of the resulting carbonates. This will allow for future enhanced carbon mineralisation studies to refine the amounts of Mg, H<sub>2</sub>O and CO<sub>2</sub> necessary to form specific carbon minerals and sequester atmospheric CO<sub>2</sub> in the most efficient manner

possible, likely through the addition of acids to liberate Mg, or H<sub>2</sub>O and CO<sub>2</sub> into the tailings to promote carbonate formation.

#### **4.6 Acknowledgements**

We would like to acknowledge funding from Carbon Management Canada and the New South Wales Department of Industry to S.A.W., G.M.D. and G.S. Work by C.C.T., J.L.H. and A.W.T. was supported by Australian Postgraduate Awards. Additionally we would like to thank Kate Maddison, Nick Staheyeff, Catherine Karpel and Brad Mullard at the NSW Department of Industry for granting us access to the field site and for their support of our work at Woodsreef.

#### **4.7 References**

- Akao, M., and Iwai, S. (1977) The hydrogen bonding of hydromagnesite. *Acta Crystallographica Section B*, 33(4), 1273-1275.
- Alexander, L., and Klug, H.P. (1948) Basic Aspects of X-Ray Absorption in Quantitative Diffraction Analysis of Powder Mixtures. *Analytical Chemistry*, 20(10), 886-889.
- Ashwal, L.D., and Cairncross, B. (1997) Mineralogy and origin of stichtite in chromite-bearing serpentinites. *Contributions to Mineralogy and Petrology*, 127(1-2), 75-86.
- Assima, G.P., Larachi, F., Beaudoin, G., and Molson, J. (2013a) Dynamics of carbon dioxide uptake in chrysotile mining residues – Effect of mineralogy and liquid saturation. *International Journal of Greenhouse Gas Control*, 12, 124-135.
- Assima, G.P., Larachi, F., Molson, J., and Beaudoin, G. (2013b) Accurate and direct quantification of native brucite in serpentine ores—New methodology and implications for CO<sub>2</sub> sequestration by mining residues. *Thermochimica Acta*, 566, 281-291.

- Bea, S.A., Wilson, S.A., Mayer, K.U., Dipple, G.M., Power, I.M., and Gamazo, P. (2012) Reactive transport modeling of natural carbon sequestration in ultramafic mine tailings. *Vadose Zone Journal*, 11(2).
- Beinlich, A., and Austrheim, H. (2012) In situ sequestration of atmospheric CO<sub>2</sub> at low temperature and surface cracking of serpentinized peridotite in mine shafts. *Chemical Geology*, 332–333, 32-44.
- Beinlich, A., Barker, S.L.L., Dipple, G.M., Gupta, M., and Baer, D.S. (2017) Stable isotope ( $\delta^{13}\text{C}$ ,  $\delta^{18}\text{O}$ ) analysis of sulfide-bearing carbonate samples using laser absorption spectrometry. *Economic geology*, 112, 693-700.
- Bish, D.L. (1980) Anion-exchange in takovite: applications to other hydroxalcalite minerals. *Bulletin Mineralogie*, 103, 170-175.
- Bish, D.L., and Brindley, G.W. (1977) A reinvestigation of takovite, a nickel aluminium hydroxy-carbonate of the pyroaurite group. *American Mineralogist*, 62, 458-464.
- Bish, D.L., and Howard, S.A. (1988) Quantitative phase analysis using the Rietveld method. *Journal of Applied Crystallography*, 21(2), 86-91.
- Bobicki, E.R., Liu, Q., Xu, Z., and Zeng, H. (2012) Carbon capture and storage using alkaline industrial wastes. *Progress in Energy and Combustion Science*, 38(2), 302-320.
- Braithwaite, R.S.W. (1994) Iowaite, a re-investigation. *Mineralogical Magazine*, 58, 79-85.
- Brantley, S.L. (2003) Reaction Kinetics of Primary Rock-forming Minerals under Ambient Conditions. *Treatise on Geochem - weathering rates of minerals*.
- Brindley, G.W. (1945) XLV. The effect of grain or particle Size on x-ray reflections from mixed powders and alloys, considered in relation to the quantitative determination of crystalline substances by x-ray methods. *Philosophical Magazine Series 7*, 36(256), 347-369.

- Catti, M., Ferraris, G., Hull, S., and Pavese, A. (1995) Static Compression and H Disorder in Brucite,  $Mg(OH)_2$ , to 11 Gpa: a Powder Neutron Diffraction Study. *Physics and Chemistry of Minerals*, 22, 200-206.
- Cavani, F., Trifirò, F., and Vaccari, A. (1991) Hydrotalcite-type anionic clays: Preparation, properties and applications. *Catalysis Today*, 11(2), 173-301.
- Chang, E.E., Chen, C.H., Chen, Y.H., Pan, S.Y., and Chiang, P.C. (2011) Performance evaluation for carbonation of steel-making slags in a slurry reactor. *J Hazard Mater*, 186(1), 558-64.
- Cheary, R.W., and Coelho, A. (1992) A fundamental parameters approach to X-ray line-profile fitting. *Journal of Applied Crystallography*, 25(2), 109-121.
- Chung, F.H. (1974) Quantitative Interpretation of X-ray Diffraction Patterns of Mixtures. 1. Matrix-Flushing Method for Quantitative Multicomponent Analysis. *Journal of Applied Crystallography*, 7(6).
- Clark, I.D., and Fritz, P. (1997) *Environmental Isotopes in Hydrogeology*. Taylor & Francis.
- Cleugh, H., Smith, M.S., Battaglia, M., and Graham, P. (2011) *Climate Change Science and Solutions for Australia*. CSIRO Publishing, 150 Oxford Street Collingwood VIC Australia.
- Davies, P.J., and Bubela, B. (1973) The transformation of nesquehonite into hydromagnesite. *Chemical Geology*, 12(4), 289-300.
- Dollase, W. (1986) Correction of intensities for preferred orientation in powder diffractometry: application of the March model. *Journal of Applied Crystallography*, 19(4), 267-272.
- Evans, D.G., and Slade, R.C.T. (2006) Structural Aspects of layered Double Hydroxides. In X. Duan, and D.G. Evans, Eds. *Layered Double Hydroxides*, 119, p. 1-87. Springer.

- Falini, G., Foresti, E., Gazzano, M., Gualtieri, A.F., Leoni, M., Lesci, I.G., and Roveri, N. (2004) Tubular-shaped stoichiometric chrysotile nanocrystals. *Chemistry*, 10(12), 3043-9.
- Fallon, S.J., Fifield, L.K., and Chappell, J.M. (2010) The next chapter in radiocarbon dating at the Australian National University: Status report on the single stage AMS. *Nuclear Instruments and Methods in Physics Research Section B: Beam Interactions with Materials and Atoms*, 268(7), 898-901.
- Gras, A., Beaudoin, G., Molson, J., Plante, B., Bussière, B., Lemieux, J.M., and Dupont, P.P. (2017) Isotopic evidence of passive mineral carbonation in mine wastes from the Dumont Nickel Project (Abitibi, Quebec). *International Journal of Greenhouse Gas Control*, 60, 10-23.
- Gras, A., Beaudoin, G., Molson, J., Plante, B., Bussière, B., Lemieux, J.M., and Kandji, B. (2015) Carbon isotope evidence for passive mineral carbonation of mine wastes from the Dumont Nickel Project (Abitibi, Quebec). 5th International Conference on Accelerated Carbonation for Environmental and Materials Engineering, New York City, USA.
- Graven, H., Allison, C.E., Etheridge, D.M., Hammer, S., Keeling, R.F., Levin, I., Meijer, H.A.J., Rubino, M., Tans, P.P., Trudinger, C.M., Vaughn, B.H., and White, J.W.C. (2017) Compiled records of carbon isotopes in atmospheric CO<sub>2</sub> for historical simulations in CMIP6. *Geoscientific Model Development*, 10, 4405-4417.
- Grguric, B.A. (2003) Minerals of the MKD5 nickel deposit, Mount Keith, Western Australia. *Australian Journal of Mineralogy*, 9(2), 55-71.
- Grguric, B.A., Madsen, I.C., and Pring, A. (2001) Woodallite, a new strontium analogue of iowaite from the Mount Keith nickel deposit, Western Australia. *Mineralogical Magazine*, 65(3), 427-435.

- Gualtieri, A.F. (2000) Accuracy of XRPD QPA using the combined Rietveld-RIR method. *Journal of Applied Crystallography*, 33(2), 267-278.
- Hagedorn, B., and Cartwright, I. (2009) Climatic and lithologic controls on the temporal and spatial variability of CO<sub>2</sub> consumption via chemical weathering: An example from the Australian Victorian Alps. *Chemical Geology*, 260(3), 234-253.
- Hamilton, J.L., Turvey, C.C., Tait, A.W., and Wilson, S.A. (in prep-a) Accelerating mineral carbonation at ultramafic mines via direct CO<sub>2</sub> reaction and heap leaching, and potential for base metal enrichment and recovery. In preparation.
- Hamilton, J.L., Wilson, S.A., Morgan, B., Turvey, C.C., Paterson, D.J., Jowitt, S., McCutcheon, J., and Southam, C. (2018) Fate of transition metals during passive carbonation of ultramafic mine tailings via air capture with potentials for metal resource recovery. *International Journal of Greenhouse Gas Control*, In Press.
- Hamilton, J.L., Wilson, S.A., Morgan, B., Turvey, C.C., Paterson, D.J., MacRae, C., McCutcheon, J., and Southam, G. (2016) Nesquehonite sequesters transition metals and CO<sub>2</sub> during accelerated carbon mineralisation. *International Journal of Greenhouse Gas Control*, 55, 73-81.
- Hamilton, J.L., Wilson, S.A., Turvey, C.C., Tait, A.W., McCutcheon, J., Fallon, S.J., and Southam, G. (in prep-b) Field-based deployment of an automated geochemical treatment system for accelerating carbonation of ultramafic mine tailings: Lessons for pilot projects and carbon accounting in mined landscapes. In preparation.
- Harrison, A.L., Dipple, G.M., Power, I.M., and Mayer, K.U. (2015) Influence of surface passivation and water content on mineral reactions in unsaturated porous media: Implications for brucite carbonation and CO<sub>2</sub> sequestration. *Geochimica et Cosmochimica Acta*, 148, 477-495.

- Harrison, A.L., Dipple, G.M., Power, I.M., and Mayer, K.U. (2016) The impact of evolving mineral–water–gas interfacial areas on mineral–fluid reaction rates in unsaturated porous media. *Chemical Geology*, 421, 65-80.
- Harrison, A.L., Dipple, G.M., Song, W., Power, I.M., Mayer, K.U., Beinlich, A., and Sinton, D. (2017) Changes in mineral reactivity driven by pore fluid mobility in partially wetted porous media. *Chemical Geology*, 463, 1-11.
- Harrison, A.L., Power, I.M., and Dipple, G.M. (2013) Accelerated carbonation of brucite in mine tailings for carbon sequestration. *Environmental Science and Technology*, 47(1), 126-134.
- Hill, R.J., and Howard, C.J. (1987) Quantitative phase analysis from neutron powder diffraction data using the Rietveld method. *Journal of Applied Crystallography*, 20(6), 467-474.
- Hitch, M., Ballantyne, S.M., and Hindle, S.R. (2010) Revaluing mine waste rock for carbon capture and storage. *International Journal of Mining, Reclamation and Environment*, 24(1), 64-79.
- Hostetler, P.B., Coleman, R.G., A., M.F., and Evans, B.W. (1966) Brucite in Alpine Serpentinities. *The American Mineralogist*, 51, 75-98.
- Houghton, J.T., Ding, Y., Griggs, D.J., Noguera, M., van der Linden, P.J., Dai, X., Maskell, K., and Johnson, C.A. (2001) *Climate Change 2001: The Scientific Basis: Contribution of Working Group 1 to the Third Assessment Report of the Intergovernmental Panel on Climate Change*. Cambridge University Press, U.K.
- Hovelmann, J., Putnis, C.V., Ruiz-Agudo, E., and Austrheim, H. (2012) Direct nanoscale observations of CO<sub>2</sub> sequestration during brucite [Mg(OH)<sub>2</sub>] dissolution. *Environ Sci Technol*, 46(9), 5253-60.

- IPCC. (2005) IPCC Special Report on Carbon Dioxide Capture and Storage. In O.D. Bert Metz, Heleen de Coninck, Manuela Loos, Leo Meyer, Ed, p. 442. Cambridge University Press, 40 West 20th Street, New York, NY 10011–4211, USA.
- IPCC. (2013) Climate Change 2013: The Physical Science Basis. In IPCC, Ed. IPCC Working Group 1.
- IPCC. (2014) Climate Change 2014 Mitigation of Climate Change. In IPCC, Ed. IPCC Working Group 3.
- Jambor, J.L. (1969) Coalingite from the Muskox Intrusion, Northwest Territories American Mineralogist, 54, 437-447.
- Johnson, T.M., and Bullen, T.D. (2003) Selenium isotope fractionation during reduction by Fe(II)-Fe(III) hydroxide-sulfate(green rust). *Geochimica et Cosmochimica Acta*, 67(3), 413-419.
- Kump, L.R., Brantley, S.L., and Arthur, M.A. (2000) Chemical Weathering, atmospheric CO<sub>2</sub> and climate. *Annual Review of Earth and Planetary Sciences*, 28, 611-67.
- Lackner, K.S. (2002) Carbonate Chemistry for Sequestering Fossil Carbon. *Annual Review of Energy and the Environment*, 27(1), 193-232.
- Lackner, K.S. (2003) A Guide to CO<sub>2</sub> Sequestration. *Science*, 300, 1677-1678.
- Laughton, C.A., and Green, N. (2002) Woodsreef Magnesium Project An example of sustainable mineral waste processing from mined ore and its utilisation to produce refined metal products. *Green Processing 2002*. New South Wales Department of Mineral Resources, St Leonards, N.S.W., Australia, Cairns, QLD.
- Lechat, K., Lemieux, J.M., Molson, J.W., Beaudoin, G., and Hebert, R. (2016) Field evidence of CO<sub>2</sub> sequestration by mineral carbonation in ultramafic milling wastes, Thetford Mines, Canada. *International Journal of Greenhouse Gas Control*, 47, 110-121.

- Leung, D.Y.C., Caramanna, G., and Maroto-Valer, M.M. (2014) An overview of current status of carbon dioxide capture and storage technologies. *Renewable and Sustainable Energy Reviews*, 39, 426-443.
- March, A. (1932) Mathematische theorie der regelung nach der korn gestalt bei affiner deformation. *Zeitschrift für Kristallographie* 81, 285-297.
- Maslen, E.N., Streltsov, V.A., Streltsova, N.R., and Ishizawa, N. (1994) Synchrotron X-ray study of the electron density in [alpha]-Fe<sub>2</sub>O<sub>3</sub>. *Acta Crystallographica Section B*, 50(4), 435-441.
- Matter, J.M., Stute, M., Snæbjörnsdóttir, S.Ó., Oelkers, E.H., Gislason, S.R., Aradóttir, E.S., Sigfusson, B., Gunnarsson, I., Sigurdardóttir, H., Gunnlaugsson, E., Axelsson, G., Alfredsson, H.A., Wolff-Boenisch, D., Mesfin, K., Taya, D.F.d.l.R., Hall, J., Dideriksen, K., and Broecker, W.S. (2016) Rapid carbon mineralization for permanent disposal of anthropogenic carbon dioxide emissions. *Science*, 352(6291), 1312-1314.
- Mavromatis, V., Bundeleva, I.A., Shirokova, L.S., Millo, C., Pokrovsky, O.S., Bénézeth, P., Ader, M., and Oelkers, E.H. (2015) The continuous re-equilibration of carbon isotope compositions of hydrous Mg carbonates in the presence of cyanobacteria. *Chemical Geology*, 404(Supplement C), 41-51.
- McCutcheon, J., Dipple, G.M., Wilson, S.A., and Southam, G. (2015) Production of magnesium-rich solutions by acid leaching of chrysotile: A precursor to field-scale deployment of microbially enabled carbonate mineral precipitation. *Chemical Geology*, 413, 119-131.
- McCutcheon, J., Turvey, C.C., Hamilton, J.L., Wilson, S.A., and Southam, G. (2017) Experimental Deployment of Microbial Mineral Carbonation at an Asbestos Mine:

- Potential Applications to Carbon Storage and Tailings Stabilization. *Minerals*, 7(191).
- McCutcheon, J., Wilson, S.A., and Southam, G. (2016) Microbially accelerated carbonate mineral precipitation as a strategy for in situ carbon sequestration and rehabilitation of asbestos mine sites. *Environmental Science & Technology*, 50(3), 1419-1427.
- Melchiorre, E.B., Bottrill, R., Huss, G.R., and Lopez, A. (2016) Conditions of Stichtite ( $\text{Mg}_6\text{Cr}_2(\text{OH})_{16}[\text{CO}_3] \cdot 4\text{H}_2\text{O}$ ) formation and its Geochemical and Isotope Record of Early Phanerozoic Serpentinizing Environments. *Geochimica et Cosmochimica Acta*.
- Melchiorre, E.B., Bottrill, R., Huss, G.R., and Lopez, A. (2018) The Early Earth Geochemical and Isotope Record of Serpentinizing Environments from Archean Stichtite ( $\text{Mg}_6\text{Cr}_2(\text{OH})_{16}[\text{CO}_3] \cdot 4\text{H}_2\text{O}$ ). *Precambrian Research*.
- Melchiorre, E.B., Huss, G.R., and Lopez, A. (2014) Carbon and hydrogen stable isotope microanalysis and data correction for rare carbonate minerals: Case studies for stichtite ( $\text{Mg}_6\text{Cr}_2[(\text{OH})_{16}[\text{CO}_3] \cdot \text{H}_2\text{O}]$ ) and malachite ( $\text{Cu}_2\text{CO}_3(\text{OH})_2$ ). *Chemical Geology*, 367, 63-69.
- Mellini, M., and Viti, C. (1994) Crystal structure of lizardite-1T from Elba, Italy. *American Mineralogist*, 79(11-12), 1194-1198.
- Merril, R.J., Butt, B.C., Forrest, V.C., Purdon, G., and Bramley-Moore, R.A. (1980) Asbestos Production at Chrysotile Corporation of Australia Pty. Limited, Barraba, N.S.W. In J.T. Woodcock, Ed. *Mining and Metallurgical Practices in Australasia*, 10, p. 669-673. The Australasian Institute of Mining and Metallurgy, Clunies Ross House, 191 Royal Parade, Parkville, Victoria, Australia 3052.
- Mervine, E., Wilson, S.A., Power, I.M., Dipple, G.M., Turvey, C.C., Hamilton, J.L., Vanderzee, S., Raudsepp, M., Southam, C., Matter, J.M., Kelemen, P.B.,

- Stiefenhofer, J., Miya, Z., and Southam, G. (in review) Carbon Storage Potential of Kimberlite Mine Tailings. *Mineralogy and Petrology*.
- Mills, S.J., Christy, A.G., Génin, J.M.R., Kameda, T., and Colombo, F. (2012) Nomenclature of the hydrotalcite supergroup: natural layered double hydroxides. *Mineralogical Magazine*, 76(5), 1289-1336.
- Mills, S.J., Whitfield, P.S., Wilson, S.A., Woodhouse, J.N., Dipple, G.M., Raudsepp, M., and Francis, C.A. (2011) The crystal structure of stichtite, re-examination of barbertonite, and the nature of polytypism in MgCr hydrotalcites. *American Mineralogist*, 96(1), 179-187.
- Miyata, S. (1983) Anion-exchange properties of hydrotalcite-like compounds. *Clays and Clay Minerals*, 31(4), 305-311.
- Miyata, S., and Okada, A. (1977) Synthesis of Hydrotalcite-like compounds and their physico-chemical properties - the systems  $Mg^{2+}-Al^{3+}-SO_4^{2-}$  and  $Mg^{2+}-Al^{3+}-CrO_4^{2-}$ . *Clays and Clay Minerals*, 25, 14-18.
- Morgan, B., Wilson, S.A., Madsen, I.C., Gozukara, Y.M., and Habsuda, J. (2015) Increased thermal stability of nesquehonite ( $MgCO_3 \cdot 3H_2O$ ) in the presence of humidity and  $CO_2$ : Implications for low temperature  $CO_2$  storage. *International Journal of Greenhouse Gas Control*, 39, 366-376.
- Mumpton, F.A., Jaffe, H.W., and S., T.C. (1965) Coalingite, a new mineral from the New Idria Serpentinite, Fresno and San Benito counties, California. *The American Mineralogist*, 50, 1893-1913.
- Mumpton, F.A., and Thompson, C.S. (1966) The Stability of Brucite in the Weathering Zone of the New Idria Serpentinite. *Clays and Clay Minerals*, 14(1), 249-257.
- O'Hanley, D.S., and Offler, R. (1992) Characterization of multiple serpentinization, Woodsreef New South Wales. *Canadian Mineralogist*, 30, 1113-1126.

- Oelkers, E.H., Gislason, S.R., and Matter, J. (2008) Mineral Carbonation of CO<sub>2</sub>. *Elements*, 4, 333-337.
- Olowe, A. (1995) Crystal structures of pyroaurite and sjoegrenite. *Advances in X-ray Analysis*, 38, 749-755.
- Oskierski, H.C., Dlugogorski, B.Z., and Jacobsen, G. (2013) Sequestration of atmospheric CO<sub>2</sub> in chrysotile mine tailings of the Woodsreef Asbestos Mine, Australia: Quantitative Mineralogy, isotopic fingerprinting and carbonation rates. *Chemical Geology*.
- Pacala, S., and Socolow, R. (2004) Stabilization Wedges: Solving the Climate Problem for the Next 50 Years with Current Technologies. *Science*, 305.
- Pastor-Rodriguez, J., and Taylor, H.F.W. (1971) Crystal structure of coalingite. *Mineralogical Magazine*, 38, 286-294.
- Pawley, G. (1981) Unit-cell refinement from powder diffraction scans. *Journal of Applied Crystallography*, 14(6), 357-361.
- Power, I., McCutcheon, J., Harrison, A., Wilson, S., Dipple, G., Kelly, S., Southam, C., and Southam, G. (2014) Strategizing Carbon-Neutral Mines: A Case for Pilot Projects. *Minerals*, 4(2), 399-436.
- Power, I.M., Dipple, G.M., and Southam, G. (2010) Bioleaching of ultramafic tailings by *Acidithiobacillus* spp. for CO<sub>2</sub> sequestration. *Environmental Science and Technology*, 44(1), 456-462.
- Power, I.M., Harrison, A.L., Dipple, G.M., Wilson, S.A., Kelemen, P.B., Hitch, M., and Southam, G. (2013a) Carbon Mineralization: From Natural Analogues to Engineered Systems. *Reviews in Mineralogy & Geochemistry*, 77, 305-360.
- Power, I.M., Wilson, S.A., and Dipple, G.M. (2013b) Serpentinite Carbonation for CO<sub>2</sub> Sequestration. *Elements*, 9, 115-121.

- Power, I.M., Wilson, S.A., Small, D.P., Dipple, G.M., Wan, W., and Southam, G. (2011) Microbially mediated mineral carbonation: roles of phototrophy and heterotrophy. *Environ Sci Technol*, 45(20), 9061-8.
- Pronost, J., Beaudoin, G., Lemieux, J.M., Hebert, R., Constantin, M., Marcouiller, S., Klein, M., Duchesne, J., Molson, J.W., Larachi, F., and Maldague, X. (2012) CO<sub>2</sub>-depleted warm air venting from chrysotile milling waste (Thetford Mines, Canada): Evidence for in-situ carbon capture from the atmosphere. *Geology*, 40(3), 275-278.
- Pronost, J., Beaudoin, G., Tremblay, J., Larachi, F., Duchesne, J., Hebert, R., and Constantin, M. (2011) Carbon sequestration kinetic and storage capacity of ultramafic mining waste. *Environ Sci Technol*, 45(21), 9413-20.
- Rietveld, H. (1969) A profile refinement method for nuclear and magnetic structures. *Journal of Applied Crystallography*, 2(2), 65-71.
- Scarlett, N.V.Y., and Madsen, I.C. (2006) Quantification of phases with partial or no known crystal structures. *Powder Diffraction*, 21(4), 278-284.
- Schellenger, A.E., and Larese-Casanova, P. (2013) Oxygen isotope indicators of selenate reaction with Fe(II) and Fe(III) hydroxides. *Environ Sci Technol*, 47(12), 6254-62.
- Seifritz, W. (1990) CO<sub>2</sub> disposal by means of silicates *Nature*, 345.
- Stuiver, M., and Polach, H.A. (1977) Reporting of <sup>14</sup>C Data. *Radiocarbon*, 19(3), 355-363.
- Tsukimura, K., Sasaki, S., and Kimizuka, N. (1997) Cation Distributions in Nickel Ferrites. *Japanese Journal of Applied Physics*, 36(6R), 3609.
- Turnbull, J.C., Mikaloff Fletcher, S.E., Ansell, I., Brailsford, G.W., Moss, R.C., Norris, M.W., and Steinkamp, K. (2017) Sixty years of radiocarbon dioxide measurements at Wellington, New Zealand: 1954–2014. *Atmospheric Chemistry and Physics*.

- Turvey, C.C., Hamilton, J.L., and Wilson, S.A. (in review) Comparison of Rietveld analysis methods for quantification of carbon dioxide fixation in ultramafic mine tailings. *American Mineralogist*, In Review.
- Turvey, C.C., Wilson, S.A., Hamilton, J.L., and Southam, G. (2017) Field-based accounting of CO<sub>2</sub> sequestration in ultramafic mine wastes using portable X-ray diffraction. *American Mineralogist*.
- Ulven, O.I., Beinlich, A., Hovelmann, J., Austrheim, H., and Jamtveit, B. (2017) Subarctic physicochemical weathering of serpentinized peridotite. *Earth and Planetary Science letters*, 468, 11-26.
- Wicks, F.J., and Whittaker, E.J.W. (1975) A reappraisal of the structures of the serpentine minerals *Canadian Mineralogist*, 13, 227-243.
- Wilson, S.A., Barker, S.L.L., Dipple, G.M., and Atudorei, V. (2010) Isotopic Disequilibrium during uptake of Atmospheric CO<sub>2</sub> into Mine Process Waters: Implications for CO<sub>2</sub> Sequestration. *Environmental Science & Technology*, 44, 9522-9529.
- Wilson, S.A., Dipple, G.M., Power, I.M., Barker, S.L.L., Fallon, S.J., and Southam, G. (2011) Subarctic Weathering of Mineral Wastes Provides a Sink for Atmospheric CO<sub>2</sub>. *Environmental Science & Technology*, 45(18), 7727-7736.
- Wilson, S.A., Dipple, G.M., Power, I.M., Thom, J.M., Anderson, R.G., Raudsepp, M., Gabites, J.E., and Southam, G. (2009a) Carbon Dioxide Fixation within Mine Wastes of Ultramafic-Hosted Ore Deposits: Examples from the Clinton Creek and Cassiar Chrysotile Deposits, Canada. *Economic geology*, 104, 95–112.
- Wilson, S.A., Harrison, A.L., Dipple, G.M., Power, I.M., Barker, S.L.L., Mayer, K.U., Fallon, S.J., Raudsepp, M., and Southam, G. (2014) Offsetting of CO<sub>2</sub> emissions by air capture in mine tailings at the Mount Keith Nickel mine, Western Australia: Rates,

controls and prospects for carbon neutral mining. *International Journal of Greenhouse Gas Control*, 25, 121-140.

Wilson, S.A., Raudsepp, M., and Dipple, G.M. (2006) Verifying and quantifying carbon fixation in minerals from serpentine-rich mine tailings using the Rietveld method with X-ray powder diffraction data. *American Mineralogist*, 91(8-9), 1331-1341.

Wilson, S.A., Raudsepp, M., and Dipple, G.M. (2009b) Quantifying carbon fixation in trace minerals from processed kimberlite; a comparative study of quantitative methods using X-ray powder diffraction data with applications to the Diavik diamond mine, Northwest Territories, Canada. *Applied Geochemistry*, 24(12), 2312-2331.

Woodhouse, J. (2006) The characterization of hydrotalcite-group minerals and their anion exchange capabilities at mount keith nickel mine, Western Australia. Unpublished masters thesis.

Zarandi, A.E., Larachi, F., Beaudoin, G., Plante, B., and Sciortino, M. (2017) Ambient mineral carbonation of different lithologies of mafic to ultramafic mining wastes/tailings – A comparative study. *International Journal of Greenhouse Gas Control*, 63, 392-400.





## Declaration for Thesis Chapter 5

Declaration by candidate

In the case of Chapter 5, the nature and extent of my contribution is as follows:

<b>Nature of Contribution</b>	<b>Extent of contribution (%)</b>
Concept, conducted fieldwork, experimental design, conducted experiments, collected and analysed data, writing and editing.	60%

The following co-authors contributed to the work. If co-authors are students at Monash University, the extent of their contribution in percentage terms must be stated:

<b>Name</b>	<b>Nature of contribution</b>	<b>Extent of Contribution (%)</b>
Hans C. Oskierski	Supervisory role, field work, assisted with data interpretation and had input into the manuscript	15%
Sasha A. Wilson	Supervisory role, field work, assisted with data interpretation and had input into the manuscript	15%
Vasileios Mavromatis	Sample preparation and data analysis	5%
Jessica L. Hamilton	Fieldwork	3%
Bogdan Dlugogorski	Fieldwork	2%

The undersigned hereby certify that the above declaration correctly reflects the nature and extent of the candidate's and co-authors contributions to this work\*.

Candidate's signature:



Date:

22/03/2018

Main supervisor's signature:



Date: 22/03/2018

\* Note: Where the responsible author is not the candidate's main supervisor, the main supervisor should consult with the responsible author to agree on the respective contributions of the authors.

## Chapter 5

### **Stable magnesium isotope signatures of alteration minerals during carbon mineralisation in ultramafic mineral wastes**

Connor C. Turvey<sup>1\*</sup>, Siobhan A. Wilson<sup>1,2</sup> Vasileios Mavromatis<sup>3,4</sup>, Jessica L. Hamilton<sup>1,5</sup>,  
Bogdan Z. Dlugogorski<sup>6</sup> and Hans C. Oskierski<sup>6</sup>

<sup>1</sup>School of Earth, Atmosphere & Environment, Monash University, Clayton, Melbourne,  
Victoria 3800, Australia

<sup>2</sup>School of Earth and Atmospheric Sciences, University of Alberta, Edmonton, Alberta  
T6G 2E3, Canada

<sup>3</sup>Géosciences Environnement Toulouse (GET), CNRS, UMR 5563, Observatoire Midi-  
Pyrénées, 14 Av. E. Belin, 31400 Toulouse, France

<sup>4</sup>Institute of Applied Geosciences, Graz University of Technology, Rechbauerstraße 12,  
8010 Graz, Austria

<sup>5</sup>School of Earth & Environmental Sciences, The University of Queensland, St Lucia,  
Queensland 4072, Australia

<sup>6</sup>School of Engineering and Information Technology, Murdoch University, Murdoch,  
Western Australia 6150, Australia

In preparation for submission to *Geochimica et Cosmochimica Acta*

## 5.0 Abstract

Stable Mg isotopes undergo significant fractionation during paired mineral dissolution and precipitation reactions at the Earth's surface. This property could make stable Mg isotopes useful tracers of reaction pathways when investigating CO<sub>2</sub> sequestration via carbon mineralisation in natural ultramafic and mafic landscapes and at mines hosted within Mg-rich rocks. Hydrotalcite supergroup minerals are commonly associated with ultramafic rocks and they can make up a significant proportion of both ores and the mineral wastes (tailings) generated by mining. Hydrotalcites undergo anion exchange reactions when exposed to aqueous solutions and they preferentially exchange anions such as sulfate and chloride to take up carbonate; thus they can act as a sink for atmospheric or industrial CO<sub>2</sub> in serpentinites. Hydrotalcites may form *in situ* within mineral wastes via reaction of Fe-bearing brucite with atmospheric CO<sub>2</sub> or they may already have been present as part of the gangue mineralogy of a mine, having formed by hydrothermal alteration of spinel minerals. Here, we test whether stable Mg isotopes can be used to distinguish metamorphic hydrotalcite minerals from secondary (sedimentary) hydrotalcite minerals. Mineral samples were taken from three ultramafic mineral deposits in Australia where one or more Mg-bearing hydrotalcite minerals are known to occur: sedimentary pyroaurite from the Woodsreef chrysotile mine (New South Wales), metamorphic iowaite–pyroaurite and woodallite–stichtite from the Mount Keith nickel mine (Western Australia) and metamorphic stichtite from the Dundas mineral field (Tasmania). Samples of Mg-bearing hydrotalcites, hydromagnesite, serpentine minerals and brucite from these sites were analysed to compare their stable Mg compositions.  $\delta^{25}\text{Mg}$  and  $\delta^{26}\text{Mg}$  values for serpentine minerals from all three localities were found to plot in two distinct regions: (1) with  $\delta^{26}\text{Mg}$  values from -0.28 ‰ to 0.00 ‰, which represents the bulk Mg content of terrestrial mafic and ultramafic rocks, and (2) with  $\delta^{26}\text{Mg}$  values from 0.00 ‰ to 0.37 ‰, which is enriched

compared to the typical Mg isotope compositions of serpentine minerals. This enriched serpentine signature may be attributed to preferential weathering of  $^{24}\text{Mg}$  from the surfaces of serpentine grains, leaving behind a leached residue that is enriched in  $^{25}\text{Mg}$  and  $^{26}\text{Mg}$ . Hydrotalcites stable Mg isotope composition was dependent on speciation rather than location or formation pathway with  $\delta^{26}\text{Mg}$  values varying between -1.23 ‰ and -0.50 ‰. The similarities between the stable Mg isotope compositions of hydrotalcites that formed via different mechanisms implies that these minerals may continuously exchange Mg with the local environment, a process that could obscure the original high temperature signature of some hydrotalcite minerals.

**Keywords:** stable Mg isotopes, ultramafic rocks, ore deposits, mine wastes, carbon mineralisation, hydrotalcites, serpentine, isotope exchange

## 5.1 Introduction

Magnesium is an important element within geological, hydrological and biological systems (Young and Galy, 2004). It occurs as three stable isotopes,  $^{24}\text{Mg}$ ,  $^{25}\text{Mg}$  and  $^{26}\text{Mg}$ , with relative abundances of 78.99%, 10.00% and 11.01% respectively (Young and Galy, 2004). The use of non-traditional stable isotopes such as those of magnesium is emerging as a powerful tool to trace a variety of Earth surface processes (Beinlich et al., 2014; Gorski and Fantle, 2017; Handler et al., 2009; Johnson et al., 2004; Li et al., 2010; Li et al., 2015; Mavromatis et al., 2014a; Mavromatis et al., 2014b; Opfergelt et al., 2012; Shirokova et al., 2013; Teng, 2017; Teng et al., 2010; Wiederhold, 2015). This is primarily because the stable Mg isotope composition of rocks and minerals has been found to be insensitive to fractionation during high temperature and mantle processes such as crustal anatexis, granite

differentiation, serpentinisation and planetary accretion (Beinlich et al., 2014; Bourdon et al., 2010; Handler et al., 2009; Li et al., 2010; Liu et al., 2010; Yang et al., 2009). Contrastingly, many processes that occur at or near the Earth's surface, such as continental weathering, carbonate formation, soil formation and plant growth, have been shown to cause large fractionations of stable Mg isotope compositions (Black et al., 2008; Bolou-Bi et al., 2010; Opfergelt et al., 2012; Shirokova et al., 2013; Teng et al., 2010; Tipper et al., 2010). Alteration phases that form during silicate rock weathering typically have stable Mg isotope compositions different to those of the original parent material. For instance, carbonate minerals tend to be enriched in isotopically light  $^{24}\text{Mg}$  (Li et al., 2012; Mavromatis et al., 2012) whereas silicate clays and epsomite ( $\text{MgSO}_4 \cdot 7\text{H}_2\text{O}$ ) are commonly enriched in isotopically heavy  $^{25}\text{Mg}$  and  $^{26}\text{Mg}$  compared to the lithologies from which they have formed (Li et al., 2011; Opfergelt et al., 2012; Wimpenny et al., 2014). Stable Mg isotopes therefore have the potential to be used to trace the formation pathways for low temperature alteration phases such as silicate clays, hydrotalcites and carbonates during naturally occurring and accelerated weathering of ultramafic rock.

Stable Mg isotopes are well suited for use as tracers of weathering reactions such as those that occur in ultramafic tailings storage facilities, where the rate of silicate weathering is accelerated due to the increased surface area of the tailings material. The use of stable Mg isotopes in this environment could provide insight into weathering reactions in natural ultramafic landscapes, including the influence sub-seafloor carbonation has upon the Mg isotopic composition of the oceans (Beinlich et al. 2014). Additionally, understanding the geochemical evolution of ultramafic mine tailings is of particular interest for environmental monitoring and tailings management, carbon sequestration through carbon mineralisation reactions and for the potential reuse and re-mining of ultramafic tailings (e.g., Blowes et al., 1991; Graupner et al., 2007; McCutcheon et al., 2015; Wilson et al., 2009a; Wilson et al.,

2014; Wilson et al., 2009b). Stable Mg isotopes could be used to fingerprint which silicate and hydroxide minerals act as sources) of Mg for CO<sub>2</sub> sequestration in Mg-carbonate minerals and hydrotalcite minerals during reaction of ultramafic rocks and mine tailings with atmospheric or industrial CO<sub>2</sub> (after Gras et al., 2017; Hamilton et al., 2018; Lechat et al., 2016; McCutcheon et al., 2017; Oskierski et al., 2013; Wilson et al., 2014, Turvey et al., in prep/Chapter 4) or during injection of industrial CO<sub>2</sub> into ultramafic rocks as proposed by Kelemen and Matter (2008) and carried out in basalt as part of the CarbFix project (e.g., Matter et al., 2016; Snæbjörnsdóttir et al., 2014).

Stable Mg isotopes could be especially useful for differentiating between minerals that can be found as either metamorphic minerals or as alteration phases within ultramafic rocks and the tailings produced by mining ultramafic-hosted orebodies. The members of the hydrotalcite supergroup (as defined by Mills et al., 2012) are layered double hydroxide (LDH) minerals that can form under a variety of environmental conditions including by low-temperature carbonation of Fe-rich brucite (Hostetler et al., 1966; Mumpton et al., 1965; Mumpton and Thompson, 1966; Oskierski et al., 2013; Turvey et al., in prep/Chapter 4), during high-temperature hydrothermal alteration of spinel minerals (Grguric, 2003; Grguric et al., 2001; Melchiorre et al., 2016; Melchiorre et al., 2018) and via direct precipitation from solution, an engineering strategy that is used for removal of aqueous contaminants from polluted water (Douglas et al., 2014; Douglas et al., 2010).

Hydrotalcite minerals are commonly present in ultramafic rocks, including orebodies and tailings material (e.g., Ashwal and Cairncross, 1997; Gras et al., 2017; Grguric, 2003; Grguric et al., 2001; Hudson and Bussell, 1981; Melchiorre et al., 2016; Oskierski et al., 2013; Turvey et al., 2017; Turvey et al., in prep/Chapter 4; Mills et al., 2011, Wilson et al., 2014). They are found as metamorphic minerals in the low-grade disseminated Ni sulphide

deposit at the Mount Keith nickel mine, Western Australia (Grguric, 2003; Grguric et al., 2001; Hudson and Bussell, 1981), and metamorphic hydrotalcites are mined as gemstones from the Dundas mineral field, Tasmania (Bottrill, 2008; Bottrill and Baker, 2008; Melchiorre et al., 2016; Melchiorre et al., 2018). Sedimentary hydrotalcite minerals have formed *in situ* within the mine tailings storage facility at the Woodsreef chrysotile mine, New South Wales, and they are known to be sequestering atmospheric CO<sub>2</sub> (Oskierski et al., 2013; Turvey et al., 2017; Turvey et al., in prep/Chapter 4). The iowaite–pyroaurite [Mg<sub>6</sub>Fe<sup>3+</sup><sub>2</sub>(Cl<sub>2</sub>)(OH)<sub>16</sub>·4H<sub>2</sub>O–Mg<sub>6</sub>Fe<sup>3+</sup><sub>2</sub>(CO<sub>2</sub>)(OH)<sub>16</sub>·4H<sub>2</sub>O] and woodallite–stichtite [Mg<sub>6</sub>Cr<sup>3+</sup><sub>2</sub>(Cl<sub>2</sub>)(OH)<sub>16</sub>·4H<sub>2</sub>O–Mg<sub>6</sub>Cr<sup>3+</sup><sub>2</sub>(CO<sub>2</sub>)(OH)<sub>16</sub>·4H<sub>2</sub>O] series minerals within the ore of the MKD5 nickel deposit at Mount Keith and the stichtite found throughout the Dundas mineral field have formed by the replacement of magnetite and chromite grains during serpentinisation (Bottrill, 2008; Grguric, 2003; Grguric et al., 2001; Melchiorre et al., 2016; Sittinger and Sittinger, 2008). The formation of carbonate-bearing hydrotalcite minerals such as pyroaurite [Mg<sub>6</sub>Fe<sup>3+</sup><sub>2</sub>(CO<sub>3</sub>)(OH)<sub>16</sub>·4H<sub>2</sub>O] and coalingite [Mg<sub>10</sub>Fe<sup>3+</sup><sub>2</sub>(CO<sub>3</sub>)(OH)<sub>24</sub>·2H<sub>2</sub>O] as alteration phases, through the carbonation of Fe-brucite, represents net sequestration of atmospheric CO<sub>2</sub>, and such reactions are known to occur within the tailings material at Woodsreef (Oskierski et al., 2013; Turvey et al., 2017; Turvey et al., in prep/Chapter 4). Additionally, owing to their capacity to exchange interlayer anions (Bish, 1980; Bish and Brindley, 1977; Miyata, 1983) there is potential for Cl-rich hydrotalcites such as iowaite and woodallite to sequester a net amount CO<sub>2</sub> after formation via anion exchange reactions, whereby interlayer Cl<sup>-</sup> is replaced by CO<sub>3</sub><sup>2-</sup> sourced from the local environment (Woodhouse 2006; Mills et al., 2011; Turvey et al., in prep/Chapter 4). Stable Mg isotopes could potentially be used to differentiate between the distinct high- and low-temperature formation pathways for hydrotalcites given that (1) greater fractionations of stable Mg isotopes occurs at low temperature and (2) hydrotalcite minerals formed from

hydrothermal fluids are likely to have similar compositions to other ultramafic minerals found in unweathered serpentinites.

Here, we investigate the stable Mg isotopic signatures of weathered serpentinite rock and mineral wastes with a specific focus on metamorphic and sedimentary hydrotalcite minerals and serpentine minerals. Hydrotalcites have the capacity to store CO<sub>2</sub> as part of the natural carbon cycle and during enhanced carbonation in mine tailings (Mills et al., 2011; Turvey et al., in prep/Chapter 4). By comparing the stable Mg isotopic compositions of Mg-bearing hydrotalcites, silicates, carbonates and hydroxides from the Dundas mineral field, Woodsreef chrysotile mine and Mount Keith nickel mine we aim to trace mobility of Mg during carbon mineralisation in ultramafic rocks and, more specifically, to investigate the stable Mg isotopic composition of hydrotalcites, which have not previously been reported, although hydrotalcite are common in ultramafic rocks. The ability of hydrotalcites to undergo anion exchange leads to changes in their stable C isotopic compositions and radiocarbon signatures due to constant re-equilibration with the local environment (Turvey et al., in prep/Chapter 4), similar to what is seen for hydrated Mg-carbonates (Mavromatis et al., 2015). Stable Mg isotope compositions offer a tracer that is potentially resistant to re-equilibration of minerals with solution over time as Mg is held in hydroxide layers within the hydrotalcite structure rather than within the easily exchangeable interlayer spaces. However, dynamic re-equilibration of stable Mg isotopes has recently been observed for the hydrated Mg-carbonate mineral, hydromagnesite (Oelkers et al., 2018). As a consequence it is also important to investigate the stable Mg isotopic compositions of hydrotalcites that have formed via both high- and low-temperature pathways to determine whether these minerals are also susceptible to Mg exchange at ambient conditions.

## 5.2 Field sites

### 5.2.1 The Woodsreef chrysotile mine

The Woodsreef chrysotile mine is located 80 km N of Tamworth in New South Wales, Australia (Figure 5.1a-b). The Woodsreef serpentinite is part of the Great Serpentinite Belt and contains partially serpentinised harzburgite, as well as massive and schistose serpentinite bodies (Glen and Butt, 1981). The massive serpentinite ore body is formed via the replacement of forsterite and pyroxenes by magnetite, brucite and the serpentine polymorphs, lizardite and chrysotile, (Glen and Butt, 1981; O'Hanley and Offler, 1992; Oskierski et al., 2013). The Woodsreef mine produced 550,000 t of long fibre chrysotile during its operational lifetime (from 1972 to 1983) as well as 24 Mt of tailings and 75 Mt of waste rock making it Australia's largest tonnage chrysotile mine (Merril et al., 1980). The tailings material at Woodsreef is finely pulverised, reactive, and has been relatively undisturbed for the past 35 years, making Woodsreef an ideal location in which to study weathering and carbonation of ultramafic rock. Consequently, the tailings storage facility at Woodsreef has been the subject of a number of studies into passive and accelerated carbon mineralisation for CO<sub>2</sub> sequestration (Hamilton et al., in prep; Hamilton et al., 2018; McCutcheon et al., 2017; McCutcheon et al., 2016; Oskierski et al., 2013; Oskierski et al., 2016; Turvey et al., in review/Chapter 3; Turvey et al., 2017; Turvey et al., in prep/Chapter 4). Previous work includes baseline studies of CO<sub>2</sub> and transition metal sequestration during carbon reactions (Hamilton et al., 2018; Oskierski et al., 2013; Turvey et al., 2017; Turvey et al., in prep/Chapter 4), estimations of the rates of CO<sub>2</sub> sequestration at Woodsreef (Oskierski et al., 2013; Turvey et al., in prep/Chapter 4), and 1-m<sup>3</sup> scale experiments for enhanced mineral reactivity and carbon uptake into tailings (Hamilton et al., in prep; McCutcheon et al., 2017; McCutcheon et al., 2016). Previous studies have also used stable C and O isotopes, and radiocarbon to trace the incorporation of atmospheric CO<sub>2</sub> into low-temperature carbonate alteration minerals at Woodsreef (Oskierski et al., 2013; Oskierski et al., 2016; Turvey et al.,

in prep/Chapter 4). The hydrotalcite minerals, pyroaurite and coalingite are common at abundances of up to 13.2 wt% and 5.8 wt%, respectively, in the upper 120 cm of the tailings storage facility at Woodsreef (Turvey et al., in prep/Chapter 4). Stable and radiogenic isotope results, quantitative X-ray diffraction data, and textural evidence from electron microscopy indicate that the coalingite and pyroaurite at Woodsreef form by carbonation of Fe-rich brucite during reaction with atmospheric CO<sub>2</sub> (Oskierski et al., 2013; Turvey et al., in prep/Chapter 4).

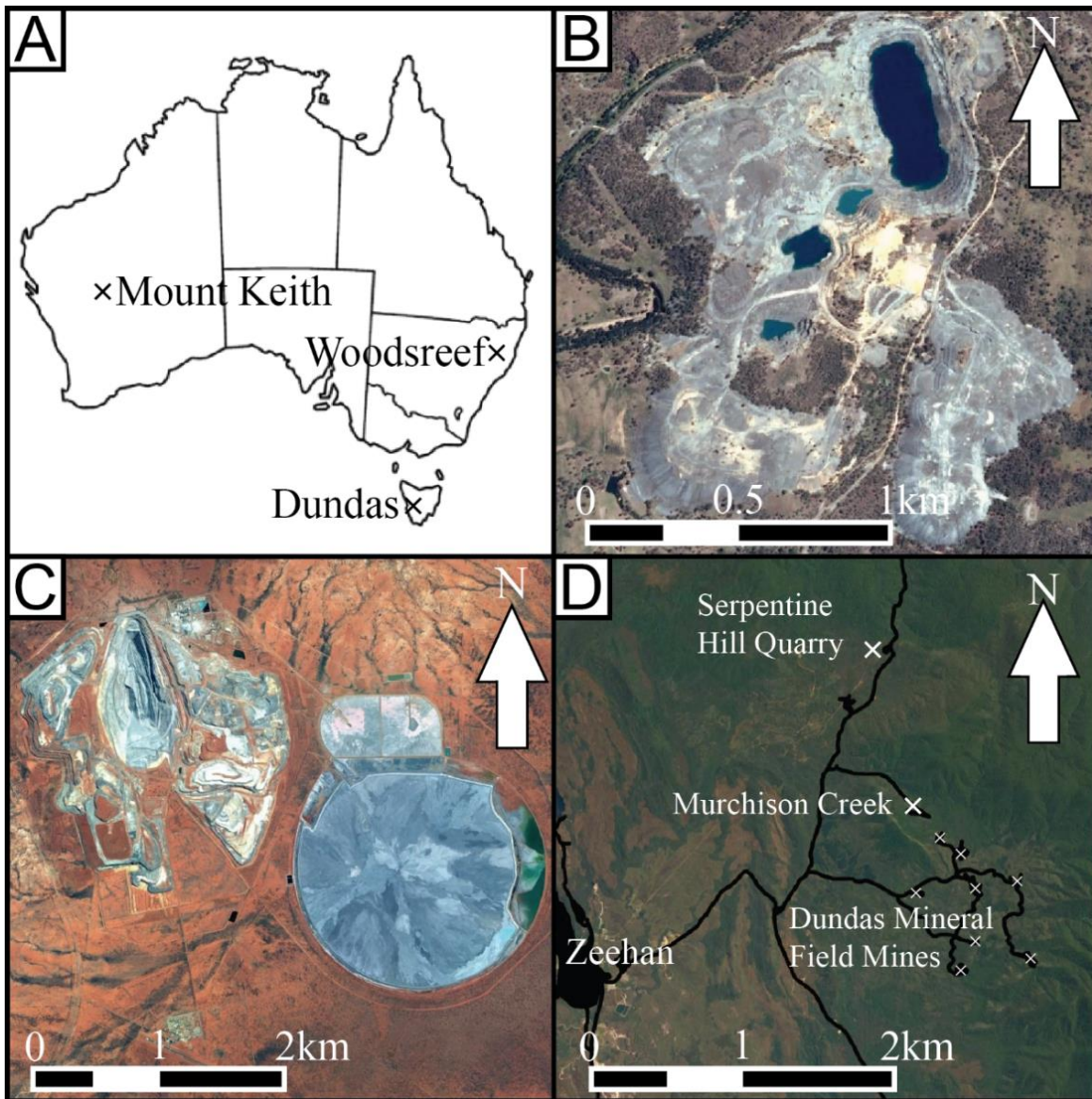


**Figure 5.1** (a) Map of Australia showing the locations of the Woodsreef chrysotile mine, Mount Keith nickel mine and Dundas mineral field. Aerial photographs of (b) the Woodsreef chrysotile mine, (c) the Mount Keith nickel mine and (d) the Dundas mineral field, highlighting the sampling locations.

### 5.2.2 The Mount Keith nickel mine

The Mount Keith nickel mine is an active mine site that is located 90 km NE of Leinster in the Goldfields district of Western Australia (Figure 5.1a, 5.1c). The Mount Keith mine is the largest nickel mine in Australia, producing an estimated 11 Mt of low-grade ore, and a comparable mass of tailings each year and emitting 370,000 t/year of CO<sub>2</sub> equivalent greenhouse gases (BHP, 2005; Grguric, 2003; Wilson et al., 2014). It has been estimated

that up to 20 wt.% of the ore at Mount Keith consists of hydrotalcite group minerals (Grguric et al., 2001). The metamorphic hydrotalcite group minerals at Mount Keith fall along the woodallite–stichtite and iowaite–pyroaurite solid solutions (Grguric, 2003). Woodallite–stichtite formed by replacement of chromite and iowaite–pyroaurite formed by replacement of magnetite and carbonation of ferroan brucite (Grguric, 2003; Grguric et al., 2001). These minerals are found in ore, coarse-grained waste rock and finely-pulverised tailings material. During mineral processing and tailings storage, it is likely that some of the pyroaurite is generated from decomposition of Mountkeithite  $[\text{Mg}_{11}\text{Fe}^{3+}_3(\text{SO}_4)_{3.5}(\text{OH})_{24}\cdot 11\text{H}_2\text{O}]$ , which is known to exchange loosely-bound  $\text{SO}_4^{2-}$  for  $\text{CO}_3^{2-}$  to form pyroaurite (Hudson and Bussell, 1981).

Mount Keith has also been the subject of field- and laboratory-based carbon mineralisation studies (Bea et al., 2012; Harrison et al., 2013; Mills et al., 2011; Wilson et al., 2010; Wilson et al., 2014). It has been estimated that the carbonation of brucite at Mount Keith currently offsets 39,800 t/yr, or 11%, of the mine’s annual  $\text{CO}_2$  equivalent ( $\text{CO}_2\text{e}$ ) greenhouse gas emissions (Wilson et al., 2014). Accelerating the rate of brucite carbonation using simple changes to tailings management practices has the potential to sequester up to 60% of Mount Keith’s annual greenhouse gas emissions (Wilson et al., 2014). Exchange of interlayer  $\text{Cl}^-$  in iowaite for  $\text{CO}_3^{2-}$  to produce pyroaurite may also be fixing an additional 40,000 t/yr of  $\text{CO}_2$  at Mount Keith (Mills et al., 2011); however, this has not been assessed in the field and the reaction is unlikely to go to completion given the limited ingress of atmospheric  $\text{CO}_2$  into the deep (<50 cm) tailings (Wilson et al., 2014). The gangue hydrotalcites at Mount Keith have the capacity to sequester atmospheric  $\text{CO}_2$  via anion exchange from  $\text{Cl}^-$  or  $\text{SO}_4^{2-}$  bearing hydrotalcites to  $\text{CO}_3^{2-}$  bearing hydrotalcites. It is also likely that gangue hydrotalcites that originally contained carbonate continuously re-equilibrate with dissolved inorganic carbonate (DIC) in tailings pore water (Turvey et al, in prep/Chapter 4), a recycling process

that does not reflect net sequestration of CO<sub>2</sub>. Given that there are multiple possible formation pathways for hydrotalcites at Mount Keith, some of which that do not sequester additional CO<sub>2</sub>, stable Mg isotopes could potentially be used to differentiate between those hydrotalcites that may be forming *in situ* within the tailings (as suggested by Turvey et al., in prep/Chapter 4) from those that were already present as gangue minerals.

### **5.2.3 The Dundas mineral field**

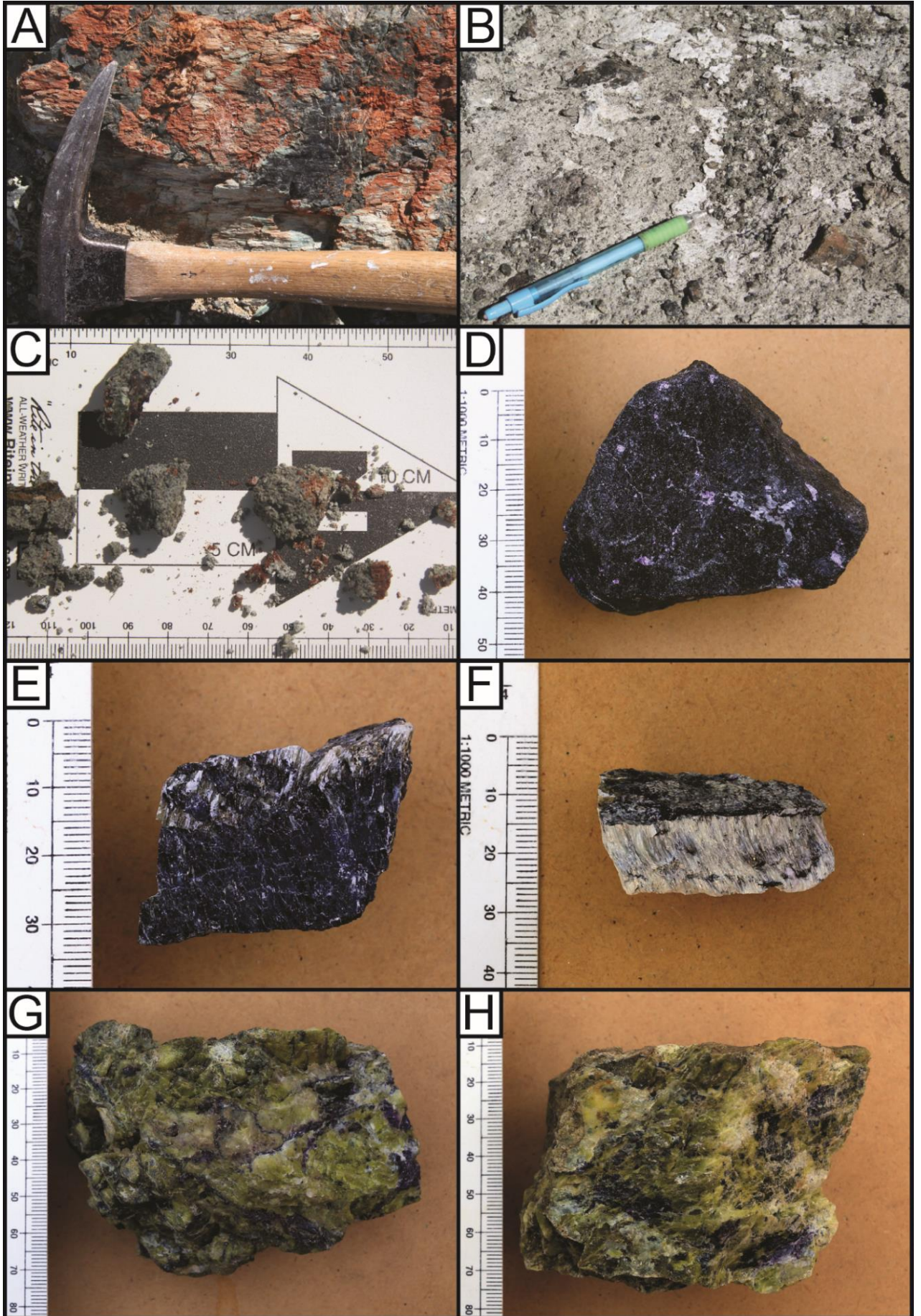
The Dundas mineral field consists of multiple disused historic and currently active mine sites, located approximately 5km E of Zeehan in Tasmania, Australia (Figure 5.1a, 5.1d). Mining of the Dundas mineral field originally began during the 1880s after the discovery of silver–lead deposits; however, over time the focus of these activities shifted onto tin and zinc–lead mining (Reid, 1925). Although the majority of the historic shafts and adits are now abandoned, several small scale mines continue operating throughout the region and the historic mines continue to be of interest to mineralogists and gem collectors for the excellent specimens of crocoite (PbCrO<sub>4</sub>), stichtite and serpentine group minerals that are found throughout the region (Bottrill, 2008; Bottrill and Baker, 2008; Sittinger and Sittinger, 2008). The stichtite and serpentine at Dundas are found within chromium-rich Cambrian serpentinites, with the Adelaide silver–lead mine being the type locality for stichtite. Both stichtite-3R and stichtite-2H (the latter originally called ‘barbertonite’ before it was recognised by Mills et al., 2011 that these are polytypes of the same mineral species) are present in Dundas serpentinite as small blebs, patches and veins that contain relict chromite grains (Ashwal and Cairncross, 1997; Bottrill, 2008; Bottrill and Baker, 2008; Melchiorre et al., 2016). This previously reported textural evidence indicates that the stichtite at Dundas has formed by high temperature alteration and carbonation of chromite (Ashwal and Cairncross, 1997; Bottrill, 2008; Bottrill and Baker, 2008; Melchiorre et al., 2016;

Melchiorre et al., 2018) rather than via low temperature alteration of Cr-brucite. The stichtite sampled from the Dundas mineral field may represent the least altered of the hydrotalcite samples collected in the course of this study as it formed during serpentinisation, whereas the hydrotalcites at Woodsreef are forming *in situ* as sedimentary minerals in the tailings storage facility and those at Mount Keith, although hydrothermal in origin, are likely reacting with atmospheric CO<sub>2</sub> as a consequence of mining and mineral processing.

#### **5.2.4 Sampling details**

Fieldwork at Woodsreef was done over several excursions from 2013 to 2015. Samples were taken from the waste rock, tailings storage facility and mine pits. These include serpentine- and pyroaurite-rich cobbles collected from the waste rock deposits, and samples of the loose tailings and surface cements that cover the surface of the tailings storage facility (Table 5.1, Figure 5.2a-c). Previous studies have determined that these surface cements consist of elevated abundances of hydromagnesite and pyroaurite that have formed *in situ* and are cementing the tailings together to form a solid crust (Oskierski et al., 2013; Turvey et al., 2017; Turvey et al., in prep/Chapter 4). Samples from Mount Keith were acquired from The University of British Columbia/BHP Billiton in 2006 and the South Australian Museum in 2016. These consisted of cobble-sized samples of woodallite–stichtite-rich serpentinite obtained from waste-rock deposits and ore stockpiles (Table 5.2, Figure 5.2d-f). Fieldwork in the Dundas mineral field was conducted in July of 2014. Samples were collected from two sites within the mineral field, the Serpentine Hill quarry and a serpentinite outcrop located off of the Murchison Highway (the ‘Murchison Creek’ site). These samples contained serpentine group minerals, chromite, and stichtite (Table 5.3, Figure 5.2g-h). GPS co-ordinates were not always available for samples obtained from museum or industry contacts as such these data are not provided in Tables 5.1-5.3.

**Figure 5.2** (a) Serpentine waste rock with pyroaurite coating at Woodsreef. (b) Thin, surficial carbonate crust formed on the Woodsreef tailings pile. (c) Serpentine tailings containing visible pyroaurite at Woodsreef. (d) Serpentine wasterock with visible grains of woodallite from the Mount Keith nickel mine. (e) Serpentine cobble with visible intergrown brucite and iowaite collected from the pit at the Mount Keith nickel mine. (f) Intergrown brucite and iowaite vein collected from the pit at the Mount Keith nickel mine. (g-h) Serpentine cobbles with visible stichtite and aragonite collected from Murchison Creek (Dundas, Tasmania).



## **5.3 Analytical methods**

### **5.3.1 Powder X-ray diffraction**

The purity of most samples analysed as part of this study was ensured through careful picking of mineral grains using tweezers under an optical microscope. The composition of all samples was determined via qualitative powder X-ray diffraction (XRD) analysis using an inXitu Terra portable X-ray diffractometer. This instrument uses a Co X-ray tube, which was operated with at 30 kV and 10 mA to collect XRD patterns over an angular range of 5 to 55° 2 $\theta$ , using a total scan time of 20 min per sample.

### **5.3.2 Selective acid extractions**

Ensuring purity through grain picking was impractical for certain samples. For 6 out of the 28 samples a dilute leach using acetic acid was employed to extract Mg from the more soluble carbonate minerals phases, while leaving behind the more recalcitrant serpentine. In such cases, each sample was exposed to an excess of 1 N acetic acid, agitated and then left to react for 1 hour. Acid-leached samples were then centrifuged at 3000 rpm for 5 minutes to separate the remaining solid sample from the aqueous phase. The more soluble fraction of each of these samples consisted of any hydromagnesite, pyroaurite and/or brucite that were present in the original material, whereas the residual material (or residue) consisted of any serpentine, magnetite and/or other more acid-resistant minerals that were not dissolved during exposure to the acetic acid. The soluble fraction that has been dissolved in the acetic acid was then decanted into a Teflon beaker and 0.4 mL of clean concentrated HNO<sub>3</sub> was added to this solution before it was allowed to evaporate at ambient laboratory conditions. Each of these residues was then washed using MilliQ water (> 18.2 M $\Omega$ ·cm) and then left to dry at ambient laboratory conditions.

### 5.3.3 Stable Mg isotope analysis

All samples, including the residual and soluble fractions of acid-leached samples, were digested in concentrated HNO<sub>3</sub> or HF–HNO<sub>3</sub> mixtures and evaporated to dryness. Afterwards, samples were re-diluted in 1 N HNO<sub>3</sub> and ~20 µg of Mg from each sample was placed in a 10 mL Bio-Rad Poly-prep column containing 1 mL AG50W-X12 resin diluted with 1.0 N HNO<sub>3</sub> for chromatic separation of Mg from matrix elements (Mavromatis et al., 2014a). Greater than >99% of the Mg loaded into the columns was recovered. The mass ratio of other cations to Mg extracted from all samples prior to stable isotope analysis was <0.001 as determined by ICP-MS analysis. The stable isotopic composition of the extracted Mg was determined after chromatic separation from the matrix elements. Stable Mg isotopic compositions were measured using a Thermo-Finnigan ‘Neptune’ Multi Collector ICP-MS at Géosciences Environnement Toulouse (GET), France. All solutions were prepared in 0.32 M HNO<sub>3</sub> and introduced into the argon plasma using a standard spray chamber. Solution concentrations were typically ~600 ppb and gave intensities of ~10 V, with total procedural blanks generally having a negligible contribution of <2 mV. Sample–standard bracketing was used to correct for instrumental mass fractionation effects and all data are presented using the δ<sup>x</sup>Mg notation with respect to the DSM-3 reference material where:

$$\delta^x Mg = \left( \frac{\left( \frac{xMg}{^{24}Mg} \right)_{sample}}{\left( \frac{xMg}{^{24}Mg} \right)_{DSM-3}} - 1 \right) \times 1000 \quad \text{Eq. 1}$$

and *x* refers to the mass of the heavy Mg isotope of interest (i.e., <sup>25</sup>Mg or <sup>26</sup>Mg). All samples were run in triplicate with the mean values presented in Tables 5.1–5.3. The reproducibility of δ<sup>26</sup>Mg analyses was assessed by replicate analyses of Mg reference standards and was typically better than 0.07 ‰. Moreover, dolomite standard JDo-1 and Mg standard CAM-1 were identically processed resulting in measured stable Mg isotope compositions that are

similar to those reported elsewhere (e.g., -1.25 ‰  $\delta^{25}\text{Mg}$  and -2.33 ‰  $\delta^{26}\text{Mg}$  for JDo-1 and -1.33 ‰  $\delta^{25}\text{Mg}$  and -2.61 ‰  $\delta^{26}\text{Mg}$  for CAM-1; Mavromatis et al., 2013; Pearce et al., 2012; Wombacher et al., 2009).

## 5.4 Results

All stable Mg isotope data are plotted in  $\delta^{25}\text{Mg}$ – $\delta^{26}\text{Mg}$  space in Figure 5.3. Data for each locality are plotted separately in Figure 5.4–5.6 and results for acid leached samples (both leachates and residues) are shown in Figure 5.7.

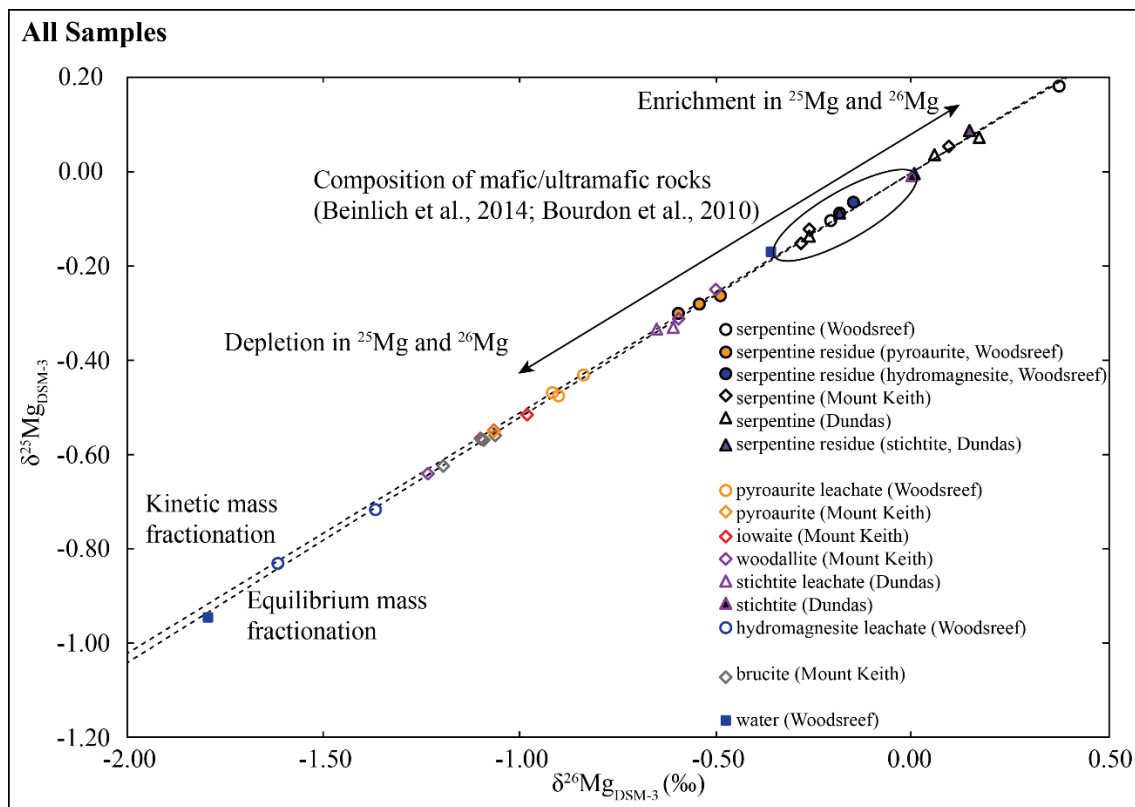


**Figure 5.3**  $\delta^{25}\text{Mg}$ – $\delta^{26}\text{Mg}$  diagram (3-isotope plot) showing the stable Mg isotopic composition of serpentine, brucite, hydrotalcite and carbonate specimens used for this study from the Woodsreef chrysotile mine, the Mount Keith nickel mine and the Dundas mineral field. Samples are differentiated depending on whether the sample was separated by picking or by acid leaching, either in the leachate or the acid leached residue. The typical  $\delta^{25}\text{Mg}$ – $\delta^{26}\text{Mg}$  compositions of mafic and ultramafic rocks (according to Beinlich et al., 2014 and Bourdon et al., 2010) are indicated as a single field. The lines indicate the slopes for equilibrium and kinetic mass dependent fractionation (Young and Galy, 2004).

#### 5.4.1 The Woodsreef chrysotile mine

Two serpentine separates that were picked by hand under a microscope and five acid leached serpentine residuals from Woodsreef have  $\delta^{26}\text{Mg}_{\text{DSM-3}}$  compositions ranging from -0.60 ‰ to 0.37 ‰ (Figures 5.3-4, Table 5.1). These values fall into three sub-groups. Three of the seven samples have the typical composition of serpentine minerals, with  $\delta^{26}\text{Mg}_{\text{DSM-3}}$  values between -0.21 ‰ and -0.15 ‰. These three samples include a pure specimen of serpentine and two acid-leached serpentine residues that remained after dissolution of hydromagnesite from tailings crust samples. These values fall within the expected range for serpentine (as described by Beinlich et al., 2014) and for terrestrial basalts, peridotites and chondrites (as described by Bourdon et al., 2010). This range is depicted as an elliptical field in  $\delta^{25}\text{Mg}$ – $\delta^{26}\text{Mg}$  space in Figure 5.3 and Figure 5.4, and all other plots of stable Mg isotope data in this study. Three acid-leached serpentine residues (for samples that also contained pyroaurite prior to acid treatment) yield  $\delta^{26}\text{Mg}_{\text{DSM-3}}$  values from -0.60 ‰ to -0.49 ‰, which is more depleted in  $^{26}\text{Mg}$  compared to what has previously been reported for serpentine minerals (Beinlich et al., 2014). One hand-picked serpentine sample is significantly enriched in heavy Mg isotopes compared to previously reported serpentine samples, with a  $\delta^{26}\text{Mg}_{\text{DSM-3}}$  value of 0.37 ‰.

Carbonate-bearing minerals at Woodsreef are significantly depleted in  $^{26}\text{Mg}$  compared with the grain-picked and acid-leached residual serpentine samples (Table 5.1, Figure 5.4). The two acid-leached hydromagnesite samples have  $\delta^{26}\text{Mg}_{\text{DSM-3}}$  compositions of -1.62 ‰ and -1.37 ‰. The stable Mg isotope data for the three acid-leached samples of pyroaurite from Woodsreef plot between the values obtained for serpentine and carbonate minerals from Woodsreef, with a composition of  $-0.92 \text{ ‰} \leq \delta^{26}\text{Mg}_{\text{DSM-3}} \leq -0.70 \text{ ‰}$ .

**Table 5.1** Woodsreef chrysotile mine sample descriptions and Mg isotope results

Sample Name	Location	GPS Co-ordinates	Description	Type	serpentine	pyroaurite	magnetite	hydromagnesite	$\delta^{26}\text{Mg}_{\text{DSM-3}}$ (‰)	$2\sigma$ (‰)	$\delta^{25}\text{Mg}_{\text{DSM-3}}$ (‰)	$2\sigma$ (‰)
13WR5-3	pit	56J 0282704 6634395	serpentinite cobble	picked	XX <sup>a</sup>				0.37	0.04	0.18	0.03
Woodsreef Serp	tailings		serpentinite cobble	picked	XX				-0.21	0.02	-0.10	0.04
14WR3-dyp	tailings	56J 0282971 6633560	surface cement	residue	XX		*	X	-0.15	0.05	-0.07	0.04
13WR2-2	tailings	56L 0282995 6633819	surface cement	leachate	XX	*		X	-1.37	0.03	-0.72	0.04
14WR2-10	pit	56J 0282328 6634244	serpentinite cobble with pyroaurite coating	residue	XX	XX	*		-0.19	0.09	-0.09	0.02
14WR2-10 3	pit	56J 0282328 6634244	serpentinite cobble with pyroaurite coating	leachate	XX	XX	*		-1.62	0.03	-0.83	0.00
14WR2-10 4	pit	56J 0282328 6634244	serpentinite cobble with pyroaurite coating	residue	XX	XX			-0.60	0.02	-0.30	0.04
WO-TU <sup>b</sup>	tailings	56J 0282852 6633858	Drip water discharging into tunnel	water	N.A				-0.92	0.06	-0.47	0.05
WO-DS <sup>b</sup>	tailings	56J 0282644 6633663	Creek water emerging downstream of tailings	water	N.A				-0.49	0.01	-0.26	0.00
				leachate					-0.84	0.05	-0.43	0.08
				leachate					-0.54	0.04	-0.28	0.04
				leachate					-0.90	0.05	-0.48	0.04
				water					-1.79	0.02	-0.95	0.02
				water					-0.36	0.04	-0.17	0.02

<sup>a</sup>XX major phase, X minor phase, \* trace phase.

<sup>b</sup>Samples originally described by Oskierski et al. (2013) and reanalysed here for their stable Mg isotope compositions

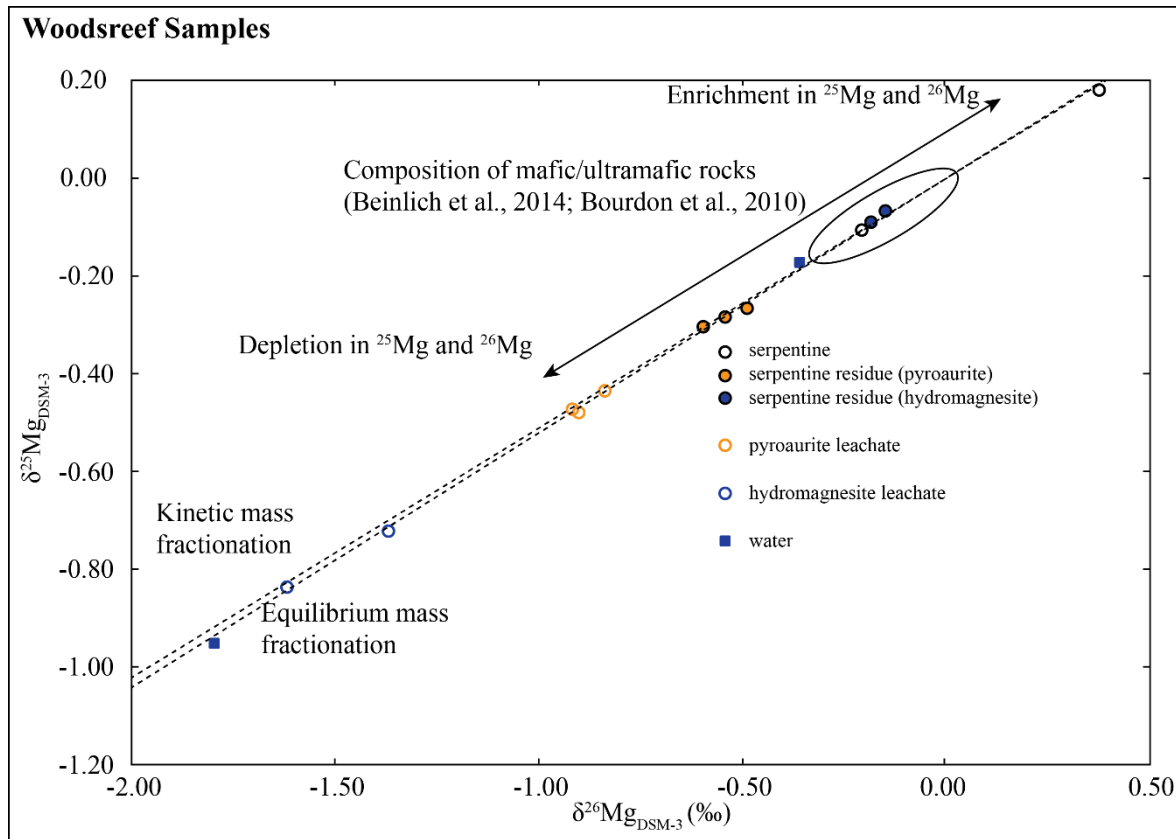


**Figure 5.4**  $\delta^{25}\text{Mg}$ – $\delta^{26}\text{Mg}$  diagram (3-isotope plot) showing the stable Mg isotopic composition of serpentinite, hydrotalcite and carbonate specimens from the Woodsreef chrysotile mine. Samples are differentiated depending on whether the sample was separated by picking or by acid leaching, either in the leachate or the acid leached residue. The typical  $\delta^{25}\text{Mg}$ – $\delta^{26}\text{Mg}$  compositions of mafic and ultramafic rocks (according to

Beinlich et al., 2014 and Bourdon et al., 2010) are indicated as a single field. The lines indicate the slopes for equilibrium and kinetic mass dependent fractionation (Young and Galy, 2004).

## 5.4.2 The Mount Keith nickel mine

The three serpentine samples from Mount Keith have similar  $\delta^{26}\text{Mg}_{\text{DSM-3}}$  compositions to those observed for serpentine minerals at Woodsreef (Table 5.2, Figure 5.3 and Figure 5.5). Two of these samples plot in the serpentine field described by Beinlich et al. (2014) with  $\delta^{26}\text{Mg}_{\text{DSM-3}}$  values of -0.28 ‰ and -0.26 ‰. A third sample is relatively enriched in  $^{26}\text{Mg}$  with a  $\delta^{26}\text{Mg}_{\text{DSM-3}}$  value of 0.09 ‰. The four samples of brucite from Mount Keith are depleted in  $^{26}\text{Mg}$  compared to the samples of serpentine, with  $\delta^{26}\text{Mg}_{\text{DSM-3}}$  values ranging from -1.20 ‰ to -1.06 ‰.

**TABLE 5.2** Mount Keith nickel mine sample descriptions and Mg isotope results

Sample Name	Location	Description	Type	serpentine	brucite	pyroaurite	iowaite	woodallite	$\delta^{26}\text{Mg}_{\text{DSM-3}}$ (‰)	2 $\sigma$ (‰)	$\delta^{25}\text{Mg}_{\text{DSM-3}}$ (‰)	2 $\sigma$ (‰)
MK serpentine 1	mine pit	serpentine cobble	picked	XX*					-0.28	0.07	-0.15	0.05
MK serpentine 2	mine pit	serpentine cobble	picked	XX					-0.26	0.01	-0.12	0.01
06MK55-1	tailings storage facility	serpentine cobble	picked	XX					0.09	0.05	0.05	0.02
MKBrucite1	mine pit	brucite vein	picked		X		*		-1.20	0.01	-0.62	0.01
MKBrucite2	mine pit	brucite vein	picked		X		*		-1.06	0.06	-0.56	0.05
MKBrucite3	mine pit	brucite vein	picked		X		*		-1.09	0.02	-0.57	0.04
MKBrucite4	mine pit	brucite vein	picked		X		*		-1.10	0.04	-0.57	0.04
Grguric Pyro	mine pit	pyroaurite separated from serpentine	picked	*	*	X			-1.07	0.08	-0.55	0.02
Grguric 1998 Iowa	mine pit	iowaite vein material	picked		*	X	XX		-0.98	0.04	-0.52	0.05
04MK Iowaite	mine pit	iowaite vein material	picked				XX		-1.07	0.02	-0.55	0.03
MK iowaite	mine pit	iowaite vein material	picked				XX		-1.10	0.04	-0.57	0.01
MK Unknown	mine pit	woodallite separated from serpentine	picked	*				XX	-1.23	0.02	-0.64	0.02
06MKhtlc-1	mine pit	woodallite separated from serpentine	picked					XX	-0.60	0.07	-0.31	0.02
MK woodallite	Ore stockpile	woodallite separated from serpentine	picked					XX	-0.50	0.03	-0.25	0.03

\*XX major phase, X minor phase, \* trace phase

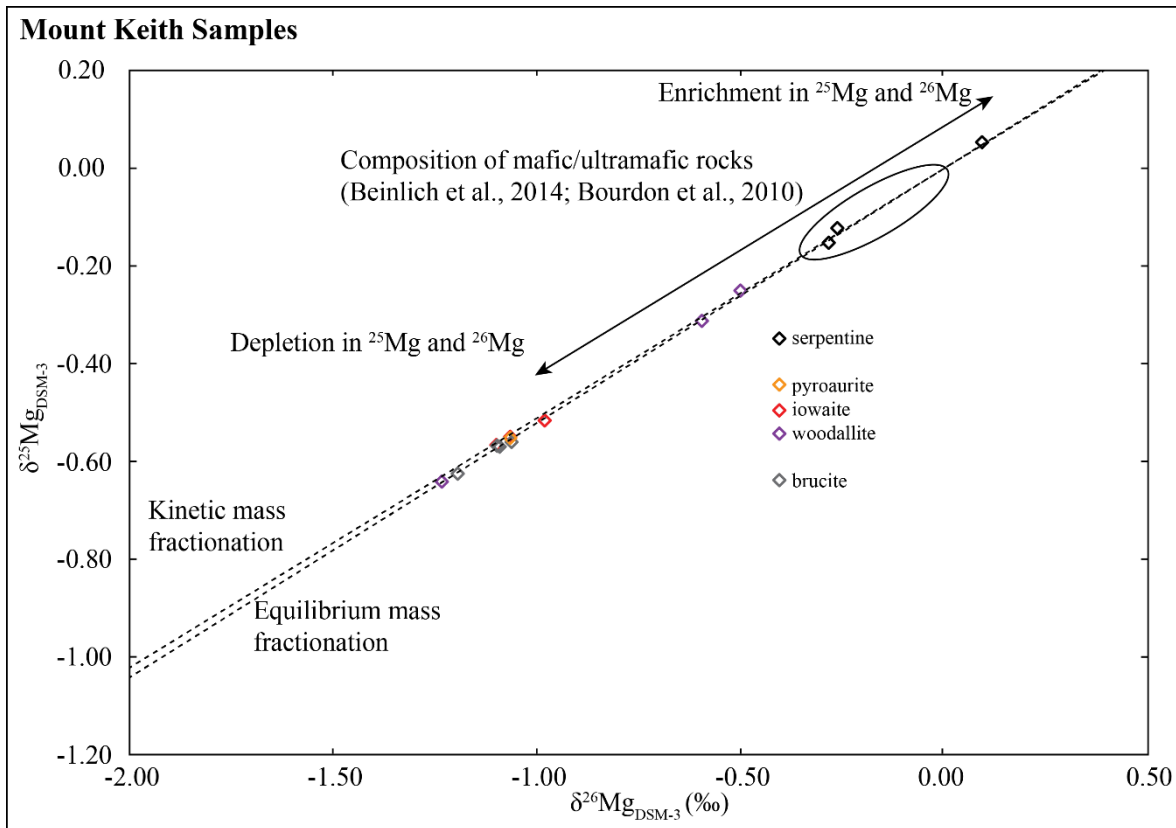


**Figure 5.5**  $\delta^{25}\text{Mg}$ – $\delta^{26}\text{Mg}$  diagram (3-isotope plot) showing the stable Mg isotopic composition of serpentine, brucite and hydrotaalcite specimens from the Mount Keith nickel mine. The typical  $\delta^{25}\text{Mg}$ – $\delta^{26}\text{Mg}$  compositions of mafic and ultramafic rocks (according to Beinlich et al., 2014 and Bourdon et al., 2010) are indicated as a single field. The lines indicate the slopes for equilibrium and kinetic mass dependent fractionation (Young and Galy, 2004).

There is a substantial amount of variation in stable Mg isotope compositions amongst the various hydrotaalcite group minerals found in the waste rock at Mount Keith. The four iowaite–pyroaurite samples are slightly enriched in heavy Mg isotopes compared to the brucite at the site, with  $\delta^{26}\text{Mg}_{\text{DSM-3}}$  values of between -1.10 ‰ and -0.98 ‰ (compared to  $-1.20 \text{ ‰} \leq \delta^{26}\text{Mg}_{\text{DSM-3}} \leq -1.06 \text{ ‰}$  for brucite, Table 5.2, Figure 5.5). Woodallite, the other common hydrotaalcite mineral sourced from Mount Keith, has more  $\delta^{26}\text{Mg}_{\text{DSM-3}}$  enriched values, with two samples plotting between the brucite and serpentine fields at -0.60 ‰ and -0.50 ‰ (Table 5.2, Figure 5.5) whereas a third sample has the most  $^{26}\text{Mg}$ -depleted composition of any sample from Mount Keith with a  $\delta^{26}\text{Mg}_{\text{DSM-3}}$  value of -1.23‰.

### 5.4.3 The Dundas mineral field

The stable Mg isotopic composition of the six serpentine samples from Dundas are similar to those seen at Woodsreef and Mount Keith (Figures 5.3 and 5.6). Three of the six samples plot in the serpentine field of Beinlich et al. (2014) with  $\delta^{26}\text{Mg}_{\text{DSM-3}}$  values from -0.26 ‰ to 0.00 ‰. The remaining three samples are relatively enriched in the heavy isotopes of Mg compared to the serpentine composition described by Beinlich et al. (2014), with  $\delta^{26}\text{Mg}_{\text{DSM-3}}$  values between 0.06 ‰ and 0.17 ‰ (Table 5.3, Figure 5.6). The three stichtite samples from Dundas have highly variable stable Mg isotope compositions, with two of the stichtite samples having similar  $\delta^{26}\text{Mg}_{\text{DSM-3}}$  values to the pyroaurite from Woodsreef and woodallite from Mount Keith with  $\delta^{26}\text{Mg}_{\text{DSM-3}}$  values of -0.65 ‰ and -0.6 ‰ (Figure 5.3); however, one sample plots at the upper limit of the serpentine field at 0.00 ‰ (Table 5.3, Figure 5.6). The latter sample is an acid-leached stichtite, 14MUR1-4 7, which is enriched in  $^{26}\text{Mg}$  compared to other hydrotalcite minerals examined in this study that were picked.

**TABLE 5.3** Dundas mineral field sample descriptions and Mg isotope results

Sample Name	Location	GPS	Description	Type	serpentine	stichtite	$\delta^{26}\text{Mg}_{\text{DSM-3}}$ (‰)		$\delta^{25}\text{Mg}_{\text{DSM-3}}$ (‰)	
								2 $\sigma$ (‰)		2 $\sigma$ (‰)
Dundas serpentine	Purchased from mineral dealer	N/A		picked	XX <sup>a</sup>		0.00	0.07	-0.01	0.05
14SH1-16	Serpentine Hill Quarry	55G 0368187 5367855	chromite bearing serpentinite cobble	picked	XX		-0.26	0.03	-0.14	0.06
14SH1-17 Dark	Serpentine Hill Quarry	55G 0368187 5367855	serpentinite cobble	picked	XX		-0.19	0.00	-0.09	0.00
14MUR1-3	Murchison Creek	55G 0368354 5365098	serpentinite cobble	picked	XX		0.06	0.04	0.04	0.03
14MUR1-9	Murchison Creek	55G 0368354 5365098	serpentinite cobble	picked	XX		0.17	0.02	0.07	0.02
14MUR1-4 7	Murchison Creek	55G 0368354 5365098	grit sized stichtite pieces	residue leachate	XX	*	0.14	0.04	0.09	0.05
Dundas stichtite	Purchased from mineral dealer	N/A		picked	*	XX	-0.65	0.07	-0.33	0.01
14MUR1-4 8	Murchison Creek	55G 0368354 5365098	grit sized stichtite pieces	picked	*	XX	-0.61	0.07	-0.33	0.02

<sup>a</sup>XX major phase, X minor phase, \* trace phase

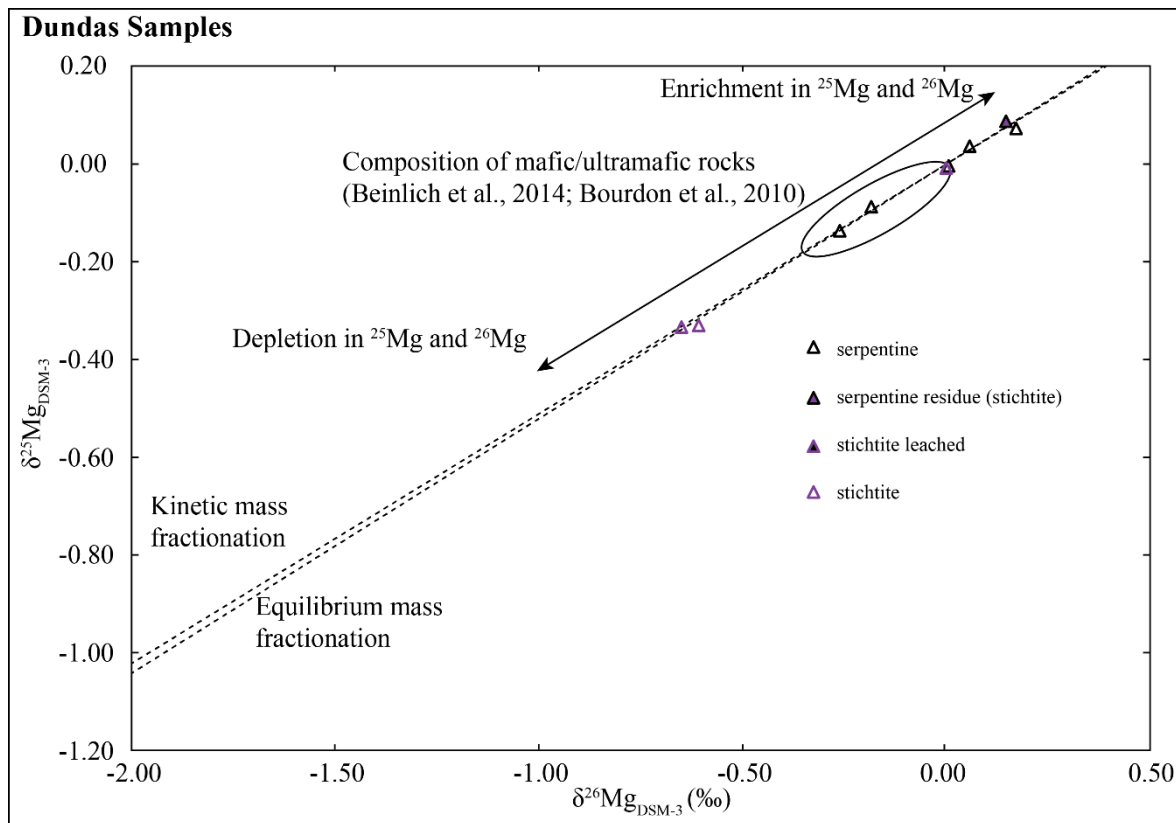


**Figure 5.6**  $\delta^{25}\text{Mg}$ – $\delta^{26}\text{Mg}$  diagram (3-isotope plot) showing the stable Mg isotopic composition of serpentine, and hydrotalcite specimens from the Dundas mineral field. Samples are differentiated depending on whether the sample was separated by picking or by acid leaching, either in the leachate or the acid leached residue. The typical  $\delta^{25}\text{Mg}$ – $\delta^{26}\text{Mg}$  compositions of mafic and ultramafic rocks (according to Beinlich et al., 2014 and Bourdon et al., 2010) are indicated as a single field. The lines indicate the slopes for equilibrium and kinetic mass dependent fractionation (Young and Galy, 2004).

## 5.5 Discussion

### 5.5.1 Stable Mg isotope signatures of serpentine undergoing weathering

The stable Mg isotope composition of the serpentine minerals is broadly consistent across all three field sites with samples of serpentine having compositions that fall into one of two ranges of values as seen in Figures 5.3. The most common  $\delta^{26}\text{Mg}_{\text{DSM-3}}$  values for serpentine were between -0.45 ‰ and 0.00 ‰, a composition that mirrors the findings of Beinlich et al. (2014) who report that the stable Mg isotope compositions of olivine and serpentine fall within the same range of values defined by terrestrial basalts, peridotites and chondrites

(Bourdon et al., 2010; Handler et al., 2009; Teng et al., 2007). Our results reaffirm that natural serpentinisation is a process that does not fractionate stable Mg isotope significantly from their primordial distribution in chondrites (Beinlich et al., 2014).

Several of the serpentine samples analysed from each of the study sites are enriched in  $^{25}\text{Mg}$  and  $^{26}\text{Mg}$  compared to the compositional field for serpentine minerals according to Beinlich et al. (2014), with  $\delta^{26}\text{Mg}_{\text{DSM-3}}$  values of between 0.06 ‰ and 0.37 ‰ (Figures 5.3–5.6). This enrichment in  $^{25}\text{Mg}$  and  $^{26}\text{Mg}$  is typical of talc, shales and sedimentary composite rocks (Beinlich et al., 2014; Li et al., 2010; Tipper et al., 2006) and has not previously been reported for serpentine minerals. This enrichment in heavy Mg isotopes can potentially be explained by the preferential loss of isotopically light, exchangeable  $^{24}\text{Mg}$  via dissolution of serpentine grains during weathering. This interpretation is consistent with the results of Wimpenny et al. (2014) who determined that acid-leaching of Mg from illite, montmorillonite and kaolinite clay produces an isotopically lighter leachate and isotopically heavier residue. They attribute this signature to preferential loss of weakly bound/exchangeable  $^{24}\text{Mg}$  to solution and retention of heavier isotopes of Mg within the octahedral, brucite-like sheets within the structures of clay minerals (Wimpenny et al., 2014). Similarly, Liu et al. (2017) found that weathering of abyssal peridotites and the subsequent formation of authigenic clays can result in the loss of  $^{24}\text{Mg}$  and subsequent enrichment in  $^{25}\text{Mg}$  and  $^{26}\text{Mg}$  of the residual abyssal peridotite. Liu et al. (2017) report  $\delta^{26}\text{Mg}$  values of  $-0.19 \pm 0.07$  ‰ in fresh serpentinised peridotites and values of  $-0.10 \pm 0.12$  ‰ in weathered peridotites. If serpentine mineral dissolution occurs incongruently, with Mg from the surface layers being preferentially dissolved relative to Si, then the isotopically lighter  $^{24}\text{Mg}$  will be released into the leachate while heavier Mg isotopes remain bound in the serpentine during formation of a passivating layer of silica (Rozalen and Huertas, 2013; Wang et al., 2006). The compositions of the isotopically heavy residue and isotopically light leachates, should

therefore depend on the relative amount of Mg leached from the serpentine which will largely be driven by the morphology of the serpentine polymorph that is undergoing dissolution, as chrysotile consists of coiled fibrils, whereas lizardite has an ideal layered topology and antigorite consists of modulated layers (Wicks and Whittaker, 1975).

The  $^{26}\text{Mg}$ -enriched stable isotope signature found in several of the serpentine samples from across all three study sites (Table 5.1–3, Figure 5.3–5.6) could be attributed to natural acid leaching that occurs as part of the weathering processes. Carbon mineralisation at Woodsreef and Mount Keith occurs via the dissolution of brucite and Mg-silicate minerals, in rainwater which contains carbonic acid, thereby providing a mechanism for acid-leaching of alkaline rocks and generation of Mg-rich fluids for carbonation reactions (Hamilton et al., 2018; McCutcheon et al., 2017; Turvey et al., 2017; Wilson et al., 2009a; Wilson et al., 2014). Exposure to carbonic acid and subsequent dissolution of Mg-bearing silicate and hydroxide minerals at Dundas, Mount Keith and Woodsreef can be considered a natural analogue to the laboratory-based acid leaching experiments of Wimpenny et al. (2014). Thus, reaction of mineral wastes and ores with carbonic acid in rainwater could lead to release of the isotopically lighter exchangeable surface  $^{24}\text{Mg}$  being released into solution whilst leaving behind a serpentine residue that is enriched in isotopically heavy Mg. It is likely that this phenomenon is more prominent in samples from this study compared to those from previous studies that have investigated the stable Mg isotopic compositions of serpentinites (e.g., Beinlich et al., 2014; Liu et al., 2017) because the increased surface area and reactivity of the serpentinite mineral wastes should lead to a higher degree of leaching than in undisturbed serpentinite landscapes.

### 5.5.2 Effects of selective acid leaching treatments on stable Mg isotope signatures of serpentinite samples

The findings of Wimpenny et al. (2014), which used multiple acid leaches to release surface-bound and structural Mg from clay minerals, imply that complications may arise from the use of selective acid leaches to analyse the stable Mg isotope compositions of serpentine and various carbonate minerals within a single sample. Several of the samples analysed as part of this study were exposed to dilute acetic acid for a period of 1 hour. This was done with the aim of extracting Mg from the more readily soluble minerals such as hydromagnesite, brucite and pyroaurite while leaving the serpentine unreacted. If we are correct that  $^{24}\text{Mg}$  is preferentially lost from the exposed surfaces of serpentine minerals, there is the possibility that light  $^{24}\text{Mg}$  from the serpentine may become a significant component in the acid leachate, and that it could obscure the true stable Mg isotopic composition of the hydromagnesite and pyroaurite. This is investigated in Figure 5.7, which reports the stable Mg isotope composition of the samples from Woodsreef and Dundas that were acid leached (no samples from Mount Keith were acid-treated). Data for both the leachate and the acid-leached residual are provided. The stable Mg isotopic compositions of leached pyroaurite (from Woodsreef), leached hydromagnesite (from Woodsreef) and leached stichtite (from Dundas) are distinct (Figure 5.7), with pyroaurite from Woodsreef enriched being in  $^{26}\text{Mg}$  ( $-0.92\text{‰} \leq \delta^{26}\text{Mg} \leq -0.84\text{‰}$ , Table 5.1) compared to the hydromagnesite from the same site ( $-1.62\text{‰} \leq \delta^{26}\text{Mg} \leq -1.37\text{‰}$ , Table 5.1). The single acid-leached stichtite sample from Dundas has a  $\delta^{26}\text{Mg}$  value of  $0.00\text{‰}$  (Table 5.3), similar to the composition of serpentine minerals from all three sites (Figure 5.3). The isotopically light values for pyroaurite and hydromagnesite imply that exchangeable Mg from the serpentine is not always a significant contributor to the Mg content of the leachate. If Mg from serpentine was a significant contributor to the

Mg content of the leachate the results from the three different minerals would likely have a more homogeneous signal, closer to the serpentine field of Beinlich et al. (2014).

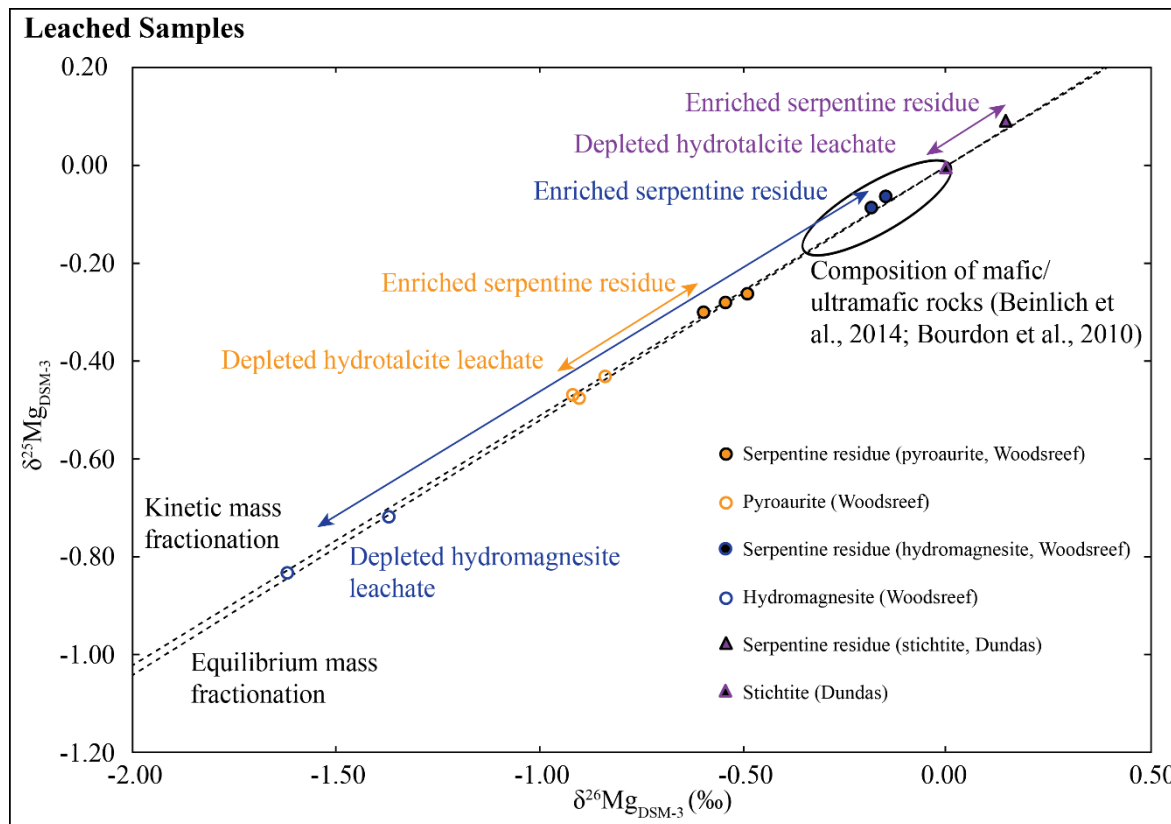


**Figure 5.7**  $\delta^{25}\text{Mg}$ – $\delta^{26}\text{Mg}$  diagram (3-isotope plot) showing the stable Mg isotopic composition of leachate and residue samples from acid leaching. Samples are differentiated depending on whether the sample is from leachate or the acid leached residue. The typical  $\delta^{25}\text{Mg}$ – $\delta^{26}\text{Mg}$  compositions of mafic and ultramafic rocks (according to Beinlich et al., 2014 and Bourdon et al., 2010) are indicated as a single field. The lines indicate the slopes for equilibrium and kinetic mass dependent fractionation (Young and Galy, 2004).

Comparing the  $\delta^{26}\text{Mg}$  values of hydrotalcite minerals that were purified via picking with the  $\delta^{26}\text{Mg}$  values of hydrotalcite leachate samples indicates that the leach has been successful. Figure 5.3 shows that leached pyroaurite from Woodsreef has a similar composition to the picked samples of pyroaurite, iowaite and brucite sourced from Mount Keith, implying that the leach is successfully sampling the pyroaurite from Woodsreef. This is encouraging as it implies that a dilute acid leach can be an effective way to separate soluble phases such as

hydromagnesite and pyroaurite for stable Mg isotope analysis. However the leached sample of stichtite from Dundas is drastically enriched compared to picked samples of stichtite from Dundas, and compared to any other hydrotalcite sample from this study (Figure 5.3 and Figure 5.6), indicating that it may be influenced by addition of Mg from the serpentine residual. For 5 out of the 6 samples the success of the other acid leaches implies that this value may also be correct and the enriched signature may be due to a contribution of Mg from the serpentine residue releasing Mg into solution.

When considering the  $\delta^{26}\text{Mg}$  results for the residual serpentine fractions however, it appears that the acetic acid leach was not completely effective at removing all of the reactive phases. Residual separates appear to have a variable stable Mg isotopic composition, ranging from -0.15 ‰ [well within the serpentine field of Beinlich et al. (2014)] to -0.60 ‰ which is significantly lighter than the serpentine field and approaching values of the pyroaurite samples (Figure 5.7). This variable composition can be attributed to an incomplete leach of hydromagnesite and pyroaurite from some samples, leaving the residual sample with an isotopically lighter composition compared to picked serpentine samples (Figure 5.3). A longer acid leach could potentially be used to overcome incomplete dissolution of carbonate-bearing minerals; however, this then has the potential to leach more exchangeable Mg from the serpentine into solution. This means acid leaching may not be the most ideal separation technique when using stable Mg isotopes as the choice may be between (1) a short leach that gives reasonable  $\delta^{26}\text{Mg}$  values for the leachate but artificially isotopically light residuals or (2) a longer leach that more accurately reflects the  $\delta^{26}\text{Mg}$  values of serpentine but leads to light exchangeable Mg from the serpentine entering the leachate alongside all the Mg from the hydromagnesite or pyroaurite. The time difference between the 'short' and 'long' leach would likely depend on the mass balance of Mg and how much Mg is held in soluble carbonate minerals compared to less soluble serpentine minerals. Determining the time

length would require calibration of experimental acid leaching methods by leaching a given sample for multiple lengths of time and comparing the relative stable Mg isotope compositions of the leachate and leached residue samples.

### 5.5.3 Stable Mg isotope signature of hydrotalcites

Results from Oskierski et al. (2013) and Turvey et al. (in prep)/Chapter 4 indicate that the pyroaurite present in the tailings material at Woodsreef is forming *in situ* by carbonation of Fe-bearing brucite. If this is the case, then the stable Mg isotopic composition of Woodsreef pyroaurite should be fractionating away from the serpentine in a predictable manner. The fractionation between stable Mg isotopes in solution and in minerals is largely dependent on the relative Mg–O bond lengths between aqueous Mg species and the mineral, with shorter bonds being enriched in heavy isotopes of Mg and longer bonds being enriched in lighter isotopes of Mg (Li et al., 2014). This has been demonstrated for serpentine (Wimpenny et al., 2010), epsomite (Li et al., 2011) and brucite (Li et al., 2014).

For the pyroaurite at Woodsreef, which is forming *in situ* within the tailings by carbonation of brucite, the findings of Li et al. (2014) would predict that pyroaurite should be enriched in heavy stable Mg isotopes compared to the solution from which it is forming {a bond length of 2.06 Å in pyroaurite compared to 2.08 Å in the aqueous Mg ion  $[\text{Mg}(\text{OH}_2)_6]^{2+}$ }. Samples of tailings pore water and pure samples of brucite from Woodsreef would be required to properly examine the stable Mg isotope results for the pyroaurite from Woodsreef. However, no samples of the tailings pore water could be extracted during our field campaigns and manual separation of pure brucite from pyroaurite and serpentine was not achievable for samples from Woodsreef. Two water samples from Woodsreef were previously collected for analysis by Oskierski et al. (2013) and these were reanalysed for their stable Mg isotope composition here. These samples have radically different stable Mg

isotope compositions, WO-DS was taken from a waterway downstream of the tailings storage facility and has a  $\delta^{26}\text{Mg}$  value of -0.36 ‰, whereas WO-TU was collected from an outflow pipe within the tailings and has a  $\delta^{26}\text{Mg}$  value of -1.79 ‰ (Table 5.1). The stable Mg isotope composition results of the pyroaurite leachate is enriched in heavy Mg isotopes compared to sample WO-TU but are depleted in heavy Mg isotopes compared to WO-DS (Figure 5.4). The cationic and anionic composition of WO-TU has been attributed to the dissolution of brucite within the tailings rather than dissolution of the bulk tailings material overall (Oskierski et al., 2016). This potentially explains the compositional differences between WO-TU and WO-DS, with WO-DS representing waters interacting with the bulk tailings and the surrounding local environment rather than being entirely dominated by interactions with brucite, which is highly reactive and more easily carbonated than serpentine minerals. If WO-TU represents waters dominated by brucite dissolution then it is likely interacting with pyroaurite in the tailings, hence the relative enrichment in heavy Mg isotopes in the pyroaurite samples compared to WO-TU (Figure 5.3–5.4).

A similar Mg fractionation trend is found in the samples from Mount Keith. No water samples were collected from the tailings, mine pit or ore stockpiles at Mount Keith. However, fractionation of stable Mg isotopes between samples of brucite and the various hydrotalcites found at the site can be observed (Table 5.2, Figure 5.5). Brucite is closely related to hydrotalcites, as it bears a similar structure and can form hydrotalcites through dissolution and precipitation under carbon limited conditions (Turvey et al., in prep/Chapter 4). As such the stable Mg isotope composition of hydrotalcites at some mine sites is likely related to the stable Mg composition of the brucite from which it forms. Brucite samples from Mount Keith typically have a lighter stable Mg isotope composition compared to hydrotalcite minerals from the same locality (Figure 5.5). The brucite samples have a  $\delta^{26}\text{Mg}_{\text{DSM-3}}$  composition of between -1.20 and -1.06 ‰, whereas iowaite–pyroaurite samples are slightly

enriched with  $\delta^{26}\text{Mg}_{\text{DSM-3}}$  values of between -1.10 ‰ and -0.98 ‰ (Table 5.2). Woodallite samples from Mount Keith are even more enriched in heavy stable Mg isotopes compared to the brucite, with a composition of between -0.60 ‰ and -0.50 ‰ (with one anomalous sample with a  $\delta^{26}\text{Mg}_{\text{DSM-3}}$  value of -1.23 ‰, Table 5.2). The relative compositions of the brucite and hydrotalcite minerals at Mount Keith are consistent with the model of Li et al. (2014) as brucite has the longest Mg–O bond at 2.09–2.10 Å while pyroaurite has a shorter bond length of 2.06 Å and stichtite has the shortest Mg–O bonds (2.01 Å) of the non-serpentine minerals analysed from Mount Keith (Allman, 1968; Mills et al., 2011). Pyroaurite and stichtite are the carbonate-bearing end members of the pyroaurite–iowaite and stichtite–woodallite solid solution series, and as such they likely provide good approximations for the Mg–O bond lengths of iowaite and woodallite. This predictable fractionation between the stable Mg isotope compositions of brucite and the various hydrotalcite minerals from Mount Keith supports a relationship between the two minerals (Figure 5.5). Furthermore there appears to be a similar relationship when comparing the stable Mg isotope composition of brucite from Mount Keith to the stable Mg isotope compositions of hydrotalcites from Woodsreef and Dundas, with the hydrotalcites from these other sites enriched compared to the brucite from Mount Keith, similar to the hydrotalcite minerals from Mount Keith (Figure 5.3). This would imply that the hydrotalcites from these sites are forming from similar brucite derived Mg pools as the hydrotalcites at Mount Keith.

#### **5.5.4 Tracing serpentinite weathering and carbonation using stable Mg isotopes**

The ultramafic rocks at Woodsreef, Mount Keith and Dundas have undergone serpentinisation and have been affected by modern weathering processes to varying degrees that have affected the stable Mg isotope compositions of both primary and alteration

minerals. Because stable Mg isotopes are largely unfractionated by high temperature processes such as serpentinisation, but undergo significant fractionation when affected by low temperature processes, such as carbonation and weathering, the bulk stable Mg isotope composition of the rocks from the three sites is likely to be similar, however the compositions of individual phases that are undergoing weathering to various degrees or are precipitating during carbonation have the potential to be significantly different, due to changing solution chemistries or different formation pathways. The stable Mg isotope compositions of serpentine minerals are similar for Woodsreef, Mount Keith and Dundas (Figure 5.3), 11 out of the 16 samples of serpentine from Woodsreef, Mount Keith and Dundas have typical  $\delta^{26}\text{Mg}$  values that are in-keeping with the results of Beinlich et al. (2014) (Tables 5.1–5.3), and 5 out of 16 are enriched in heavy stable Mg isotopes, most likely due to loss of  $^{24}\text{Mg}$  through weathering processes (Tables 5.1–5.3). The similar stable Mg isotope compositions for serpentine from Woodsreef, Mount Keith and Dundas occur as the serpentine minerals from all three sites have a similar starting composition (the stable Mg composition shared by basalts, peridotites and chondrites, Bourdon et al., 2010) and have then undergone similar processes, with the stable Mg isotope compositions being unfractionated during serpentinisation (Beinlich et al., 2014) and then slightly enriched during the weathering of exposed serpentine at the Earth's surface. The samples of brucite from Mount Keith are enriched in  $^{24}\text{Mg}$  compared to the serpentine samples from Mount Keith (Table 5.2, Figure 5.5), indicating that even though it formed during the same serpentinisation process as the serpentine (Grguric, 2003) it has a distinct stable Mg composition, driven by the preference for  $^{24}\text{Mg}$  due to the length of the Mg–O bond in brucite.

Unlike the serpentine minerals, the hydrotalcites from the three sites have different formation pathways, with the pyroaurite from Woodsreef forming from dissolution and replacement of brucite during carbonation (Oskierski et al., 2013; Turvey et al., 2017; Turvey et al., in

prep/Chapter 4) and the hydrotalcite minerals from Mount Keith and Dundas forming via hydrothermal alteration of magnetite and chromite during serpentinisation (Bottrill, 2008; Bottrill and Baker, 2008; Grguric, 2003; Grguric et al., 2001; Melchiorre et al., 2016). This could potentially lead to pyroaurite from Woodsreef having a different stable Mg composition than hydrotalcites from Mount Keith and Dundas, as the Mg source for pyroaurite from Woodsreef is dissolving brucite while the Mg source for hydrotalcites from Dundas and Mount Keith was serpentinising magnetite and chromite. However what is observed in Figure 5.3 is that the stable Mg isotope composition of hydrotalcites are highly variable and appear to be determined by mineral species, not by formation pathway. The hydrotalcite minerals appear as three main clusters (Figure 5.3), the most depleted of which are all the samples of pyroaurite, iowaite and one of the three woodallite samples from Mount Keith, and the pyroaurite from Woodsreef. These samples occupy a  $\delta^{26}\text{Mg}_{\text{DSM-3}}$  range from -1.23 ‰ to -0.84 ‰ (a range of values that also incorporates the stable Mg composition of samples of brucite from Mount Keith, Table 5.1–5.2). The second cluster (Figure 5.3) consists of the 2 picked stichtite samples from Dundas and 2 of the 3 samples of Woodallite from Mount Keith, these hydrotalcites have  $\delta^{26}\text{Mg}_{\text{DSM-3}}$  values between -0.65 ‰ and -0.50 ‰ (Table 5.2–5.3). The hydrotalcite mineral with the most enriched stable Mg isotope composition was the acid leachate-derived stichtite sample from Dundas which has a  $\delta^{26}\text{Mg}_{\text{DSM-3}}$  value of 0.00 ‰ (Table 5.3), this  $^{26}\text{Mg}$  enriched signature likely occurs as a result of dissolution of serpentine during the acid leaching procedure that was used for this sample. Similarities between the stable Mg isotope composition of the woodallite from Mount Keith and the stichtite from Dundas (the second cluster, Figure 5.3) is expected as they are both derived from the alteration of chromite during the two serpentinisation events that formed the serpentinite at Mount Keith and Dundas respectively (Grguric, 2003; Grguric et al., 2001; Melchiorre et al., 2014). However the similarities between the iowaite–pyroaurite samples

from Mount Keith and the pyroaurite from Woodsreef is more surprising, given that the iowaite–pyroaurite from Mount Keith has formed from high temperature alteration of magnetite during serpentinisation (Grguric, 2001) and the pyroaurite from Woodsreef has formed from low temperature carbonation of brucite under carbon limited conditions (Turvey et al., in prep/Chapter 4). There are multiple possible explanations to the similarities between the iowaite–pyroaurite from Mount Keith and the pyroaurite from Woodsreef; either (1) the magnetite from which the minerals at Mount Keith are forming has a similar Mg composition to that of the brucite from Woodsreef, resulting in a fluid with a similar stable Mg composition to that of the brucite; (2) the dissolution and carbonation of brucite is a larger contributor to the formation of hydrotalcites at Mount Keith than has been previously indicated (Grguric, 2003); or (3) the hydrotalcites from Mount Keith and Woodsreef are undergoing continuous re-equilibration with Mg-rich pore water that is a result of weathering reactions in the tailings. Stable isotope exchange with the local environment has been reported for stable Mg isotopes in epsomite (Li et al., 2014), brucite (Li et al., 2014) and hydromagnesite (Oelkers et al., 2018), stable C isotopes in hydromagnesite and dypingite (Mavromatis et al., 2015), and stable Fe isotopes in hematite and goethite (Friedrich et al., 2015; Joshi et al., 2017). If the hydrotalcites we analysed have undergone stable Mg isotope exchange with aqueous Mg in pore or surface waters, then this could explain why the iowaite–pyroaurite from Mount Keith which has a hydrothermal origin (Grguric, 2003) has similar  $\delta^{26}\text{Mg}_{\text{DSM-3}}$  values to the Woodsreef pyroaurite which has a low temperature origin derived from weathering and carbonation of Fe-rich brucite (Figure 3.3, Turvey et al., in prep/Chapter 4). Continuous re-equilibration of Mg would progressively overwrite the hydrothermal stable Mg isotope signature that the hydrotalcites from Mount Keith would have originally preserved, and replaced it with a low temperature stable Mg isotope signature, indistinguishable from that of low temperature pyroaurite from Woodsreef.

It is well known that hydrotalcite minerals undergo anion exchange (Bish, 1980; Bish and Brindley, 1977; Mills et al., 2012; Miyata, 1983), and that this process can go to completion on the timescale of hours or days (Bish, 1980; Miyata, 1983). It has been demonstrated by Turvey et al. (in prep)/Chapter 4 that a resetting of stable and radiogenic carbon isotopes occurs as a result of this anion exchange. If hydrotalcites exchange stable Mg isotopes with the local environment in a similar manner to that observed for stable C and O and radiocarbon isotopes, metamorphic hydrotalcites may reach the same composition as weathering-derived hydrotalcites that have formed by low-temperature carbonation of brucite. This would make it unlikely that stable Mg isotopes can be used to discriminate between hydrothermal and sedimentary hydrotalcite minerals. The extent to which this process occurs is currently unknown, as is the time scale over which this re-equilibration might occur. Hydrotalcite minerals in undisturbed outcrops of serpentinite, fresh ore and relatively fresh waste rock may still preserve the original stable Mg isotopic signatures of metamorphic hydrotalcites; however, it is possible stable Mg isotope exchange is very rapid, on the scale of anion exchange in hydrotalcites (Bish, 1980; Miyata, 1983; Miyata and Okada, 1977). If exchange between hydrotalcites and fluid in the surrounding environment is occurring it is of potential concern as hydrotalcites have been proposed for use in sequestering heavy metals and other contaminants (Douglas et al., 2014; Douglas et al., 2010), and such an exchange process would represent a mechanism by which these contaminants may be rereleased back into the tailings environment or pit water where they are forming.

## **5.6 Conclusions**

The stable Mg isotopic compositions of ultramafic outcrops and mine wastes are altered by a combination of multiple processes that are occurring simultaneously. Serpentinisation does

not cause significant fractionation away from the stable Mg isotope composition of basalts peridotites and chondrites (Beinlich et al., 2014; Bourdon et al., 2010); however, the leaching of Mg from serpentine minerals during weathering can lead to the formation of residual serpentine that is enriched in heavy  $^{25}\text{Mg}$  and  $^{26}\text{Mg}$ . This is likely due to the preferential loss of isotopically light  $^{24}\text{Mg}$  from mineral surfaces, which will contribute to  $^{24}\text{Mg}$  enriched signature of riverine and ocean waters which has been reported, alongside preferential dissolution of  $^{24}\text{Mg}$  enriched minerals such as carbonates and brucite (Teng et al., 2010; Beinlich et al., 2014). The stable Mg isotope composition of minerals, such as hydromagnesite and various hydrotalcites, that form as alteration phases in serpentinites are depleted in  $^{25}\text{Mg}$  and  $^{26}\text{Mg}$ , consistent with other reported carbonate mineral compositions (Beinlich et al., 2014). The depleted stable Mg isotope signature in hydromagnesite occurs as it is forming from  $^{25}\text{Mg}$  and  $^{26}\text{Mg}$  depleted fluids. The depleted stable Mg isotope signature in hydrotalcites occurs for both hydrotalcites that have formed from hydrothermal replacement of magnetite and chromite and for hydrotalcites that are forming by low temperature carbonation of brucite. The consistent depleted stable Mg isotope signature for hydrotalcites that have formed via different formation pathways could occur if the spinel minerals and brucite which are the Mg sources for the hydrotalcites have a similar stable Mg isotope composition or if post-formation the hydrotalcite minerals are undergoing Mg exchange with fluids (tailings pore water, rain water, mine pit water etc.) in the local environment. This Mg exchange would lead to re-equilibration of stable Mg isotope compositions over time, overprinting high temperature stable Mg isotope compositions with low temperature weathering-derived stable Mg isotope compositions. Exchange of Mg with the local environment affects our ability to trace the origins of hydrotalcite minerals using stable Mg isotopes, and may lead to potential rerelease of contaminants trapped within hydrotalcite minerals.

## 5.7 Acknowledgements

Funding for this work was provided by an Australian Research Council DECRA Fellowship and grants from Carbon Management Canada and the New South Wales Department of Industry to S.A.W, and a grant from INSU/CNRS to V.M. We would like to acknowledge the contributions of Simon Jowitt (University of Nevada, Las Vegas) and Ben Mililli (BHP Billiton) for their assistance with sampling at the Dundas mineral field, Ben Grguric and Greg Dipple for providing us with samples from Mount Keith, Anna Harrison for transporting samples for Mg isotope analysis, and Andreas Beinlich for advice on stable Mg isotope analyses. We would also like to thank Kate Maddison, Nick Staheyeff, Catherine Karpiel and Brad Mullard for granting us access to Woodsreef and supporting us in the field.

## 5.8 References

- Allman, R. (1968) The Crystal Structure of Pyroaurite. *Acta Crystallographica Section B*, B24, 972-977.
- Ashwal, L.D., and Cairncross, B. (1997) Mineralogy and origin of stichtite in chromite-bearing serpentinites. *Contributions to Mineralogy and Petrology*, 127(1-2), 75-86.
- Bea, S.A., Wilson, S.A., Mayer, K.U., Dipple, G.M., Power, I.M., and Gamazo, P. (2012) Reactive transport modeling of natural carbon sequestration in ultramafic mine tailings. *Vadose Zone Journal*, 11(2).
- Beinlich, A., Mavromatis, V., Austrheim, H., and Oelkers, E.H. (2014) Inter-mineral Mg isotope fractionation during hydrothermal ultramafic rock alteration - Implications for the global Mg-cycle. *Earth and Planetary Science letters*, 392(166-176).
- BHP. (2005) Mt Keith Nickel Operations: Environmental Data. BHP Billiton Sustainable Development Reports.

- Bish, D.L. (1980) Anion-exchange in takovite: applications to other hydrotalcite minerals. *Bulletin Mineralogie*, 103, 170-175.
- Bish, D.L., and Brindley, G.W. (1977) A reinvestigation of takovite, a nickel aluminium hydroxy-carbonate of the pyroaurite group. *American Mineralogist*, 62, 458-464.
- Black, J.R., Epstein, E., Rains, W.D., Yin, Q.-z., and Casey, W.H. (2008) Magnesium-Isotope Fractionation During Plant Growth. *Environmental Science & Technology*, 42(21), 7831-7836.
- Blowes, D.W., Reardon, E.J., Jambor, J.L., and Cherry, J.A. (1991) The formation and potential importance of cemented layers in inactive sulfide mine tailings. *Geochimica et Cosmochimica Acta*, 55(4), 965-978.
- Bolou-Bi, E.B., Poszwa, A., Leyval, C., and Vigier, N. (2010) Experimental determination of magnesium isotope fractionation during higher plant growth. *Geochimica et Cosmochimica Acta*, 74(9), 2523-2537.
- Bottrill, R.S. (2008) A mineralogical field guide for a Western tasmania minerals and museums tour. In E.a.R. Department of Infrastructure, Ed. Mineral Resources Tasmania.
- Bottrill, R.S., and Baker, W.E. (2008) A Catalogue of The Minerals of Tasmania. In E.a.R. Department of Infrastructure, Ed. Mineral resources Tasmania.
- Bourdon, B., Tipper, E.T., Fitoussi, C., and Stracke, A. (2010) Chondritic Mg isotope composition of the Earth. *Geochimica et Cosmochimica Acta*, 74(17), 5069-5083.
- Douglas, G., Shackleton, M., and Woods, P. (2014) Hydrotalcite formation facilitates effective contaminant and radionuclide removal from acidic uranium mine barren lixiviant. *Applied Geochemistry*, 42(0), 27-37.

- Douglas, G.B., Wendling, L.A., Pleysier, R., and Trefry, M. (2010) Hydrotalcite Formation for Contaminant Removal from Ranger Mine Process Water. *MINE WATER AND THE ENVIRONMENT*, 29, 108-115.
- Friedrich, A.J., Helgeson, M., Liu, C., Wang, C., Rosso, K.M., and Scherer, M.M. (2015) Iron Atom Exchange between Hematite and Aqueous Fe(II). *Environmental Science & Technology*, 49(14), 8479-8486.
- Glen, R.A., and Butt, B.C. (1981) Chrysotile asbestos at Woodsreef, New South Wales. *Economic Geology and the Bulletin of the Society of Economic Geologists*, 76(5), 1153-1169.
- Gorski, C.A., and Fantle, M.S. (2017) Stable mineral recrystallization in low temperature aqueous systems: A critical review. *Geochimica et Cosmochimica Acta*, 198, 439-465.
- Gras, A., Beaudoin, G., Molson, J., Plante, B., Bussière, B., Lemieux, J.M., and Dupont, P.P. (2017) Isotopic evidence of passive mineral carbonation in mine wastes from the Dumont Nickel Project (Abitibi, Quebec). *International Journal of Greenhouse Gas Control*, 60, 10-23.
- Graupner, T., Kassahun, A., Rammlmair, D., Meima, J.A., Kock, D., Furche, M., Fiege, A., Schippers, A., and Melcher, F. (2007) Formation of sequences of cemented layers and hardpans within sulfide-bearing mine tailings (mine district Freiberg, Germany). *Applied Geochemistry*, 22(11), 2486-2508.
- Grguric, B.A. (2003) Minerals of the MKD5 nickel deposit, Mount Keith, Western Australia. *Australian Journal of Mineralogy*, 9(2), 55-71.
- Grguric, B.A., Madsen, I.C., and Pring, A. (2001) Woodallite, a new chromium analogue of iowaite from the Mount Keith nickel deposit, Western Australia. *Mineralogical Magazine*, 65(3), 427-435.

- Hamilton, J.L., Turvey, C.C., Tait, A.W., and Wilson, S.A. (in prep) Accelerating mineral carbonation at ultramafic mines via direct CO<sub>2</sub> reaction and heap leaching, and potential for base metal enrichment and recovery. In preparation.
- Hamilton, J.L., Wilson, S.A., Morgan, B., Turvey, C.C., Paterson, D.J., Jowitt, S., McCutcheon, J., and Southam, C. (2018) Fate of transition metals during passive carbonation of ultramafic mine tailings via air capture with potentials for metal resource recovery. *International Journal of Greenhouse Gas Control*, In Press.
- Hamilton, J.L., Wilson, S.A., Morgan, B., Turvey, C.C., Paterson, D.J., MacRae, C., McCutcheon, J., and Southam, G. (2016) Nesquehonite sequesters transition metals and CO<sub>2</sub> during accelerated carbon mineralisation. *International Journal of Greenhouse Gas Control*, 55, 73-81.
- Handler, M.R., Baker, J.A., Schiller, M., Bennett, V.C., and Yaxley, G.M. (2009) Magnesium stable isotope composition of Earth's upper mantle. *Earth and Planetary Science Letters*, 282(1), 306-313.
- Harrison, A.L., Power, I.M., and Dipple, G.M. (2013) Accelerated carbonation of brucite in mine tailings for carbon sequestration. *Environmental Science and Technology*, 47(1), 126-134.
- Hostetler, P.B., Coleman, R.G., A., M.F., and Evans, B.W. (1966) Brucite in Alpine Serpentinities. *The American Mineralogist*, 51, 75-98.
- Hudson, D.R., and Bussell, M. (1981) Mountkeithite, a new pyroaurite-related mineral with an expanded interlayer containing exchangeable MgSO<sub>4</sub>. *Mineralogical Magazine*, 44, 345-350.
- Johnson, C.M., Beard, B.L., Albarède, F., Meeting, A.G.U., and Meeting, C.G.U. (2004) *Geochemistry of Non-traditional Stable Isotopes*. Mineralogical Society of America.

- Joshi, P., Fantle, M.S., Larese-Casanova, P., and Gorski, C.A. (2017) Susceptibility of Goethite to Fe<sup>2+</sup>-Catalyzed Recrystallization over Time. *Environmental Science & Technology*, 51(20), 11681-11691.
- Kelemen, P.B., and Matter, J. (2008) In situ carbonation of peridotite for CO<sub>2</sub> storage. *Proceedings of the National Academy of Sciences*, 105(45), 17295-17300.
- Lechat, K., Lemieux, J.M., Molson, J.W., Beaudoin, G., and Hebert, R. (2016) Field evidence of CO<sub>2</sub> sequestration by mineral carbonation in ultramafic milling wastes, Thetford Mines, Canada. *International Journal of Greenhouse Gas Control*, 47, 110-121.
- Li, W.-Y., Teng, F.-Z., Ke, S., Rudnick, R.L., Gao, S., Wu, F.-Y., and Chappell, B.W. (2010) Heterogeneous magnesium isotopic composition of the upper continental crust. *Geochimica et Cosmochimica Acta*, 74(23), 6867-6884.
- Li, W., Beard, B.L., and Johnson, C.M. (2011) Exchange and fractionation of Mg isotopes between epsomite and saturated MgSO<sub>4</sub> solution. *Geochimica et Cosmochimica Acta*, 75, 1814-1828.
- Li, W., Beard, B.L., Li, C., and Johnson, C.M. (2014) Magnesium isotope fractionation between brucite [Mg(OH)<sub>2</sub>] and Mg aqueous species: Implications for silicate weathering and biogeochemical processes. *Earth and Planetary Science letters*, 394, 82-93.
- Li, W., Beard, B.L., Li, C., Xu, H., and Johnson, C.M. (2015) Experimental calibration of Mg isotope fractionation between dolomite and aqueous solution and its geological implications. *Geochimica et Cosmochimica Acta*, 157, 164-181.
- Li, W., Chakraborty, S., Beard, B.L., Romanek, C.S., and Johnson, C.M. (2012) Magnesium isotope fractionation during precipitation of inorganic calcite under laboratory conditions. *Earth and Planetary Science letters*, 333-334, 304-316.

- Liu, P.-P., Teng, F.-Z., Dick, H.J.B., Zhou, M.-F., and Chung, S.-L. (2017) Magnesium isotopic composition of oceanic mantle and oceanic Mg cycling. *Geochimica et Cosmochimica Acta*.
- Liu, S.-A., Teng, F.-Z., He, Y., Ke, S., and Li, S. (2010) Investigation of magnesium isotope fractionation during granite differentiation: Implication for Mg isotopic composition of the continental crust. *Earth and Planetary Science Letters*, 297(3), 646-654.
- Matter, J.M., Stute, M., Snæbjörnsdóttir, S.Ó., Oelkers, E.H., Gislason, S.R., Aradóttir, E.S., Sigfusson, B., Gunnarsson, I., Sigurdardóttir, H., Gunnlaugsson, E., Axelsson, G., Alfredsson, H.A., Wolff-Boenisch, D., Mesfin, K., Taya, D.F.d.l.R., Hall, J., Dideriksen, K., and Broecker, W.S. (2016) Rapid carbon mineralization for permanent disposal of anthropogenic carbon dioxide emissions. *Science*, 352(6291), 1312-1314.
- Mavromatis, V., Bundeleva, I.A., Shirokova, L.S., Millo, C., Pokrovsky, O.S., Bénézech, P., Ader, M., and Oelkers, E.H. (2015) The continuous re-equilibration of carbon isotope compositions of hydrous Mg carbonates in the presence of cyanobacteria. *Chemical Geology*, 404(Supplement C), 41-51.
- Mavromatis, V., Gautier, Q., Bosc, O., and Schott, J. (2013) Kinetics of Mg partition and Mg stable isotope fractionation during its incorporation in calcite. *Geochimica et Cosmochimica Acta*, 114, 188-203.
- Mavromatis, V., Meister, P., and Oelkers, E.H. (2014a) Using stable Mg isotopes to distinguish dolomite formation mechanisms: A case study from the Peru Margin. *Chemical Geology*, 385, 84-91.
- Mavromatis, V., Pearce, C.R., Shirokova, L.S., Bundeleva, I.A., Pokrovsky, O.S., Benezeth, P., and Oelkers, E.H. (2012) Magnesium isotope fractionation during hydrous

magnesium carbonate precipitation with and without cyanobacteria. *Geochimica et Cosmochimica Acta*, 76, 161-174.

Mavromatis, V., Prokushkin, A.S., Pokrovsky, O.S., Viers, J., and Korets, M.A. (2014b) Magnesium isotopes in permafrost-dominated Central Siberian larch forest watersheds. *Geochimica et Cosmochimica Acta*, 147, 76-89.

McCutcheon, J., Dipple, G.M., Wilson, S.A., and Southam, G. (2015) Production of magnesium-rich solutions by acid leaching of chrysotile: A precursor to field-scale deployment of microbially enabled carbonate mineral precipitation. *Chemical Geology*, 413, 119-131.

McCutcheon, J., Turvey, C.C., Hamilton, J.L., Wilson, S.A., and Southam, G. (2017) Experimental Deployment of Microbial Mineral Carbonation at an Asbestos Mine: Potential Applications to Carbon Storage and Tailings Stabilization. *Minerals*, 7(191).

McCutcheon, J., Wilson, S.A., and Southam, G. (2016) Microbially accelerated carbonate mineral precipitation as a strategy for in situ carbon sequestration and rehabilitation of asbestos mine sites. *Environmental Science & Technology*, 50(3), 1419-1427.

Melchiorre, E.B., Bottrill, R., Huss, G.R., and Lopez, A. (2016) Conditions of Stichtite ( $\text{Mg}_6\text{Cr}_2(\text{OH})_{16}[\text{CO}_3] \cdot 4\text{H}_2\text{O}$ ) formation and its Geochemical and Isotope Record of Early Phanerozoic Serpentinizing Environments. *Geochimica et Cosmochimica Acta*.

Melchiorre, E.B., Bottrill, R., Huss, G.R., and Lopez, A. (2018) The Early Earth Geochemical and Isotope Record of Serpentinizing Environments from Archean Stichtite ( $\text{Mg}_6\text{Cr}_2(\text{OH})_{16}[\text{CO}_3] \cdot 4\text{H}_2\text{O}$ ). *Precambrian Research*.

Merril, R.J., Butt, B.C., Forrest, V.C., Purdon, G., and Bramley-Moore, R.A. (1980) Asbestos Production at Chrysotile Corporation of Australia Pty. Limited, Barraba,

- N.S.W. In J.T. Woodcock, Ed. Mining and Metallurgical Practices in Australasia, 10, p. 669-673. The Australasian Institute of Mining and Metallurgy, Clunies Ross House, 191 Royal Parade, Parkville, Victoria, Australia 3052.
- Mills, S.J., Christy, A.G., Génin, J.M.R., Kameda, T., and Colombo, F. (2012) Nomenclature of the hydrotalcite supergroup: natural layered double hydroxides. *Mineralogical Magazine*, 76(5), 1289-1336.
- Mills, S.J., Whitfield, P.S., Wilson, S.A., Woodhouse, J.N., Dipple, G.M., Raudsepp, M., and Francis, C.A. (2011) The crystal structure of stichtite, re-examination of barbertonite, and the nature of polytypism in MgCr hydrotalcites. *American Mineralogist*, 96(1), 179-187.
- Miyata, S. (1983) Anion-exchange properties of hydrotalcite-like compounds. *Clays and Clay Minerals*, 31(4), 305-311.
- Miyata, S., and Okada, A. (1977) Synthesis of Hydrotalcite-like compounds and their physico-chemical properties - the systems  $Mg_{2+}-Al_{3+}-SO_4^{2-}$  and  $Mg_{2+}-Al_{3+}-CrO_4^{2-}$ . *Clays and Clay Minerals*, 25, 14-18.
- Mumpton, F.A., Jaffe, H.W., and S., T.C. (1965) Coalingite, a new mineral from the New Idria Serpentinite, Fresno and San Benito counties, California. *The American Mineralogist*, 50, 1893-1913.
- Mumpton, F.A., and Thompson, C.S. (1966) The Stability of Brucite in the Weathering Zone of the New Idria Serpentinite. *Clays and Clay Minerals*, 14(1), 249-257.
- O'Hanley, D.S., and Offler, R. (1992) Characterization of multiple serpentinization, Woodsreef New South Wales. *Canadian Mineralogist*, 30, 1113-1126.
- Oelkers, E.H., Berninger, U.-N., Pérez-Fernández, A., Chmeleff, J., and Mavromatis, V. (2018) The temporal evolution of magnesium isotope fractionation during

hydromagnesite dissolution, precipitation, and at equilibrium. *Geochimica et Cosmochimica Acta*, 226, 36-49.

Opfergelt, S., Georg, R.B., Delvaux, B., Cabidoche, Y.M., Burton, K.W., and Halliday, A.N. (2012) Mechanisms of magnesium isotope fractionation in volcanic soil weathering sequences, Guadeloupe. *Earth and Planetary Science Letters*, 341(Supplement C), 176-185.

Oskierski, H.C., Dlugogorski, B.Z., and Jacobsen, G. (2013) Sequestration of atmospheric CO<sub>2</sub> in chrysotile mine tailings of the Woodsreef Asbestos Mine, Australia: Quantitative Mineralogy, isotopic fingerprinting and carbonation rates. *Chemical Geology*.

Oskierski, H.C., Dlugogorski, B.Z., Oliver, T.K., and Jacobsen, G. (2016) Chemical and isotopic signatures of waters associated with the carbonatio of ultramafic mine tailings, Woodsreef Asbestos Mine, Australia. *Chemical Geology*.

Pearce, C.R., Saldi, G.D., Schott, J., and Oelkers, E.H. (2012) Isotopic fractionation during congruent dissolution, precipitation and at equilibrium: Evidence from Mg isotopes. *Geochimica et Cosmochimica Acta*, 92, 170-183.

Rozalen, M., and Huertas, F.J. (2013) Comparative effect of chrysotile leaching in nitric, sulfuric and oxalic acids at room temperature. *Chemical Geology*, 352, 134-142.

Reid, M. (1925) The Dundas Mineral Field. In *D.o. Mines*, Ed, John Vail, Government Printer, Hobart.

Shirokova, L.S., Mavromatis, V., Bundeleva, I., Pokrovsky, O.S., Benezeth, P., Gerard, E., Pearce, C., and Oelkers, E.H. (2013) Using Mg isotopes to Trace Cyanobacterially Mediated Magnesium Carbonate Precipitation in Alkaline lakes. *Aquatic Geochemistry*, 19, 1-24.

- Sittinger, R., and Sittinger, C. (2008) July 2008 Mineral of the Month: Stichtite. Mineral of the Month. Mineral of the Month Club, 1770 Orville Avenue Cambria, CA.
- Snæbjörnsdóttir, S.Ó., Wiese, F., Fridriksson, T., Armansson, H., Einarsson, G.M., and Gislason, S.R. (2014) CO<sub>2</sub> storage potential of basaltic rocks in Iceland and the oceanic ridges. *Energy Procedia*, 63, 4585-4600.
- Teng, F.-Z. (2017) Magnesium Isotope Geochemistry. *Reviews in Mineralogy & Geochemistry*, 82(1), 219-287.
- Teng, F.-Z., Li, W., Li, Y., Rudnick, R.L., and Gardner, L.R. (2010) Contrasting lithium and magnesium isotope fractionation during continental weathering. *Earth and Planetary Science Letters*, 300(1), 63-71.
- Teng, F.-Z., Wadhwa, M., and Helz, R.T. (2007) Investigation of magnesium isotope fractionation during basalt differentiation: Implications for a chondritic composition of the terrestrial mantle. *Earth and Planetary Science Letters*, 261(1), 84-92.
- Tipper, E.T., Gaillardet, J., Louvat, P., Capmas, F., and White, A.F. (2010) Mg isotope constraints on soil pore-fluid chemistry: Evidence from Santa Cruz, California. *Geochimica et Cosmochimica Acta*, 74(14), 3883-3896.
- Tipper, E.T., Galy, A., and Bickle, M.J. (2006) Riverine evidence for a fractionated reservoir of Ca and Mg on the continents: Implications for the oceanic Ca cycle. *Earth and Planetary Science letters*, 247, 267-279.
- Turvey, C.C., Hamilton, J.L., and Wilson, S.A. (in review) Comparison of Rietveld analysis methods for quantification of carbon dioxide fixation in ultramafic mine tailings. *American Mineralogist*, In Review.
- Turvey, C.C., Wilson, S.A., Hamilton, J.L., and Southam, G. (2017) Field-based accounting of CO<sub>2</sub> sequestration in ultramafic mine wastes using portable X-ray diffraction. *American Mineralogist*.

- Turvey, C.C., Wilson, S.A., Hamilton, J.L., Tait, A.W., McCutcheon, J., and Southam, G. (in prep) Hydrotalcites as a carbon sink at the Woodsreef Chrysotile Mine (NSW, Australia). In preparation.
- Wang, L., Lu, A., Wang, C., Zheng, X., Zhao, D., and Liu, R. (2006) Nano-fibriform production of silica from natural chrysotile. *Journal of Colloid and Interface Science*, 295(2), 436-439.
- Wicks, F.J., and Whittaker, E.J.W. (1975) A reappraisal of the structures of the serpentine minerals *Canadian Mineralogist*, 13, 227-243.
- Wiederhold, J.G. (2015) Metal Stable Isotope Signatures as Tracers in Environmental Geochemistry. *Environmental Science & Technology*, 49(5), 2606-2624.
- Wilson, S.A., Barker, S.L.L., Dipple, G.M., and Atudorei, V. (2010) Isotopic Disequilibrium during uptake of Atmospheric CO<sub>2</sub> into Mine Process Waters: Implications for CO<sub>2</sub> Sequestration. *Environmental Science & Technology*, 44, 9522-9529.
- Wilson, S.A., Dipple, G.M., Power, I.M., Thom, J.M., Anderson, R.G., Raudsepp, M., Gabites, J.E., and Southam, G. (2009a) Carbon Dioxide Fixation within Mine Wastes of Ultramafic-Hosted Ore Deposits: Examples from the Clinton Creek and Cassiar Chrysotile Deposits, Canada. *Economic geology*, 104, 95–112.
- Wilson, S.A., Harrison, A.L., Dipple, G.M., Power, I.M., Barker, S.L.L., Mayer, K.U., Fallon, S.J., Raudsepp, M., and Southam, G. (2014) Offsetting of CO<sub>2</sub> emissions by air capture in mine tailings at the Mount Keith Nickel mine, Western Australia: Rates, controls and prospects for carbon neutral mining. *International Journal of Greenhouse Gas Control*, 25, 121-140.
- Wilson, S.A., Raudsepp, M., and Dipple, G.M. (2009b) Quantifying carbon fixation in trace minerals from processed kimberlite; a comparative study of quantitative methods

- using X-ray powder diffraction data with applications to the Diavik diamond mine, Northwest Territories, Canada. *Applied Geochemistry*, 24(12), 2312-2331.
- Wimpenny, J., Colla, C.A., Yin, Q.-Z., Rustad, J.R., and Casey, W.H. (2014) Investigating the behaviour of Mg isotopes during the formation of clay minerals. *Geochimica et Cosmochimica Acta*, 128, 178-194.
- Wimpenny, J., Gislason, S.R., James, R.H., Gannoun, A., Pogge Von Strandmann, P.A.E., and Burton, K.W. (2010) The behaviour of Li and Mg isotopes during primary phase dissolution and secondary mineral formation in basalt. *Geochimica et Cosmochimica Acta*, 74, 5259-5279.
- Wombacher, F., Eisenhauer, A., Heuser, A., and Weyer, S. (2009) Separation of Mg, Ca and Fe from geological reference materials for stable isotope ratio analyses by MC-ICP-MS and double-spike TIMS. *Journal of Analytical Atomic Spectrometry*, 24(5), 627-636.
- Yang, W., Teng, F.-Z., and Zhang, H.-F. (2009) Chondritic magnesium isotopic composition of the terrestrial mantle: A case study of peridotite xenoliths from the North China craton. *Earth and Planetary Science Letters*, 288(3-4), 475-482.
- Young, E.D., and Galy, A. (2004) The Isotope Geochemistry and Cosmochemistry of Magnesium. *Reviews in Mineralogy & Geochemistry*, 55, 197-230.







## Declaration for Thesis Chapter 6

Declaration by candidate

In the case of Chapter 6, the nature and extent of my contribution is as follows:

<b>Nature of Contribution</b>	<b>Extent of contribution (%)</b>
Concept, experimental design, conducted experiments, collected and analysed data, writing and editing.	75%

The following co-authors contributed to the work. If co-authors are students at Monash University, the extent of their contribution in percentage terms must be stated:

<b>Name</b>	<b>Nature of contribution</b>	<b>Extent of Contribution (%)</b>
Andrew J. Frierdich	Supervisory role, experimental design, data analysis and interpretation and had input into the manuscript	20
Sasha A. Wilson	Supervisory role, assisted with data interpretation and had input into the manuscript	5%

The undersigned hereby certify that the above declaration correctly reflects the nature and extent of the candidate's and co-authors contributions to this work\*.

Candidate's signature:



Date:

22/03/2018

Main supervisor's signature:



Date: 22/03/2018

\* Note: Where the responsible author is not the candidate's main supervisor, the main supervisor should consult with the responsible author to agree on the respective contributions of the authors.

## Chapter 6

### **Mg exchange between pyroaurite [Mg<sub>6</sub>Fe<sup>3+</sup><sub>2</sub>CO<sub>3</sub>(OH)<sub>16</sub>·4H<sub>2</sub>O] and aqueous Mg(II): Implications for carbon mineralisation and contaminant release**

Connor C. Turvey<sup>1\*</sup>, Siobhan A. Wilson<sup>1,2</sup> and Andrew J. Friedrich<sup>1</sup>

<sup>1</sup>School of Earth, Atmosphere & Environment, Monash University, Clayton, Melbourne,  
Victoria 3800, Australia

<sup>2</sup>Department of Earth and Atmospheric Sciences, University of Alberta, Edmonton,  
Alberta, T6G 2E3, Canada

In preparation for submission to *Environmental Science & Technology*

## 6.0 Abstract

Hydrotalcite supergroup minerals are anionic clays that are under increasing interest for their ability to sequester atmospheric and aqueous contaminants, including atmospheric CO<sub>2</sub> and heavy metals in mine tailings ponds. Hydrotalcites are commonly carbonate-bearing, however, it is challenging to trace their formation pathways using stable C and O isotopes because they undergo anion exchange with CO<sub>3</sub><sup>2-</sup><sub>(aq)</sub> from the local environment. Stable Mg isotopes may be used as an alternative tracer that is potentially less likely to undergo exchange and continuously re-equilibrate with solution; however, the robustness of this remains to be tested. Here, we expose synthetic pyroaurite [Mg<sub>6</sub>Fe<sup>3+</sup><sub>2</sub>(CO<sub>3</sub>)(OH)<sub>16</sub>·4H<sub>2</sub>O], which is a common hydrotalcite mineral, to <sup>25</sup>Mg-enriched Mg<sup>2+</sup><sub>(aq)</sub> in order to determine whether it undergoes exchange with aqueous Mg. The experiment was conducted over 90 days, with the solid analysed by powder X-ray diffraction (XRD) and the solution composition analysed by Inductively Coupled Plasma Mass Spectrometry (ICP-MS) over the course of the experiment. ICP-MS results were used to determine that <sup>24</sup>Mg and <sup>26</sup>Mg from pyroaurite was entering solution while <sup>25</sup>Mg from solution was incorporated into the pyroaurite, indicating that exchange between the pyroaurite and solution was occurring and began immediately upon contact. Rietveld refinements of the XRD data revealed that the crystallite size of the pyroaurite is constant over time, suggesting that Mg exchange is occurring predominantly at mineral surfaces and does not involve wholesale recrystallisation of the mineral. Exchange of Mg and other cations between pyroaurite and solution may complicate the interpretation of stable Mg isotope data in tracer studies. It also means there is the potential for contaminants sequestered in hydrotalcites to be released over time.

## 6.1 Introduction

Hydrotalcite supergroup minerals are layered double hydroxide (LDH) minerals with the general formula  $[M^{2+}_{1-x}M^{3+}_x(OH)_2]^{x+}A^{n-}_{x/n} \cdot mH_2O$ . Hydrotalcite minerals consist of stacked ‘brucite-like’ hydroxide layers that contain divalent and trivalent cations, which are separated by interlayer galleries containing H<sub>2</sub>O molecules and various small anions (Evans and Slade, 2006; Mills et al., 2012). These minerals are being investigated for their ability to remove heavy metals and other aqueous contaminants from mine tailings ponds during their precipitation (Douglas et al., 2014; Douglas et al., 2010), and for their ability to sequester atmospheric CO<sub>2</sub> (Douglas et al., 2014; Douglas et al., 2010; Oskierski et al., 2013; Turvey et al., in prep-a/Chapter 4; Turvey et al., in prep-b/Chapter 5) via precipitation, or anion exchange with dissolved inorganic carbon (DIC) post precipitation (Bish, 1980; Miyata, 1983). Carbon mineralisation of mine tailings is being considered as a low-cost method for reducing the CO<sub>2</sub> emissions of some ultramafic mine sites (e.g., Gras et al., 2017, Wilson et al., 2014; Turvey et al., in prep/Chapter 4; Oskierski et al., 2013). At several of these mines hydrotalcite minerals are present and may represent net sequestration of CO<sub>2</sub> (Gras et al., 2017, Wilson et al., 2014; Turvey et al., in prep/Chapter 4; Oskierski et al., 2013).

Understanding the origins of hydrotalcite minerals is important when considering their potential to sequester atmospheric CO<sub>2</sub> in mining environments (Turvey et al., in prep-a/Chapter 4). Hydrotalcites form by multiple pathways and under both high- and low-temperature conditions. For instance, the hydrotalcite minerals pyroaurite  $[Mg_6Fe^{3+}_2(CO_3)(OH)_{16} \cdot 4H_2O]$  and coalingite  $[Mg_5Fe^{3+}_2(CO_3)(OH)_{24} \cdot 2H_2O]$  can form at Earth’s surface conditions from the low temperature carbonation of Fe-rich brucite (Hostetler et al., 1966; Mumpton et al., 1965; Mumpton and Thompson, 1966). This reaction is occurring in

the tailings storage facility at the Woodsreef chrysotile mine, New South Wales, Australia, via the reaction of atmospheric CO<sub>2</sub> with brucite, making hydrotalcite minerals an important carbon sink at Woodsreef (Oskierski et al., 2013; Turvey et al., 2017; Turvey et al., in prep-a/Chapter 4; Turvey et al., in prep-b/Chapter 5). Hydrotalcites may already be present in the tailings of some other ultramafic hosted mines as gangue minerals (Grguric 2003; Grguric et al., 2001, Wilson et al., 2014), having formed during hydrothermal alteration of spinel minerals (Grguric, 2003; Grguric et al., 2001; Melchiorre et al., 2016; Melchiorre et al., 2018). In this case, it is important to understand whether hydrotalcites are forming *in situ* within mine tailings, and thus sequestering atmospheric CO<sub>2</sub>, if they were already present in the ore during mining and are not contributing to the net carbon sequestration, or if they are gangue minerals that originally contained non-carbonate anions but have undergone anion exchange and so are sequestering atmosphere CO<sub>2</sub>. The combined use of stable C and O isotopes with radiocarbon is typically used to trace sources of carbon within minerals and to account for CO<sub>2</sub> sequestration in ultramafic mines (e.g., Beinlich and Austrheim, 2012; Gras et al., 2017; Oskierski et al., 2013; Turvey et al., in prep-a/Chapter 4; Wilson et al., 2009; Wilson et al., 2011; Wilson et al., 2014). Although this methodology works well for anhydrous and hydrous Mg-carbonate minerals, determining the origins of hydrotalcites using stable C and O isotopes and radiocarbon is made more complex by the ability of hydrotalcites to exchange interlayer anions for aqueous carbonate in the local environment (Bish, 1980; Miyata, 1983). Anion exchange will therefore cause the radiocarbon and stable C and O isotopic signatures of hydrotalcites to change over time until they no longer reflect the original isotopic composition of the minerals (Bish, 1980; Miyata, 1983; Turvey et al., in prep-a/Chapter 4). Stable Mg isotopes are potentially a more robust tracer of whether or not a hydrotalcite minerals formed at high or low temperature, as the Mg in hydrotalcite minerals is part of the hydroxide layer, and so may be more resistant to exchange than

elements which are held in the interlayer galleries (e.g., C and some of the O within carbonate groups).

Non-traditional stable isotopes, such as those of Mg are emerging as a tool to identify and examine surface processes such as continental weathering, the transport and fate of metal contaminants and carbonate formation (Beinlich et al., 2014; Gorski and Fantle, 2017; Handler et al., 2009; Johnson et al., 2004; Li et al., 2010; Li et al., 2015; Mavromatis et al., 2014a; Mavromatis et al., 2014b; Opfergelt et al., 2012; Shirokova et al., 2013; Teng et al., 2010; Teng et al., 2017; Wiederhold, 2015). Stable Mg isotopes can be used as geochemical tracers as they are indifferent to many high temperature processes such as serpentinisation, planetary accretion, granite differentiation and crustal anataxis (Beinlich et al., 2014; Bourdon et al., 2010; Handler et al., 2009; Li et al., 2010; Liu et al., 2010; Yang et al., 2009). However, they do undergo significant fractionation when under the influence of low temperature and Earth surface processes such as soil and carbonate formation, crustal weathering and plant growth (Black et al., 2008; Bolou-Bi et al., 2010; Opfergelt et al., 2012; Shirokova et al., 2013; Teng et al., 2010; Tipper et al., 2010). As such, stable Mg isotopes may potentially be used to differentiate between hydrotalcites of high- and low-temperature origin (Turvey et al., in prep-b/Chapter 5).

There is a growing body of evidence that some minerals, such as Mg-carbonates and Fe-oxyhydroxides continuously re-equilibrate their stable Fe and Mg isotopic composition with the local environment (Friedrich et al., 2015a; Friedrich et al., 2015b; Friedrich et al., 2016; Gorski and Fantle, 2017; Handler et al., 2014; Mavromatis et al., 2015; Mavromatis et al., 2012; Oelkers et al., 2018; Pedersen et al., 2005; Shirokova et al., 2013). Mavromatis et al. (2012), Shirokova et al. (2013) and (Oelkers et al., 2018) observed continuous re-equilibration of stable Mg isotopes in hydromagnesite  $[\text{Mg}_5(\text{CO}_3)_4(\text{OH})_2 \cdot 4\text{H}_2\text{O}]$ , dypingite

[ $\text{Mg}_5(\text{CO}_3)_4(\text{OH})_2 \cdot \sim 5\text{H}_2\text{O}$ ] and co-existing aqueous fluids. Pedersen et al. (2005) investigated exchange of aqueous Fe(II) for structural Fe(III) in hematite, goethite and lepidocrocite and they found that at pH 6.5 goethite and lepidocrocite exchanged Fe(III) with aqueous Fe(II), whereas hematite did not. However a later study by Friedrich et al. (2015b) found that hematite did undergo exchange, and that the rate of Fe exchange was influenced by particle size, pH and the concentration of Fe(II) in solution.

If hydrotalcites exchange stable Mg isotopes in a similar manner to that of other Mg-carbonate minerals, it may erase the isotopic record of their formation conditions over time. Turvey et al. (in prep-b)/Chapter 5 compared the stable Mg isotope compositions of hydrotalcite and serpentine minerals from three different ultramafic mine sites in Australia. They did not observe an appreciable difference between the stable Mg isotopic composition of hydrotalcites formed during high-temperature alteration of spinels and low-temperature carbonation of brucite (Turvey et al., in prep-b/Chapter 5), and suggest that this could be indicative of Mg exchange occurring between hydrotalcite minerals and pore waters in the local tailings environment. Furthermore, if hydrotalcites exchange both anions in their interlayer galleries, and cations from their hydroxide layers there is potential for them to slowly release contaminants back into surface water and groundwater after formation, necessitating careful storage if they are being used to sequester aqueous and atmospheric contaminants such as metals, metalloids or  $\text{CO}_2$ .

Understanding how minerals exchange isotopes with dissolved species is necessary to (1) assess the robustness with which they preserve isotopic information about their conditions of formation and (2) to determine their suitability for immobilizing contaminants (Gorski and Fantle, 2017). This study investigates whether hydrotalcites undergo recrystallization in aqueous solutions and readily exchange structural Mg with dissolved Mg(II). We examine

stable Mg isotope exchange between the hydrotalcite mineral, pyroaurite, that has a natural Mg isotopic composition and  $^{25}\text{Mg}$ -enriched aqueous Mg(II) to determine if exchange occurs between pyroaurite and solution, and whether the exchange results in a phase change or crystallite growth.

## 6.2 Materials and methods

### 6.2.1 Pyroaurite synthesis

Pyroaurite with a natural Mg isotopic composition (i.e., the natural abundance of stable Mg isotopes is 78.99%  $^{24}\text{Mg}$ , 10.00%  $^{25}\text{Mg}$  and 11.01%  $^{26}\text{Mg}$ ; Young and Galy, 2004) was synthesised using a modified version of the Vucelic et al. (1997) synthesis method. Pyroaurite was produced by direct synthesis, with 250 mL of a metal nitrate solution containing both 6.1 g of  $\text{Fe}(\text{NO}_3)_3 \cdot 9\text{H}_2\text{O}$  and 11.7 g of  $\text{Mg}(\text{NO}_3)_2 \cdot 6\text{H}_2\text{O}$  added at a rate of ~4 mL/min into a vessel containing 250 mL of a base solution (containing 5.1 g of dissolved NaOH and 10.1 g of dissolved  $\text{Na}_2\text{CO}_3$ ). The base solution was heated to 75°C and was mixed using a stir bar at 300 rpm using a heated stir plate. Once the two solutions were completely combined, the vessel was enclosed and the combined solution was left at 75°C and 300 rpm for 92 hours to allow crystallites to grow. The resulting solid was filtered from the solution using 11  $\mu\text{m}$  cellulose filters and was allowed to air-dry at room temperature (~22°C).

The identity of the resulting solid was confirmed as being pyroaurite through qualitative XRD. Samples were analysed using a Bruker D8 Advance X-ray diffractometer at the Monash X-ray Platform. The instrument was equipped with a Cu X-ray tube that operated at 40 kV and 40 mA. Data were collected using a LynxEye 1D Position Sensitive Detector over a  $2\theta$  range of 3-80°, using a dwell time of 1s/step and a step size of 0.02°. Pyroaurite was identified using the software package DIFFRAC.EVA V2.1 (Bruker AXS) with

reference to standard patterns from the ICDD PDF-2 database and Crystallography Open Database. The surface area of the synthetic pyroaurite was calculated as being 88.24 m<sup>2</sup>/g prior to exchange via the Brunauer-Emmett-Teller (BET) method using a Quantachrome Autosorb-1 series Surface Area and Pore Size analyser located in the Department of Materials Engineering at the University of British Columbia. The starting stable Mg isotope composition of the pyroaurite was analysed by Inductively Coupled Plasma Mass Spectrometry (ICP-MS) prior to the exchange experiment and was reported as 76.2 % <sup>24</sup>Mg, 12.4 % <sup>25</sup>Mg and 11.3 % <sup>26</sup>Mg.

### 6.2.2 Isotopic exchange experiments

An enriched <sup>25</sup>Mg<sup>2+</sup><sub>(aq)</sub> solution was made to test the exchange of Mg with natural abundance Mg<sup>2+</sup> in the synthetic pyroaurite (hereafter referred to as ‘pyroaurite’ for simplicity). The <sup>25</sup>Mg solution was produced by dissolving 0.04 g of MgO (99.2% <sup>25</sup>Mg, Isoflex USA) into 5.5 mL of 0.5 M HCl. A 60-μL volume of the <sup>25</sup>Mg-enriched solution was added to reactors (15-mL sterile centrifuge tubes) containing 10-mL of a 0.1 M carbonate–bicarbonate pH buffer (buffering the solution to pH 11.2). The molar ratio of Mg in the pyroaurite compared to Mg<sup>2+</sup><sub>(aq)</sub> in solution was 30:1. Initial control experiments were conducted to ensure that (1) combining the <sup>25</sup>Mg tracer with the carbonate–bicarbonate pH buffer would not precipitate Mg-carbonate minerals and (2) that the pH buffer would ensure the stability of the pyroaurite and prevent it from undergoing net dissolution over time (see S.I. Section S1. for details of the control experiments, Evans and Slade, 2006). Hydrotalcites are known to undergo anion exchange at ambient conditions, and to have a strong preference for taking up carbonate over other anions, meaning that carbonate-bearing hydrotalcites are the most stable species and unlikely to undergo anion exchange into non-carbonate bearing hydrotalcite minerals (Bish, 1980; Bish and Brindley, 1977; Miyata, 1983). Furthermore the

excess carbonate present in the buffer ensured that no anion exchange would occur between pyroaurite and chloride in solution.

Reactions were initiated by adding 0.02 g of the pyroaurite to a 15 mL reactor containing 10 mL of the  $^{25}\text{Mg}$ -enriched carbonate–bicarbonate buffer solution. The exchange experiment was conducted over a period of 90 days and 22 identical reactors were prepared in parallel allowing for duplicate reactors to be sacrificed at various time points. Reactors were sealed and placed on a shaking table to keep the suspension mixed. Two samples of the unreacted starting pyroaurite were dissolved in 1M HCl and saved for later stable Mg isotope analysis using ICP-MS. Duplicate samples of the unreacted  $^{25}\text{Mg}$ -enriched carbonate-bicarbonate buffer were also saved for analysis.

Reactors were sacrificed at 9 time points between 0 and 90 days: 0, 1, 3, 5, 10, 15, 30, 60 and 90 days. The contents of each reactor were separated into a solid and liquid component for later analysis by centrifugation for 2 minutes at 4000 rpm. A 9 mL volume of the supernatant was then filtered using a 0.22  $\mu\text{m}$  syringe filter into a clean test tube, acidified using 1 mL of 1 M HCl and saved for ICP-MS analysis. The solid component was removed following centrifuging, rinsed with ethanol, left to dry and saved for XRD analysis. For the ‘0 day’ samples, sample collection occurred immediately after combining the pyroaurite and  $^{25}\text{Mg}$ -bearing buffer solution at the initiation of the experiment; as such, the 0 day samples are distinct from the unreacted pyroaurite and  $^{25}\text{Mg}$ -bearing buffer solution, as they reacted for approximately 2 minutes whilst in the centrifuge during separation and sample preparation.

### **6.2.3 ICP-MS Analysis and %Mg exchange calculations**

Isotopic analysis was conducted at the School of Earth, Atmosphere and Environment, Monash University using an ICAP-Q ICP-MS. Aqueous samples were diluted 100 $\times$  using

0.1 M HCl prior to analysis. Stable Mg isotope concentrations were calculated using a calibration curve derived from standards of a known Mg concentration. Stable Mg isotope mole fractions,  $f^n\text{Mg}$  were calculated by dividing the counts per second (cps) recorded for isotope  $n$  by the total cps value for all magnesium isotopes as given in Equation 1:

$$f^n\text{Mg} = \frac{n_{\text{cps}}}{^{24}\text{cps} + ^{25}\text{cps} + ^{26}\text{cps}} \quad (\text{Eq. 1})$$

A modified version of the Handler et al. (2014) method for calculating Fe exchange between solution and goethite was used to estimate the amount of Mg exchange over time (Handler et al., 2014; Mikutta et al., 2009). This method can be used to determine the relative amount of Mg in the solid that has equilibrated with the fluid, and can be considered as analogous to the amount of Mg exchange that has occurred. The degree of exchange was calculated using the initial mole fraction for the stable Mg isotopes and the total Mg concentrations of the aqueous solution and pyroaurite, as seen in Equation 2:

$$\%Mg \text{ Exchange} = \frac{N_{aq} \times (f_{aq}^i - f_{Mg}^t)}{N_{pyro}^{tot} \times (f_{Mg}^t - f_{pyro}^i)} \times 100 \quad (\text{Eq. 2})$$

Where  $N_{aq}$  is the total moles of aqueous  $\text{Mg}^{2+}$  in the system,  $N_{pyro}^{tot}$  is the total moles of Mg in pyroaurite,  $f_{aq}^i$  is the initial isotope composition of aqueous  $\text{Mg}^{2+}$ ,  $f_{Mg}^t$  is the isotope composition of the aqueous  $\text{Mg}^{2+}$  at time  $t > 0$  and  $f_{pyro}^i$  is the initial isotope composition of the pyroaurite, these calculations were calculated using  $f^{25}\text{Mg}$  (see S.I. Section S2. for complete calculation details). Previous isotopic exchange studies have attempted to quantify the amount of exchangeable atoms at mineral surfaces to determine whether exchange is occurring solely as a result of surface absorption, or whether atoms within the mineral structure are being exchanged. We used the method outlined in Handler et al. (2014) in order to estimate the proportion of Mg in the pyroaurite that was exposed as the surfaces of the mineral (see S.I. Section S3. for complete details).

## 2.4 Crystallite size analysis

Crystallite size analyses was performed on XRD patterns that were collected from samples of the dried pyroaurite powder mounted on a zero-background Si [single crystal (9 1 1)] holder. Rietveld refinements of the XRD patterns were done using the software package Topas V.5 (Bruker AXS) using the fundamental parameters approach (Cheary and Coelho, 1992), to calculate crystallite size and strain. The contribution of instrumental peak broadening to XRD patterns collected from experimental samples was modelled using an instrument profile refined from a pattern of NIST SRM 660b LaB<sub>6</sub>. The single variable reciprocal space expression outlined in Whitfield et al. (2010) was used to overcome anisotropic peak broadening in pyroaurite. The volume-weighted crystallite size, denoted *LVol-IB* in Topas V.5 was calculated from refined values for Lorentzian and Gaussian integral breadth, while microstrain  $e_0$  was calculated from refined values for Lorentzian and Gaussian strain (see the S.I. Section S4. for further details).

## 6.3 Results and discussion

### 6.3.1 Interactions between pyroaurite and aqueous Mg

The results of our control experiments indicated that no precipitation of Mg carbonates occurred during interaction of pyroaurite with the buffer solution and that the pyroaurite remained stable for a period of 3 days with no evidence of dissolution (see S.I. Section S1. for details of the control experiments).

For the exchange experiments, ICP-MS analysis of the solution was used to trace the movement of stable Mg isotopes between the pyroaurite and solution. ICP-MS data for aqueous solution (Figure 6.1) were used to determine the concentration of Mg in solution. Figure 6.1 illustrates that the concentration of Mg in solution immediately changes upon contact with the pyroaurite at day 0, decreasing from an initial concentration of ~540  $\mu\text{M}$  to

a concentration of  $\sim 435 \mu\text{M}$  (0 days, Table 6.1). The total Mg content of the solution continues to decrease after initial contact from  $\sim 435 \mu\text{M}$  (0 days) to  $\sim 230 \mu\text{M}$  after 3 days (Table 6.1), and eventually appears to stabilise at  $\sim 220 \mu\text{M}$  from days 10–90.

**Table 6.1** Mg concentration and Mg fraction

Sample	Time	Concentration	Fraction Mg		
		Total Mg ( $\mu\text{M}$ )	$f^{24}\text{Mg}$	$f^{25}\text{Mg}$	$f^{26}\text{Mg}$
pyroaurite	NA	16161.6	0.74	0.11	0.15
(dup)	NA	16342.8	0.74	0.11	0.15
Mg <sup>2+</sup>	NA	530.1	0.01	0.99	0.01
(dup)	NA	561.2	0.01	0.99	0.00
0 days	0.1	440.0	0.28	0.66	0.05
(dup)	0.1	430.2	0.27	0.68	0.05
1 days	1	246.8	0.47	0.44	0.09
(dup)	1	260.0	0.46	0.45	0.09
3 days	3	230.3	0.49	0.40	0.10
(dup)	3	232.1	0.51	0.40	0.09
5 days	5	202.5	0.51	0.37	0.12
(dup)	5	203.2	0.51	0.39	0.09
7 days	7	224.2	0.55	0.34	0.10
(dup)	7	172.8	0.56	0.34	0.10
10 days	10	200.7	0.57	0.33	0.11
(dup)	10	193.5	0.54	0.36	0.10
15 days	15	224.7	0.60	0.28	0.12
(dup)	15	234.2	0.57	0.32	0.11
30 days	30	211.1	0.60	0.28	0.12
(dup)	30	211.6	0.60	0.28	0.12
60 days	60	205.6	0.63	0.25	0.12
(dup)	60	223.8	0.62	0.25	0.12
90 days	90	212.7	0.63	0.25	0.12
(dup)	90	216.3	0.63	0.24	0.12

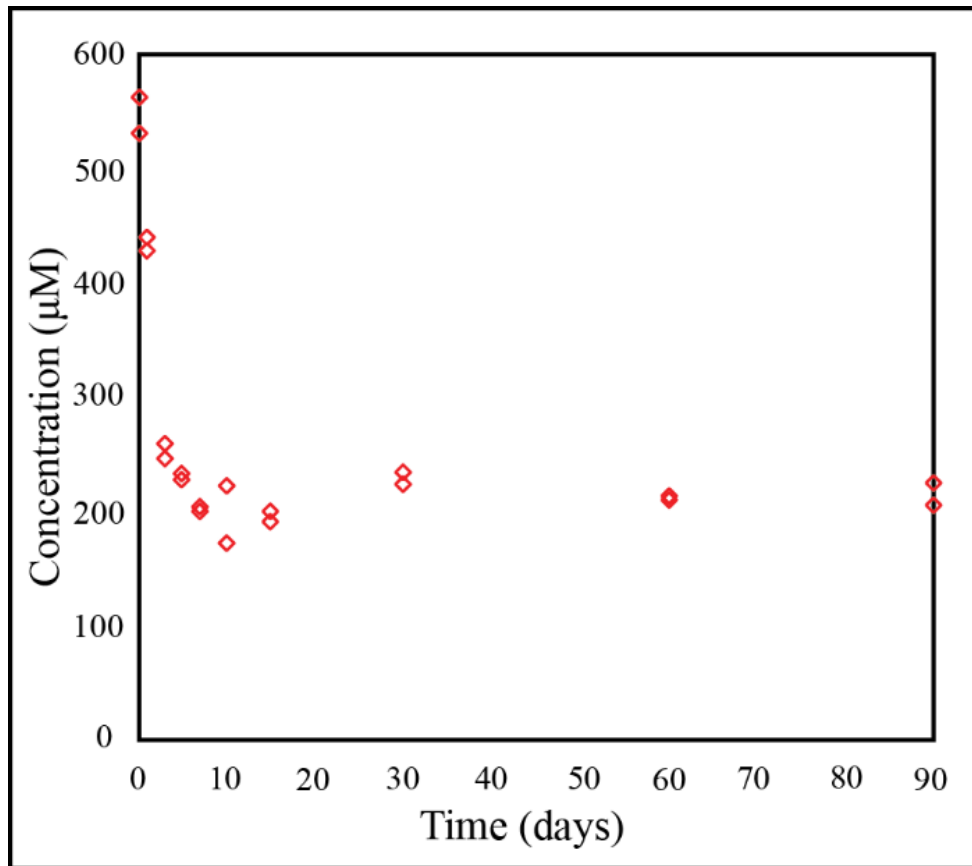


**Figure 6.1** Graph of the total Mg concentration in solution over time. Duplicate results are included for each time step.

Figure 6.2 reveals that changes occur to the stable Mg isotope composition of the solution throughout the experiment. The initial stable Mg isotope composition of the solution was  $\geq 99\%$   $^{25}\text{Mg}$  before contact with the pyroaurite (Table 6.1). However, upon contact with the pyroaurite, the stable Mg isotope composition of the solution begins to change immediately (Figure 6.2). Over the first 24 hours of the experiment the fraction of  $^{25}\text{Mg}$  in solution changed from 0.99 (i.e., unreacted solution) to 0.67 after approximately 2 minutes (i.e., for the 0 day samples made by combining the pyroaurite and solution and then immediately sacrificing the 0 day reactors) to 0.45 in the 1 day reactors (Table 6.1).  $f^{24}\text{Mg}$  in the solution increased, from  $\leq 0.01$  to 0.27 upon contact with the pyroaurite, and it continued to increase in magnitude, reaching a value of 0.47 within the first 24 hours of the experiment (Table 6.1, Figure 6.2). The value of  $f^{26}\text{Mg}$  increased to a lesser extent than  $f^{24}\text{Mg}$  from  $\leq 0.01$  for the

unreacted solution to a value of 0.09 within the first 24 hours of the experiment. The larger increase in  $f^{24}\text{Mg}$  compared to that for  $f^{26}\text{Mg}$  is likely due to the variation in abundance between  $^{24}\text{Mg}$  and  $^{26}\text{Mg}$  in the starting pyroaurite, with  $^{24}\text{Mg}$  being ~6 times more prevalent in the original material (i.e., the pyroaurite starting composition was 76.2 %  $^{24}\text{Mg}$ , 12.4 %  $^{25}\text{Mg}$ , 11.3 %  $^{26}\text{Mg}$ ). After the highly transient first 24 hours, the rate of change for the stable Mg isotopic composition of solution begins to slow (Figure 6.2). The  $f^{25}\text{Mg}$  of the solution continues to decline from 1 to 15 days, from a value of 0.45 to 0.30.  $f^{24}\text{Mg}$  increases from 0.47 to 0.59 and  $f^{26}\text{Mg}$  increases from 0.09 to 0.12 over the same period of time (Table 6.1). Beyond 15 days, the composition appears to be approaching a steady state, with the composition approaching  $f^{25}\text{Mg}$  0.25,  $f^{24}\text{Mg}$  0.63 and  $f^{26}\text{Mg}$  0.12 after 90 days of reaction (Table 6.1).

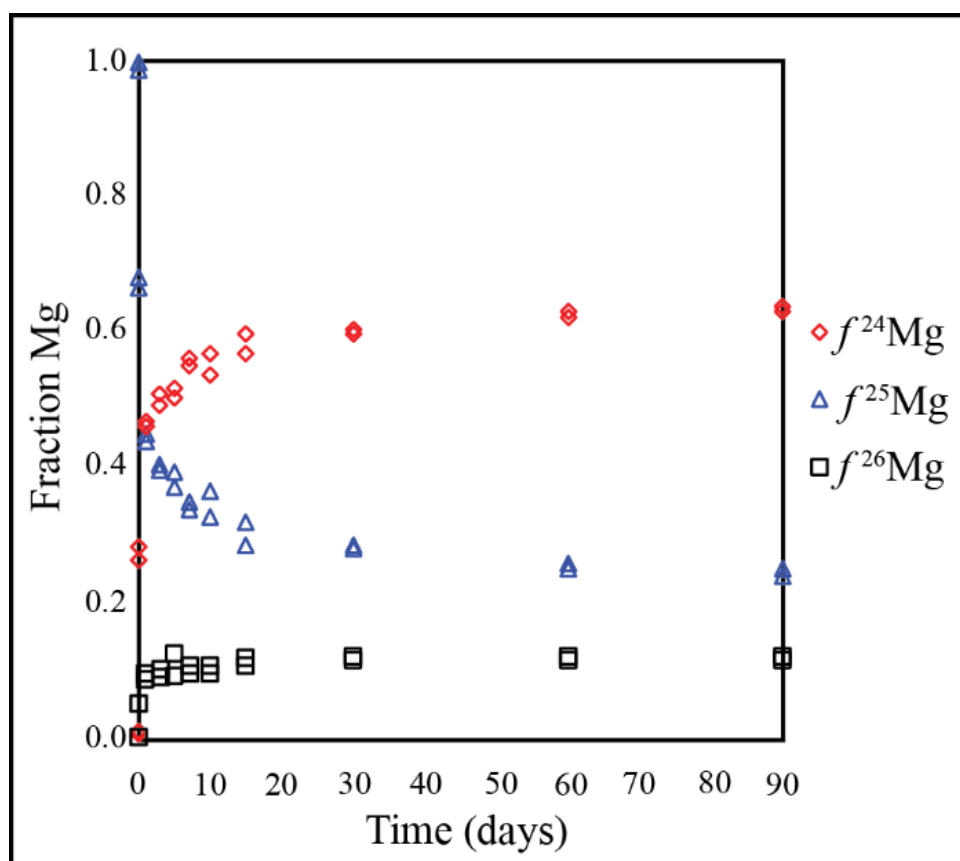


**Figure 6.2** Graph of the evolving fraction Mg composition of the solution over time. Duplicate results are included for each time step.

The changing stable Mg isotopic composition of the solution indicates that interactions are occurring between the pyroaurite and solution. The loss of Mg from solution observed in Figure 6.2 could be occurring due to (1) absorption and exchange with the pyroaurite, (2) adsorption onto the surface of the pyroaurite grain, or (3) through formation of Mg-carbonate minerals. Results from the control experiments (see S.I. Section S1.) indicate that the solution was undersaturated with respect to Mg-carbonates, with the formation of new Mg-carbonate minerals likely kinetically inhibited by the hydration shell surrounding  $\text{Mg}^{2+}_{(\text{aq})}$  ions. XRD patterns were collected for the pyroaurite over the course of the experiment to confirm that no new carbonate mineral phases were forming, and to trace changes to crystallite size of the pyroaurite. Figure 6.3 compares the intensity-normalised (0 0 3) peak of pyroaurite (Figure 6.3a) and whole XRD patterns (Figure 6.3b) of the starting pyroaurite, as well as the pyroaurite after 1, 5, 10, 30 and 60 days of the experiment. Figure 6.3b shows there is no formation of other hydrated Mg-carbonate minerals occurring. The only trace phase that appears is trona  $[\text{Na}_3(\text{CO}_3)(\text{HCO}_3)\cdot 2(\text{H}_2\text{O})]$ , a hydrated sodium carbonate mineral that is likely forming due to incomplete removal of the aqueous solution during washing and drying of the pyroaurite after the experiment had been completed (with the sodium likely sourced from the sodium carbonate and sodium bicarbonate salts used to make the carbonate–bicarbonate buffer).

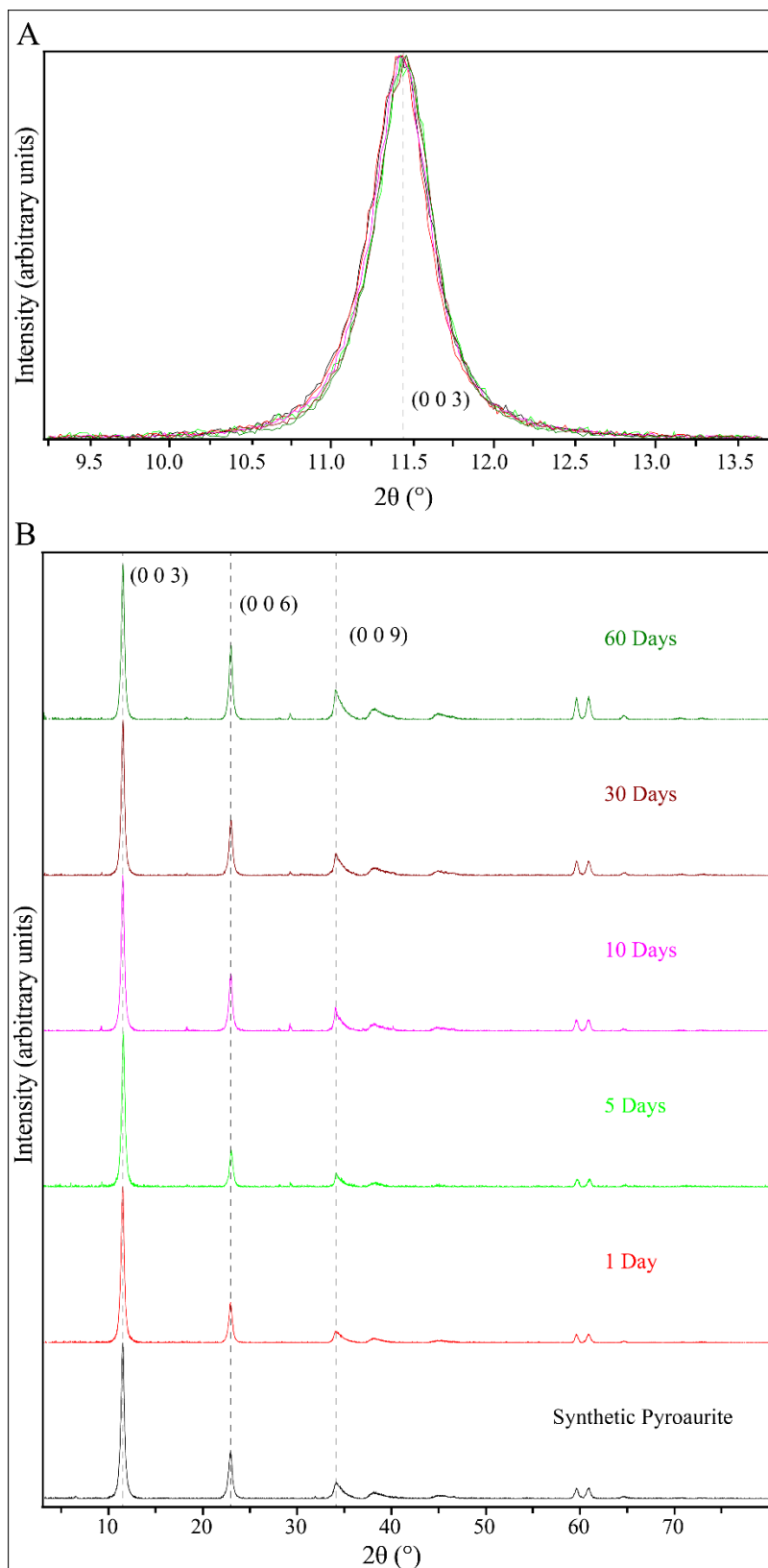


**Figure 6.3** Comparison between normalised XRD patterns of **a)** the (0 0 3) peak and **b)** whole pattern for the pyroaurite before reaction and after 1, 10 and 60 days. XRD patterns are normalised to intensity the (0 0 3) peak ( $\sim 12^\circ 2\theta$ ) to allow for comparison between individual patterns.

The peaks shapes for pyroaurite in Figure 6.3 potentially indicate changes to the crystal structure of the pyroaurite over time. The (0 0 3) reflection, the most prominent pyroaurite reflection, and the one to which the patterns were normalised shows no obvious change in peak shape with time (Figure 6.3a). However, there is a discernible sharpening and increase in relative intensity of the (0 0 6) and (0 0 9) reflections in patterns of pyroaurite from 10 days onwards (Figure 6.3b). This could be attributed to the crystal undergoing regrowth and improving the higher order symmetry of the crystal structure, or it could be due to other factors such as specimen transparency during analysis. Crystallite size and strain calculations that were made using Rietveld refinements in Topas V.5 (see S.I. Section S4.) to assess whether pyroaurite crystallites were changing size (an indication of mineral dissolution and reprecipitation). The results (reported as *LVol-IB* in S.I. Section S4.) indicate there is no discernible increase in crystallite size over time, with *LVol-IB* values staying stable at ~15 nm from the starting pyroaurite up to 60 days of reaction, and strain values slightly decreasing over time from 0.001 to 0.000. The constant crystallite size over time indicates that neither dissolution nor crystal regrowth is occurring on a large scale, making it likely that the changes to the (0 0 6) and (0 0 9) reflections are artefacts of sample preparation rather than the result of structural changes to the pyroaurite over time. The constant crystallite size of pyroaurite is likely occurring as dissolution and precipitation rates are balanced, with excess dissolution prevented by the use of the carbonate-bicarbonate pH buffer to ensure maintenance of alkaline conditions (as confirmed by one of the control experiments, see S.I. S.I. Section S1.). Another likely reason for the lack of variation in the crystallite size is that formation of more pyroaurite is inhibited in the reactions as there is no source of Fe<sup>3+</sup> in the system, other than the Fe<sup>3+</sup> that is already held in the pyroaurite structure. Thus, substantial dissolution and regrowth of pyroaurite may require introduction of an additional source of Fe into solution.

The changes that are occurring to the solution composition, and the lack of new pyroaurite or other Mg-carbonate phases forming in the experiments, indicates that exchange of stable Mg isotopes is occurring between the  $\text{Mg}^{2+}_{(\text{aq})}$  in solution and the surface Mg of the pyroaurite. The net loss of Mg from solution indicates that the system was supersaturated with regards to Mg, leading it to sorb onto the surface of the pyroaurite (Figure 6.1). However the changing composition of the remaining Mg in solution (Figure 6.2) illustrates that over time  $^{24}\text{Mg}$  and  $^{26}\text{Mg}$  are entering solution from the pyroaurite. This is likely occurring via coupled dissolution-reprecipitation reactions which are exchanging the Mg in solution and in pyroaurite without affecting the bulk pyroaurite sample. This indicates that pyroaurite does undergo Mg exchange with fluids from the local environment, whether that is pore water in ultramafic mine tailings (such as the pyroaurite forming in the tailings at the Woodsreef chrysotile mine, Turvey et al., in prep-a/Chapter 4, or the hydrotalcites in the tailings at the Mount Keith nickel mine, Grguric, 2003; Wilson et al., 2014), mine pit water (when using hydrotalcites to trap heavy metals and other contaminants, Douglas et al., 2010; Douglas et al., 2014) or rainfall falling onto natural ultramafic outcrops that contain hydrotalcites (such as the exposed serpentinites at the Dundas mineral field, Melchiorre et al., 2016; Melchiorre et al., 2018; Turvey et al., in prep-b/Chapter 5).

### **6.3.2 Degree of Mg exchange**

The method of Handler et al. (2014) has been used in multiple previous studies to estimate the amount of exchange that a mineral has undergone (Friedrich et al., 2015b; Handler et al., 2014); however, it assumes that any reacted mineral (in this case, pyroaurite) is constantly in isotopic equilibrium with the remaining solution, and it is thus called the ‘homogeneous model’ by Gorski and Fantle (2017). Another model that could be used to describe the degree of Mg exchange is the ‘heterogeneous model’, which assumes that the recrystallised solid is

not in isotopic equilibrium with the fluid as the fluid composition is continuously changing (Gorski and Fantle, 2017). A third model uses a combination of the heterogeneous and homogeneous models, where some of the new material is still considered to be in equilibrium with the solution; the ‘exchanged’ fraction (after the homogeneous model); and some material is no longer in equilibrium and is referred to as the ‘buried’ fraction (after the heterogeneous model) (Joshi et al., 2017). Joshi et al. (2017) used a combined model to estimate how much Fe(II) in goethite and solution was ‘exchanged’ (homogeneous) and ‘buried’ (heterogeneous). They found that for Fe(II) in goethite, the calculated extent of exchange employing their model may be significantly lower than that calculated using the method of Handler et al. (2014). This could mean that the amount of Mg exchange calculated using the homogeneous model (Eq. 2) represents the upper bound for this process in minerals, including in pyroaurite. When considering the application of pyroaurite as a sink for aqueous and atmospheric contaminants it is more appropriate to assume the homogeneous model, which will give the highest amount of Mg exchange (Gorski and Fantle, 2017) and so would represent the ‘worst case scenario’ for exchange, where there is the most potential for divalent cations that are substituted into sites for structural Mg to be exchanged back into the local environment (e.g., in a tailings pond, in scenarios such as those described by Douglas et al., 2010 and Douglas et al., 2014).

Calculating the relative amount of Mg in the solid in equilibrium with the fluid, using Eq. 2, gives an estimate of the degree of Mg exchange that has occurred between the solution and pyroaurite over time. Figure 6.4 shows the degree of Mg exchange that occurs over time, calculated using  $f^{25}\text{Mg}$  values.  $f^{25}\text{Mg}$  was used to trace the exchange as it has the greatest isotopic contrast between dissolved Mg and structural Mg in pyroaurite (Figure 6.2, Table 6.2). 1.9 % of Mg in the pyroaurite becomes equilibrated with the Mg in solution upon contact with the solution as seen in the 0 day samples (produced by combining the pyroaurite

and solution and then immediately sacrificing the reactors) and 5.4 % was exchanged in the first 24 hours of the experiment (Table 6.2). After the first 24 hours of rapid exchange, a more steady increase in the amount of Mg exchanged between pyroaurite and solution occurs for the remainder of the experiment, with up to 29.0 % of Mg exchanged after 90 days when using  $f^{25}\text{Mg}$ . For the majority of time points, this increase occurs in an approximately linear manner, with the exception of the data point for 15 days which is uncharacteristically high at 17.1 % (when calculated using  $f^{25}\text{Mg}$ ). The % Mg exchange values were also calculated using  $f^{24}\text{Mg}$  and  $f^{26}\text{Mg}$  (S.I. Section S2.). Using the other stable isotopes of Mg results in different % Mg exchange values. The use of  $f^{24}\text{Mg}$  in calculations produced similar results as for  $f^{25}\text{Mg}$  (S.I. Section S2., Figure S5.), with an increasing divergence between the values obtained using  $f^{24}\text{Mg}$  and  $f^{25}\text{Mg}$  with higher degrees of exchange. Using  $f^{26}\text{Mg}$  for the calculation leads to significantly lower % Mg exchange values, a discrepancy that likely occurs as there is less isotopic contrast between the dissolved Mg and structural Mg than there is for the  $^{24}\text{Mg}$  and  $^{25}\text{Mg}$ .

**Table 6.2** % Mg Exchange

Sample	Time	% Mg Exchange*
0 days	0.1	1.9
1 days	1	5.4
3 days	3	6.8
5 days	5	7.5
7 days	7	9.4
10 days	10	10.4
15 days	15	17.1
30 days	30	19.8
60 days	60	26.0
90 days	90	29.1

\*Calculated using  $f^{25}\text{Mg}$

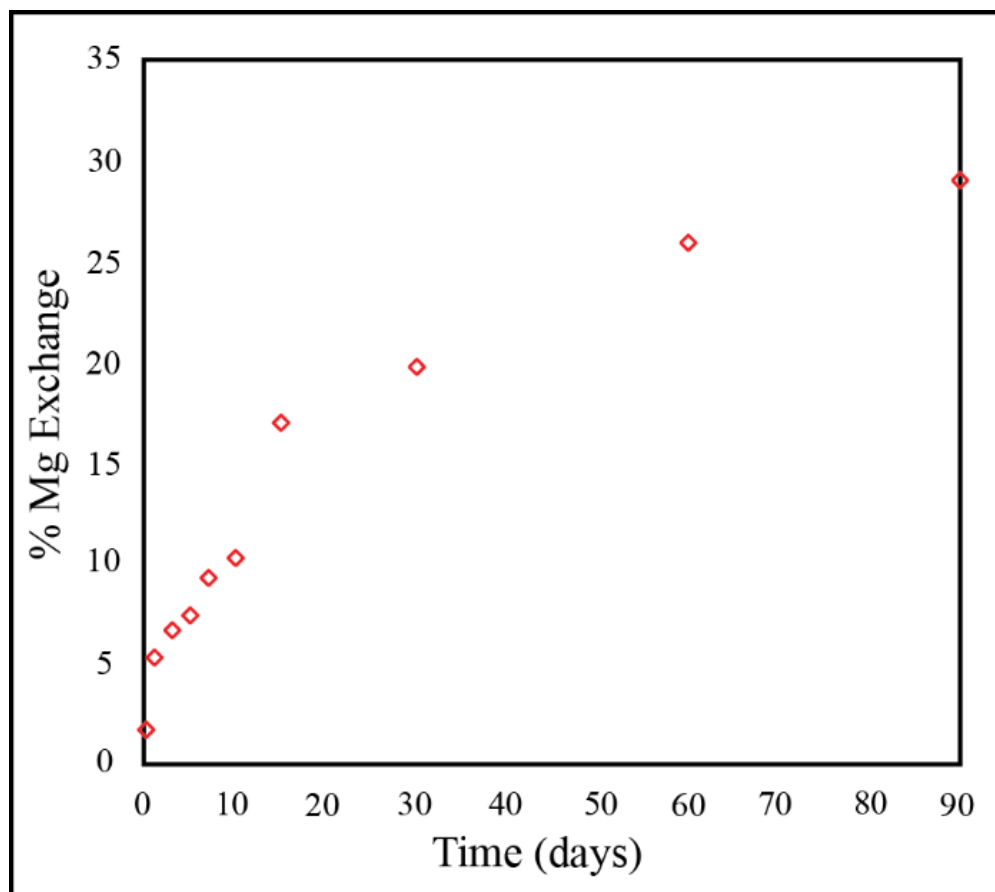


**Figure 6.4** Graph of the % Mg exchange over time calculated using  $f^{25}\text{Mg}$ .

It is estimated that 31.8% of Mg in pyroaurite is located at the surface using methods reported previously in Handler et al. (2014) for calculating the degree of exchange and the proportion of an element that is exposed at the surface of a mineral. By the end of the experiment, after 90 days of reaction, 29.1% of the Mg in the pyroaurite was in equilibrium with the solution. Combined with the crystallite size data, which indicated there was no apparent change in crystallite size over time, it is likely that the majority of exchange is occurring between the solution and Mg at the surface of the pyroaurite and that if exchange is occurring for Mg held deeper into the pyroaurite structure it is not leading to large scale recrystallisation that would alter the crystallite size of the pyroaurite.

Previous studies have found that dissolution of Mg-bearing minerals typically leads to the formation of a  $^{24}\text{Mg}$ -enriched solution and a  $^{25}\text{Mg}$ - and  $^{26}\text{Mg}$ -enriched weathering residue

(Teng, 2017; Turvey et al., in prep-b; Wimpenny et al., 2014; Wimpenny et al., 2010). Wimpenny et al. (2014) used exchange experiments to determine that the Mg that is absorbed onto the interlayer spaces and surface sites of illite  $[K_{0.6}(H_3O)_{0.4}Al_{1.3}Mg_{0.3}Fe^{2+}_{0.1}Si_{3.5}O_{10}(OH)_2 \cdot H_2O]$ , montmorillonite  $[(M_y^+nH_2O)(Al_{2-y}Mg_y)Si_4O_{10}(OH)_2]$  where  $M^+$  is the monovalent cation] and kaolinite  $[Al_2Si_2O_5(OH)_4]$  is more labile and typically enriched in isotopically light  $^{24}Mg$ . The exchange that is occurring in pyroaurite in this study is likely analogous to what is observed for silicate clay minerals in Wimpenny et al. (2014) and Wimpenny et al. (2010). Except instead of seeing the loss of this labile Mg to solution we are seeing exchange of the labile Mg for  $^{25}Mg$ . Comparisons can also be drawn between the exchange of Mg in hydrotalcites and the work Neumann et al. (2015) who investigated the exchange of aqueous  $^{57}Fe(II)$  and structural Fe(III) in nontronite  $[(M_y^+nH_2O)Fe_2^{3+}(Al_{4-x}Al_x)Si_4O_{10}(OH)_2]$ . Neumann et al. (2015) observed similar trends, with fast initial decreases in the concentration of aqueous  $^{57}Fe$ , and stabilization after about 50 days of reaction. The authors also estimated that 5–20 % of structural Fe in the clay exchanged with solution, which is significantly higher than the amount of Fe which is exposed directly to solution without considering the interlayer spaces of smectites (Neumann et al., 2015). The structural and behavioural similarities between Fe-bearing smectite minerals such as nontronite and Mg hydrotalcites such as pyroaurite, along with the similar results for isotope exchange makes it likely that we are seeing similar processes occurring in both minerals groups. It is most likely that the isotopes of divalent and trivalent cations in both cationic and anionic clay minerals, such as nontronite and pyroaurite respectively, are able to exchange with isotopes of the same element in solution via their interlayer galleries, and that actual exchange rates may be higher if exchange occurs not along through exposed mineral surfaces but within individual clay layers.

### **6.3.3 Implications for tracing the origins of hydrotalcite minerals and for contaminant release**

The exchange of Mg between pyroaurite and solution poses an issue when considering the use of stable Mg isotopes to trace the origins of pyroaurite and other hydrotalcites. As stable Mg isotopes only undergo significant fractionation due to low temperature or surface alteration processes (Black et al., 2008; Bolou-Bi et al., 2010; Opfergelt et al., 2012; Shirokova et al., 2013; Teng et al., 2010; Tipper et al., 2010) it has been proposed that they may provide one way of distinguishing between low-temperature and high-temperature hydrotalcite minerals (Turvey et al., in prep-a/Chapter 4; Turvey et al., in prep-b/Chapter 5). Given the rapid exchange of stable C and O isotopes between hydrotalcites and solution, a more robust isotopic tracer (i.e., one that is less susceptible to exchange) might be used to distinguish between low-temperature hydrotalcites that capture atmospheric CO<sub>2</sub> during their formation in mineral wastes, from their high-temperature counterparts that exchange metamorphic CO<sub>2</sub> for atmospheric CO<sub>2</sub>. However, the results of this study indicate that the stable Mg isotope compositions of naturally occurring hydrotalcite minerals are likely exchanging with the local environment in a similar manner to stable C and O isotopes. This helps to elucidate the results of Turvey et al. (in prep-b/Chapter 5) who found a similar Mg isotope composition for hydrotalcites that were known to have a hydrothermal origin, and those that were known to have a sedimentary origin across various ultramafic mine sites and natural serpentinite outcrops. At sites where hydrotalcites are sequestering CO<sub>2</sub> via carbon mineralisation (i.e., via carbonation of brucite), starting stable Mg, C and O isotope compositions will be overprinted by interactions with the Mg- and carbonate-rich fluids that are created during the weathering of ultramafic rock. In the case of hydrotalcites in tailings storage facilities, exchange of Mg with the local environment means that hydrotalcites originally formed by the high-temperature alteration of spinel minerals will rapidly lose their

original stable Mg isotope signature and adopt a signature indicative of formation in a low-temperature environment as they interact with pore waters that contain Mg released by brucite and serpentine dissolution. This could potentially invalidate the use of stable Mg isotopes as a method for differentiating hydrotalcite formation pathways as was suggested in Turvey et al. (in prep-b)/Chapter 5, as original compositions will over time be erased through interactions with Mg-rich fluids within the tailings material, leading to indistinguishable Mg compositions for hydrotalcite minerals, regardless of formation pathway.

The exchange occurring between pyroaurite and aqueous  $Mg^{2+}$  also has larger implications for how hydrotalcite minerals will sequester contaminants over time. It has been well established that hydrotalcite minerals can undergo exchange with aqueous anions that are present in sufficient concentrations (Bish, 1980; Bish and Brindley, 1977; Miyata, 1983). The propensity of pyroaurite to also undergo Mg exchange with solution implies that it is likely that hydrotalcites are exchanging both their interlayer anions as well as the divalent metal cations that are held in the hydroxide layers of the mineral. The fate of trivalent cations in the hydrotalcite structure (such as the  $Fe^{3+}$  in pyroaurite) remains an open question; however, it is unlikely that they will exchange, as dissolution studies have revealed that pyroaurite-type synthetic hydrotalcites tend to leave behind an Fe(III) enriched phase during dissolution (Imran et al., 2016). Hydrotalcites are being used to capture uranium and other contaminants from wastewater (Douglas et al., 2014; Douglas et al., 2010), and they have been considered for sequestering atmospheric  $CO_2$  (Gras et al., 2017; Mills et al., 2011; Oskierski et al., 2013; Turvey et al., 2017; Turvey et al., in review/Chapter 3; Turvey et al., in prep-a/Chapter 4; Turvey et al., in prep-b/Chapter 5; Woodhouse, 2006). These results indicate that hydrotalcites may continue to undergo both cation and anion exchange with the local environment where initially they have been selected to act as reservoirs for

contaminants. This may be important to consider when sequestering atmospheric CO<sub>2</sub> and other industrial contaminants within hydrotalcites as they may potentially rerelease contaminants into solution via anion exchange and structural cation exchange.

#### **6.4 Acknowledgements**

Funding for this work was provided by an Australian Research Council Discovery Early Career Researcher Award and grants from Carbon Management Canada and the New South Wales Department of Industry to S.A.W. and from an Australian Research Council Discovery Early Career Researcher Award (DE170100417) to A.J.F. We would like to thank Massimo Raveggi and Yona Nebel-Jacobsen for their assistance with ICP-MS analysis, Sally Finora for her BET surface area analysis of the pyroaurite, Jessica Hamilton for her assistance using PHREEQC, Hans Oskeirski and Vasileios Mavromatis for their insights in Mg isotope research and to Helen Brand for her insight into X-ray diffraction and crystallography.

#### **6.5 References**

- Beinlich, A., Mavromatis, V., Austrheim, H., and Oelkers, E.H. (2014) Inter-mineral Mg isotope fractionation during hydrothermal ultramafic rock alteration - Implications for the global Mg-cycle. *Earth and Planetary Science letters*, 392(166-176).
- Beinlich, A., and Austrheim, H. (2012) In situ sequestration of atmospheric CO<sub>2</sub> at low temperature and surface cracking of serpentinized peridotite in mine shafts. *Chemical Geology*, 332–333, 32-44.
- Bish, D.L. (1980) Anion-exchange in takovite: applications to other hydrotalcite minerals. *Bulletin Mineralogie*, 103, 170-175.
- Bish, D.L., and Brindley, G.W. (1977) A reinvestigation of takovite, a nickel aluminium hydroxy-carbonate of the pyroaurite group. *American Mineralogist*, 62, 458-464.

- Black, J.R., Epstein, E., Rains, W.D., Yin, Q.-z., and Casey, W.H. (2008) Magnesium-Isotope Fractionation During Plant Growth. *Environmental Science & Technology*, 42(21), 7831-7836.
- Bolou-Bi, E.B., Poszwa, A., Leyval, C., and Vigier, N. (2010) Experimental determination of magnesium isotope fractionation during higher plant growth. *Geochimica et Cosmochimica Acta*, 74(9), 2523-2537.
- Bourdon, B., Tipper, E.T., Fitoussi, C., and Stracke, A. (2010) Chondritic Mg isotope composition of the Earth. *Geochimica et Cosmochimica Acta*, 74(17), 5069-5083.
- Cheary, R.W., and Coelho, A. (1992) A fundamental parameters approach to X-ray line-profile fitting. *Journal of Applied Crystallography*, 25(2), 109-121.
- Douglas, G., Shackleton, M., and Woods, P. (2014) Hydrotalcite formation facilitates effective contaminant and radionuclide removal from acidic uranium mine barren lixiviant. *Applied Geochemistry*, 42(0), 27-37.
- Douglas, G.B., Wendling, L.A., Pleysier, R., and Trefry, M. (2010) Hydrotalcite Formation for Contaminant Removal from Ranger Mine Process Water. *MINE WATER AND THE ENVIRONMENT*, 29, 108-115.
- Evans, D.G., and Slade, R.C.T. (2006) Structural Aspects of layered Double Hydroxides. In X. Duan, and D.G. Evans, Eds. *Layered Double Hydroxides*, 119, p. 1-87. Springer.
- Friedrich, A.J., Beard, B.L., Rosso, K.M., Scherer, M.M., Spicuzza, M.J., Valley, J.W., and Johnson, C.M. (2015a) Low temperature, non-stoichiometric oxygen-isotope exchange coupled to Fe(II)-goethite interactions. *Geochimica et Cosmochimica Acta*, 160, 38-54.
- Friedrich, A.J., Helgeson, M., Liu, C., Wang, C., Rosso, K.M., and Scherer, M.M. (2015b) Iron Atom Exchange between Hematite and Aqueous Fe(II). *Environmental Science & Technology*, 49(14), 8479-8486.

- Friedrich, A.J., Spicuzza, M.J., and Scherer, M.M. (2016) Oxygen Isotope Evidence for Mn(II)-Catalyzed Recrystallization of Manganite ( $\gamma$ -MnOOH). *Environmental Science & Technology*, 50(12), 6374-6380.
- Gorski, C.A., and Fantle, M.S. (2017) Stable mineral recrystallization in low temperature aqueous systems: A critical review. *Geochimica et Cosmochimica Acta*, 198, 439-465.
- Gras, A., Beaudoin, G., Molson, J., Plante, B., Bussière, B., Lemieux, J.M., and Dupont, P.P. (2017) Isotopic evidence of passive mineral carbonation in mine wastes from the Dumont Nickel Project (Abitibi, Quebec). *International Journal of Greenhouse Gas Control*, 60, 10-23.
- Grguric, B.A. (2003) Minerals of the MKD5 nickel deposit, Mount Keith, Western Australia. *Australian Journal of Mineralogy*, 9(2), 55-71.
- Grguric, B.A., Madsen, I.C., and Pring, A. (2001) Woodallite, a new chromium analogue of iowaite from the Mount Keith nickel deposit, Western Australia. *Mineralogical Magazine*, 65(3), 427-435.
- Handler, M.R., Baker, J.A., Schiller, M., Bennett, V.C., and Yaxley, G.M. (2009) Magnesium stable isotope composition of Earth's upper mantle. *Earth and Planetary Science Letters*, 282(1), 306-313.
- Handler, R.M., Friedrich, A.J., Johnson, C.M., Rosso, K.M., Beard, B.L., Wang, C., Latta, D.E., Neumann, A., Pasakarnis, T., Premaratne, W.A.P.J., and Scherer, M.M. (2014) Fe(II)-Catalysed Recrystallization of Goethite Revisited *Environmental Science & Technology*, 48, 11302-11311.
- Hostetler, P.B., Coleman, R.G., A., M.F., and Evans, B.W. (1966) Brucite in Alpine Serpentinites. *The American Mineralogist*, 51, 75-98.

- Imran, A., López-Rayó, S., Magid, J., and Hansen, H.C.B. (2016) Dissolution kinetics of pyroaurite-type layered double hydroxide doped with Zn: Perspectives for pH controlled micronutrient release. *Applied Clay Science*, 123(Supplement C), 56-63.
- Johnson, C.M., Beard, B.L., Albarède, F., Meeting, A.G.U., and Meeting, C.G.U. (2004) *Geochemistry of Non-traditional Stable Isotopes*. Mineralogical Society of America.
- Joshi, P., Fantle, M.S., Larese-Casanova, P., and Gorski, C.A. (2017) Susceptibility of Goethite to Fe<sup>2+</sup>-Catalyzed Recrystallization over Time. *Environmental Science & Technology*, 51(20), 11681-11691.
- Li, W.-Y., Teng, F.-Z., Ke, S., Rudnick, R.L., Gao, S., Wu, F.-Y., and Chappell, B.W. (2010) Heterogeneous magnesium isotopic composition of the upper continental crust. *Geochimica et Cosmochimica Acta*, 74(23), 6867-6884.
- Li, W., Beard, B.L., Li, C., Xu, H., and Johnson, C.M. (2015) Experimental calibration of Mg isotope fractionation between dolomite and aqueous solution and its geological implications. *Geochimica et Cosmochimica Acta*, 157, 164-181.
- Liu, S. A., Teng, F. Z., He, Y., Ke, S., and Li, S. (2010) Investigation of magnesium isotope fractionation during granite differentiation: Implication for Mg isotopic composition of the continental crust. *Earth and Planetary Science Letters*, 297(3), 646-654.
- Mavromatis, V., Bundeleva, I.A., Shirokova, L.S., Millo, C., Pokrovsky, O.S., Bénézech, P., Ader, M., and Oelkers, E.H. (2015) The continuous re-equilibration of carbon isotope compositions of hydrous Mg carbonates in the presence of cyanobacteria. *Chemical Geology*, 404(Supplement C), 41-51.
- Mavromatis, V., Meister, P., and Oelkers, E.H. (2014a) Using stable Mg isotopes to distinguish dolomite formation mechanisms: A case study from the Peru Margin. *Chemical Geology*, 385, 84-91.

- Mavromatis, V., Pearce, C.R., Shirokova, L.S., Bundeleva, I.A., Pokrovsky, O.S., Benezeth, P., and Oelkers, E.H. (2012) Magnesium isotope fractionation during hydrous magnesium carbonate precipitation with and without cyanobacteria. *Geochimica et Cosmochimica Acta*, 76, 161-174.
- Mavromatis, V., Prokushkin, A.S., Pokrovsky, O.S., Viers, J., and Korets, M.A. (2014b) Magnesium isotopes in permafrost-dominated Central Siberian larch forest watersheds. *Geochimica et Cosmochimica Acta*, 147, 76-89.
- Melchiorre, E.B., Bottrill, R., Huss, G.R., and Lopez, A. (2016) Conditions of Stichtite ( $\text{Mg}_6\text{Cr}_2(\text{OH})_{16}[\text{CO}_3] \cdot 4\text{H}_2\text{O}$ ) formation and its Geochemical and Isotope Record of Early Phanerozoic Serpentinizing Environments. *Geochimica et Cosmochimica Acta*.
- Melchiorre, E.B., Bottrill, R., Huss, G.R., and Lopez, A. (2018) The Early Earth Geochemical and Isotope Record of Serpentinizing Environments from Archean Stichtite ( $\text{Mg}_6\text{Cr}_2(\text{OH})_{16}[\text{CO}_3] \cdot 4\text{H}_2\text{O}$ ). *Precambrian Research*.
- Mikutta, C., Wiederhold, J.G., Cirpka, O.A., Hofstetter, T.B., Bourdon, B., and Gunten, U.V. (2009) Iron isotope fractionation and atom exchange during sorption of ferrous iron to mineral surfaces. *Geochimica et Cosmochimica Acta*, 73(7), 1795-1812.
- Mills, S.J., Christy, A.G., Génin, J.M.R., Kameda, T., and Colombo, F. (2012) Nomenclature of the hydrotalcite supergroup: natural layered double hydroxides. *Mineralogical Magazine*, 76(5), 1289-1336.
- Mills, S.J., Whitfield, P.S., Wilson, S.A., Woodhouse, J.N., Dipple, G.M., Raudsepp, M., and Francis, C.A. (2011) The crystal structure of stichtite, re-examination of barbertonite, and the nature of polytypism in MgCr hydrotalcites. *American Mineralogist*, 96(1), 179-187.

- Miyata, S. (1983) Anion-exchange properties of hydrotalcite-like compounds. *Clays and Clay Minerals*, 31(4), 305-311.
- Mumpton, F.A., Jaffe, H.W., and S., T.C. (1965) Coalingite, a new mineral from the New Idria Serpentinite, Fresno and San Benito counties, California. *The American Mineralogist*, 50, 1893-1913.
- Mumpton, F.A., and Thompson, C.S. (1966) The Stability of Brucite in the Weathering Zone of the New Idria Serpentinite. *Clays and Clay Minerals*, 14(1), 249-257.
- Neumann, A., Wu, L., Li, W., Beard, B.L., Johnson, C.M., Rosso, K.M., Friedrich, A.J., and Scherer, M.M. (2015) Atom Exchange between Aqueous Fe(II) and Structural Fe in Clay Minerals. *Environmental Science & Technology*, 49(5), 2786-2795.
- Oelkers, E.H., Berninger, U.-N., Pérez-Fernández, A., Chmeleff, J., and Mavromatis, V. (2018) The temporal evolution of magnesium isotope fractionation during hydromagnesite dissolution, precipitation, and at equilibrium. *Geochimica et Cosmochimica Acta*, 226, 36-49.
- Opfergelt, S., Georg, R.B., Delvaux, B., Cabidoche, Y.M., Burton, K.W., and Halliday, A.N. (2012) Mechanisms of magnesium isotope fractionation in volcanic soil weathering sequences, Guadeloupe. *Earth and Planetary Science Letters*, 341(Supplement C), 176-185.
- Oskierski, H.C., Dlugogorski, B.Z., and Jacobsen, G. (2013) Sequestration of atmospheric CO<sub>2</sub> in chrysotile mine tailings of the Woodsreef Asbestos Mine, Australia: Quantitative Mineralogy, isotopic fingerprinting and carbonation rates. *Chemical Geology*.
- Pedersen, H.D., Postma, D., Jakobsen, R., and Larsen, O. (2005) Fast transformation of iron oxyhydroxides by the catalytic action of aqueous Fe(II). *Geochimica et Cosmochimica Acta*, 69(16), 3967-3977.

- Shirokova, L.S., Mavromatis, V., Bundeleva, I., Pokrovsky, O.S., Benezeth, P., Gerard, E., Pearce, C., and Oelkers, E.H. (2013) Using Mg isotopes to Trace Cyanobacterially Mediated Magnesium Carbonate Precipitation in Alkaline lakes. *Aquatic Geochemistry*, 19, 1-24.
- Teng, F.-Z. (2017) Magnesium Isotope Geochemistry. *Reviews in Mineralogy & Geochemistry*, 82, 219-287.
- Teng, F.-Z., Li, W.-Y., Rudnick, R.L., and Gardner, L.R. (2010) Contrasting lithium and magnesium isotope fractionation during continental weathering. *Earth and Planetary Science Letters*, 300(1), 63-71.
- Teng, F.Z., Watkins, J., and Dauphas, N. (2017) *Non-Traditional Stable Isotopes*. De Gruyter.
- Tipper, E.T., Gaillardet, J., Louvat, P., Capmas, F., and White, A.F. (2010) Mg isotope constraints on soil pore-fluid chemistry: Evidence from Santa Cruz, California. *Geochimica et Cosmochimica Acta*, 74(14), 3883-3896.
- Turvey, C.C., Wilson, S.A., Hamilton, J.L., and Southam, G. (2017) Field-based accounting of CO<sub>2</sub> sequestration in ultramafic mine wastes using portable X-ray diffraction. *American Mineralogist*.
- Turvey, C.C., Hamilton, J.L., and Wilson, S.A. (in review) Comparison of Rietveld analysis methods for quantification of carbon dioxide fixation in ultramafic mine tailings. *American Mineralogist*, In Review.
- Turvey, C.C., Wilson, S.A., Hamilton, J.L., Tait, A.W., McCutcheon, J., and Southam, G. (in prep-a) Hydrotalcites as a carbon sink at the Woodsreef Chrysotile Mine (NSW, Australia). In preparation.

- Turvey, C.C., Wilson, S.A., Mavromatis, V., Hamilton, J.L., Dlugogorski, B.Z., and Oskierski, H.C. (in prep-b) Tracing the origins of hydrotalcites in ultramafic wastes using stable magnesium isotopes. In preparation.
- Vucelic, M., Jones, W., and Moggridge, G.D. (1997) Cation Ordering in Synthetic Layered Double Hydroxides. *Clays and Clay Minerals*, 45(6), 803-813.
- Whitfield, P.S., Davidson, I.J., Mitchell, L.D., Wilson, S.A., and Mills, S.J. (2010) Problem Solving with the TOPAS Macro Language: Corrections and Constraints in Simulated Annealing and Rietveld Refinement. *Materials Science Forum*, 651, 11-25.
- Wiederhold, J.G. (2015) Metal Stable Isotope Signatures as Tracers in Environmental Geochemistry. *Environmental Science & Technology*, 49(5), 2606-2624.
- Wilson, S.A., Barker, S.L.L., Dipple, G.M., and Atudorei, V. (2010) Isotopic Disequilibrium during uptake of Atmospheric CO<sub>2</sub> into Mine Process Waters: Implications for CO<sub>2</sub> Sequestration. *Environmental Science & Technology*, 44, 9522-9529.
- Wilson, S.A., Harrison, A.L., Dipple, G.M., Power, I.M., Barker, S.L.L., Mayer, K.U., Fallon, S.J., Raudsepp, M., and Southam, G. (2014) Offsetting of CO<sub>2</sub> emissions by air capture in mine tailings at the Mount Keith Nickel mine, Western Australia: Rates, controls and prospects for carbon neutral mining. *International Journal of Greenhouse Gas Control*, 25, 121-140.
- Wimpenny, J., Colla, C.A., Yin, Q.-Z., Rustad, J.R., and Casey, W.H. (2014) Investigating the behaviour of Mg isotopes during the formation of clay minerals. *Geochimica et Cosmochimica Acta*, 128, 178-194.
- Wimpenny, J., Gislason, S.R., James, R.H., Gannoun, A., Pogge Von Strandmann, P.A.E., and Burton, K.W. (2010) The behaviour of Li and Mg isotopes during primary phase

dissolution and secondary mineral formation in basalt. *Geochimica et Cosmochimica Acta*, 74, 5259-5279.

Woodhouse, J. (2006) The characterization of hydrotalcite-group minerals and their anion exchange capabilities at mount keith nickel mine, Western Australia. Unpublished masters thesis.

Yang, W., Teng, F.-Z., and Zhang, H.-F. (2009) Chondritic magnesium isotopic composition of the terrestrial mantle: A case study of peridotite xenoliths from the North China craton. *Earth and Planetary Science Letters*, 288(3–4), 475-482.

# **Chapter 7**

## **Conclusions and future research**

Connor C. Turvey<sup>1</sup>

<sup>1</sup>School of Earth, Atmosphere & Environment, Monash University, Clayton, Melbourne,  
Victoria 3800, Australia

## 7.1 Outcomes of the thesis

As the threat of increasingly major changes to the Earth's climate loom, it is becoming more and more important to find methods to combat, and adapt to, anthropogenic global warming (Cleugh et al., 2011; Houghton et al., 2001; IPCC, 2005; IPCC, 2013; IPCC, 2014; Millar et al., 2017). The power of carbon sequestration is to actively lower emissions and greenhouse gas concentrations within the atmosphere (IPCC, 2014; Lackner, 2002; Lackner et al., 1995; Seifritz, 1990; Yang et al., 2008). If implemented correctly, CO<sub>2</sub> sequestration will help us to transition from the greenhouse gas heavy present to a low emissions future, buying time to change practices and adopt carbon neutral technologies (IPCC, 2014; Pacala and Socolow, 2004). Carbon mineralisation in ultramafic mine tailings has the capacity to make this change a reality for the minerals industry, which has historically been a major emitter with a poor track record on environmentally sustainable practices. Hydrotalcites are present at many of the ultramafic mine sites that have been investigated for their carbon sequestration potential. However, prior to this thesis, the impact that they could have upon carbon sequestration at mine sites was an open question. This thesis aimed to turn the presence of hydrotalcite minerals in ultramafic wastes from a relative unknown to a potential asset for carbon sequestration.

The chapters of this thesis covered a wide variety of topics, all relating to the formation of hydrotalcite minerals and carbon sequestration, including understanding how hydrotalcites form and interact with their local environment, their contribution to CO<sub>2</sub> sequestration at some mines, and how to trace their formation in the tailings environment. In **Chapter 3**, we detailed the results of using the PONCKS and Rietveld/RIR methods on synthetic tailings of a known composition, to determine which would give us the most accurate results when analysing the tailings at Woodsreef and other mineralogically similar ultramafic tailings

storage facilities. The XRD methods developed in **Chapter 3** were applied in **Chapter 4** and combined with elemental C data to estimate the amount of CO<sub>2</sub> sequestered in the tailings at the Woodsreef chrysotile mine. XRD results revealed a relationship between the formation of pyroaurite, coalingite and brucite in the tailings, and textural analysis with SEM was used to confirm the formation of pyroaurite/coalingite at the expense of Fe-rich brucite. Radiocarbon results illustrate that both hydromagnesite and hydrotalcite minerals at Woodsreef contain predominantly modern atmospheric carbon. Stable C and O data show that hydromagnesite and pyroaurite have distinct stable isotopic compositions, with pyroaurite tending to be depleted in heavy stable C and O isotopes compared to hydromagnesite. Our use of an anion exchange experiment shows that this isotopically depleted stable C and O isotopic signature is typical of carbon uptake by pyroaurite under carbon limited conditions. All of these aspects indicate that the pyroaurite and coalingite at Woodsreef are forming *in situ* within the tailings via reaction of Fe-rich brucite, with atmospheric CO<sub>2</sub>, but under carbon limited conditions.

The stable C and O isotope results of **Chapter 4** demonstrate the variable nature of hydrotalcite compositions. In **Chapter 5** we investigated the stable Mg isotope signatures of hydrotalcites, serpentine minerals and associated phases at three ultramafic sites in Australia. The aim was to understand the compositional changes that occur in the tailings as they undergo carbon mineralisation, and to also investigate the stable Mg isotopic composition of hydrotalcites and to determine if the origin of hydrotalcites can be identified by their stable Mg isotope composition. We found that serpentine minerals within the tailings at the Woodsreef chrysotile mine, Mount Keith nickel mine and Dundas mineral field are uniquely enriched in <sup>25</sup>Mg and <sup>26</sup>Mg, likely as a result of the carbonic acid leaching that occurs during carbon mineralisation via reaction with rainwater. However, there did not appear to be a significant compositional difference in stable Mg isotopes between hydrotalcite minerals

with a metamorphic origin and those that formed from the carbonation of brucite at Earth's surface conditions. This was investigated further in **Chapter 6**, where we conducted a Mg isotope exchange experiment between synthetic pyroaurite and  $^{25}\text{Mg}$  enriched aqueous  $\text{Mg}^{2+}$ . We found that exchange between the Mg in the pyroaurite and Mg in solution begins immediately upon contact between the two reservoirs and that exchange of Mg occurs largely through surface absorption. This result potentially explains the stable Mg isotope composition of hydrotalcites as seen in **Chapter 5**, as even though some of these minerals are known to have formed under hydrothermal or sedimentary circumstances, they will all be exchanging with Mg in the local environment regardless of their original stable Mg isotopic composition. This result, along with the stable C and O isotope data from **Chapter 4**, confirms how complicated the stable isotope compositions of hydrotalcites are. The continuous re-equilibration of stable Mg, C and O isotopes in these minerals with the local environment means that hydrotalcite stable isotope signatures are hard to interpret and tracing the origins of hydrotalcite minerals requires multiple lines of evidence to support any conclusions that are drawn from isotope data.

The results of the thesis will improve our ability to trace and quantify carbon sequestration at mine sites, to better understand the carbon sequestration that is occurring at the Woodsreef chrysotile mine, and to improve our fundamental understanding of how the hydrotalcite minerals form and behave in the environment.

## **7.2 Improved methods for tracing carbon mineralisation**

Tracing carbon mineralisation reactions, is essential for assessing carbon sequestration rates and the untapped potential of ultramafic mine tailings storage facilities, and other natural and engineered landscapes, to sequester  $\text{CO}_2$  (Hamilton et al., in prep-a; Turvey et al., 2017; Wilson et al., 2006; Wilson et al., 2009b). The results in this thesis help to both develop new

methods and improve upon existing methods for identifying and tracing carbonation reactions so that carbon mineralisation may be accounted for at mine sites that are undergoing passive carbonation, and during laboratory and field scale enhanced carbon mineralisation trials.

Quantitative XRD using Rietveld refinements has been a staple of carbon accounting at mine sites undergoing carbon mineralisation, as it can be used to rapidly produce results compared to other quantitative XRD methods, and can separately quantify multiple carbonate bearing phases, to differentiate between metamorphic carbonates such as calcite or magnesite and carbonates such as hydromagnesite and pyroaurite that are forming *in situ* due to interactions with the atmosphere (Oskierski et al., 2013; Wilson et al., 2006; Wilson et al., 2009b). This is particularly important for sites that contain multiple carbonate minerals, some of which are forming *in situ* within the tailings like hydromagnesite and (in some cases) hydrotalcites, whereas others are present as gangue minerals such as bedrock calcite, magnesite and, depending on context, hydrotalcites (e.g., Gras et al., 2017; Oskierski et al., 2013; Wilson et al., 2009a; Wilson et al., 2006; Wilson et al., 2009b). The main disadvantage of using Rietveld refinements for quantitative XRD is that the method becomes problematic when trying to quantify CO<sub>2</sub> sequestered in either poorly crystalline or amorphous carbonate phases (Oskierski et al., 2013; Turvey et al., 2017; Wilson et al., 2009a; Wilson et al., 2006; Wilson et al., 2009b). Various non-Rietveld methods such as using the reference intensity ratio (RIR) method have been compared with the Rietveld method in the past to help when quantifying amorphous or poorly crystalline phases such as serpentine minerals (Oskierski et al., 2013; Wilson et al., 2006; Wilson et al., 2009b). However, modified Rietveld methods that rely upon structureless pattern fitting can be used to accurately quantify the abundances of poorly ordered minerals while still maintaining the advantages that Rietveld refinements provide (Scarlett and Madsen, 2006; Turvey et al., 2017; Wilson et al., 2006; Wilson et al.,

2009b). **Chapter 3** presents the first direct comparison between the Partial Or No Known Crystal Structure method (PONKCS, Scarlett and Madsen, 2006) and the Pawley/internal standard method (Wilson et al., 2006). The results of **Chapter 3** reveal that the Pawley/internal standard method produces more accurate results for both major disordered phases, such as serpentine, and also minor carbonate-bearing phases such as hydromagnesite and pyroaurite compared to the PONKCS method. This indicates that when accuracy in carbon accounting is the most important aspect to be considered, the Pawley/internal standard method is ideal. The increased sample preparation time required for the Pawley/internal standard method (i.e., introduction of a known weight of a well crystallised standard material) means that in some cases where rapid analysis is required (such as carbon accounting in the field, Turvey et al., 2017) the PONKCS method may be better suited, as it requires no internal standard but still produces reasonably accurate results (Turvey et al., 2017). The results of **Chapter 3** also demonstrated the difficulty in quantifying the abundance of hydrotalcite minerals such as pyroaurite using XRD. The high degree of preferred orientation displayed by the pyroaurite in the samples led to overestimation of pyroaurite abundance for samples that contained low abundances of pyroaurite (<3 wt.%) and underestimation for samples that contained higher abundances of pyroaurite (>3 wt.%). Furthermore, the use of a combined PONKCS/internal standard method offers a way to test the goodness of fit of the PONKCS method and could potentially be used for quantifying multiple separate amorphous or poorly crystalline phases using Rietveld refinements.

The methods developed in **Chapter 3** were used in **Chapter 4** to quantify the abundances of the various carbonate-bearing hydrotalcite minerals at Woodsreef. Quantitative XRD results indicate the presence of multiple reaction fronts as a function of depth within the tailings at Woodsreef. Here, hydromagnesite forms in the shallow tailings (where the supply of atmospheric carbon is abundant) whereas coalingite and pyroaurite form from Fe-rich

brucite under more carbon limited conditions deeper into the tailings pile. The RIR method (Chung, 1974) was used to quantify the abundance of coalingite in the tailings pile as a suitable crystal structure for this phase is not available. By combining the quantitative XRD data with total C data (as recommended by Hamilton et al., in prep) we were able to provide a robust carbon sequestration estimate for the tailings material. Using the results **Chapter 3** we determined that quantitative XRD results provide a naturally conservative estimate of CO<sub>2</sub> sequestration, as this method (1) cannot be used to account for the presence of X-ray amorphous carbonate phases, and (2) typically underestimates the abundances of minor phases such as carbonates. Elemental C data provides a maximum estimate of carbon sequestration potential as it cannot be used to distinguish between modern atmospheric and non-atmospheric sources for carbon (Hamilton et al., in prep-a). The combined use of quantitative XRD and elemental C data provides minimum and maximum carbon sequestration values that can be used in the future for accounting of carbon sequestration in minerals.

Stable Mg isotopes have been used to trace various surface processes including soil formation and carbonate mineral formation (e.g., Opfergelt et al., 2012; Shirokova et al., 2013). Stable Mg isotopes have the potential to highlight the movement of magnesium that is occurring at sites that are undergoing carbon mineralisation. This was investigated in **Chapter 5** where serpentine, brucite, hydromagnesite and hydrotalcite minerals from the Woodsreef chrysotile mine, Mount Keith nickel mine and Dundas mineral field were analysed for their stable Mg isotope composition. The composition of some of the serpentinite samples from the three sites showed an enriched <sup>25</sup>Mg and <sup>26</sup>Mg signature that had not previously been reported for serpentine minerals, as they are typically unfractionated from the mantle/condrritic Mg compositional field described by Beinlich et al. (2014) and Bourdon et al. (2010). Similar enriched stable Mg isotope signatures are seen for minerals

that are exposed to acid leaching during laboratory experiments (Wimpenny et al., 2014; Liu et al., 2017), where light Mg is preferentially liberated from serpentine by the acid leach, leaving behind a mineral residue that is enriched in heavy Mg isotopes. In samples that have not been deliberately exposed to acids, this signature can be attributed to reaction of serpentine with rainwater containing carbonic acid since exposure to rainwater and carbonation of tailings material is analogous to a long term dilute acid leach. This process leads to the formation of an isotopically light Mg-rich fluid and an isotopically heavy serpentine residue. It is likely that this signature has not been seen in other studies because they were conducted on natural serpentinite outcrops, rather than pulverised serpentinite tailings where carbon mineralisation reactions are occurring at a faster rate. This  $^{25}\text{Mg}$ - and  $^{26}\text{Mg}$ -depleted signature could be used in the future to identify sites where carbon sequestration is occurring or infer the degree to which carbon sequestration is occurring by tracing the loss of heavy Mg isotopes due to the weathering reactions that occur in serpentinite mine tailings.

The results of **Chapter 5** showed that the use of acid leaches to separate out various mineral phases for Mg isotope analysis may be problematic. The acid leaches conducted on tailings samples that contained hydromagnesite showed complete leaching of the hydromagnesite, with the serpentine residue having a typical serpentine Mg isotope composition. However, for the tailings samples containing pyroaurite and serpentine, the stable Mg isotope signatures of the leachate and residue were less well defined. The pyroaurite-derived leachate was depleted in  $^{25}\text{Mg}$  and  $^{26}\text{Mg}$ , much like the hydromagnesite, however the serpentine residue was more depleted in  $^{25}\text{Mg}$  and  $^{26}\text{Mg}$  than typical serpentine minerals, indicating that the acid leach may have been incomplete and that unleached pyroaurite may be causing the bulk stable Mg isotopic composition of the residue to be isotopically lighter than that of pure serpentine samples. A longer acid leach could potentially dissolve all the

hydrotalcites; however, it may also begin to liberate isotopically light  $^{24}\text{Mg}$  from the exchangeable surface sites of serpentine minerals, potentially resulting in a stable Mg isotope signature that is not representative of the bulk serpentine mineral. This highlights the potential issues that must be overcome when using stable Mg isotopes to identify carbon mineralisation processes in tailings storage facilities, the understanding of which can be used by future studies to improve analysis techniques.

### **7.3 Determining the origin of hydrotalcites at the Woodsreef chrysotile mine**

The origins of the pyroaurite and coalingite at the Woodsreef chrysotile mine has been an open question, and one that is important to understand when determining the amount of atmospheric carbon sequestered at the site as well as its future carbonation potential (Oskierski et al., 2013; Turvey et al., 2017).

The results of **Chapter 4** show that pyroaurite and coalingite are forming by the carbonation of Fe-rich brucite within the tailings at Woodsreef. **Chapter 4** also demonstrates that a multi-analytical approach is required to determine the origin of hydrotalcite minerals in this setting owing to their complicated environmental behaviour. The presence of radiocarbon within pure samples of pyroaurite at Woodsreef indicates uptake of  $\text{CO}_2$  from the modern atmosphere, either by *in situ* formation from Fe-rich brucite following tailings deposition or via exchange of metamorphic carbonate (if pyroaurite had a hydrothermal origin) for aqueous carbonate derived from the modern atmosphere. The XRD results for samples taken from various depths below the tailings surface show that there is an inverse relationship between brucite and pyroaurite abundances, similar to what is observed for hydromagnesite and brucite at Woodsreef and other mines. This implies that pyroaurite forms at the expense of brucite within the tailings pile at Woodsreef. The presence of coalingite deeper into the tailings compared to pyroaurite implies a depth-dependent control on mineralogy, with the

more carbon-poor coalingite forming under more carbon-limited conditions deeper into the tailings pile. Finally, SEM images reveal that there is textural evidence supporting the formation of pyroaurite via carbonation of brucite in the tailings pile at Woodsreef. Brucite from the tailings shows dissolution features and small platy crystals can be seen forming on the surfaces of brucite, with EDS data confirming the presence of Mg, Fe and C in these crystals and indicating that they are either pyroaurite, coalingite or Fe-rich hydromagnesite. As XRD data of the same sample did not show detectable levels of hydromagnesite it implies that the crystals are either pyroaurite or coalingite forming at the expense of the Fe-rich brucite. Together, these multiple lines of evidence can be used to confirm that the pyroaurite found in the tailings at Woodsreef is forming from the carbonation of Fe-rich brucite, with rainwater containing carbonic acid falling onto the tailings, dissolving brucite and then re-precipitating pyroaurite and coalingite, with more coalingite found deeper into the tailings where the infiltration of CO<sub>2</sub> gas and DIC-rich waters will be lesser than the upper tailings.

With the atmospheric origin of CO<sub>2</sub> in the pyroaurite and coalingite at Woodsreef confirmed, the results of **Chapter 4** allow for a more accurate estimate of the amount of carbon sequestered at Woodsreef. The quantitative XRD and elemental C results from **Chapter 4** were used to estimate the amount of CO<sub>2</sub> that has been sequestered in the tailings at Woodsreef within the hydromagnesite-dominated surface crusts and also within the deeper pyroaurite- and coalingite-rich tailings within the site. Using the compositional data taken from various depths into the tailings, we were able to improve our understanding of how limitations on CO<sub>2</sub> infiltration into the tailings pile controls alteration mineralogy. The average mineralogical compositions for various depths were used to produce a carbon sequestration estimate that was depth sensitive, rather than assuming an identical mineralogy throughout the entire tailings pile at Woodsreef, as has generally been done in previous studies. Using XRD data, we estimate that Woodsreef has sequestered 3,900 t of CO<sub>2</sub> within

the upper 120 cm of the tailings since mine closure, at a carbonation rate of  $230 \text{ g CO}_2 \text{ m}^{-2} \text{ y}^{-1}$ , whereas using elemental C data suggest that Woodsreef has sequestered 6,900 t of  $\text{CO}_2$ , at a rate of  $410 \text{ g CO}_2 \text{ m}^{-2} \text{ y}^{-1}$ . These upper and lower estimates on the rate of carbonation are 3 orders of magnitude higher than typical rates for  $\text{CO}_2$  uptake in the Australian Victorian Alps (Hagedorn and Cartwright, 2009), and they are comparable to the  $\text{CO}_2$  uptake rates determined for other ultramafic mine sites, higher than what is calculated for the Diavik Diamond mine ( $102\text{--}114 \text{ g CO}_2 \text{ m}^{-2} \text{ y}^{-1}$ , Wilson et al. 2011) and similar to what is calculated for the Mount Keith nickel mine ( $162\text{--}2,400 \text{ g CO}_2 \text{ m}^{-2} \text{ y}^{-1}$ , Bea et al. 2012; Wilson et al., 2014).

By confirming the origin of pyroaurite and coalingite at Woodsreef we are able to determine the amount of  $\text{CO}_2$  that is being sequestered, and also show that hydrotalcites at this site are making up a significant portion of the carbon budget, alongside the hydromagnesite. Enhanced carbon mineralisation studies which seek to increase the rate of carbon mineralisation at a site could potentially use hydrotalcites in the future, by promoting uptake of  $\text{CO}_2$  in carbon limited conditions (where hydrated Mg-carbonates cannot form) to form hydrotalcites, or within pre-existing hydrotalcite minerals using anion exchange.

#### **7.4 Implications of *in situ* formation of hydrotalcite minerals for carbon sequestration in ultramafic tailings storage facilities**

The concepts explored in this thesis and its findings have broader implications for carbon sequestration research beyond the Woodsreef Chrysotile mine. Estimating the amount of atmospheric  $\text{CO}_2$  that has already been sequestered within tailings, and determining the total amount of  $\text{CO}_2$  that could potentially be sequestered in the future, are important pieces of information vital to understanding carbon mineralisation at mine sites (e.g., Oskierski et al., 2013; Wilson et al., 2009a; Wilson et al., 2014; Wilson et al., 2006; Wilson et al., 2009b),

as is determining ways to monitor passive CO<sub>2</sub> uptake and to enhance carbonation through biotic and abiotic methods (e.g., Gras et al., 2017; Hamilton et al., in prep-b; Lechat et al., 2016; McCutcheon et al., 2017). **Chapter 3** improves upon existing carbon accounting techniques by comparing the accuracy of three quantitative XRD methods, ultimately determining that the Pawley/internal standard method provides the most accurate estimates for the hydromagnesite and pyroaurite in a sample. It also shows that quantitative XRD methods underestimate the amount of CO<sub>2</sub> contained within a sample, meaning that Rietveld refinement results are likely to give a conservative estimate of the amount of CO<sub>2</sub> sequestered at any given mine.

The formation of pyroaurite from Fe-rich brucite has potentially wide-reaching implications for carbon sequestration in ultramafic rocks, including ultramafic mine tailings. Many ultramafic ore deposits and tailings storage facilities contain hydrotalcite minerals and brucite at wt% abundances (e.g., Gras et al., 2017; Wilson et al., 2014). **Chapter 4** shows that hydrotalcites have sequestered approximately 60% of the total C stored at Woodsreef. It is possible that hydrotalcites also contribute to CO<sub>2</sub> sequestration at other sites such as the Mount Keith nickel mine, where hydrotalcites make up ~20 wt% of the tailings material (Grguric, 2003), or the Dumont nickel project, where the hydrotalcites at the site have similar stable C isotope compositions to the pyroaurite at Woodsreef (Gras et al., 2017). Because hydrotalcites can potentially sequester atmospheric CO<sub>2</sub> during precipitation, or via anion exchange with atmosphere-derived DIC, they may have a role to play in carbon sequestration even at sites where they were originally present as part of the gangue mineralogy (e.g., Mount Keith). The pyroaurite at Woodsreef is forming at greater extent than hydromagnesite, and is commonly present within deeper tailings under more carbon-limited conditions. This means that hydrotalcites form under a wider range of conditions than hydromagnesite, even under non-ideal conditions, this might offer an extra advantage for implementing enhanced

passive carbonation at mines where the supply of CO<sub>2</sub> into tailings cannot be readily enhanced through changes to tailings management or reaction of tailings with CO<sub>2</sub>-rich waste gases. Recent field experiments for enhanced passive carbonation have mainly focussed on optimising pore-water saturation and increasing supply of CO<sub>2</sub> and Mg into solution to promote formation of hydrated Mg-carbonate minerals (Hamilton et al., in prep.; McCutcheon et al., 2017; McCutcheon et al., 2016). However, in addition to forming hydrated Mg-carbonate minerals under geochemically conditions, these strategies are likely to also be forming hydrotalcite minerals in less than ideal conditions, creating multiple carbonation fronts that are sequestering CO<sub>2</sub> in several mineral species. Additionally, this means that if geochemical conditions can be improved in the deeper tailings at Woodsreef (likely through the introduction of additional CO<sub>2</sub>) it may be possible to convert the hydrotalcites to a mineral phase such as hydromagnesite which has a lower Mg:CO<sub>2</sub> and is a more volume-efficient sink for CO<sub>2</sub>.

### **7.5 Understanding stable isotopic signatures and elemental exchange in hydrotalcites**

Stable isotopes are widely used in geochemistry for tracing the origins of minerals (e.g., Friedrich et al., 2015; Gras et al., 2017; Opfergelt et al., 2012; Shirokova et al., 2013; Teng, 2017; Young and Galy, 2004). They have previously been used in carbon sequestration studies to confirm the origin of carbonates and to understand what formation mechanisms are creating the carbonate minerals that are forming (Beinlich and Austrheim, 2012; Gras et al., 2017; Gras et al., 2015; Harrison et al., 2013; Oskierski et al., 2013; Wilson et al., 2011; Wilson et al., 2009a; Wilson et al., 2014). Investigating the origins of hydrotalcites using stable C and O isotope data and radiocarbon data has been complicated because few studies report results for pure samples of hydrotalcite minerals or even multiphase samples containing hydrotalcites (e.g., O'Neil and Barnes, 1971; Gras et al., 2017; Oskierski et al.,

2013; Wilson et al., 2009a; Wilson et al., 2014). This thesis adds substantially to the available data on the stable C, O and Mg isotope compositions of hydrotalcite minerals and gives a first assessment of how these can change over time due to environmental conditions.

Stable C and O isotope signatures for pyroaurite-bearing samples at Woodsreef have been previously reported in Oskierski et al. (2013). Results from **Chapter 4** provide more context for these previously published results, by showing that the pyroaurite at Woodsreef is depleted in  $^{13}\text{C}$  and  $^{18}\text{O}$  relative to the hydromagnesite, and that the stable C and O isotope composition of bulk tailings samples is likely due to mechanical mixing of these two carbonate minerals. The high radiocarbon content of the pyroaurite at Woodsreef (with pyroaurite at the surface of the tailings pile having the highest  $F^{14}\text{C}$  values), unambiguously indicates that pyroaurite contains modern  $\text{CO}_2$  either through *in situ* formation within the tailings or by undergoing anion exchange post deposition (in the case it had formed during serpentinisation). As there is limited organic carbon available in the tailings pile, the only likely modern source for carbon is atmospheric  $\text{CO}_2$ . The results of the anion exchange experiment in **Chapter 4** indicate that this style of reaction can produce radically different stable C and O isotope compositions in hydrotalcites depending the availability of carbon. The experiment showed that hydrotalcites gain a  $^{13}\text{C}$ -depleted stable C isotope signature if they undergo anion exchange (or form) in carbon limited conditions, similar to other carbonate minerals (Harrison et al., 2013; Wilson et al., 2010). This supports the XRD and SEM evidence that pyroaurite and coalingite are forming under carbon limited conditions in the deep tailings, as the pyroaurite at Woodsreef is depleted in  $^{13}\text{C}$  compared to the hydromagnesite which is forming under more carbon-rich conditions. The exchangeable nature of stable C and O isotopes in hydrotalcites means that they are not the most reliable recorders of formation conditions, as it is likely their stable C and O isotope and radiocarbon signatures evolved over time to reflect recent environmental conditions.

No stable Mg isotope data had previously been reported for hydrotalcite minerals. We hypothesised that the stable Mg isotope composition of hydrotalcite minerals would be immune to exchange with the environment, and suggested that stable Mg isotopes could potentially be used to differentiate between hydrotalcites formed during high-temperature hydrothermal alteration and those that formed from low-temperature carbonation of brucite, since (1) the two formation mechanisms should lead to different stable Mg isotopic signatures and (2) we expected that Mg would be less likely to exchange with solution than interlayer anions (such as  $\text{CO}_3^{2-}$ ). The results of **Chapter 5** reveal that stable Mg isotope composition for hydrotalcites sourced from the Woodsreef chrysotile mine (low temperature), Mount Keith nickel mine (high temperature) and Dundas mineral field (high temperature) is dependent of mineral species not formation conditions. These unexpectedly homogeneous results likely imply that hydrotalcites may be undergoing stable Mg isotope exchange with the local environment, similar to what has been overserved for structural Fe in the Fe-clay minerals such as nontronite and ferruginous smectite (Neumann et al., 2015). This phenomenon was further investigated in **Chapter 6** where a Mg exchange experiment was conducted between synthetic pyroaurite and a  $^{25}\text{Mg}$ -enriched  $\text{Mg}^{2+}_{(\text{aq})}$  solution. The results of the experiment indicate that a substantial amount of Mg exchange (up to 29.1%) occurs between the solid pyroaurite and the local environment over the 90 days the experiments were conducted. Rietveld refinement results for crystallite size and strain for the synthetic pyroaurite showing no obvious changes over time, implying that most of this exchange occurred at the mineral surfaces. This exchange offers an explanation for the homogeneous stable Mg isotope signatures found in hydrotalcites from Woodsreef, Mount Keith and Dundas that were investigated in Chapter 5. Interactions with Mg-rich fluids can be expected to slowly alter the stable Mg isotope signature of a high-temperature hydrotalcite mineral until it is indistinguishable from hydrotalcites that have formed in the low-

temperature tailings environment. The ease and rapidity of Mg exchange has further implications for the uses of hydrotalcites. Although they are well known to undergo anion exchange at ambient conditions, the discovery that they also exchange cations from their hydroxide layers mean that contaminants sequestered within these brucite-like sheets could potentially be remobilised. This may be cause for concern as the formation of hydrotalcites has been suggested a method of sequestering contaminants other than atmospheric CO<sub>2</sub> at some mine sites (Douglas et al., 2014; Douglas et al., 2010).

### **7.6 Suggestions for future research**

The results of this thesis have raised a new series of questions to be answered by future research, some of which are summarised below.

In **Chapter 3**, the combined PONKCS-Pawley/internal standard method was used to demonstrate potential to separately quantify multiple disordered phases without having to build robust PONKCS models for all phases. It would require further analyses of synthetic tailings of a known composition that also include various amounts of a truly amorphous material to test the sensitivity of the combined PONKCS-Pawley/internal standard method to the presence of amorphous material and the accuracy with which it can be used to quantify the abundances of mineral phases.

**Chapter 4** demonstrated that pyroaurite formation at Woodsreef contributes significantly to net carbon sequestered. The presence and origins of hydrotalcites will be important considerations for future studies into carbon sequestration at other active and abandoned mines. Additionally, as this field of carbon sequestration research transitions from analysing the results of passive carbon mineralisation in mines to accelerating carbonation in field trials and demonstration projects, the formation of hydrotalcites should be viewed as a potential asset that bolsters carbon sequestration rates under suboptimal conditions where

hydrated Mg-carbonates do not readily form. Future laboratory studies into the reactivity of Fe-rich brucite at Earth's surface conditions should be performed, as much of the literature regarding the formation of pyroaurite from brucite does not delve into the fundamental nature of why brucite carbonates to form several different minerals, depending on environmental conditions.

The stable C and O isotope results for Woodsreef, and the anion exchange experiment of **Chapter 4** indicate that the extent of C and O isotope fractionation observed in hydrotalcites is dependent on carbon availability in tailings pore water. This fractionation trend occurs in hydrotalcites regardless of the mechanism by which they are incorporating carbonate, either (1) anion exchange, or (2) forming from the carbonation of Fe-rich brucite. There remains an unanswered question regarding the magnitude of this fractionation for pyroaurite–DIC and pyroaurite–H<sub>2</sub>O, and under what specific environmental conditions <sup>13</sup>C and <sup>18</sup>O depletion in pyroaurite occurs. This could be better explored in a dedicated stable C and O isotope fractionation study for hydrotalcites, where the compositions of hydrotalcites could be compared under a variety of carbon availabilities using both anion exchange and precipitation experiments.

**Chapter 5** is the first investigation into the stable Mg isotope composition of hydrotalcites; as such, there remain unanswered questions regarding how the stable Mg isotope compositions of Mg-carbonates and Mg-hydrotalcites that are forming from the same Mg-rich solutions and/or brucite relate to each other. Additionally, a larger data set of stable Mg isotope results from different mine sites and weathered serpentinites would serve to improve our understanding of Mg cycling during carbon mineralisation. It would also be beneficial to expand upon the results of **Chapter 6** to determine an equilibrium stable Mg isotope fractionation factor between pyroaurite and aqueous Mg<sup>2+</sup>, and to investigate the stable Mg

isotope compositions of fresh samples of waste rock hydrotalcites from Mount Keith or Dundas to show how they vary over time via exchange with Mg-rich pore waters in the tailings.

Hydrotalcites have the potential to be exploited for a wide variety of uses, from carbon sequestration and contaminant removal, to nutrient delivery of drugs and fertilizers. All of these uses rely upon the hydrotalcite minerals ability to sequester and release molecules and elements of our choosing. Improving our understanding of how hydrotalcites form in the natural environment, and the ways they interact with the environment and change over time is essential for fully utilising their unique sequestration and exchange capacities. By doing so, this will enable us to use hydrotalcite minerals to fulfil a myriad of tasks into the future, including trapping atmospheric CO<sub>2</sub> and helping to reduce the negative impacts we are having upon our planet.

## 7.7 References

- Beinlich, A., and Austrheim, H. (2012) In situ sequestration of atmospheric CO<sub>2</sub> at low temperature and surface cracking of serpentinized peridotite in mine shafts. *Chemical Geology*, 332–333, 32-44.
- Beinlich, A., Mavromatis, V., Austrheim, H., and Oelkers, E.H. (2014) Inter-mineral Mg isotope fractionation during hydrothermal ultramafic rock alteration - Implications for the global Mg-cycle. *Earth and Planetary Science letters*, 392(166-176).
- Bourdon, B., Tipper, E.T., Fitoussi, C., and Stracke, A. (2010) Chondritic Mg isotope composition of the Earth. *Geochimica et Cosmochimica Acta*, 74(17), 5069-5083.
- Chung, F.H. (1974) Quantitative Interpretation of X-ray Diffraction Patterns of Mixtures. 1. Matrix-Flushing Method for Quantitative Multicomponent Analysis. *Journal of Applied Crystallography*, 7(6).
- Cleugh, H., Smith, M.S., Battaglia, M., and Graham, P. (2011) *Climate Change Science and Solutions for Australia*. CSIRO Publishing, 150 Oxford Street Collingwood VIC Australia.
- Douglas, G., Shackleton, M., and Woods, P. (2014) Hydrotalcite formation facilitates effective contaminant and radionuclide removal from acidic uranium mine barren lixiviant. *Applied Geochemistry*, 42(0), 27-37.
- Douglas, G.B., Wendling, L.A., Pleysier, R., and Trefry, M. (2010) Hydrotalcite Formation for Contaminant Removal from Ranger Mine Process Water. *MINE WATER AND THE ENVIRONMENT*, 29, 108-115.
- Friedrich, A.J., Beard, B.L., Rosso, K.M., Scherer, M.M., Spicuzza, M.J., Valley, J.W., and Johnson, C.M. (2015) Low temperature, non-stoichiometric oxygen-isotope exchange coupled to Fe(II)–goethite interactions. *Geochimica et Cosmochimica Acta*, 160, 38-54.

- Gras, A., Beaudoin, G., Molson, J., Plante, B., Bussière, B., Lemieux, J.M., and Dupont, P.P. (2017) Isotopic evidence of passive mineral carbonation in mine wastes from the Dumont Nickel Project (Abitibi, Quebec). *International Journal of Greenhouse Gas Control*, 60, 10-23.
- Gras, A., Beaudoin, G., Molson, J., Plante, B., Bussière, B., Lemieux, J.M., and Kandji, B. (2015) Carbon isotope evidence for passive mineral carbonation of mine wastes from the Dumont Nickel Project (Abitibi, Quebec). 5th International Conference on Accelerated Carbonation for Environmental and Materials Engineering, New York City, USA.
- Grguric, B.A. (2003) Minerals of the MKD5 nickel deposit, Mount Keith, Western Australia. *Australian Journal of Mineralogy*, 9(2), 55-71.
- Hagedorn, B., and Cartwright, I. (2009) Climatic and lithologic controls on the temporal and spatial variability of CO<sub>2</sub> consumption via chemical weathering: An example from the Australian Victorian Alps. *Chemical Geology*, 260(3), 234-253.
- Hamilton, J.L., Turvey, C.C., Tait, A.W., and Wilson, S.A. (in prep-a) Accelerating mineral carbonation at ultramafic mines via direct CO<sub>2</sub> reaction and heap leaching, and potential for base metal enrichment and recovery. In preparation.
- Hamilton, J.L., Wilson, S.A., Turvey, C.C., Tait, A.W., McCutcheon, J., Fallon, S.J., and Southam, G. (in prep-b) Field-based deployment of an automated geochemical treatment system for accelerating carbonation of ultramafic mine tailings: Lessons for pilot projects and carbon accounting in mined landscapes. In preparation.
- Harrison, A.L., Power, I.M., and Dipple, G.M. (2013) Accelerated carbonation of brucite in mine tailings for carbon sequestration. *Environmental Science and Technology*, 47(1), 126-134.

- Houghton, J.T., Ding, Y., Griggs, D.J., Noguer, M., van der Linden, P.J., Dai, X., Maskell, K., and Johnson, C.A. (2001) *Climate Change 2001: The Scientific Basis: Contribution of Working Group 1 to the Third Assessment Report of the Intergovernmental Panel on Climate Change*. Cambridge University Press, U.K.
- IPCC. (2005) *IPCC Special Report on Carbon Dioxide Capture and Storage*. In O.D. Bert Metz, Heleen de Coninck, Manuela Loos, Leo Meyer, Ed, p. 442. Cambridge University Press, 40 West 20th Street, New York, NY 10011–4211, USA.
- IPCC. (2013) *Climate Change 2013: The Physical Science Basis*. In IPCC, Ed. IPCC Working Group 1.
- IPCC. (2014) *Climate Change 2014 Mitigation of Climate Change*. In IPCC, Ed. IPCC Working Group 3.
- Lackner, K.S. (2002) Carbonate Chemistry for Sequestering Fossil Carbon. *Annual Review of Energy and the Environment*, 27(1), 193-232.
- Lackner, K.S., Wendt, C.H., Butt, D.P., Joyce Jr, E.L., and Sharp, D.H. (1995) Carbon dioxide disposal in carbonate minerals. *Energy*, 20(11), 1153-1170.
- Lechat, K., Lemieux, J.M., Molson, J.W., Beaudoin, G., and Hebert, R. (2016) Field evidence of CO<sub>2</sub> sequestration by mineral carbonation in ultramafic milling wastes, Thetford Mines, Canada. *International Journal of Greenhouse Gas Control*, 47, 110-121.
- Liu, P.-P., Teng, F.-Z., Dick, H.J.B., Zhou, M.-F., and Chung, S.-L. (2017) Magnesium isotopic composition of oceanic mantle and oceanic Mg cycling. *Geochimica et Cosmochimica Acta*.
- McCutcheon, J., Turvey, C.C., Hamilton, J.L., Wilson, S.A., and Southam, G. (2017) *Experimental Deployment of Microbial Mineral Carbonation at an Asbestos Mine:*

- Potential Applications to Carbon Storage and Tailings Stabilization. *Minerals*, 7(191).
- McCutcheon, J., Wilson, S.A., and Southam, G. (2016) Microbially accelerated carbonate mineral precipitation as a strategy for in situ carbon sequestration and rehabilitation of asbestos mine sites. *Environmental Science & Technology*, 50(3), 1419-1427.
- Millar, R.J., Fuglestedt, J.S., Friedlingstein, P., Rogelj, J., Grubb, M.J., Matthews, H.D., Skeie, R.B., Forster, P.M., Frame, D.J., and Allen, M.J. (2017) Emission budgets and pathways consistent with limiting warming to 1.5°C. *Nature Geoscience*, 10, 741-748.
- Neumann, A., Wu, L., Li, W., Beard, B.L., Johnson, C.M., Rosso, K.M., Friedrich, A.J., and Scherer, M.M. (2015) Atom Exchange between Aqueous Fe(II) and Structural Fe in Clay Minerals. *Environmental Science & Technology*, 49(5), 2786-2795.
- O'Neil, J.R., and Barnes, I. (1971) C13 and O18 compositions in some fresh-water carbonates associated with ultramafic rocks and serpentinites; western United States. *Geochimica et Cosmochimica Acta*, 35, 687-697.
- Opfergelt, S., Georg, R.B., Delvaux, B., Cabidoche, Y.M., Burton, K.W., and Halliday, A.N. (2012) Mechanisms of magnesium isotope fractionation in volcanic soil weathering sequences, Guadeloupe. *Earth and Planetary Science Letters*, 341(Supplement C), 176-185.
- Oskierski, H.C., Dlugogorski, B.Z., and Jacobsen, G. (2013) Sequestration of atmospheric CO<sub>2</sub> in chrysotile mine tailings of the Woodsreef Asbestos Mine, Australia: Quantitative Mineralogy, isotopic fingerprinting and carbonation rates. *Chemical Geology*.
- Pacala, S., and Socolow, R. (2004) Stabilization Wedges: Solving the Climate Problem for the Next 50 Years with Current Technologies. *Science*, 305.

- Scarlett, N.V.Y., and Madsen, I.C. (2006) Quantification of phases with partial or no known crystal structures. *Powder Diffraction*, 21(4), 278-284.
- Seifritz, W. (1990) CO<sub>2</sub> disposal by means of silicates *Nature*, 345.
- Shirokova, L.S., Mavromatis, V., Bundeleva, I., Pokrovsky, O.S., Benezeth, P., Gerard, E., Pearce, C., and Oelkers, E.H. (2013) Using Mg isotopes to Trace Cyanobacterially Mediated Magnesium Carbonate Precipitation in Alkaline lakes. *Aquatic Geochemistry*, 19, 1-24.
- Teng, F.-Z. (2017) Magnesium Isotope Geochemistry. *Reviews in Mineralogy & Geochemistry*, 82(1), 219-287.
- Turvey, C.C., Wilson, S.A., Hamilton, J.L., and Southam, G. (2017) Field-based accounting of CO<sub>2</sub> sequestration in ultramafic mine wastes using portable X-ray diffraction. *American Mineralogist*.
- Wilson, S.A., Barker, S.L.L., Dipple, G.M., and Atudorei, V. (2010) Isotopic Disequilibrium during uptake of Atmospheric CO<sub>2</sub> into Mine Process Waters: Implications for CO<sub>2</sub> Sequestration. *Environmental Science & Technology*, 44, 9522-9529.
- Wilson, S.A., Dipple, G.M., Power, I.M., Barker, S.L.L., Fallon, S.J., and Southam, G. (2011) Subarctic Weathering of Mineral Wastes Provides a Sink for Atmospheric CO<sub>2</sub>. *Environmental Science & Technology*, 45(18), 7727-7736.
- Wilson, S.A., Dipple, G.M., Power, I.M., Thom, J.M., Anderson, R.G., Raudsepp, M., Gabites, J.E., and Southam, G. (2009a) Carbon Dioxide Fixation within Mine Wastes of Ultramafic-Hosted Ore Deposits: Examples from the Clinton Creek and Cassiar Chrysotile Deposits, Canada. *Economic geology*, 104, 95–112.
- Wilson, S.A., Harrison, A.L., Dipple, G.M., Power, I.M., Barker, S.L.L., Mayer, K.U., Fallon, S.J., Raudsepp, M., and Southam, G. (2014) Offsetting of CO<sub>2</sub> emissions by air capture in mine tailings at the Mount Keith Nickel mine, Western Australia: Rates,

- controls and prospects for carbon neutral mining. *International Journal of Greenhouse Gas Control*, 25, 121-140.
- Wilson, S.A., Raudsepp, M., and Dipple, G.M. (2006) Verifying and quantifying carbon fixation in minerals from serpentine-rich mine tailings using the Rietveld method with X-ray powder diffraction data. *American Mineralogist*, 91(8-9), 1331-1341.
- Wilson, S.A., Raudsepp, M., and Dipple, G.M. (2009b) Quantifying carbon fixation in trace minerals from processed kimberlite; a comparative study of quantitative methods using X-ray powder diffraction data with applications to the Diavik diamond mine, Northwest Territories, Canada. *Applied Geochemistry*, 24(12), 2312-2331.
- Wimpenny, J., Colla, C.A., Yin, Q.-Z., Rustad, J.R., and Casey, W.H. (2014) Investigating the behaviour of Mg isotopes during the formation of clay minerals. *Geochimica et Cosmochimica Acta*, 128, 178-194.
- Yang, H., Xu, Z., Fan, M., Gupta, R., Slimane, R.B., Bland, A.E., and Wright, I. (2008) Progress in carbon dioxide separation and capture: A review. *Journal of Environmental Sciences*, 20, 14-27.
- Young, E.D., and Galy, A. (2004) The Isotope Geochemistry and Cosmochemistry of Magnesium. *Reviews in Mineralogy & Geochemistry*, 55, 197-230.



# Appendix 1

## **Supplemental Information for Chapter 6: Mg exchange between pyroaurite [ $\text{Mg}_6\text{Fe}^{3+}_2\text{CO}_3(\text{OH})_{16}\cdot 4\text{H}_2\text{O}$ ] and aqueous Mg(II): Implications for carbon mineralisation and contaminant release**

Connor C. Turvey<sup>1</sup>

<sup>1</sup>School of Earth, Atmosphere & Environment, Monash University, Clayton, Melbourne,  
Victoria 3800, Australia

## S1. Control experiments

Two control experiments were conducted to ensure that Mg-carbonate minerals, such as hydromagnesite  $[\text{Mg}_5(\text{CO}_3)_4(\text{OH})_2 \cdot 4\text{H}_2\text{O}]$ , dypingite  $[\text{Mg}_5(\text{CO}_3)_4(\text{OH})_2 \cdot \sim 5\text{H}_2\text{O}]$  and nesquehonite ( $\text{MgCO}_3 \cdot 3\text{H}_2\text{O}$ ), would not precipitate and that pyroaurite remained stable in the buffer solution. The precipitation of Mg carbonates would disrupt the exchange experiments as Mg would be lost from solution into a sink other than the pyroaurite, while the dissolution of pyroaurite over time would lead to the release of Mg back into solution via a mechanism other than exchange.

The first control experiment placed varying concentrations of  $\text{Mg}^{2+}_{(\text{aq})}$  (450 or 1800  $\mu\text{M}$ ) into carbonate–bicarbonate pH buffers at various pH values (9.4–11.5). This was done to see whether either the concentration of  $\text{Mg}^{2+}_{(\text{aq})}$  or the pH conditions had an effect on the precipitation of Mg carbonate minerals. ICP-MS results for the first experiment showed that  $\text{Mg}^{2+}_{(\text{aq})}$  stayed in solution over 3 days (Figure S1.), for both  $\text{Mg}^{2+}_{(\text{aq})}$  concentrations and over the full range of pH values that were tested (Figure S2.), indicating the no precipitation of Mg carbonates was occurring. The lack of precipitation is likely occurring thanks to kinetic inhibition thanks to the hydration of the  $\text{Mg}^{2+}_{(\text{aq})}$  ion.

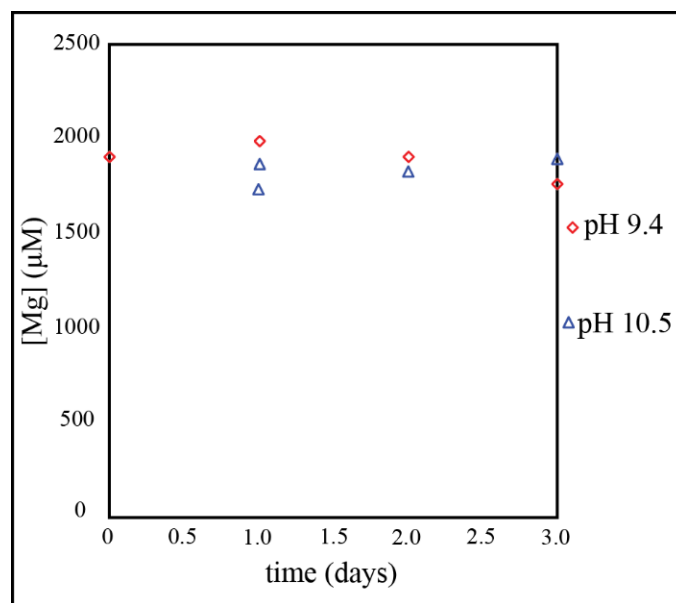


**Figure S1.** ICP-MS results for control experiment 1, showing change in concentration over time for experiments using pH 9.4 and pH 10.5 carbonate-bicarbonate buffers (experiments using pH 10, 10.3, 10.6 and 11.5 are not included as they were only collected at one time point).

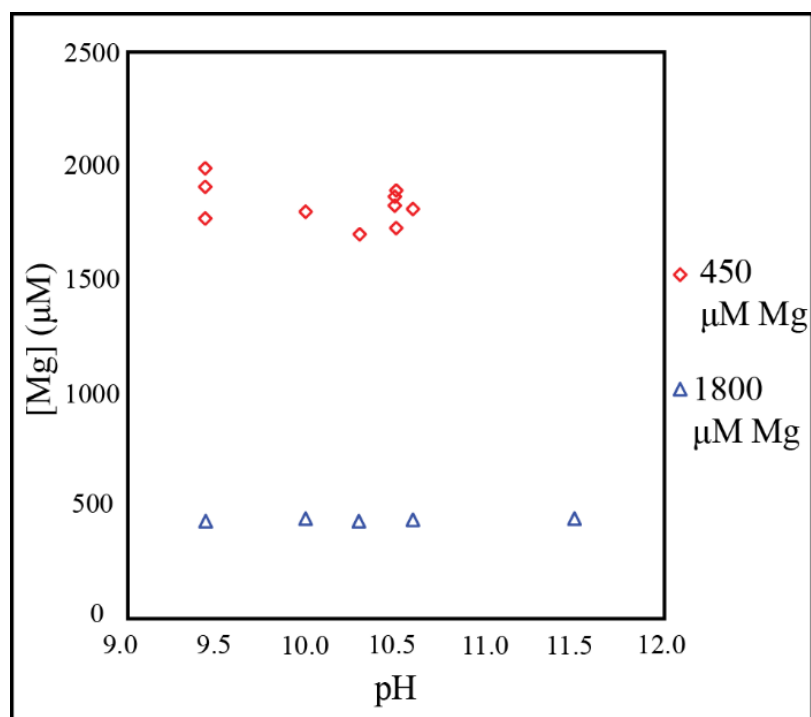


**Figure S2.** ICP-MS results for control experiment 1, showing negligible change in Mg concentration for a range of pH values (for pH 9.4 and pH 10.5 multiple data points are from various time points see Figure S1.).

The second experiment combined 5–20 mg of the pyroaurite with the carbonate–bicarbonate buffers (pH 9.4–11.5). This experiment which was run prior to the exchange experiment was designed to investigate the amount of Mg that would be released into solution by leaving the pyroaurite in contact with the carbonate–bicarbonate buffer over 90 days. ICP-MS results show that pyroaurite was most stable at high pH values, releasing less  $\text{Mg}^{2+}_{(\text{aq})}$  into solution (Figure S3.). Figure S3. Plots the amount of Mg released (as Mg concentration, [Mg]) into solution at various pH conditions and masses of pyroaurite, while Figure S4. plots the proportion of total Mg in the system that is released for various pH conditions and masses of pyroaurite. When considering the amount of pyroaurite placed into the solution, it was found that the addition of 20 mg of pyroaurite led to the highest concentrations of  $\text{Mg}^{2+}_{(\text{aq})}$  compared to 10 mg and 5 mg (Figure S3.); however, when considering the total amount of Mg from the system which had entered the solution, 20 mg released relatively little Mg into solution (Figure S4.).

The results of the control experiments reveal that the (1) risk of Mg-carbonate mineral formation was negligible in the pH conditions under consideration and that (2) higher pH conditions minimise loss of Mg into solution via dissolution.

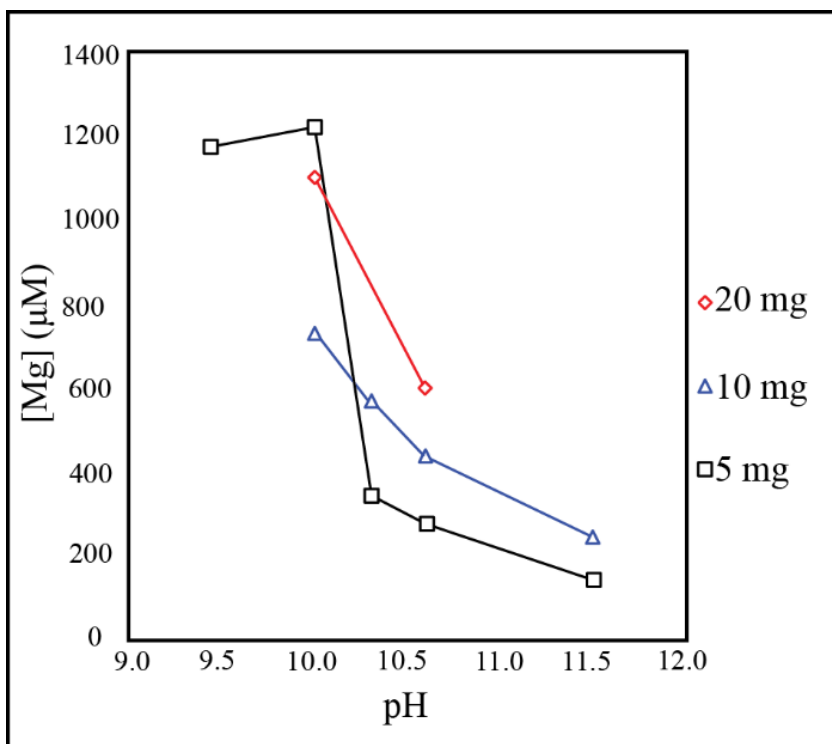


**Figure S3.** ICP-MS results for control experiment 2, showing change in concentration for multiple pyroaurite masses, over a range of pH values.

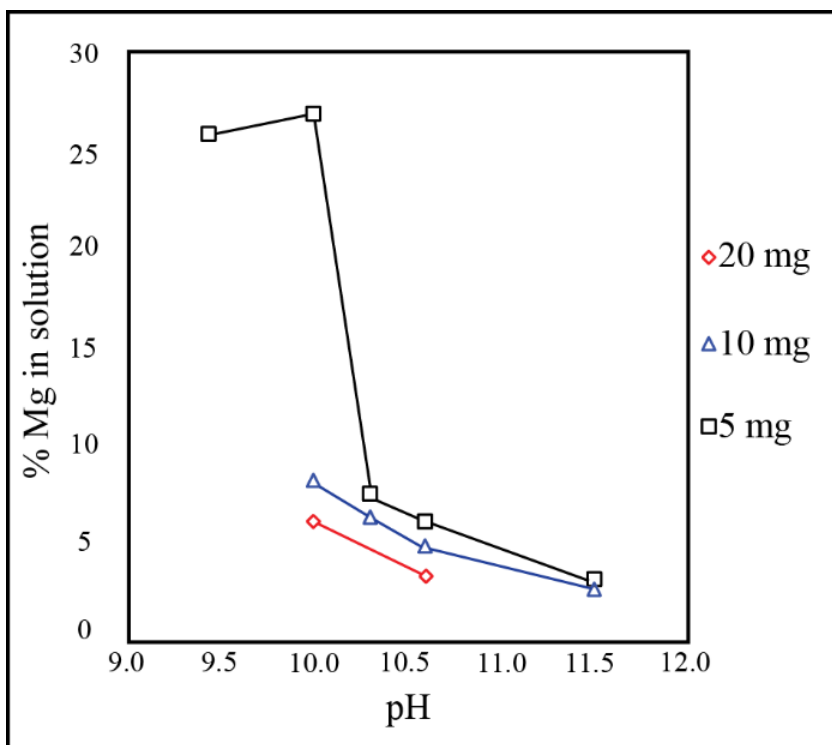


**Figure S4.** % Mg results for control experiment 2, showing the amount of Mg which has entered solution for multiple pyroaurite masses, over a range of pH values.

## S2. Mg % Exchange calculations

The % Mg exchanged was estimated using Eq. 2 and the  $f^x\text{Mg}$  values determined via ICP-MS (after the method of Handler et al., 2014). The calculated % Mg exchange values are largely similar when using  $f^{24}\text{Mg}$  and  $f^{25}\text{Mg}$ , with the results being within 3% of each other for a given time step and reactor, and with the use of  $f^{24}\text{Mg}$  typically resulting in slightly higher exchange values. The use of  $f^{26}\text{Mg}$  results in significantly lower % Mg exchange values than are obtained with either of the two lighter isotopes (Figure S5). After 90 days of reaction, there is a difference of 12.6% between the values calculated for % Mg when using  $f^{25}\text{Mg}$  and  $f^{26}\text{Mg}$ .

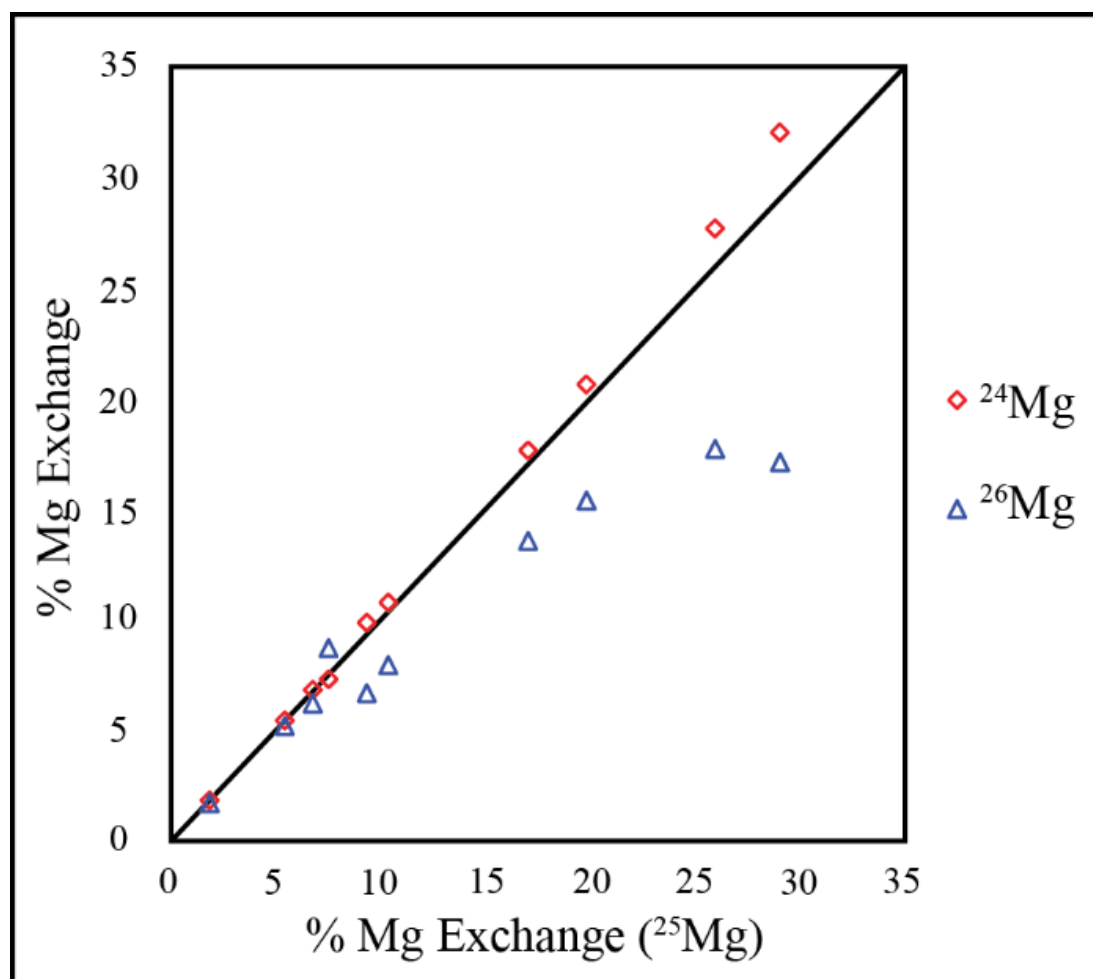


**Figure S5.** Comparison of the % Mg exchange values calculated using  $f^{24}\text{Mg}$  and  $f^{26}\text{Mg}$  relative to using  $f^{25}\text{Mg}$ .

Of the three isotopes,  $^{24}\text{Mg}$  and  $^{25}\text{Mg}$  are more likely to give accurate values for the amount of Mg exchange as they are present in significantly higher abundances than the  $^{26}\text{Mg}$  in the system. This is because the pyroaurite is the largest reservoir of Mg in the system and consists of mostly  $^{24}\text{Mg}$  while the solution contains almost pure  $^{25}\text{Mg}$ . The  $^{26}\text{Mg}$  is present at comparatively low abundances in the pyroaurite, it is nearly absent from the starting solution, and it is present at close to the detection limit of the instrument in all analyses from the exchange experiment, making it far more unreliable for use in calculating the degree of exchange. The extent of exchange that occurs between the two reservoirs is largely driven by exchange of  $^{25}\text{Mg}$  from the solution with  $^{24}\text{Mg}$  in the pyroaurite, making it likely that these isotopes provide more accurate estimates. The results shown in Figure S5. are consistent with this interpretation given the nearly 1:1 correspondence between values of % Mg exchange obtained using  $f^{24}\text{Mg}$  and  $f^{26}\text{Mg}$ .

### S3. Estimate of the fraction of Mg atoms at the pyroaurite surface

An estimate of the fraction of Mg atoms at the surface of the pyroaurite grains is was done using a similar method to that of Handler et al. (2014) who calculated the fraction of Fe atoms at goethite surfaces relative to those within the volume of crystals. Surface Mg atom densities for the (0 0 1), (1 0 0) and (0 1 0) surfaces of pyroaurite were calculated using crystallographic information files (CIF) that were visualised in CrystalMaker X for Windows (Ingram and Taylor, 1967).

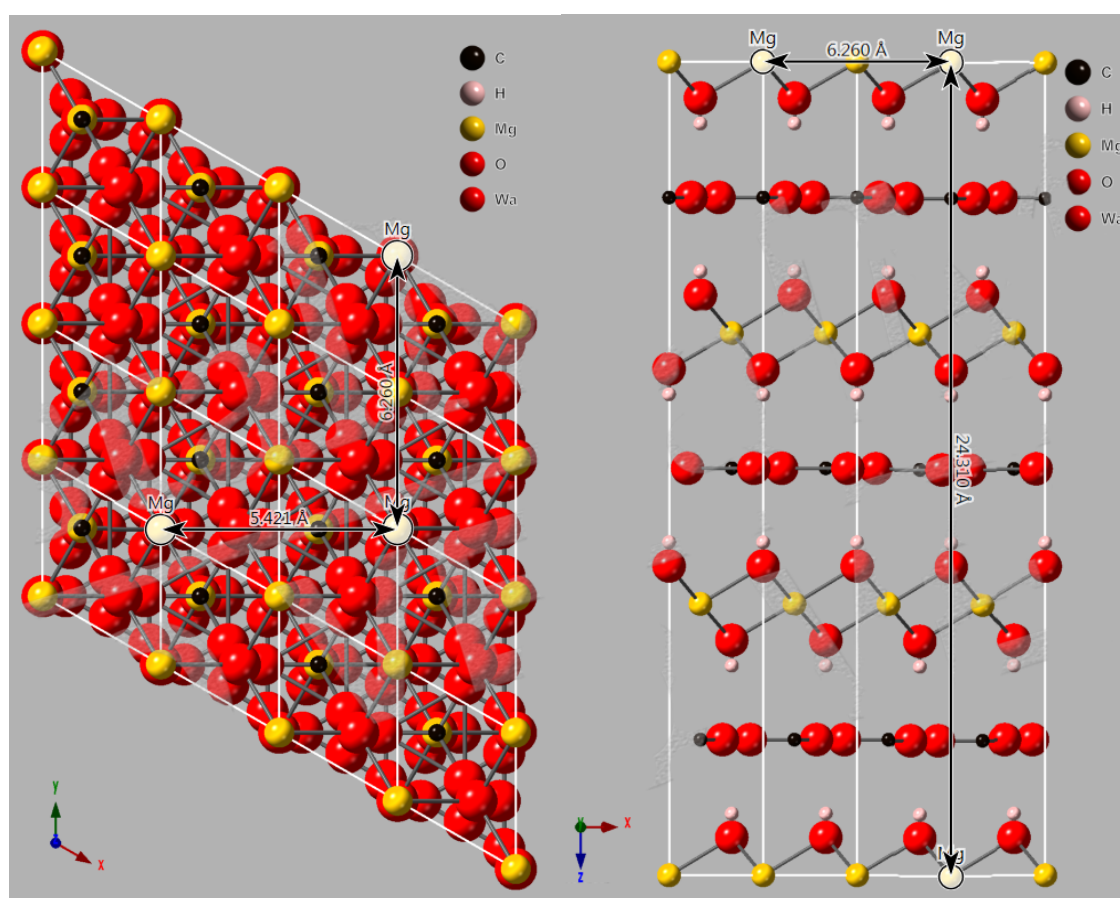


**Figure S6.** Geometry of Mg atoms (yellow) at the pyroaurite surface for the (0 0 1) and (1 0 0), (0 1 0) surfaces.

The number of Mg atoms for a given surface area was calculated using the CIF file in CrystalMaker X (Figure S6.), this was used to calculate density of Mg atoms at the (0 0 1), (1 0 0) and (0 1 0) surfaces (Table S1). To simplify the calculations only the outer (0 0 1),

(1 0 0) and (0 1 0) surfaces were considered, rather than considering interlayer positions. This was combined with BET surface data to determine the number of atoms found at the pyroaurite surface (in atoms/gram), this was compared to the total number of Mg atoms in a gram of pyroaurite to determine the fraction of Mg atoms that are at the surface of the mineral grain.

**Table S1.** Surface fraction calculations

	(0 0 1) Surface	(1 0 0) and (0 1 0) Surfaces
Surface Mg atoms per area (see Figure S3)	$2 + 2 \times \frac{1}{2} + 4 \times \frac{1}{4} = 4$	$4 + 2 \times \frac{1}{2} + 4 \times \frac{1}{4} = 4$
Area (Å <sup>2</sup> )	5.42 x 6.26	24.31 x 6.26
Surface atom density (atoms/nm <sup>2</sup> )	11.79	3.94
BET Specific Surface Area (m <sup>2</sup> /g)		88.24
No. of Mg atoms at pyroaurite surface (atoms/ gram)	1.04 x 10 <sup>21</sup>	3.48 x 10 <sup>20</sup>
No. of Mg atoms in a gram of pyroaurite		5.46 x 10 <sup>21</sup>
Fraction of Mg atoms at the surface (%)	19.05	6.37
Total fraction of Mg atoms at the surface (%)		31.79

#### S4. Crystallite size calculations and results

Calculating the crystallite size of the pyroaurite before and during the exchange reaction allows for determination of whether if the pyroaurite crystallites are (1) growing, which would imply that Mg exchange is causing regrowth of the crystallites to occur, (2) shrinking, which would imply that dissolution is occurring over time or (3) staying the same size, which would imply that any exchange occurring is not affecting the larger crystal structure of the mineral. Figure S7. Reports the crystallite size of the pyroaurite over various time points (Table S2.)

**Table S2.** Crystallite size and strain for pyroaurite over time

Time (days)	LVol-IB (nm)	$2\sigma$	$e_{\theta}$
0	15.7	1.7	0.001
1	18.6	4.0	0.001
5	20.6	2.8	0.002
10	14.8	1.1	0.000
30	15.3	1.1	0.000
60	14.9	1.4	0.000

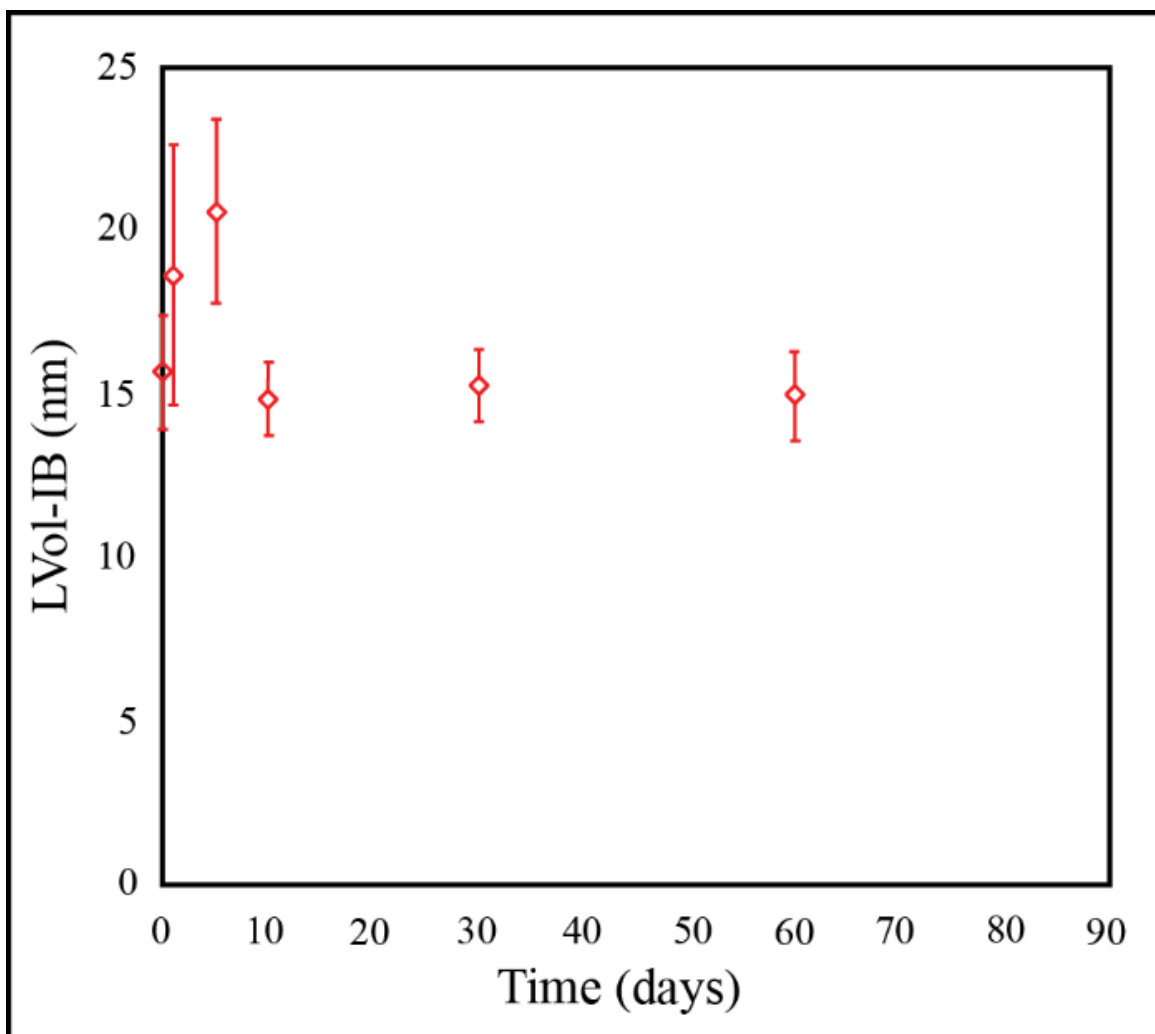


**Figure S7.** Crystallite size (*LVol-IB*) over time for pyroaurite undergoing Mg exchange. Error bars represent the estimated standard deviation ( $2\sigma$ ) that was calculated using Topas V.5 (BrukerAXS).

### **S.I. 1.5 References**

Cheary, R.W., and Coelho, A. (1992) A fundamental parameters approach to X-ray line-profile fitting. *Journal of Applied Crystallography*, 25(2), 109-121.

Gualtieri, A.F. (2000) Accuracy of XRPD QPA using the combined Rietveld-RIR method. *Journal of Applied Crystallography*, 33(2), 267-278.

Ingram L, Taylor H.F.W. (1967) The crystal structures of sjoegrenite and pyroaurite. *Mineralogical Magazine*, 36,465 - 479

Handler, R.M., Friedrich, A.J., Johnson, C.M., Rosso, K.M., Beard, B.L., Wang, C., Latta, D.E., Neumann, A., Pasakarnis, T., Premaratne, W.A.P.J., and Scherer, M.M. (2014) Fe(II)-Catalysed Recrystallization of Goethite Revisited *Environmental Science & Technology*, 48, 11302-11311.

Whitfield, P.S., Davidson, I.J., Mitchell, L.D., Wilson, S.A., and Mills, S.J. (2010) Problem Solving with the TOPAS Macro Language: Corrections and Constraints in Simulated Annealing and Rietveld Refinement. *Materials Science Forum*, 651, 11-25.

